Studies of Volcanic Influence on Aerosols, Clouds and Climate

Friberg, Johan

2016

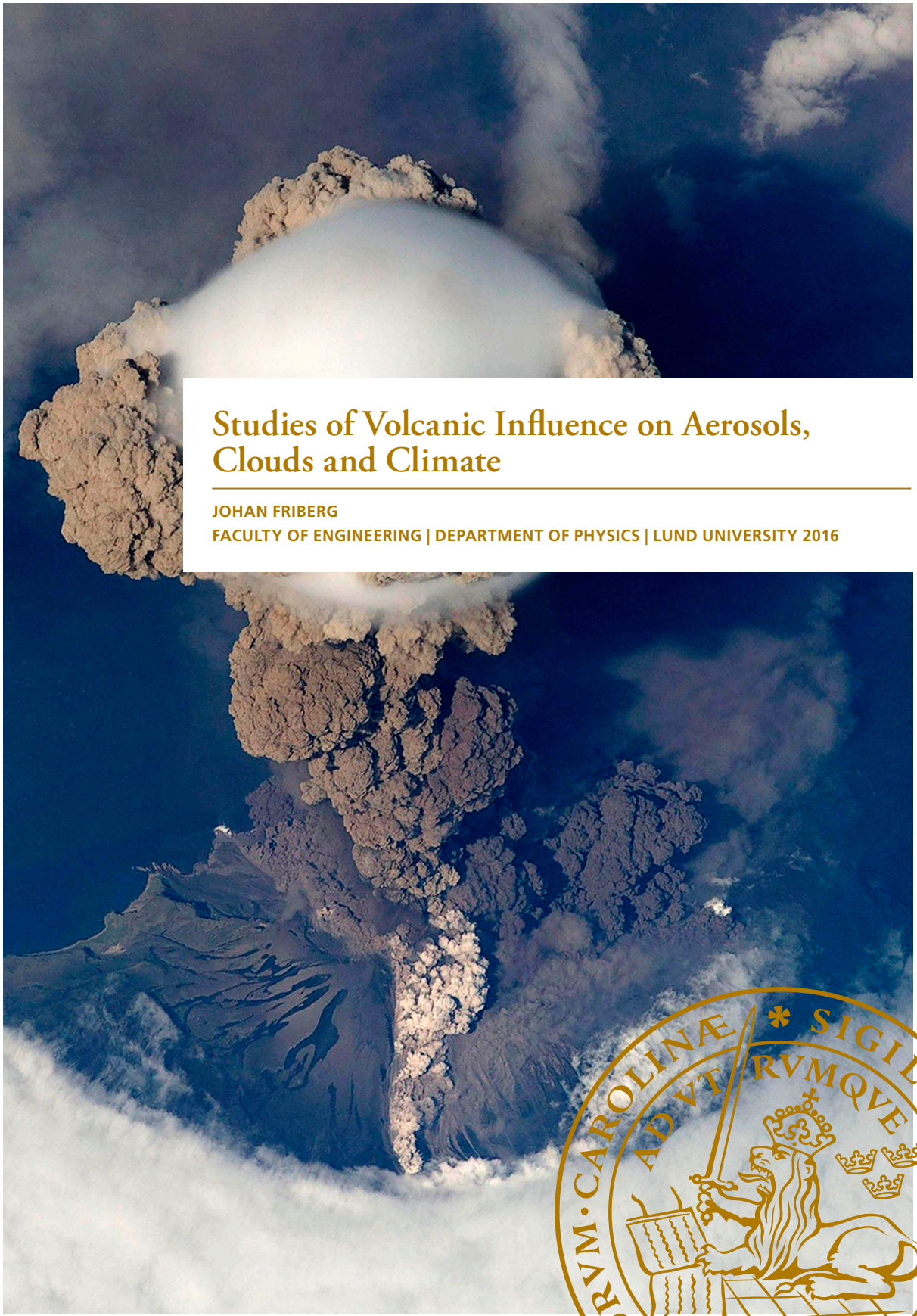

Studies of Volcanic Influence on Aerosols, Clouds and Climate

JOHAN FRIBERG
FACULTY OF ENGINEERING | DEPARTMENT OF PHYSICS | LUND UNIVERSITY 2016

Studies of Volcanic Influence on Aerosols, Clouds and Climate

Johan Friberg

LUND
UNIVERSITY

DOCTORAL DISSERTATION
which, by due permission of the Faculty of Engineering, Lund University, Sweden,

will be defended in Rydbergsalen, Department of Physics, Professorsgatan 1, Lund,
on February 26th 2016, at 9.15.

Faculty opponent

Professor Veli-Matti Kerminen

Department of Physics, University of Helsinki, Finland

Organization:
LUND UNIVERSITY
Division of Nuclear Physics
P.O. Box 118, SE-22100, Lund
Author: Johan Friberg

Document name:
DOCTORAL DISSERTATION

Date of issue: 2016-02-02

Title: Studies of Volcanic Influence on Aerosols, Clouds and Climate

Abstract:

This thesis focuses on the influence of volcanism on the compositions of the aerosols in the upper troposphere (UT) and lowermost stratosphere (LMS), and their direct and indirect impact on climate. Aerosol data were obtained by aircraft-borne sampling, using the CARIBIC (Civil Aircraft for the Regular Investigation of the Atmosphere Based on an Instrument Container) platform, and laboratory-based ion beam analysis of aerosol samples at the Lund Ion Beam Analysis Facility (LIBAF). Aerosol composition data were compared to particle size distributions obtained from onboard optical particle counter (OPC) measurements, demonstrating good agreement between the two analysis systems. The impact on climate was investigated using satellite observations of aerosol and optical properties of cirrus clouds. These were provided by the CALIOP and MODIS instruments onboard the NASA satellites CALIPSO, Terra and Aqua.

The aerosol load in the LMS has varied considerably since 2000, mainly due to volcanic injections of particles and particle-forming gases. Tropical volcanoes affect the LMS for up to two years after eruption, through transport within the Brewer-Dobson circulation. In contrast, extra-tropical volcanoes inject aerosols directly into the LMS, which subside to the UT within months. The eruption of Kasatochi in August 2008 increased the aerosol load in the northern hemisphere LMS by a factor of ~10. Apart from sulfate and ash, both fresh and aged volcanic aerosols contain surprisingly large amounts of carbonaceous aerosols, and the value of the oxygen:carbon ratio (O/C) of ~2 indicates an organic origin. Entrainment of the organic aerosol present in the tropospheric background within volcanic jets and plumes was suggested to be the cause.

Using CALIOP data, it was shown that the stratospheric aerosol at altitudes below 15 km constitutes a significant part of the volcanic forcing. During the period from 2008 to the middle of 2012, volcanic forcing in the LMS constituted 30% of that in the rest of the stratosphere. In addition, volcanism was found to have a significant influence on aerosol concentrations in the UT of the northern hemisphere. Comparison with cirrus reflectance (CR) data obtained using the MODIS instrument revealed a strong anti-correlation between the CR and particulate sulfur mass concentration, suggesting that the volcanic aerosol affected midlatitude cirrus clouds. In 2011, the CR was 8% lower than in 2001. Since cirrus clouds warm the Earth, this decrease is associated with regional cooling.

The results of these studies show that previous estimates of the impact of volcanism on climate have been underestimated. The investigations of the direct and indirect radiative effects of volcanism on the UT and LMS presented here provide new information on the effect of volcanism on the Earth's climate. This will allow more realistic estimates of the impact of volcanism on climate variability, and improve climate models providing more realistic projections of future global temperatures.

Key words: Stratosphere, volcanism, volcanic aerosol, lowermost stratosphere, upper troposphere, sulfurous aerosol, carbonaceous aerosol, radiative forcing, direct effect, indirect effect, ion beam analysis

Classification system and/or index terms (if any)

Supplementary bibliographical information

Language: English

ISRN: LUTFD2/(TFKF-1047)/1-73 (2015)

ISBN: 978-91-7623-591-1(print)
ISBN: 978-91-7623-592-8(pdf)

Recipient's notes

Number of pages: 73

Price

Signature  Date 2016-01-18

Studies of Volcanic Influence on Aerosols, Clouds and Climate

Johan Friberg

LUND
UNIVERSITY

Front cover taken by NASA
from the International Space Station

Faculty of Engineering, Department of Physics
ISRN LUTFD2/(TFKF-1047)/1-73 (2015)
ISBN 978-91-7623-591-1 (print)
ISBN 978-91-7623-592-8 (pdf)

Printed in Sweden by Media-Tryck, Lund University
Lund 2013

”Min mamma jobbar med satelliter,
men min pappa har faktiskt ett flygplan”

-Elsa Sporre Friberg, three years old

Table of Contents

Abstract

This thesis focuses on the influence of volcanism on the compositions of the aerosols in the upper troposphere (UT) and lowermost stratosphere (LMS), and their direct and indirect impact on climate. Aerosol data were obtained by aircraft-borne sampling, using the CARIBIC (Civil Aircraft for the Regular Investigation of the Atmosphere Based on an Instrument Container) platform, and laboratory-based ion beam analysis of aerosol samples at the Lund Ion Beam Analysis Facility (LIBAF). Aerosol composition data were compared to particle size distributions obtained from onboard optical particle counter (OPC) measurements, demonstrating good agreement between the two analysis systems. The impact on climate was investigated using satellite observations of aerosol and optical properties of cirrus clouds. These were provided by the CALIOP and MODIS instruments onboard the NASA satellites CALIPSO, Terra and Aqua.

The aerosol load in the LMS has varied considerably since 2000, mainly due to volcanic injections of particles and particle-forming gases. Tropical volcanoes affect the LMS for up to two years after eruption, through transport within the Brewer-Dobson circulation. In contrast, extra-tropical volcanoes inject aerosols directly into the LMS, which subside to the UT within months. The eruption of Kasatochi in August 2008 increased the aerosol load in the northern hemisphere LMS by a factor of ~10. Apart from sulfate and ash, both fresh and aged volcanic aerosols contain surprisingly large amounts of carbonaceous aerosols, and the value of the oxygen:carbon ratio (O/C) of ~2 indicates an organic origin. Entrainment of the organic aerosol present in the tropospheric background within volcanic jets and plumes was suggested to be the cause.

Using CALIOP data, it was shown that the stratospheric aerosol at altitudes below 15 km constitutes a significant part of the volcanic forcing. During the period from 2008 to the middle of 2012, volcanic forcing in the LMS constituted 30% of that in the rest of the stratosphere. In addition, volcanism was found to have a significant influence on aerosol concentrations in the UT of the northern hemisphere. Comparison with cirrus reflectance (CR) data obtained using the MODIS instrument revealed a strong anti-correlation between the CR and particulate sulfur mass concentration, suggesting that the volcanic aerosol affected midlatitude cirrus clouds. In 2011, the CR was 8% lower than in 2001. Since cirrus clouds warm the Earth, this decrease is associated with regional cooling.

The results of these studies show that previous estimates of the impact of volcanism on climate have been underestimated. The investigations of the direct and indirect radiative effects of volcanism on the UT and LMS presented here provide new information on the effect of volcanism on the Earth's climate. This will allow more realistic estimates of the impact of volcanism on climate variability, and improve climate models providing more realistic projections of future global temperatures.

Populärvetenskaplig sammanfattning

I atmosfären finns mikroskopiskt små luftburna partiklar. Till skillnad från makroskopiska partiklar sedimenterar dessa så kallade 'aerosol-partiklar' så sakta att de följer med den omgivande luftens rörelser. I atmosfärens nedre luftlager (troposfären) avlägsnas aerosolpartiklarna från atmosfären av nederbörd. Partiklarna deponerar därför inom någon vecka. Ovanför troposfären uppstår däremot ingen nederbördsbildning. I detta luftlager (stratosfären) följer partiklarna därför med luftens rörelser. Eftersom lufttransporten ner till troposfären är långsam kan aerosolpartiklar som nått stratosfären stanna kvar i luften i flera år.

Ett flygplan, tre satelliter och en partikelaccelerator

I denna avhandling presenteras forskning kring förekomsten av aerosolpartiklar i främst stratosfären och övre troposfären, deras beståndsdelar, geografiska och vertikala spridning, variationer över tiden, samt deras påverkan på Jordens klimat. Studierna baseras på data från aerosolprov och -mätningar tagna (mellan år 1999-2013) på 10-12 km höjd med ett passerarflygplan inom forskningskonsortiet CARIBIC, samt data ifrån tre satelliter (CALIPSO, Terra och Aqua). Satelliterna använder olika optiska mätmetoder för att undersöka strålningsegenskaperna för partiklar och moln, medan en annan optisk metod via flygplansmätning genererar data över partiklarnas storlek. I ett laboratorium bombarderas proverna från flygplansmätningar med protoner accelererade med en partikelaccelerator för att även mäta aerosolpartiklarnas kemiska beståndsdelar och masskoncentrationer utav dessa.

Aerosolpartiklarnas sammansättning

Partiklar i stratosfären antas vanligtvis bestå utav svavelsyra och vatten. Därutöver innehåller partiklarna stora mängder kolmaterial och diverse föreningar med metaller. En ny upptäckt är att kolfraktionen i stratosfäriska partiklar huvudsakligen är organisk (ej sot). Svavelsyran bildas främst från karbonylsulfid och svaveldioxid. Vid förbränning av fossila bränslen emitteras stora mängder svaveldioxid, varav det mesta deponerar på marken som surt regn. Karbonylsulfid, som huvudsakligen har naturliga källor, kan däremot överleva den långsamma transporten upp till stratosfären, där den bryts ner av UV-ljus och bildar svavelsyrapartiklar. Kraftiga vulkanutbrott kan dock transportera vulkanisk svaveldioxid upp till 10-tals km höjd.

Vulkaniska aerosolpartiklar och deras klimatpåverkan

Aerosolpartiklar påverkar Jordens klimat på flera sätt. Genom att reflektera tillbaka solens strålning ut i rymden hindrar partiklarna solljuset från att värma upp Jordens yta, vilket ger en kylande effekt på klimatet. Under de senaste 10 åren har mängden partiklar i stratosfären varierat mycket, främst pga. flera vulkanutbrott. De vulkaniska partiklarna har under denna period kylt klimatet och därmed bidragit till att dölja en del av den globala uppvärmningen som människans växthusgasutsläpp genererar.

Vulkanutbrott kan transportera stora mängder partiklar och partikelbildande gaser till hög höjd. När det vulkaniska molnet stratosfären blir partiklarnas kylande effekt långvarig. Efter vulkanen Pinatubos kraftiga utbrott i Filipinerna år 1991 sjönk Jordens medeltemperatur med cirka 0,5°C under det efterföljande året.

Trots att 40% av stratosfärens luft ligger under 15 km höjd inkluderas vanligtvis inte partiklarna i denna luftmassa (lägsta stratosfären) vid uppskattningar av klimatpåverkan från vulkanism. I denna avhandling presenteras forskning som visar att lägsta stratosfären var påverkad av vulkaniska partiklar under större delen av perioden 2005-2013. Mellan vintern 2008 och sommaren 2012 gav partiklar i lägsta stratosfären en klimatpåverkan som motsvarar cirka 30% utav den från övriga stratosfärens partiklar. Deras kylande effekt bidrog därmed till att motverka den globala uppvärmningen.

Vulkanismen kan också ha påverkat molnen, eftersom vattenånga behöver ytor att kondensera på för att bilda moln. I stratosfären bildar vattenånga inte moln, men i troposfären sker all molnbildning i samverkan med aerosolpartiklar. I den kalla övre troposfären består molnen utav små iskristaller. Dessa så kallade cirrusmoln isolerar och värmer Jorden genom att stänga inne en andel av dess värmestrålning. En ny upptäckt är att nedtransport av luft ifrån stratosfären starkt påverkar förekomsten av partiklar i övre troposfären. Samtidiga variationer i cirrusmolnens reflektion tyder på att partiklarna har påverkat dem. Från 2001 till 2011 sjönk reflektansen för cirrusmolnen på norra halvklotet med 8%, vilket sannolikt gett en kylande effekt på Jordens klimat. Störst var förändringen över Europa, Atlanten och Nordamerika, områden med tät flygtrafik. En möjlig förklaring till cirrusmolnens förändrade egenskaper kan vara att partiklar i övre troposfären (t.ex. sot ifrån flygplanen) kan bli sämre på att binda vattenånga när de blandas med de vulkaniska partiklarna. Idag vet vi inte hur stor påverkan vulkaniska partiklar har på cirrusmolnen. Kanske kan ytterligare flyplansmätningar och satellitobservationer kombineras med modellberäkningar för att ge klarhet i detta.

Papers included in this thesis

I. S. M. Andersson, B. G. Martinsson, **J. Friberg**, C. A. M. Brenninkmeijer, A. Rauthe-Schöch, M. Hermann, P. F. J. van Velthoven, and A. Zahn, *Composition and evolution of volcanic aerosol from eruptions of Kasatochi, Sarychev and Eyjafjallajökull in 2008-2010 based on CARIBIC observations*, Atmos. Chem. Phys., 13, doi: 10.5194/acp-13-1781 (2013).

I contributed to the sample analysis, the data analysis and discussions on the manuscript.

II. **J. Friberg**, B. G. Martinsson, S. M. Andersson, C. A. M. Brenninkmeijer, M. Hermann, P. F. J. van Velthoven, and A. Zahn, *Sources of increase in lowermost stratospheric sulphurous and carbonaceous aerosol background concentrations during 1999-2008 derived from CARIBIC flights*, Tellus B, 66, doi: 10.3402/tellusb.v66.23428 (2014).

I contributed to the sample analysis, performed the data analysis and wrote the paper.

III. B. G. Martinsson, **J. Friberg**, S. M. Andersson, A. Weigelt, M. Hermann, D. Assmann, J. Voigtländer, C. A. M. Brenninkmeijer, P. J. F. van Velthoven, and A. Zahn, *Comparison between CARIBIC aerosol samples analysed by accelerator-based methods and optical particle counter measurements*, Atmos. Meas. Tech., 7, doi: 10.5194/amt-7-2581 (2014).

I contributed to the ion beam analysis, assisted in the data evaluation and contributed to discussions on the manuscript.

IV. S. M. Andersson, B. G. Martinsson, J. P. Vernier, **J. Friberg**, C. A. M. Brenninkmeijer, M. Hermann, P. F. J. van Velthoven, and A. Zahn, *Significant radiative impact of volcanic aerosol in the lowermost stratosphere*, Nature Communications, 6, doi: 10.1038/ncomms8692 (2015).

I contributed to the ion beam analysis, assisted in the data evaluation, and took part in discussions on the manuscript.

V. **J. Friberg**, B. G. Martinsson, M. K. Sporre, S. M. Andersson, C. A. M. Brenninkmeijer, M. Hermann, P. F. J. van Velthoven, and A. Zahn, *Influence of volcanic eruptions on midlatitude upper tropospheric aerosol and consequences for cirrus clouds*, Earth and Space Science, 2, doi: 10.1002/2015EA000110 (2015).

I contributed to the sample analysis, performed the aerosol-related data analysis, and wrote most of the paper. I also contributed to the cirrus data evaluation.

Abbreviations and Acronyms

AOD	Aerosol optical depth
BD	Brewer-Dobson (refers to the meridional transport in the stratosphere)
CALIOP	Cloud-Aerosol Lidar with Orthogonal Polarization
CARIBIC	Civil Aircraft for the Regular Investigation of the Atmosphere Based on an Instrument Container
CR	Cirrus reflectance
ENSO	El Niño southern oscillation
GHG	Greenhouse gas
IBA	Ion beam analysis
IN	Ice nuclei
IPCC	Intergovernmental Panel on Climate Change
LIBAF	Lund Ion Beam Analysis Facility
LMS	Lowermost stratosphere
MODIS	Moderate-Resolution Imaging Spectroradiometer
NH	Northern hemisphere
OCS	Carbonyl sulfide
OPC	Optical particle counter
PDO	Pacific decadal oscillation
PESA	Particle elastic scattering analysis
PIXE	Particle-induced X-ray emission
PV	Potential vorticity
QI	Quality indicator
RF	Radiative forcing
S/PV_{LMS}	S_{LMS} to PV ratio
SH	Southern hemisphere
S_{LMS}	Particulate sulfur concentration in the LMS
STP	Standard temperature (273.15 K) and pressure (1013.25 hPa)
S_{UT}	Particulate sulfur concentration in the UT
TTL	Tropical transition layer
UT	Upper troposphere

Acknowledgements

Thank you…

Bengt, for your guidance and support, and sharing of your experience and knowledge, within science, football and life in general. You have always been available, no matter the timing or the question.

Sandra, for still helping out, even though you don't have the time. Together with Bengt we turned the research focus to answer some big questions.

Lotta, for taking the time to mentor me. It has in many ways been challenging, but also a lot of fun.

Per, Staffan and Göran, for all help with our experimental work.

All colleagues within the CARIBIC project. Carl, Markus, Peter and Andreas. You are especially acknowledged for fruitful collaboration, welcoming attitude and appreciation of my research.

Cerina. ^5.

Pico, Maciek, Maria and Kilian. It was one legendary summer.

Anneli and Britt-Marie for helping a confused PhD student with all the administrative stuff.

Charlotta, for helping out with teaching assignments and general organizational matters.

All other PhD students, and the rest of the staff at the division of nuclear physics, for friendly company and for maintaining a great atmosphere that I so much enjoy.

Inger with colleagues. Together you helped me back on track, in a time of great need.

David. On some winding roads we made it through. Apparently sometimes the less likely students end up in the forefront of science.

Dad and Mom, for introducing me to mathematics and the natural sciences, and for encouraging my curiosity and childhood needs of knowledge and explanations. Many were the hours you spent reading and discussing inventions, phenomena and theories with your four year old son (volcanic eruptions, aircrafts and satellites included). And my Grand-dads, Walter and Gunnar, who inspired me further.

Elsa and Vilgot. Not only are you adorable. Your creativity, imagination and joy are contagious. And Moa, the love of my life. Thank you for your endless love and support. Together we strive into the unknown. And that journey has just begun.

1.Background

1.1. Volcanism and climate

Atmospheric aerosol particles affect the radiation budget of the Earth both directly, via absorption and scattering of solar radiation, and indirectly, through their influence on clouds. The effect of aerosols on climate depends on many factors, such as particle shape, composition, size, and morphology, as well as their residence time in the atmosphere. Typically, tropospheric aerosol particles are deposited on the ground within days or weeks, whereas aerosol particles in the stratosphere can remain suspended in the air for years. The volcanic eruption of Mount Pinatubo (in the Philippines) in 1991 perturbed the stratospheric aerosol load for several years, and it was estimated that it resulted in a temperature decrease of 0.5°C in the following year. The stratospheric aerosol load then decreased, reaching background levels at the end of the 20th century.

The stratospheric aerosol load has varied considerably during the first decade of the present millennium, mainly due to a number of large volcanic eruptions. Concurrent with these events, observations of the global temperature indicated a ~15-20 year period without global warming, often referred to as the 'hiatus'. This has attracted much attention in recent years, and factors such as changes in vertical heat distribution in the oceans, solar forcing and the impact of volcanism on the stratospheric aerosol load, have been suggested as possible drivers. However, evidence presented during 2015 indicates that the global warming seen in the late 1900s has continued into the 21st century.

1.2. Aircraft- and satellite-borne observations

Most aerosol particle measurements are carried out in the lowest layer of the troposphere, the so-called atmospheric boundary layer. *In situ* measurements of particles at higher altitudes are rare. The aerosol data used in the work presented in this thesis were obtained via aircraft sampling and measurements, and satellite observations of the tropical troposphere, the extra-tropical upper troposphere (UT) and the overlying stratosphere.

The CARIBIC (Civil Aircraft for the Regular Investigation of the Atmosphere Based on an Instrument Container) project provides a platform for *in situ* sampling of aerosol particles and trace gases, using commercial intercontinental aircraft. Aerosol samples have been collected on monthly flights since 1999, and particle elemental concentrations are measured using ion beam techniques to obtain detailed information on the chemical composition of the aerosol. CARIBIC also provides particle size distributions using an optical particle counter (OPC). Satellite observations using the CALIOP (Cloud-Aerosol Lidar with Orthogonal Polarization) instrument provided spatial and temporal distributions of the global aerosol load. In addition, observations of cirrus cloud reflectance using the MODIS (Moderate-Resolution Imaging Spectroradiometer) instrument were used to investigate possible particle-associated perturbations of midlatitude cirrus clouds.

1.3. Aims of this work

The first objective of the studies presented in this thesis was to investigate the influence of air dynamics on aerosol concentrations in the lowermost stratosphere (LMS) and upper troposphere. Since the stratosphere was perturbed by volcanic aerosols during much of the period studied, the second objective was to explore the influence of volcanism on variations in aerosol concentrations in the LMS.

Recent volcanic perturbations of the stratosphere have masked the global warming effects of greenhouse gases (GHGs). Previous estimates of the effects of volcanic eruptions on climate have neglected the impact of aerosols in the LMS. In addition, the stratospheric aerosol eventually subsides into the extra-tropical UT, where it may influence cirrus clouds, inducing further perturbation of the Earth's radiative balance. Two further aims of this work were, therefore, to investigate the direct effects of volcanism in the LMS, in order to estimate the associated radiative forcing in absolute terms, as well as in relation to that of the stratospheric portion above the LMS; and to investigate possible indirect effects of volcanism in the UT through changes in the optical properties of cirrus clouds. Aerosol composition data from aircraft-borne sampling were compared with data from satellite observations (CALIOP), extending the studies to a near-global scale. Regarding indirect effects, the influence of the subsidence of aerosol from the stratosphere was established, so that the volcanic impact on the UT aerosol could be compared to changes in the reflectance of midlatitude cirrus clouds.

2. Introduction

The atmosphere contains suspended particles, and although they constitute only a very small proportion of the atmospheric mass, these so-called aerosol particles affect the Earth's climate in many ways. They play an important role in the radiative balance by scattering solar radiation back into space, and through particle-cloud interactions. Hence, changes in the amount of atmospheric aerosol particles will affect our climate. One example of this is volcanic eruptions, which generate large amounts of aerosol particles that occasionally perturb the aerosol load for many years. Blocking of sunlight by volcanic particles has caused significant cooling throughout history, as well as in the modern era.

The studies in this thesis focus on aerosol particles in the tropical middle troposphere, the extra-tropical upper troposphere and the overlying stratosphere. The vertical motion of air in the troposphere is mainly driven by convection, induced by solar heating of the Earth's surface. The temperature in the troposphere decreases with altitude by, on average, 6.5 K km^{-1}, while the temperature increases above the tropopause (i.e. the boundary between the troposphere and the stratosphere) through the stratosphere, due to heating by UV absorption in the O_3 layer (Figure 2.1). The difference in lapse rates (temperature gradients) results in different dynamics in the two air masses, leading to very limited and slow vertical air motion in the stratosphere, which limits the mixing and transport across the tropopause. Therefore, the compositions of these air masses differ significantly.

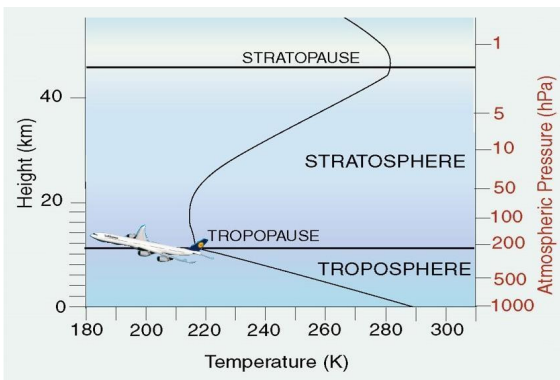

Figure 2.1.
The vertical temperature structure of the Earth's atmosphere. [after *Bennett*, 2006].

The troposphere contains, on average, 90% of the atmosphere's mass [*Appenzeller et al.*, 1996], more than 99% of its water, and most of the aerosol particles. Also, most of the weather systems are formed in the troposphere. The stratosphere extends up to an altitude of ~50 km, but contains much less mass than the troposphere, and water concentrations of only ppm. In the middle stratosphere, O_3 is produced by UV radiation, forming the O_3 layer, located at an altitude of ~20-30 km. Subsidence of stratospheric air brings O_3 rich air to the tropopause region, where it mixes with tropospheric air.

2.1. The tropopause

The tropopause acts as an upper boundary for adiabatically driven air motion, limiting the transport of air between the troposphere and the stratosphere. The altitude of the tropopause depends on the average temperature of the atmosphere below the tropopause, and is therefore located at a higher altitude in the tropics (17 km) than in polar regions (8 km). The World Meteorological Organization defines the (thermal) tropopause as the lowest level at which the temperature decrease is 2 K km^{-1} or less, given that the average decrease from that level to any higher level within 2 km is less than 2 K km^{-1}.

The tropopause can also be defined by its chemistry; preferably by atmospheric trace gases that are more abundant in either the troposphere or the stratosphere. For example, gradients of O_3, CO and water are used to define the chemical tropopause [*Zahn and Brenninkmeijer*, 2003]. Since the troposphere and stratosphere differ in their dynamics (e.g. their lapse rates), the dynamic properties of the air can also be used to determine the altitude of the tropopause [*Hoerling et al.*, 1991; *Hoinka*, 1997]. The dynamical tropopause was used in the studies described in Papers I, II, III and V, based on modeling of the air dynamics, while in Paper IV, the thermal tropopause was employed, based on satellite observations.

2.2. Stratospheric dynamics

Aerosol particles are removed from the troposphere by sedimentation and wet deposition (removal through precipitation). Submicron aerosol particles can remain suspended in the air for several years, owing to the absence of wet deposition in the stratosphere and their low settling rates. Therefore, the transport of air is of major importance for understanding the variability in concentrations of particulate matter in the stratosphere.

While the extra-tropical tropopause acts as a barrier to transport, slowly ascending air in the tropical transition layer (TTL), located at an altitude of 15-17 km [*SPARC*, 2015], reaches the stratosphere on time scales of months, allowing sufficient time for particles to sediment. During ascent, the temperature falls causing freeze-drying of air entering the stratosphere, which results in the low stratospheric water concentrations. Aerosol particles are also scavenged from the TTL, as they act as seeds for droplet and ice crystal formation. Thus, the sedimentation of large ice crystals acts as a sink for aerosol particles (in-cloud scavenging), and coagulation on settling ice crystals provides a further sink (below-cloud scavenging).

In the tropical stratosphere, upwelling air is incorporated in a meridional transport mechanism called the Brewer-Dobson (BD) circulation [*Brewer*, 1949; *Dobson*, 1956], bringing air from the tropics to midlatitudes and polar regions, in a deep branch and shallow branches (Figure 2.2). The shallow branches transport air at low stratospheric altitudes, while the deep branch extends into the overlying mesosphere. Whereas the shallow branches have weak seasonality, the strength of the deep branch varies considerably with season, being stronger in the winter hemisphere. These paths transport air on very different time scales. In the deep branch, transport from the tropics to midlatitudes takes years, starting with slow ascent in the tropical stratosphere. In contrast, the shallow branches can transport air from the tropics to midlatitudes in a matter of weeks [*Bourassa et al.*, 2012].

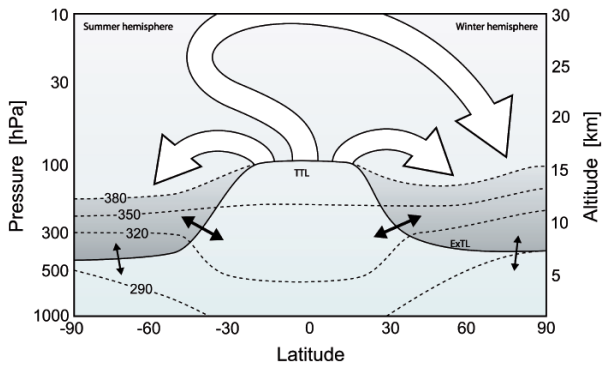

Figure 2.2.
The stratospheric circulation and stratosphere-troposphere exchange during northern hemispheric winter. Solid line marks the tropopause, the dashed lines the 290-380 K isentropes, and the dark shaded volume the LMS. The black arrows indicate cross-tropopause mixing. The deep and shallow branches of the BD circulation are indicated by the white arrows. [based on *Birner and Bönisch*, 2011; *Holton et al.*, 1995]

In the extratropics, air downwells to the troposphere, passing through the LMS. The LMS constitutes the stratospheric air mass below the 380 K isentrope (potential temperature level, ~15 km altitude at midlatitudes), containing >40% of the stratospheric mass [*Appenzeller et al.*, 1996]. The air exchange between the

troposphere and stratosphere varies with season. In the northern hemisphere (NH), subsidence across the 380 K isentrope peaks in midwinter (January), but it takes months for the downwelling air to reach the tropopause. As a result, the net transport across the tropopause peaks in May. In addition, the mass of the LMS varies with season, by a factor of ~30% at northern midlatitudes [*Appenzeller et al.*, 1996]. In spring and summer (fall), the tropopause ascends (descends) due to warming (cooling) of the underlying troposphere, while the upper limit of the LMS (the 380 K isentrope) remains at a more constant altitude. Air transport in the southern hemisphere (SH) is shifted by six months, compared with that in the NH, and the variation in the LMS mass and transport is smaller.

The composition of the LMS depends on transport. In the LMS, tropospheric air mixes with downwelling stratospheric air, inducing concentration gradients of trace gases [*Zahn et al.*, 2002] and particulate matter [*Martinsson et al.*, 2005]. In contrast to the overlying part of the stratosphere, the LMS has isentropes that cross the tropopause causing bidirectional transport, allowing rapid local cross-tropopause mixing. Closest to the tropopause, such mixing forms a ~2-3 km layer [*Gettelman et al.*, 2011], with steep concentration gradients of, for example, CO, O_3, water and particulate matter. A large fraction of the aerosol samples analyzed in the present work were sampled in this so-called extra-tropical transition layer. Non-local, cross-tropopause transport occurs from the TTL, in the vicinity of the subtropical jet. Weakening of the jet results in higher transport during summer [*Sprenger and Wernli*, 2003], bringing large amounts of tropospheric air into the midlatitude LMS. This phenomenon is referred to as the flushing of the LMS [*Hoor et al.*, 2002], as it greatly reduces the proportion of stratospheric air.

The combined effect of seasonally varying strengths of the many transport paths is seasonally varying amounts of stratospheric and tropospheric air in the LMS. *Bönisch et al.* [2009] described this as a seasonally varying mean age of LMS air, decreasing from spring to fall; the age being a measure of the time since the air was transported from the troposphere. Finally, the stratospheric air enters the UT, contributing O_3 [*Roelofs and Lelieveld*, 1997] and stratospheric aerosol [*Friberg et al.*, 2015] to the tropospheric background.

2.3. Atmospheric aerosol particles

An aerosol is defined as a collection of solid or liquid particles suspended in a gas. The size of aerosol particles ranges from ~1 nm-100 μm; the upper limit being roughly the maximum size of a particle that can remain suspended, and the lower the minimum size for the formation of stable molecular clusters. The particles are formed either by the disintegration of solids or liquids (primary particle production), or via the conversion of gases to particles (secondary particle production). Vapor can interact

with, and add mass to, existing particles, or form nm-sized clusters, creating new particles that may grow by vapor condensation and coagulation. Primary particles are generally super-micron sized.

Atmospheric aerosol particles are produced by a vast number of sources, both natural and anthropogenic. Agriculture and combustion processes emit large quantities of particles and particle-forming vapors. For example, combustion generates not only soot, but also a large number of gases, such as SO_2, NO_x and VOCs. Some typical natural sources of particles are: upwelling dust, sea spray, volcanic and biogenic particle-forming compounds, pollen and particulates from forest fires.

Aerosol particles vary greatly in their chemical composition, size, shape and density. Liquid particles are generally spherical, while solid particles often have irregular shapes. Therefore, equivalent diameters, based on particle properties or behavior (e.g. aerodynamic or optical diameters), are frequently used to describe a particle, or a collection of particles. Furthermore, atmospheric aerosols are polydisperse; their size distribution often being close to a log-normal distribution [*Seinfeld and Pandis*, 2012]. Hence, the physical properties of particles are conveniently described by particle size distributions, in terms of number, surface or volume.

2.4. Stratospheric and UT aerosols

2.4.1. The sulfurous aerosol

The sulfurous aerosol constitutes the largest component of the stratospheric aerosol [*Deshler*, 2008]. Using a combination of balloon-borne and aircraft-borne measurements, *Junge et al.* [1961] found a layer of stratospheric aerosol located at an altitude of 20 km, later named the 'Junge layer'. Later studies on the composition indicated particulate mixtures of sulfuric acid and water [*Rosen*, 1971], and it was subsequently suggested that these were formed from carbonyl sulfide (OCS) [*Crutzen*, 1976] and SO_2. Large amounts of OCS are emitted from the oceans [*Brühl et al.*, 2012; *Kremser et al.*, 2015], as the surface water is often supersaturated with OCS. OCS is also produced from other sulfurous trace gases, such as dimethyl sulfide and CS_2, with some anthropogenic contribution. OCS is relatively inert in the troposphere. However, OCS transported in the deep BD branch is photo-oxidized to SO_2 by the intense UV radiation in the tropical stratosphere. In contrast to OCS, SO_2 is oxidized also in the shallow BD branches. In the LMS, downwelling sulfur-rich stratospheric air mixes with air from the UT, inducing a concentration gradient of sulfurous aerosol throughout the LMS.

2.4.2. The carbonaceous aerosol

In the 1990s, a carbonaceous component was identified in the LMS aerosol [*Murphy et al.*, 1998], often occurring together with the sulfurous aerosol. Morphology studies showed LMS particles to be composed of branched frameworks of carbonaceous matter surrounded by the sulfurous component [*Nguyen et al.*, 2008].

Large forest fires sometimes entrain smoke to high altitudes [*Guan et al.*, 2010; *Jost et al.*, 2004], carrying soot and particle-forming organic trace gases. In 2001, a massive firestorm in Alberta Canada, called the Chisholm fire, formed pyro-cumulonimbus that penetrated the extra-tropical tropopause. This episode was estimated to have increased the aerosol load of the NH lower stratosphere by >5% [*Fromm et al.*, 2010]. However, such events are rare. *Guan et al.* [2010] estimated that, on average, less than 5 events per year reach altitudes exceeding 5 km. Furthermore, biomass burning effluents contain particulate K. K was undetected in a majority of the carbonaceous UT [*Murphy et al.*, 2006] and LMS [*Murphy et al.*, 2014] particles, suggesting biomass burning to be a minor source of carbonaceous aerosol in the UT and LMS.

Furthermore, a number of authors [*Carn et al.*, 2011; *Martinsson et al.*, 2009; *Schmale et al.*, 2010] have recently reported the presence of carbonaceous aerosol in volcanic clouds in the UT/LMS, with organic fractions on the order of 20-50%, suggesting that volcanism is an important source of carbonaceous aerosol in the UT/LMS.

2.4.3. Volcanic impact

Volcanic eruptions penetrating the tropopause provides the largest source of variability in the stratospheric aerosol concentrations [*Robock*, 2000], adding ash and particle-forming gases such as SO_2. A single volcanic eruption in the tropics can perturb the stratospheric aerosol concentrations of both hemispheres for several years. In the 20th century, several large volcanic eruptions induced periods of stratospheric perturbations lasting for a year or more. The years after the eruption of the tropical volcano Mount Pinatubo in 1991 is probably the single most-studied such period. The Pinatubo cloud reached an altitude of at least 30 km [*GVP*, 2015], injecting ~10 Tg of S into the tropical stratosphere, increasing its aerosol load by a factor of over 100. Subsequent transport by the BD circulation eventually brought the sulfurous aerosol to midlatitudes. In the aftermath of Pinatubo, the stratospheric aerosol concentrations decreased over a period of several years.

During the first decade of this millennium, the aerosol load in the NH stratosphere increased again [*Hofmann et al.*, 2009], mainly as a result of three eruptions in the tropics in 2005 and 2006 (Manam and Rabaul in Papua New Guinea, and Soufrière Hills, Monserrat)[*Vanhellemont et al.*, 2010; *Vernier et al.*, 2011]. Ground-based lidar measurements of the aerosol load showed that the volcanic aerosol had spread to both the NH [*Bazhenov et al.*, 2012; *Hofmann et al.*, 2009] and the SH [*Nagai et al.*,

2010]. While super-micron ash particles are deposited quickly, the sulfurous aerosol injected into the tropical stratosphere is transported together with the air in the BD circulation. Part of the aerosol was incorporated into the deep branch, perturbing the stratosphere for several years. The volcanic aerosol was subsequently removed by downwelling through the LMS, where it caused the sulfurous aerosol concentrations to increase by a factor of ~2 , before reaching the UT [*Friberg et al.*, 2014].

Volcanism at mid- and high-latitudes generally affects the stratosphere on shorter time scales. The aerosol injected into the extra-tropical stratosphere is ventilated to the UT within a few months to more than half a year, depending on the altitude distribution of the injection [e.g. *Andersson et al.*, 2015]. While cross-hemispheric transport is slow, the aerosol spreads latitudinally within a hemisphere. In recent years, several extra-tropical eruptions have injected aerosols and precursor gases into the LMS, starting with the eruption of Kasatochi (Alaska) in August 2008, followed by the eruptions of Redoubt (Alaska) and Sarychev (Kuril Islands, Russia) in 2009, and Grimsvötn (Iceland) and Puyehue-Cordón Caulle (Chile) in 2011.

2.5. Climate impact of aerosol particles

Aerosol particles affect the radiative balance of the Earth directly, via scattering and absorption, and indirectly, by altering the occurrence and properties of clouds. Thus, perturbations in the atmospheric aerosol load may affect the Earth's radiative budget. In the latest assessment report from the Intergovernmental Panel on Climate Change (IPCC) [*IPCC*, 2013], anthropogenic interference was identified as the main cause of perturbations in the Earth's radiative budget since the beginning of the industrial era. Figure 2.3 illustrates the relative importance of the major factors contributing to global warming (expressed in terms of radiative forcing (RF)), where aerosol particles are estimated to have a cooling effect on climate.

RF is often used to indicate the impact of a single factor or combinations of multiple factors on climate, where positive forcing indicates warming, and *vice versa*. For a given perturbation of the atmospheric radiation budget, the RF (in units of Wm^{-2}) is the corresponding net change in the difference between the incoming and outgoing radiative fluxes that would occur if the temperature were unchanged. Thus, a reference period is needed for comparison, preferably a time when the anthropogenic impact was negligible (or small). The year 1750 is often used as the reference (as in Figure 2.3). Estimates of RF are usually globally averaged values, where the upper boundary is defined as the tropopause or sometimes the 'top of the atmosphere'. Besides RF, the corresponding climate impact eventually depends on feedback systems.

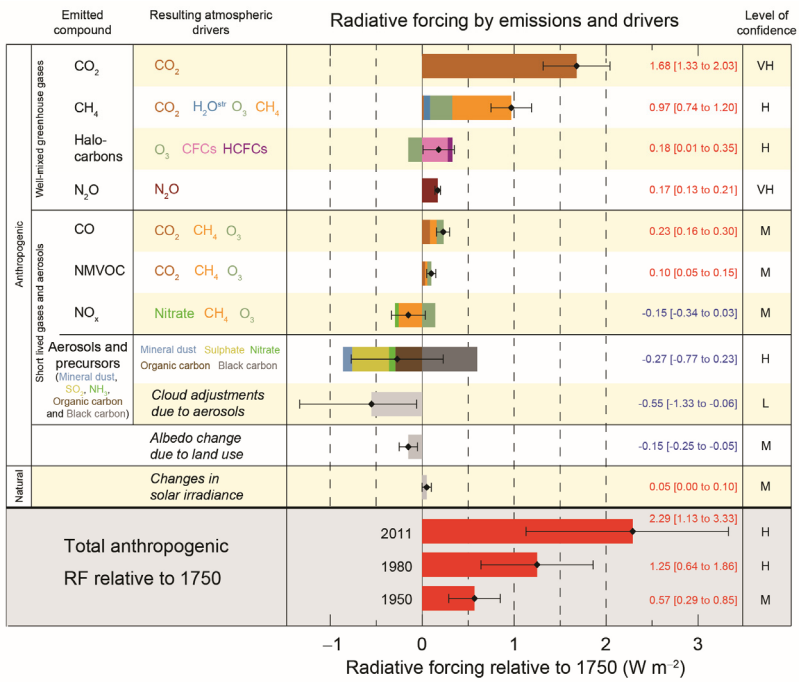

Figure 2.3.
RF estimates in 2011 relative to 1750 and aggregated uncertainties for the main drivers of climate change. Values are global average RF, partitioned according to the emitted compounds or processes that result in a combination of drivers. The best estimates of the net RF are shown as black diamonds with corresponding uncertainty intervals; the numerical values are provided on the right of the figure, together with the confidence level in the net forcing (VH – very high, H – high, M – medium, L – low, VL – very low). Albedo forcing due to black carbon on snow and ice is included in the black carbon aerosol bar. Small forcings due to contrails (0.05 W m^{-2}, including contrail induced cirrus), and HFCs, PFCs and SF_6 (total 0.03 W m^{-2}) are not shown. Concentration-based RFs for gases can be obtained by summing the like-coloured bars. Volcanic forcing is not included as its episodic nature makes it difficult to compare to other forcing mechanisms. Total anthropogenic RF is provided for three different years relative to 1750. [IPCC, 2013].

It is evident from Figure 2.3 that the uncertainty in the estimated impact of aerosol particles is greater than in any other component. The large uncertainties in both the direct and indirect effects of aerosol particles lead to a large error in the estimated total anthropogenic forcing. These uncertainties will naturally affect the prediction of future temperature evolution.

To avoid dangerous impacts of climate change, the aim of mitigation strategies has been to restrict global warming to below 2°C (or recently 1.5°C, compared to that of the preindustrial era), by decreasing GHG emissions. Cooling by aerosols has probably masked a large part of the committed warming [*Ramanathan and Feng*, 2008]. Thus, future temperatures will to a large degree depend not only on the

GHGs', but also on aerosol particles. Since combustion produces both components (GHGs and aerosols), reducing the usage of fossil-fuels might result in short-term accelerated warming. Hence, more knowledge is required on aerosol forcing to be able to make better predictions of the climatic consequences of human exploitation of the planet.

2.5.1. The direct radiative effect and geo-engineering

All aerosol particles scatter radiation, while only some absorb it. Backscattering of incoming solar radiation cools the Earth's surface, while other particles, such as soot, which absorb it, lead to warming of the surrounding air. The direct effect of the anthropogenically emitted aerosol is estimated to be greater on shortwave than on longwave radiation [*Myhre et al.*, 2013], leading to a net cooling of the Earth's surface. The cooling effect depends on the amount and residence time of the emitted aerosol.

The injection of volcanic aerosol into the stratosphere can have a considerable impact on surface temperature; tropical eruptions generally perturbing the stratosphere for longer periods than extra-tropical ones (as explained above). The eruption of Mount Tambora (Indonesia) in 1815 caused a considerable decrease in temperature in the following year, with concomitant crop failure and food shortages. 1816 was thereafter called 'the year without a summer'. The volcanic SO_4 from the Pinatubo eruption in 1991, one of the largest eruptions of the 20th century, is estimated to have reduced the global temperature by ~0.5°C in the following year [*McCormick et al.*, 1995]. While an eruption of this magnitude has not occurred since 1991, there has been an increase in the stratospheric aerosol load resulting from a number of smaller tropical eruptions in the last decade. It has been estimated that these have induced a negative RF of 0.1 Wm^{-2} [*Solomon et al.*, 2011]. Extra-tropical volcanism [*Andersson et al.*, 2015] added further cooling.

The observed cooling effect of volcanic aerosol has resulted in discussions on the potential of deliberately injecting sulfur into the stratosphere to counteract anthropogenic warming [e.g. *Crutzen*, 2006]. This controversial 'geo-engineering' strategy appears to be a relatively cheap and easy solution, and many imaginative techniques have been proposed [e.g. *Vaughan and Lenton*, 2011]. However, apart from the ethical aspects of tampering with the climate, questions regarding feasibility and possible side effects of geo-engineering must be addressed. In the meantime, volcanic eruptions provide a means of studying stratospheric aerosol forcing.

2.5.2. The indirect radiative effect: cirrus clouds in the UT

Clouds reflect shortwave solar radiation, but also absorb longwave radiation emitted by the Earth. The RF associated with these have been estimated to be ~-50 Wm^{-2} (shortwave) and ~30 Wm^{-2} (longwave), leading to a net cooling effect of ~20 Wm^{-2} [*Boucher et al.*, 2013].

Cirrus clouds are the most relevant to the work presented in this thesis. These clouds consist of ice crystals, and are formed at altitudes ranging from about 5 km to the tropopause. Cirrus ice crystal formation is generally divided into two categories depending on cloud microphysics:

homogeneous freezing, i.e., freezing of supercooled solution droplets

heterogeneous freezing, crystallization of water directly on existing ice nuclei (IN).

Homogeneous freezing requires temperatures below 236 K [*Rosenfeld and Woodley*, 2000]. IN lower the supersaturation required for ice crystal formation, thus heterogeneous freezing also occurs at higher temperatures. Homogeneous (heterogeneous) freezing is characterized by high (low) number concentrations and small (large) ice crystals.

Cirrus cloud 'seeding', by deliberately adding IN, has been proposed as a means of counteracting the anthropogenic warming of the planet. However, such a technique may not have the desired effect [*Storelvmo et al.*, 2013]. The outcome depends on which mechanism dominates ice crystal formation. Adding IN to a homogeneously dominated freezing regime may alter ice crystal formation to the heterogeneous regime, resulting in fewer, larger ice crystals. Hence, seeding could cause optical thinning of cirrus clouds, leading to a cooling effect. In contrast, seeding in a heterogeneous freezing regime would provide more IN, increasing the available surface area. This would result in smaller ice crystals and higher number concentrations, giving optically thicker clouds, and increased warming.

It is still not known which mechanism dominates cirrus cloud formation on a global scale. Campaign-based results presented by *Cziczo et al.* [2013] suggest that heterogeneous freezing dominates over Central and North America, where crustal and metallic particles were found to be major constituents of sampled ice residuals. In contrast, modeling has indicated that homogeneous freezing is dominant over most parts of the globe, apart from some continental regions [*Barahona et al.*, 2014].

Soot and volcanic ash can also act as IN [*Campbell et al.*, 2012; *Schumann et al.*, 2013; *Shibata et al.*, 2012]. For example, ash from Eyjafjallajökull (Iceland) was observed to induce ice crystal formation in all clouds below -15°C [*Seifert et al.*, 2011]. Similarly, aircraft engine soot emitted in flight corridors may alter the dominant freezing mechanism from homogeneous to heterogeneous [*Zhou and Penner*, 2014], inducing a cooling effect.

2.5.3. Volcanism and decreased warming

Observations of global surface temperatures have indicated a decrease or lack in global warming since the end of the 1990s, termed the 'hiatus'. Since a hiatus was not predicted by climate models, much effort has been devoted to explaining it. The CMIP5 models used by the IPCC seemed to overestimate the observed temperature evolution of the past ~15-20 years. Factors such as internal variability (e.g. changes in ocean heat sequestration), errors in model response, or inaccurate estimates of RF (e.g. solar forcing and volcanism) [*Flato et al.*, 2013; *Fyfe et al.*, 2013], have been discussed as possible causes. *Santer et al.* [2014] suggested volcanism to be an important factor behind the discrepancy. The existence of a hiatus has recently been called into question, where authors conclude that there likely neither been a hiatus [*Karl et al.*, 2015], nor a slowdown of the global temperature increase [*Rajaratnam et al.*, 2015]. However, several cooling factors have been identified in the search for potential drivers of a hiatus.

During volcanically quiescent periods, the stratospheric aerosol accounts for a minor fraction of the aerosol forcing [*Solomon et al.*, 2011]. However, the increased stratospheric aerosol burden during the 21st century, suggests that volcanism has had a masking effect on the ongoing tropospheric warming [*Andersson et al.*, 2015; *Ridley et al.*, 2014].

3. Methodology

3.1. The CARIBIC platform

CARIBIC is a collaborative project involving 11 research groups in 5 European countries, with the aim of studying the tropopause region. In the period 1997-2002, 76 intercontinental flights were conducted with the first-generation (Phase 1) instrument container [*Brenninkmeijer et al.*, 2007] using a Boeing 767-300 ER run by the German company LTU International Airways. In May 2005, a second-generation (Phase 2) sampling system was installed in a Lufthansa Airbus 340-600 [*Brenninkmeijer et al.*, 2007]. The sampling system consists of a permanently mounted, multiple probe inlet, connected to a 1.6 ton instrument container loaded in the cargo bay, sampling at an altitude of 9-12 km. It provides *in situ* measurements of aerosol particles and trace gases (CO, NO/NO_y, O_3, VOCs, gaseous and condensed water), and air and aerosol samples for laboratory analysis (GHGs, hydro- and halocarbons [*Baker et al.*, 2010; *Brenninkmeijer et al.*, 2007; *Oram et al.*, 2012; *Schuck et al.*, 2009], and aerosol particle composition [*Martinsson et al.*, 2014]).

3.2. Aerosol sampling

3.2.1. The impactors

The aerosol inlet is mounted in the lower aircraft fuselage in front of the engines, well outside the aircraft's boundary layer [*Brenninkmeijer et al.*, 2007]. This arrangement prevents sampling of aircraft exhaust and ensures that the samples are representative of the atmospheric conditions. Steel tubing connects the inlet to a cyclone, where large particles are deposited. The remaining aerosol is sampled on thin polymer films for later analysis at the Lund Ion Beam Analysis Facility (LIBAF). Sampling is terminated when the pressure exceeds 350 hPa.

Aerosol particles were sampled using different inlet systems for the CARIBIC Phase 1 and 2. Phase 1 used an inlet system with 90% sampling efficiency for particles of 0.1-1 µm [*Hermann et al.*, 2001]. The presently used system (Phase 2) has penetrations of 60% for 5 µm particles and over 90% for submicron particles [*Martinsson et al.*,

2014; *Rauthe-Schöch et al.*, 2012]. The cyclone has almost 100% penetration for submicron particles [*Nguyen et al.*, 2006], and a cut-off size of 2 μm is used to minimize the transmission of larger particles.

The aerosol passing through the cyclone is sampled with an automated impactor system [*Nguyen et al.*, 2006]. The Phase 2 system was developed based on a previous impactor system used during Phase 1, and has very similar sampling characteristics. In the Phase 1 device, a single orifice was used to create one well defined deposition spot [*Papaspiropoulos et al.*, 1999]. In the Phase 2 device, particles are deposited in four spots (forming a square pattern) to meet analytical requirements [*Nguyen et al.*, 2006] (see Section 3.3). The Phase 1 (Phase 2) system collects particles with aerodynamic diameters of 0.07-2 (0.08-2) μm using 12 (14) impactors for sequential sampling, and 2 (2) for integral sampling. Integral samples are used as a safety measure to detect contamination. Sequential samples are collected over a period of 150 (100) minutes, corresponding to a flight distance of 2200 (1500) km and a sampling volume of 0.09 (0.25) m^3 at STP (standard temperature: 273.15 K, and pressure: 1013.25 hPa).

3.2.2. The optical particle counter

In 2010, the CARIBIC platform was equipped with an OPC, measuring particle size distributions, using a diode laser of 830 nm wavelength. The OPC generates reliable data for particles larger than 130 nm, in 16 size bins, with an upper limit of 1-1.3 μm, depending on the particle refractive index and calibration curve [*Martinsson et al.*, 2014; *Rauthe-Schöch et al.*, 2012]. In the study described in Paper III, a refractive index of 1.479-0.0143i was applied to the entire size range, computed from literature values of UT aerosol composition (44% sulfuric acid, 44% ammonium sulfate, 10% organic carbon and 2% soot) and mixing rules.

3.3. Composition analysis

The elemental constituents of the aerosol particles were identified using a combination of two ion beam analysis (IBA) techniques: PIXE (particle-induced X-ray emission) [*Johansson and Campbell*, 1988] and PESA (particle elastic scattering analysis) [*Nguyen and Martinsson*, 2007], at the LIBAF. In IBA, samples are bombarded by charged particles accelerated in an electric field. In the current study, the substrates were irradiated by protons with an energy of 2.55 MeV.

PIXE is similar to the electron microscopy technique XEDS (X-ray energy dispersive spectroscopy). A fraction of the irradiating protons interacts with the electrons in the thin substrates, leading to the ejection of electrons, most likely from inner shells, resulting in vacancies. When these vacancies are filled by outer-shell electrons,

photons are emitted with energies in the keV range that are characteristic of each element. The X-ray spectrum also contains a background consisting mainly of bremsstrahlung. The composition of the substrate is then determined by comparison with standards, i.e. specimens with known compositions. X-rays can be detected over a broad energy range using energy-dispersive spectroscopy, allowing many elements to be analyzed simultaneously. Integration of the peaks in the spectrum yields the concentrations of the detected elements.

The possibility of detecting an element is highly dependent on the background in the spectrum. The advantage of PIXE over electron microscopy is that less bremsstrahlung is generated with heavier projectiles, resulting in lower detection limits for PIXE. Thin samples are desirable as they not only minimize bremsstrahlung, but thick-target corrections, such as self-absorption and changes in ionization cross-section due to slowing down of the projectile in the target, can be avoided. It is also important that the substrate backing has as little contamination as possible. The thin polymer films used in the CARIBIC project (AP1, 0.2 μm) are well suited in both these respects.

The UT/LMS aerosol consists mainly of sulfurous and carbonaceous aerosols [*Friberg et al.*, 2014; *Murphy et al.*, 2007]. S is generally easily detected in PIXE spectra, while C is difficult to detect as the lower X-ray energies emitted by C are mostly absorbed before reaching the detector. Therefore PIXE is often combined with other measurement methods.

PESA uses the scattering of impinging protons for element or isotope analysis. A fraction of the protons in the impinging beam interacts with atomic nuclei in the substrates, causing them to be scattered and lose energy. The amount of energy lost depends on the mass of the target nucleus, the mass of the projectile and the scattering angle. The energy and number of protons scattered by the target can be measured using a particle detector. The separation between the peaks in the spectrum is largest for low mass numbers. Hence, this method is best suited for the lightest elements. The PESA technique was introduced into the CARIBIC project in 2005 [*Nguyen and Martinsson*, 2007], to obtain knowledge on the amount and composition of the carbonaceous aerosol in the UT/LMS.

The aerosol samples were analyzed using a combination of PIXE and PESA. Quantitative PIXE measurements were performed using a 5.5 mm collimator to allow all four aerosol deposit spots to be analyzed together, with a current of typically 150-180 nA, and a charge of 30 μC. This provides absolute concentrations of elements with atomic numbers higher than 15. The analysis of lighter elements, e.g. Al and Si, is often not possible with PIXE due to interference from the tail of the large S peak.

The second method employed relative PIXE and PESA analysis. C, N and O concentrations were measured with a particle detector positioned at an angle of 165 degrees from the beam, i.e. to analyze backscattered protons, while protons scattered by H nuclei are measured with a particle detector in the forward direction. In contrast

to PIXE, PESA suffers from high background resulting from the specimen backing, i.e. the polymer film. To reduce the background, a smaller collimator (1 mm) is employed in the PIXE measurements so only one of the four aerosol deposit spots is analyzed. The smaller beam width requires less charge and current (3 μC and 15-18 nA, respectively). Furthermore, a background correction is applied based on the irradiation of two regions of blank backing, 4 mm from the center of the deposition area, on opposite sides of the aerosol deposit centre [*Nguyen and Martinsson*, 2007]. Finally, H, C, N and O are quantified based on a comparison of the S peaks in the X-ray spectra from the quantitative and relative PIXE measurements. When combined in this way, these IBA methods yield absolute concentrations of the major and minor UT/LMS aerosol constituents. Typical detection limits for the most commonly detected elements (in units of ng m^{-3} at STP) are: 1 (H),15 (C), 3 (N), 7 (O), 2 (S), 0.2 (K) and 0.1 (Fe).

3.4. Tracing stratospheric air

As stated in Section 2.1, the stratosphere and troposphere differ in both their air dynamics and chemical composition, leading to gradients, for example, in water, O_3, and sulfuric acid particles. In the current studies, two stratospheric tracers were used: the *in situ* measured O_3 concentrations, and the modeled dynamic parameter, potential vorticity (PV).

The presently used O_3 instrument combines two techniques: a dual-beam UV photometer for high accuracy, serving as a calibrated standard, and a solid state chemiluminescence detector with high measurement frequency. The total uncertainty in 10 Hz measurements is estimated to be 2% [*Brenninkmeijer et al.*, 2007; *Zahn et al.*, 2012]. In the Phase 1 system, UV absorption measurements had an uncertainty of 4% or 4 ppbv, whichever was largest [*Zahn et al.*, 2002]. In the current studies, O_3 data were integrated over the corresponding aerosol sampling times.

PV increases from the tropopause into the stratosphere. The dynamical tropopause is generally considered to lie in the PV range of 1.5-3.5 PVU (potential vorticity units: 1 PVU = 10^{-6} K m^2 kg^{-1} s^{-1}) [*Hoerling et al.*, 1991; *Hoinka*, 1997], and this was the range used in these studies. The PV values were calculated by the Royal Netherlands Meteorological Institute from archived ECMWF (European Centre for Medium-Range Weather Forecasts) analyses with a horizontal resolution of 1×1 degrees at 91 vertical hybrid sigma-pressure model levels. The derived PV values were interpolated linearly in latitude, longitude, log pressure and time to fit the position of the aircraft, and averaged over the duration of sampling.

3.5. Sampling artefacts

The sampling efficiency of an impactor depends on the properties of the particles and the mass deposited. When calibrated with liquid particles, the aerosol sampler showed excellent qualities [*Nguyen et al.*, 2006]. However, several factors may result in underestimation of the sampled aerosol mass.

Bounce-off: Solid particles may bounce off the samples, resulting in particle loss or secondary deposition somewhere else on the substrate.

Blow-off: Solid particles could be blown off the specimen, if it is overloaded.

Wetting: When sampling liquid aerosols with high concentrations, the large amount of deposited mass wetting the surface may cause migration on the substrate.

The effects listed above can all cause deposition of particulate matter outside the area irradiated by the ion beam (5.5 mm), resulting in underestimation of the sampled aerosol mass. Paper III describes a thorough study of such effects based on photographs of 106 samples, collected in the period April 2011-March 2012. Figure 3.1 illustrates typical appearances of the four types of deposition patterns identified: ideal appearance (a), samples with radial filament structures resulting from wetting (b), secondary deposition located between the four primary aerosol deposit spots (c), and very small deposition spots outside the deposition area (d). A quality indicator (QI) was introduced as a means of qualitatively describing the problem with particle losses: no significant losses (QI = 0), discernible losses (QI = 1), and, serious losses (QI = 2).

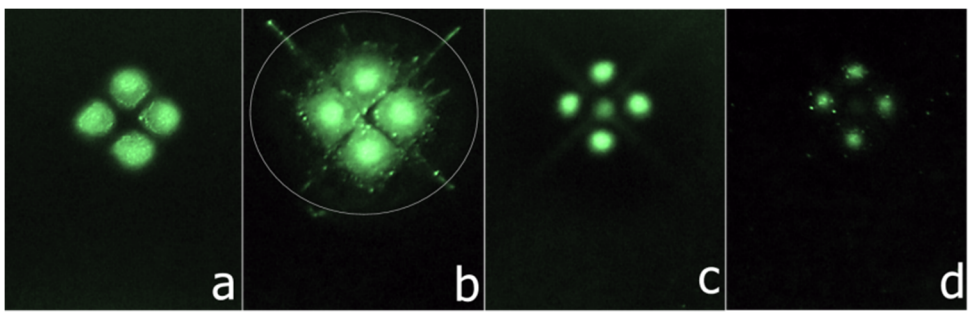

Figure 3.1.
Photographic images of aerosol deposits from the CARIBIC aerosol sampler, where particles are collected from four impactor orifices. (a) Ideal appearance; four spots. (b) Thin filaments of liquid aerosol radiating out from the main deposit. (c) Secondary deposition between the four main spots. (d) Several very small spots outside the main deposition area. The ellipse in (b) illustrates the beam size which is 5.5 mm vertically and 5.5/cos(23°) mm horizontally.

The artefacts described above occurred at different frequencies in the UT and LMS samples, due to the different particle compositions in these air masses. The high concentrations of sulfurous aerosol in the stratosphere resulted in a higher frequency of wetting in LMS samples, while higher concentrations of crustal particles in the UT resulted in more frequent bounce-off. In addition, some of the UT samples were found to be affected by Ni particles generated in the sampling inlet while flying in ice clouds (see Section 3.5.1).

The amount of aerosol deposited outside the four main spots was estimated using S concentrations from the irradiation of blank areas of the film 4 mm from the center of the deposition area. It can be seen from Figure 3.2 that undetected mass usually constituted a few percent of the total mass deposited.

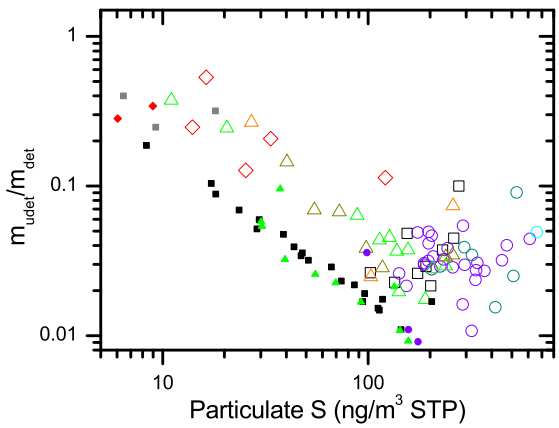

Figure 3.2.
Scatter plot of the ratio of the estimated particulate mass of S outside the analytical beam area (m_{udet}) to the detected mass (m_{det}) as a function of the atmospheric particulate S concentration. Particulate S was detected in the analytical area of all samples. Open symbols indicate cases where S was also detected outside the analytical area, whereas the small, closed symbols denote samples where S was undetected outside the analytical area.

3.5.1. The cloud-generated 'Ni-ice' defect

Impaction of large particles on the Ni-plated aerosol inlet of the aerosol sampler can cause the release of submicron Ni particles. Evidence of artefactual Ni was observed specifically when cruising through ice clouds, accompanied by higher concentrations of particles larger than those normally observed by the OPC in the UT/LMS [*Martinsson et al.*, 2014]. The Ni-ice defect is illustrated in Figure 3.3. The ten samples in the upper right corner were identified as being significantly affected by ice clouds. Of these ten samples, four showed signs of losses, and four of secondary

deposition, both being typical bounce-off patterns of the solid Ni particles. Occasional tropopause crossing sometimes results in combined samples being taken from both the UT and LMS. However, in this 1-year study only one sample taken above the UT (i.e. >1.5 PVU) suffered from this Ni-ice defect.

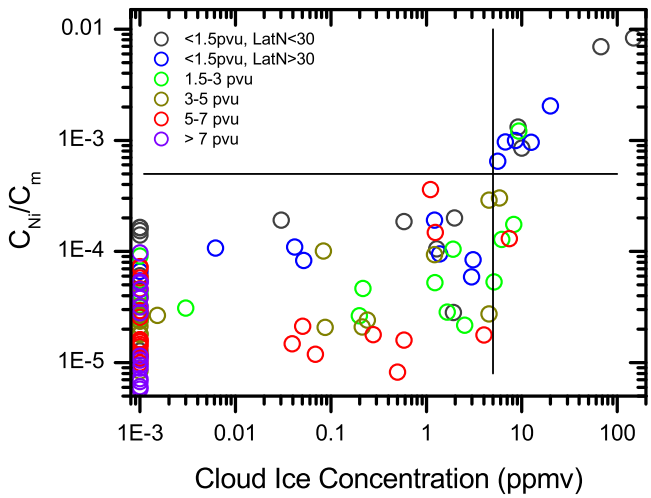

Figure 3.3.
Correlation of the ratio of Ni in the sample (C_{Ni}) to the total mass (C_m) obtained from IBA measurements, with the average cloud ice concentration during the sampling period for each sample. Note, in order to display zero cloud ice concentration on the logarithmic scale, 10^{-3} ppmv was added to each data point.

3.6. Comparison of impactor and OPC

Mass concentrations determined by applying the combined PIXE/PESA method to impactor samples were compared to particle size distributions obtained from the OPC, over the 1-year period mentioned above (April 2011-March 2012) (Paper III). Particle volume concentrations (C_v) were computed by integration of the size distributions (over the size interval 130-900 nm) and compared to mass concentrations (C_m) from the impactor samples (80-2000 nm size interval). Out of the 106 samples, 89 were within a C_v/C_m range of 0.55-1.55 $cm^3\ g^{-1}$ (Figure 3.4), showing good correlation over a size range of a factor of approximately 50, despite the fundamentally different measurement methods (optical vs. aerodynamic diameters).

Deviations were identified as being caused by a mismatch in the size range of the two measurement methods, deviation of particle refractive index from the calibration, or aerosol sampling defects. Sampling of crustal particles suffers from all these problems,

leading to elevated C_v/C_m. Low C_v/C_m were associated with large fractions of carbonaceous aerosol, probably of organic origin [*Friberg et al.*, 2014], with size distributions indicating large amounts of small particles, probably not fully resolved by the OPC.

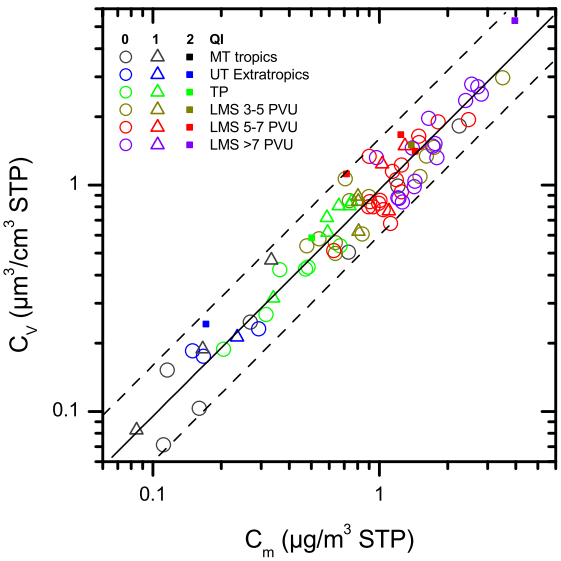

Figure 3.4.
Particle volume concentration obtained from the OPC as a function of mass concentration determined from aerosol samples collected at three PV levels in the stratosphere, the tropopause, the extra-tropical UT and the middle troposphere of the tropics. The colors of the symbols indicates the sampling location, and the shape the QI of the samples.

The apparent particle density for the samples shown in Figure 3.4 was estimated to be 1.08 g cm^{-3}. Excluding samples subject to defects increased the apparent density to 1.15 g cm^{-3}. This is a rather low value compared to typical densities of atmospheric particles. For example, particle densities for compounds containing the major constituent S are: 1.84 (sulfuric acid), 1.77 (ammonium sulfate), and 1.78 g cm^{-3} (ammonium bisulfate). The presence of organic compounds will probably decrease the particle density somewhat. Studies on submicron aerosol particles at an urban [*Hu et al.*, 2012] and remote [*Kannosto et al.*, 2008; *Saarikoski et al.*, 2005] locations have revealed particle densities of approximately 1.5 g cm^{-3}. The lower estimates obtained in this work are within the combined uncertainties of the OPC and aerosol sampler.

3.7. Satellite-based observations

3.7.1. MODIS: cirrus reflectance

A MODIS instrument is installed on each of the satellites Terra and Aqua, which were launched in December 1999 and May 2002, respectively. The cirrus reflectance (CR) obtained with this instrument was used in a comparison of aerosol data and cirrus cloud properties in the northern midlatitudes (30-60°N). NASA provides MODIS data in several formats, with different spatial and time resolutions. MODIS level 3 monthly averages, with a global coverage of 1×1° horizontal resolution were used in the present work.

MODIS uses 36 spectral bands in the wavelength range 0.415-14.235 µm [*King et al.*, 2003; *Platnick et al.*, 2003]. The band centered at 1.38 µm is used to determine CR, since the solar radiation measured at this wavelength is scattered by cirrus clouds or completely absorbed by the humid underlying atmosphere. The 1.38 µm signal is somewhat attenuated by water vapor located above the cirrus clouds. The attenuation is quantified from the slope of a scatter plot of the reflectance from the 1.38 µm and 0.66 µm channels, and a correction factor is computed. In too dry an atmosphere, part of the 1.38 µm radiation is reflected by underlying clouds or, in some cases, the Earth's surface. A lower limit of the atmospheric water vapor product from MODIS was used to exclude such pixels, minimizing the bias in the CR product. After recommendations from B. C. Gao (personal communication), and investigations of the atmospheric water vapor data, this limit was set to 0.4 cm water (i.e. the resulting column height if all atmospheric water was condensed). The method resulted in the exclusion of pixels mostly over the North American and Asian continents, as can be seen in Figure 3.5.

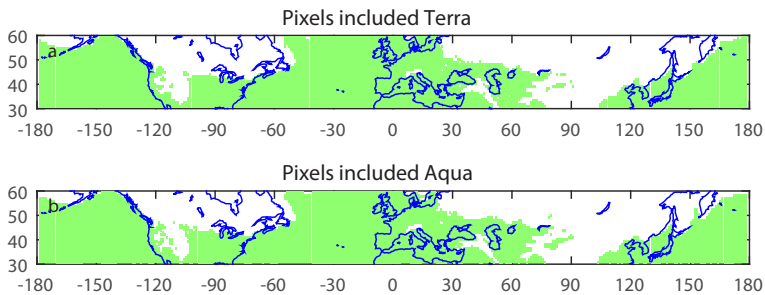

Figure 3.5.
The geographical areas included in the calculations of the cirrus reflectance, shaded in green, for the satellites Terra (a) and Aqua (b).

3.7.2. CALIOP: scattering ratios and aerosol optical depth

The influence of volcanic eruptions on the stratosphere was investigated using a combination of CARIBIC aerosol composition data and night-time aerosol light-scattering data obtained from the CALIOP instrument onboard the CALIPSO satellite. CALIPSO has provided data since June 2006.

CALIOP uses pulsed polarized laser beams with wavelengths of 1064 and 532 nm. The beam is directed towards the Earth's surface and is attenuated not only by scattering from aerosol particles and clouds, but also by air molecules. Vertical profiles of an aerosol can be generated using the ratio of the measured scattering to modeled scattering of the air molecules. The computation employs a modeled reference molecular scattering (air and O_3) from a particle-free part of the atmosphere. For the level 1 data from NASA Langley Research Center, an altitude band of 30-34 km is used, regarded to contain low aerosol concentrations. This approach was found to generate an underestimation of the scattering in the tropics by 6% [*Vernier et al.*, 2009], as the tropical aerosol extends to an altitude of 35 km. Therefore, the data used in the study presented in Paper IV were generated by recalibration of the scattering ratio using the 36-39 km altitude band. Furthermore, to obtain the clear-sky conditions, the influence of ice clouds was removed by applying a cloud mask excluding depolarization ratios greater than 5%. The cloud mask was expanded downwards to the lowest altitudes used (4 km) and upwards 360 m (2 pixels) to avoid bias from attenuated signals or misclassification of cloud tops. Finally, the aerosol optical depth (AOD) was computed [*Andersson et al.*, 2015] based on the aerosol scattering, using a conversion factor (which depends on particle size distribution [*Jäger and Deshler*, 2002]) of 50 [*Jäger and Deshler*, 2003], and integration over the stratospheric depth. Number size distributions obtained with the OPC following the eruptions of Grimsvötn and Nabro were similar to observations of stratospheric background [*Jäger and Deshler*, 2002], and values prior to these eruptions [*Andersson et al.*, 2015], confirming the validity of the procedure described above.

4. Results and Discussion

The LMS contains a mixture of tropospheric and stratospheric air. Since the aerosol concentrations in the UT are far lower than those in the stratosphere, the LMS aerosol concentrations depend to a large degree on those in the stratosphere. In periods of perturbed stratospheric aerosol load, subsidence of stratospheric air is expected to generate steeper S gradients in the LMS than during background conditions. Thus, stratospheric aerosol concentrations are to various degrees reflected in the LMS aerosol as the air passes through it during subsidence to the troposphere. Since CARIBIC started to provide data on the UT/LMS aerosol composition (1999), the stratospheric aerosol load has varied considerably. Investigating the causes and implications of these variations was a central part of the work presented in this thesis. In this chapter the composition, distribution and sources of the LMS and UT aerosol, as well as implications for the climate, will be discussed, based on the findings presented in Papers I, II, IV and V.

4.1. Composition of aerosol in the UT and LMS

4.1.1. The sulfurous aerosol

The concentration of the sulfurous component varies considerably with geographical location. Figure 4.1a illustrates the geographical distribution of particulate S concentrations at cruise altitudes (9-12 km), in the periods 1999-2002 and 2005-2013. A strong latitudinal gradient is evident, with higher concentrations being seen at northern midlatitudes than in the subtropics and tropics. Based on CARIBIC data from 1999-2002, *Martinsson et al.* [2005] found a gradient of S in the LMS, caused by downwelling of stratospheric aerosol. The PV can be used as a measure of the distance from the tropopause. Comparison of the S concentration with the PV distribution (Figure 4.1b) shows good agreement with their finding, indicating that the aerosol was of stratospheric origin.

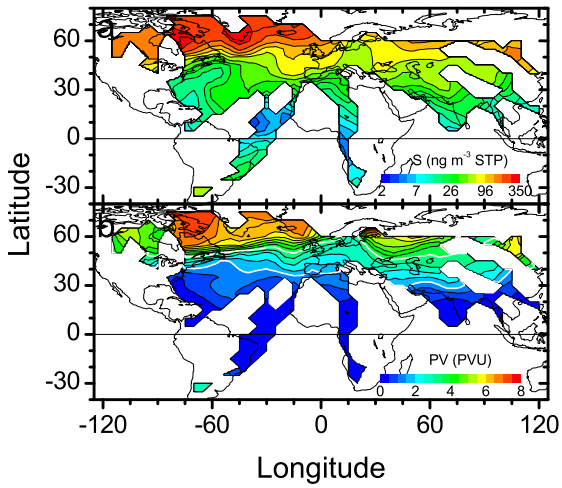

Figure 4.1.
Contour graphs illustrating the geographical distribution of (a) particulate S concentrations and (b) PV, based on all aerosol samples collected by CARIBIC in the period 1999-2013 (including samples taken in the extra-tropical UT and LMS, and in the tropical troposphere). The white lines in (b) indicate the PV isopleths of 1.5 and 3.5 PVU, the range in which the dynamical tropopause is normally defined.

During the 15 years from 1999 to 2013, the concentration of the sulfurous component varied by a factor of over 100. A large part of this variation was attributed to the S gradient in the LMS. Together with stratospheric O_3, the deep BD branch carries S formed from OCS that induces gradients of S and O_3 in the LMS through subsidence and mixing with tropospheric air. During background conditions, the S and O_3 therefore correlates in the LMS, and the S/O_3 ratio is rather stable. In order to compensate for the S gradient in the LMS, the S concentrations were divided by the O_3 mixing ratios. Thus, perturbations in the LMS aerosol concentrations are easily identified as positive deviations of the S/O_3 from that during background conditions (Figure 4.2).

The period 1999-2002, known to be volcanically quiescent, shows the lowest S/O_3 ratio. Due to the low volcanic influence during this period, it was used to represent the 'background concentrations' of S in the LMS and also of that in the UT. Figure 4.2 illustrates the temporal trend of the S/O_3 ratio normalized to the average for the period 1999-2002, revealing the deviations of S/O_3 from the background levels. In the years following 2002, most of the data are found above the average for that period, indicating perturbation of the LMS aerosol.

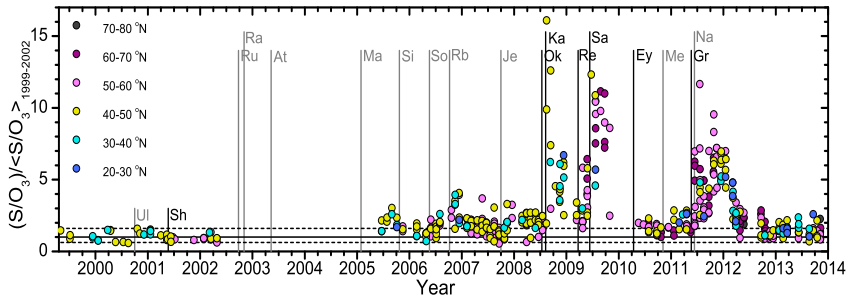

Figure 4.2.
Identification of volcanic aerosol components in the LMS in the NH showing values of the S/O_3 ratio (ng m^{-3} STP $ppbv^{-1}$) normalized to the average S/O_3 ratio during the period 1999-2002 (a period of low volcanic activity). The larger tick marks indicate January 1 in each year. The measurements were made at altitudes of 9-12 km, and the color indicates the latitude band of aerosol sampling. The full line indicates the geometric average and the dashed lines the minimum and maximum S/O_3 ratio during the period 1999-2002, normalized to the geometric average for that period. The starting dates of tropical (gray) and NH extra-tropical (black) eruptions that affected the stratosphere of the NH are denoted by vertical lines. The eruptions are: Ul (Ulawun), Sh (Sheveluch), Ru (Ruang), Ra (Reventador), At (Anatahan), Ma (Manam), Si (Sierra Negra), So (Soufrière Hills), Rb (Rabaul), Je (Jebel at Tair), Ok (Okmok), Ka (Kasatochi), Re (Redoubt), Sa (Sarychev), Ey (Eyjafjallajökull), Me (Merapi), Gr (Grimsvötn) and Na (Nabro). (See Table 4.1 for details of the eruptions.)

The largest peaks in the S/O_3 ratio are clearly related to volcanic eruptions penetrating the tropopause (vertical lines in Figure 4.2, from Table 4.1). These deviations were mainly caused by the addition of volcanic aerosol, either injected into the LMS by extra-tropical eruptions, or by subsidence of aerosol transported from the tropical stratosphere.

The Kasatochi eruption in August 2008 injected 1.7 Tg SO_2 into the NH extra-tropical stratosphere, increasing the S/O_3 ratio by up to 10 times. In the following year, two strong eruptions (Redoubt in March, and Sarychev in June) occurred, which prolonged the period of significant volcanic perturbations, until reaching close to background conditions at the end of 2010. In May 2011, the extra-tropical volcano Grimsvötn erupted causing a short, intense peak in the S/O_3 ratio, and in June the same year the tropical volcano Nabro erupted. In contrast to the extra-tropical eruptions, SO_2 from Nabro was injected into the tropical stratosphere. Subsequent transport and oxidation brought high concentrations of S in the shallow BD branches to the northern midlatitudes [*Bourassa et al.*, 2012], increasing the S/O_3 ratio by a factor of 5 to 10.

Table 4.1.
Volcanic eruptions in the 21st century that affected (or had the potential to affect) the stratospheric aerosol load [from *Andersson et al.*, 2015].

Volcano	Eruption date	Long. (°E)	Lat. (°N)	SO_2
Ulawun	Sep. 29, 2000	151	-5	
Sheveluch	May 22, 2001	161	57	
Ruang	Sep. 25, 2002	125	2	0.03[a]
Reventador	Nov. 3, 2002	-78	0	0.07[a]
Anatahan	May 10, 2003	146	16	0.03[a]
Manam	Jan. 27, 2005	145	-4	0.09[a]
Sierra Negra	Oct. 22, 2005	-91	-1	
Soufrière Hills	May 20, 2006	-62	17	0.2[b]
Rabaul	Oct. 7, 2006	152	-4	0.2[a]
Jebel at Tair	Sep. 30, 2007	42	16	0.08[c]
Chaitén	May 2, 2008	-73	-43	0.01[d]
Okmok	Jul. 12, 2008	-168	53	0.1[c]
Kasatochi	Aug. 7, 2008	-176	52	1.7[c]
Redoubt	Mar. 23, 2009	-153	60	0.01[e]
Sarychev	Jun. 12, 2009	153	48	1.2[f]
Eyjafjallajökull	Apr. 14, 2010	-20	64	
Merapi	Nov. 5, 2010	110	-8	0.4[g]
Grimsvötn	May 21, 2011	-17	64	0.4[h]
Puyehue-Cordón Caulle	Jun. 6, 2011	-72	-41	0.3[h]
Nabro	Jun. 12, 2011	42	13	1.5[h]

[a] *Prata and Bernardo* [2007] , [b] *Carn and Prata* [2010], [c] *Thomas et al.* [2011],[d] *Prata et al.* [2008], [e] *Lopez et al.* [2013], [f] *Haywood et al.* [2010],[g] *Surono et al.* [2012], and [h] *Clarisse et al.* [2012].

The S/O_3 ratio is higher than the background level during the period May 2005-August 2008, and for most of the time between the strong peaks. These high values have been attributed to subsidence of volcanic aerosol transported from the tropics [*Friberg et al.*, 2014]. The eruptions of Manam (January 2005), Soufrière Hills (May 2006) and Rabaul (October 2006) perturbed the aerosol load of the stratosphere for several years [*Vanhellemont et al.*, 2010; *Vernier et al.*, 2011], while the transport of the Nabro aerosol in the deep BD branch increased the S/O_3 ratio slightly in 2013. In addition to the eruptions discussed here, a number of additional volcanic eruptions occurred (see Table 4.1) that could have made minor contributions to the variation in the S/O_3 ratio in the NH LMS presented in Figure 4.2. Volcanic perturbations in the stratosphere and UT are discussed further below.

4.1.2. The carbonaceous aerosol

Besides the sulfurous component, large amounts of carbonaceous aerosol are found in the CARIBIC samples. *Schwarz et al.* [2010] reported black carbon concentrations of

0.1-4 ng m^{-3} in the LMS, which is about one to two orders of magnitude lower than particulate C in the CARIBIC samples. In other studies [*Murphy et al.*, 1998; *Schmale et al.*, 2010] it has been found that a fraction of the UT/LMS aerosol is organic, suggesting that organic C accounts for the discrepancy. Although IBA allows detailed elemental analysis, the chemical composition cannot be determined directly. However, organic aerosol contains more oxygen than soot. Hence, the oxygen content in the carbonaceous fraction provides information on the nature of the C in the UT/LMS. In Paper II, the average O/C ratio was computed, using stoichiometric relations. The method was based on a scatter plot of the O/S ratio vs. the C/S ratio (Figure 4.3). Most of the data scatter at O/S values >4 (the dotted line in the figure, representing sulfate), indicating that the carbonaceous aerosol is organic. Linear regression revealed the O/C ratio to be ~0.2.

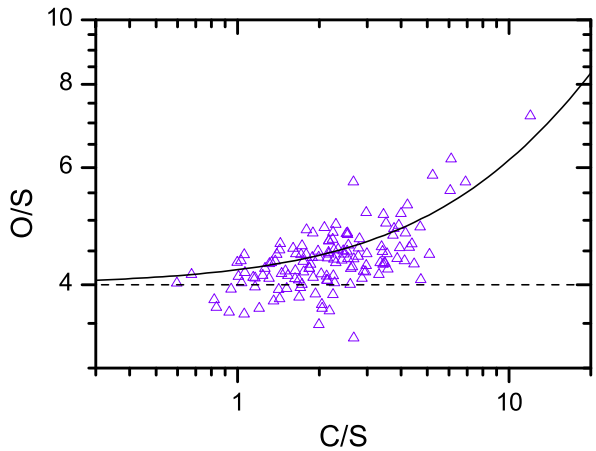

Figure 4.3.
O/S vs. C/S molar ratios. The dashed line represents O/S = 4 (the ratio in sulfate), and the curve shows the best fit to the data, i.e. O/S = 4 + 0.2 C/S. The O contribution from crustal elements was subtracted based on the average crust composition [*Rudnick and Fountain*, 1995] and the Fe concentrations obtained using PIXE. (See Paper II for further details.)

4.1.3. Composition and evolution of volcanic aerosol

The composition and evolution of volcanic aerosol were investigated based on aerosol composition measurements and satellite observations of aerosol from the eruptions of Kasatochi (August 2008), Sarychev (June 2009) and Eyjafjallajökull (April 2010) (Paper I). The eruption of Eyjafjallajökull emitted large amounts of ash, mainly to the free troposphere and the UT. Some ash components, such as silicates, can damage aircraft jet engines, and large regions of European airspace were closed to regular passenger flights during April 15-21 as a safety measure. However, dedicated CARIBIC flights were made over northern Europe, at altitudes of 4-12 km, to obtain

measurements in fresh volcanic clouds. The Eyjafjallajökull aerosol was found to be dominated by sulfate and ash, in contrast to aerosol from Kasatochi and Sarychev, which consisted mainly of SO_4 and C (Figure 4.4).

Several authors have reported large amounts of carbonaceous matter in volcanic aerosols [*Carn et al.*, 2011; *Martinsson et al.*, 2009; *Schmale et al.*, 2010]. Explosive volcanoes, such as those studied in Paper I, generally do not emit CO_3. Low values of the O/C ratio also indicated that there were other sources of the sampled particulate C. Furthermore, low amounts of K in the carbonaceous fraction indicated that biomass burning could not explain the volcanically associated C. The source of the C was instead suggested to be entrainment of air from low tropospheric altitudes containing particulate C and organic trace gases (that could form particulate matter)[*Andersson et al.*, 2013]. In the boundary layer, organic concentrations range from hundreds to tens of thousands of ng m^{-3}, i.e. up to several orders of magnitude higher than in the tropopause-region. Entrained organic trace gases could have formed additional particulate C.

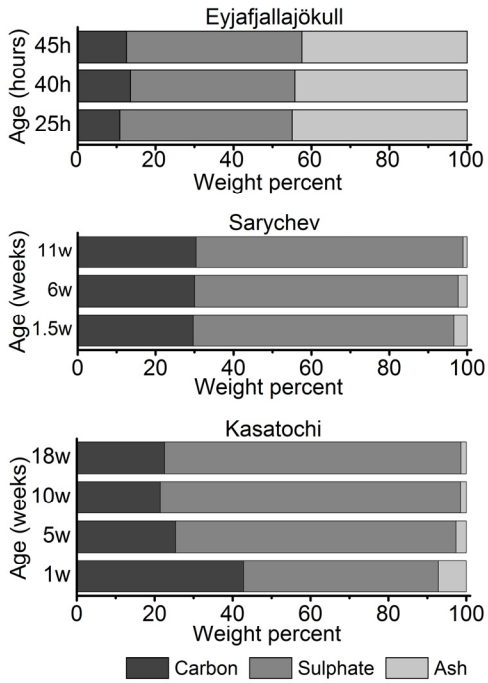

Figure 4.4.
Major components of aerosol samples collected following eruptions of Eyjafjallajökull, Sarychev and Kasatochi. Aerosol collected 1.5, 6 and 11 weeks after the eruption of Sarychev are shown as averages of 3, 6 and 2 samples, respectively. The composition of aerosol samples collected 18 weeks after the Kasatochi eruption is an average of 3 samples. The remaining aerosol compositions are each represented by one sample only. The carbonaceous fraction is averaged over all samples of the aerosol from Sarychev. (See Paper I for further details.)

Following extra-tropical eruptions, SO_2 in the LMS is oxidized to SO_4. Thus, after the Kasatochi, Sarychev and Eyjafjallajökull eruptions, the sulfurous mass increased, resulting in increasing aerosol load in the LMS, and decreasing ash/sulfate ratios (Fe was used as a proxy for ash, Figure 4.4). Estimates indicated that differences in particle sizes of SO_4 and ash (potentially causing differences in coagulation and deposition rates), had negligible influence on composition [*Andersson et al.*, 2013]. Hence, the change in composition was driven by the conversion of SO_2. Based on the declining Fe/S ratio (Figure 4.5), the conversion rate was estimated to be 45±22 days, which is within the broad range (9 to 62 days) of previous estimates of SO_2 emitted by Kasatochi [*Jurkat et al.*, 2010; *Karagulian et al.*, 2010; *Krotkov et al.*, 2010].

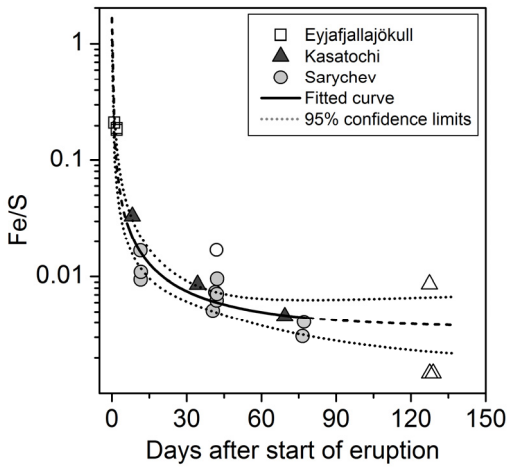

Figure 4.5.
Mass ratio of Fe to S in aerosol samples influenced by three volcanoes (indicated by different symbols) vs. time since the start of the eruptions. The solid line shows a fit to the Fe/S ratio for the samples influenced by the Sarychev and Kasatochi eruptions. Samples denoted by open symbols were excluded from the fit.

4.1.4. Cross-tropopause transport of volcanic aerosol

CALIPSO lidar images show that the Kasatochi eruption in August 2008 injected SO_2 and ash into the stratosphere, forming two layers (Figure 4.6), the lower located in the LMS, and the upper at altitudes above 15 km. While the lower cloud was confined to latitudes higher than 45°N, the upper cloud also spread to the equator. Subsequent oxidation of SO_2 produced increasing aerosol load. Thereafter, the aerosol load in the LMS decreased by cross-tropopause transport.

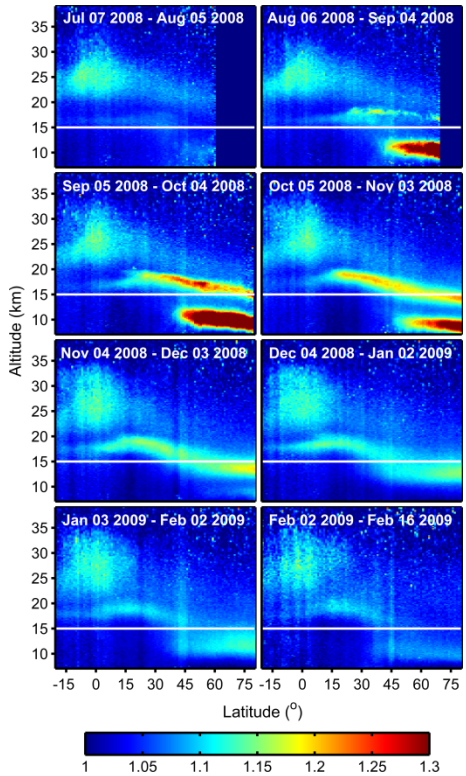

Figure 4.6.
Distributions of the Kasatochi volcanic aerosol with latitude and altitude based on CALIPSO lidar measurements. Results are monthly and zonally averaged scattering ratios ((measured total scattering)/(modeled air molecular scattering)) from July 2008 to February 2009. (For Feb. 2009, only 2 weeks of data were available.) The feature in the tropics at an altitude of 25 km, which is enhanced in the scattering ratio due to the weak scattering from air molecules at high altitudes, is already present before the eruption of Kasatochi, and is probably related to tropical upwelling and particle formation. High-latitude data are missing in the two upper panels due to the limited latitudinal extent of the CALIPSO night-time data during the summer season. The white line indicates an altitude of 15 km.

Figure 4.6 indeed illustrates the impact of Kasatochi's eruption on the stratospheric aerosol concentrations, but it also provides the possibility to study transport patterns and transport times. Figure 4.7 provides further insight into the removal rate of aerosol in the tropopause-region, in this case during fall. The lower layer obviously affected the LMS for a period of ~2.5 months, which is also observed in the temporal trend of S/O_3 (Figure 4.2). Concurrent downwelling of the upper cloud, resulted in a second peak in the aerosol load and the S/O_3 ratio in the LMS (December in Figure 4.2), which extended the volcanic influence of the Kasatochi eruption throughout the winter.

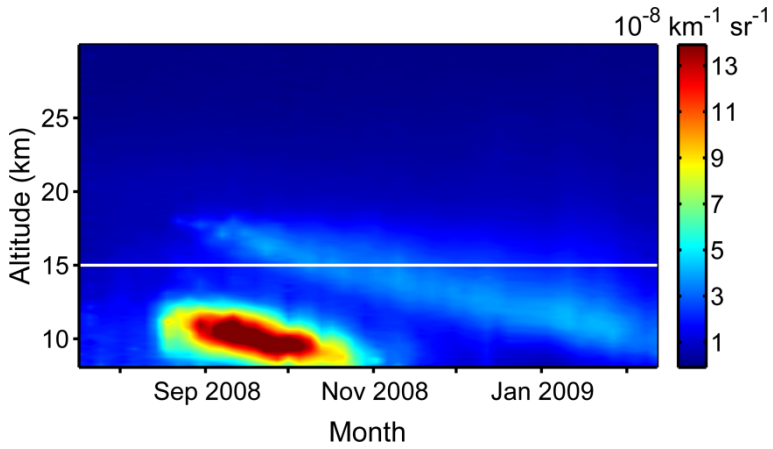

Figure 4.7.
Downward transport of the Kasatochi volcanic aerosol, showing the temporal evolution of aerosol scattering as a function of altitude, from July 2008 to February 2009, spatially averaged over 40°N-80°N. Tick marks indicate the first day of the month. Results are shown as total backscatter from CALIPSO data minus molecular backscatter. The white line indicates an altitude of 15 km.

4.2. Volcanic aerosol forcing in the LMS

In the previous section, it was shown that the Kasatochi eruption mostly affected the LMS (Figures 4.6 and 4.7). However, the IPCC estimate of RF due to volcanism (-0.15 to -0.08 Wm^{-2}) does not include altitudes below the 380 K isentrope, i.e. the upper cloud was only partly included, while the lower one was completely excluded. Similarly, the influence of volcanic aerosol injected by tropical volcanism is underestimated by the IPCC method, since transport through the LMS is excluded. In a recent study, the aerosol at stratospheric altitudes below15 km (basically the LMS), was estimated to constitute ~30-70% of the total stratospheric AOD [*Ridley et al.*, 2014].

In the present work (Paper IV), the LMS contribution to the total volcanic forcing was estimated based on lidar data from CALIPSO. Figure 4.8a illustrates the global AOD during the period 2008 to mid-2012, in the altitude ranges 15-35 km (thin lines) and tropopause-35 km (heavy lines). It is evident that the LMS constituted a large fraction of the stratospheric AOD during that period (Figure 4.8b). Furthermore, large variations in AOD, coupled to volcanic eruptions, were observed in the NH. After the northern midlatitude eruptions of Kasatochi and Sarychev, and the tropical Nabro eruption, the fraction of the stratospheric AOD in the NH LMS peaked at approximately 60%, 50%, and 45%, respectively. The corresponding aerosol forcing below 15 km (Figure 4.8d) was 56% (Kasatochi), 44% (Sarychev), and 23% (Nabro). In contrast, periods of low volcanic impact such as the year 2010,

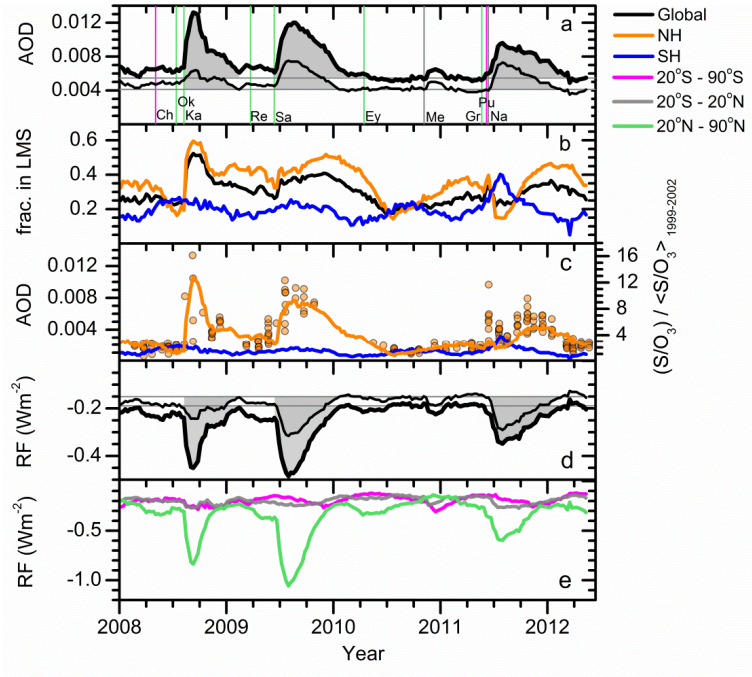

Figure 4.8.
Volcanic influence on global and regional aerosol radiative parameters. (a) Global AOD at 532 nm calculated using integrated CALIPSO aerosol scattering from 15 to 35 km altitude (thin line), and from the tropopause to 35 km (heavy line). Major tick marks indicate January 1. The dates of volcanic eruptions are indicated by vertical lines, color-coded according to latitude. The eruptions are: Ch (Chaitén), Ok (Okmok), Ka (Kasatochi), Re (Redoubt), Sa (Sarychev), Ey (Eyjafjallajökull), Me (Merapi), Gr (Grimsvötn), Pu (Puyehue-Cordón Caulle) and Na (Nabro) (see Table 4.1 for details). The horizontal gray lines indicate the estimated background AOD during the period 2008 to mid-2012, and the shading indicates the total integrated volcanic AOD from the Kasatochi, Sarychev and Nabro eruptions. (b) The fraction of total AOD from the LMS. (c) AOD in the LMS from CALIPSO data (lines) and S/O_3 in the NH from CARIBIC data (circles). (d) As in (a), but net RF calculated from the AOD shown in (a). (e) Stratospheric net RF in three regions equal in surface area.

indicate that the LMS constitute ~20% of the stratospheric AOD during background conditions. These eruptions affected the radiation budget mostly in the NH, where the total stratospheric aerosol forcing varied between ~-0.2 and -1 Wm^{-2} (Figure 4.8e). Including the LMS (altitudes below 15 km) increased the global stratospheric RF (AOD) by more than 30% (45%). This is in the lower part of the range presented by *Ridley et al.* [2014] (30-70%), who computed the RF based on sun photometer data from the AERONET network. However, the AERONET AOD is not vertically resolved. Instead, their stratospheric AOD estimate is based on modeling of the vertical distribution of the aerosol in the troposphere. Also, the time resolution is limited, i.e. the impact of the AOD of individual volcanic eruptions is not clearly resolved. Thus, the CALIOP data are expected to provide a more realistic estimate of

the stratospheric AOD due to their vertical resolution and superior time resolution [*Andersson et al.*, 2015]. Nevertheless, the LMS constitutes a large fraction of the total volcanically induced direct RF that was excluded in previous estimates of volcanically associated RF.

In conclusion, the CALIOP and CARIBIC data mostly showed good agreement (Figure 4.8c). However, one exception is the peak in CARIBIC aerosol data after the Grimsvötn eruption. CALIOP night-time data are not available for the higher latitudes during the summer (see uppermost left panel in Figure 4.6). Most of the aerosol samples were taken at latitudes above 55°N in June, i.e. the CARIBIC samples were taken outside the reach of CALIOP. Also, the CARIBIC data were collected from relatively fresh aerosol during patchy conditions, while the averaging of the CALIOP data suppressed the signal of the Grimsvötn aerosol. Therefore, patchiness in aerosol concentrations was taken into account in later analyses (Sections 4.4 and 4.5) by allowing ample time (30 days) for dilution of the volcanic aerosol with the LMS background. After dealing with the large perturbations in the LMS, the smaller ones will be discussed in the following sections.

4.3. Tropical volcanic impact on the LMS

The tendency of increased particulate S concentrations in the LMS (S_{LMS}) in the period May 2005-July 2008, as shown in Figure 4.2, was investigated (Paper II). Subsidence of air from the overlying stratosphere induces O_3 and S gradients in the LMS by mixing with air from the troposphere. The concentrations of O_3 and particulate S in the LMS vary with season, as a result of their long lifetimes and seasonally dependent transport. The mass fluxes of both stratospheric and tropospheric air into and out of the LMS vary with season, as does the strength of the subsidence via the deep BD branch carrying O_3. In a first attempt to illustrate the increase above background levels, differences in the S concentrations between the periods 2005-2008 (denoted 05-08) and 1999-2002 (denoted 99-02) were investigated using scatter plots of S vs. O_3 (Figure 4.9) for each season separately. The S gradients were indeed steeper in the later period. To highlight the difference between the 99-02 and 05-08 data, a linear fit of the 99-02 data, was employed based on all seasons (to increase the statistical significance). More than 90% of the 05-08 data are found above the fit to the 99-02 data. The 05-08 S gradient is strongest in winter, after which it decreases in strength, in spring and summer, to almost vanish in the fall. Together with the low O_3 levels, this shows that the influence of the stratosphere is weaker in fall than in the other seasons. Hence, in fall, a larger fraction of the LMS air originates from the troposphere.

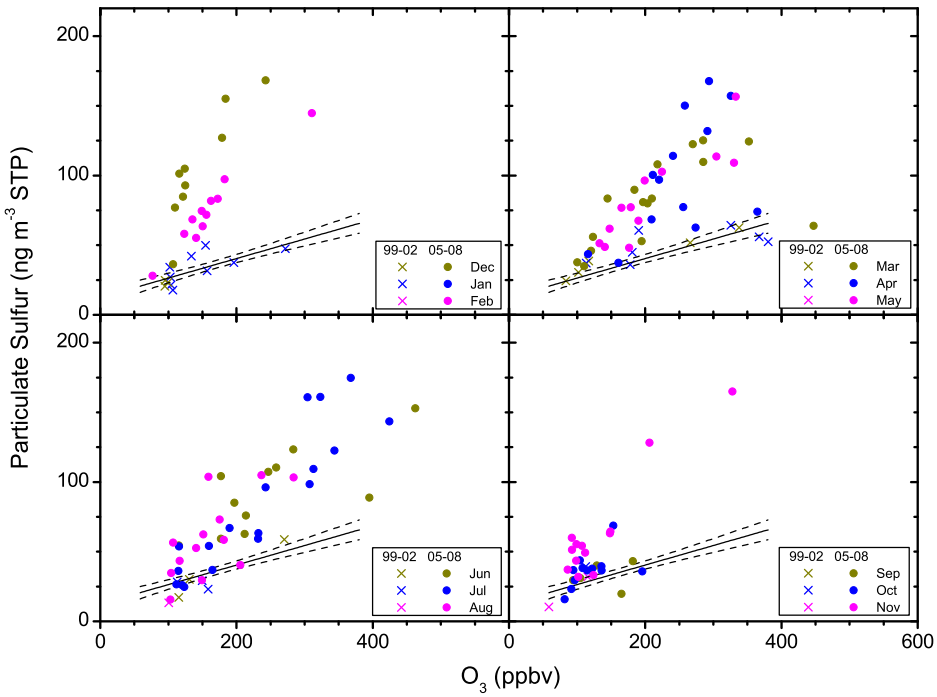

Figure 4.9.
Concentration of particulate S vs. O_3 for LMS samples (PV >2 PVU) collected in the NH. Upper left: Winter (December, January, February). Upper right: Spring (March, April, May). Lower left: Summer (June, July, August). Lower right: Fall (September, October, November). Linear regression (full line), with 95% confidence intervals (dashed lines) based on the background concentrations was applied to the 1999-2002 data to facilitate the comparison of the data from the two periods.

4.3.1. Temporal trends of particulate matter and O_3

The relation between S and O_3 was further investigated using temporal trends of the ratios of S and O_3 to PV, as illustrated in Figure 4.10. C was also included in the analysis, providing additional information on the aerosol. An advantage of this method is the possibility to compare seasonal variations between the trace gas and particulate components. A sinus function was fitted to the O_3/PV ratio, showing an annually repeating trend, with a maximum in May, for both the 99-02 and 05-08 data. The ratio of the maximum and minimum values is 1.9. In comparison, the concentration at the 380 K isentrope shows a maximum (minimum) in March (September), and a seasonal variation of a factor of ~2 [*Fortuin and Kelder*, 1998; *Martinsson et al.*, 2005]. Hence, the seasonality in O_3 concentrations at the tropopause is similar to that at the upper boarder of the LMS, with a phase shift of

two months, illustrating that subsidence of stratospheric air is the main driver in the LMS seasonal O_3 cycle.

Similarly, the S concentrations observed in the LMS depend on the S concentrations in the downwelling air (i.e., above the 380 K isentrope). While SO_4 is formed via photo-oxidation of OCS in the deep BD branch, it can also be formed from SO_2 at lower altitudes, i.e. particulate S produced from SO_2 can be carried in the shallow BD branches. In order to differentiate between the influence of the deep and shallow branches, and to resolve any dissimilarities between the 99-02 and 05-08 data, separate sine functions were fitted to the data for the two periods, using the same relative amplitude and phase as for the O_3/PV fit (in Figure 4.10a). In the period 99-02, the S/PV ratio shows good agreement with the O_3/PV ratio, confirming that during background conditions S is carried by the deep BD branch. In contrast, large deviations from the fit were observed for some of the 05-08 data, indicating that additional S formation occurred in the shallow branches.

The same method was applied to the C data for the period 05-08 (Figure 4.10c). The C/PV ratios showed poor agreement with the fit to the O_3/PV ratio, indicating that photo-oxidation deep in the stratosphere is less important, in relative terms, for the formation of C than for S. (Unfortunately, no C data are available for the period 99-02.)

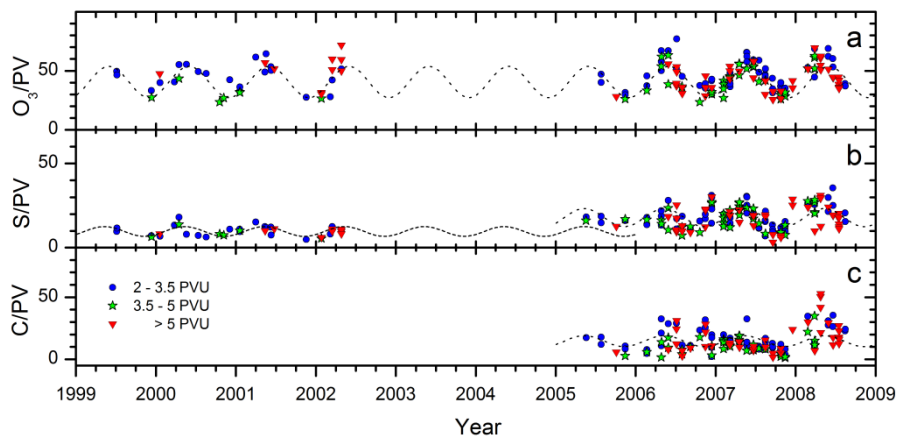

Figure 4.10.
Temporal trends of ratios of C, S and O_3 to PV. (a) O_3/PV (ppbv PVU^{-1}), (b) S/PV (ng m^{-3} STP PVU^{-1}) and (c) C/PV (ng m^{-3} STP PVU^{-1}). Sine functions, based on the O_3/PV ratio in (a) are shown in (b) and (c) to highlight any deviations from transport in the deep BD branch.

4.3.2. Influence of the shallow BD branches

The importance of the shallow BD branches was further investigated in a comparison of the seasonal variation of the S/O_3 ratio for the two periods (99-02 and 05-08) (Figure 4.11). While there is a weak seasonal variation in the period 99-02, a large increase can be seen at the end of the year in the period 05-08, which cannot be caused by subsidence via the deep BD branch. It can be seen from the temporal trend of the S/O_3 ratio in Figure 4.12a that these high values occur at the end of 2006 and 2007. Thus, the source of S causing (i) higher S/O_3 ratios in 05-08 than in 99-02, and (ii) the deviations in the S/O_3 ratio during the period 05-08, affects the aerosol load rather sporadically. This sporadic behavior is also evident in the temporal trend of the S/PV ratio presented in Figure 4.10b.

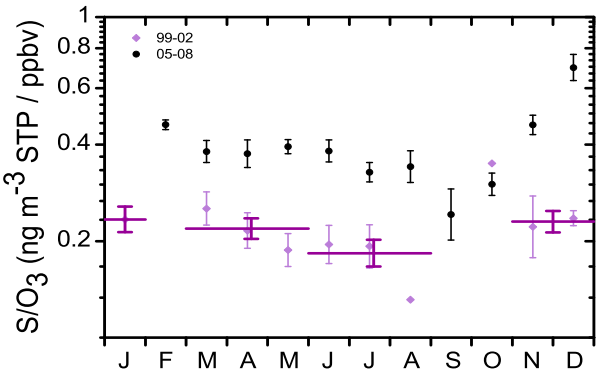

Figure 4.11.
Ratios of particulate S to O_3 (units: ng m^{-3} STP $ppbv^{-1}$) for the periods 1999-2002 and 2005-2008, expressed as monthly geometric averages (black and pale purple symbols). The horizontal dark purple lines denote averages in the period 1999-2002 for the months of January, March-May, June-August and November-December. Error bars represent standard errors.

4.3.3. Identification of tropical volcanic aerosol in midlatitudes

In the period 2005-2008, the stratospheric aerosol load increased due to injection of S into the tropical stratosphere by one eruption in 2005 (Manam), and two in 2006 (Soufrière Hills and Rabaul) [*Vanhellemont et al.*, 2010; *Vernier et al.*, 2011]. Rapid transport and transformation of SO_2 in the shallow BD branches probably caused the rapid increase at the end of 2006. Satellite-based observations show that the aerosol was ascending in the tropics in the fall of 2006 and winter of 2007, at a rate of ~0.6 km per month [*Vernier et al.*, 2009]. Thus, in 2007, the volcanic aerosol was located at higher altitudes than during 2006, resulting in a later increase in S at the end of that year.

Part of the volcanic aerosol was transported to high altitudes within the deep BD branch, prolonging the influence of volcanism on the stratospheric aerosol load. Satellite observations showed the Junge layer to be heavily perturbed in 2007, both in the tropics and the midlatitudes [*Vanhellemont et al.*, 2010]. Subsequent subsidence increased the S_{LMS} during 2008, causing higher S/O_3 ratios during 2008 than in preceding years (Figure 4.12a). A comparison of the S_{LMS} during the season of large subsidence in the stratosphere (February-August) revealed a trend of increasing S_{LMS}, with approximately a doubling compared to the background conditions.

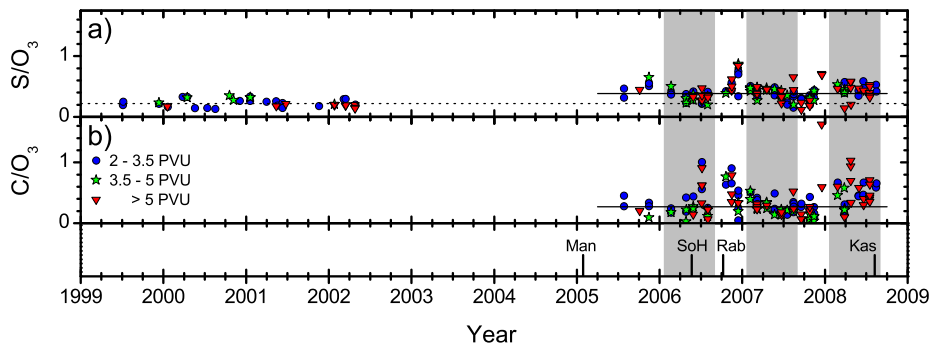

Figure 4.12.
Ratios of S (a) and C (b) to O_3 (units: ng m^{-3} STP $ppbv^{-1}$) for NH LMS samples. Full and dashed horizontal lines represent geometric averages for the periods 2005-2008 and 1999-2002, respectively. The period February-August is shaded gray. Vertical lines indicate the volcanic eruptions of Manam (Man), Soufrière Hills (SoH), Rabaul (Rab) and Kasatochi (Kas).

The C/O_3 ratio shows a similar pattern as the S/O_3 ratio, e.g. the peaks at the end of 2006 and 2007, and the higher values in 2008, indicating that the concentration of C in the LMS was also influenced by volcanism. Entrainment within volcanic jets and plumes, bringing low tropospheric air containing C and organic trace gases into the stratosphere, was proposed as the cause of these observations [*Andersson et al.*, 2013]. The resulting increases from 2006 to 2008 were 23% and 70% for S/O_3 and C/O_3, respectively.

The stronger inter-annual trend of C/O_3 than S/O_3 indicates that C is less abundant in the stratospheric background than S. While the S/O_3 ratio increases gradually, a large step is observed in the C/O_3 ratio from 2007 to 2008. Investigating the C/S ratio revealed a significant difference between these years. The eruption of Soufrière Hills reached a higher altitude (>20 km) than the eruption of Rabaul (<18 km, just above the tropical tropopause). Therefore, the Rabaul aerosol was mostly transported in the shallow branches, influencing the LMS mainly at the end of 2006 and during the beginning of 2007. In contrast, the Soufrière Hills aerosol chiefly impacted the LMS in 2008, indicating that the Soufrière Hills eruption transported aerosol with a higher C/S ratio than the Rabaul eruption did. Interestingly, the concentrations of

organics in the aerosol have been reported to be higher in the vicinity of Soufrière Hills than around Rabaul [*Spracklen et al.*, 2008; *Stramska*, 2009].

In summary, volcanic aerosol that was injected into the tropical stratosphere, transported to midlatitudes and subsequently downwelling to the LMS, doubled the S load compared with background conditions. Once transported across the tropopause, this volcanically induced doubling could potentially affect aerosol concentrations in the UT.

4.4. S in the UT coupled to subsidence

The Nabro eruption injected about an order of magnitude more SO_2 into the stratosphere than any of the tropical eruptions in the previous decade. In the evaluation of the influence of stratosphere-troposphere transport on the S concentrations in the UT (S_{UT}), periods of data with similar concentration levels were combined, to avoid interfering with the high S concentrations resulting from the eruption of Nabro (for details see Paper V). The analysis included three periods: one with background levels (1999-2002), one intermediately influenced by volcanism (2005 to July 2008 and 2013; denoted the period 05-08/13), and a period strongly influenced by volcanism (most of the period from August 2008 to 2012).

4.4.1. Volcanic influence on northern midlatitude S_{UT}

Figure 4.13 shows a considerable difference between the S_{UT} in the two periods 05-08/13 and 99-02. In the period 99-02, a latitudinal correlation is observed with, on average, higher values of S_{UT} in northern midlatitudes than in the subtropics and tropics. A similar, but stronger, trend was observed in the period 05-08/13. A direct comparison of these periods (Figure 4.13c) reveals that the difference between them is greatest at the midlatitudes. At 45°N, the value of S_{UT} approximately doubled from the earlier to the later period, indicating volcanic perturbation of the UT aerosol concentrations. Interestingly however, no significant difference was observed south of 30°N.

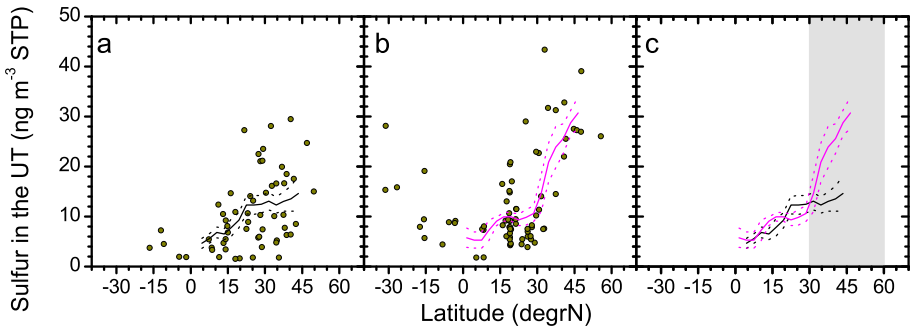

Figure 4.13.
The latitudinal variation of particulate S in the UT during (a) March-July 99-02 and (b) March-July 05-08/13. (c) Direct comparison of the averaged profiles shown as lines in (a) and (b). The dashed lines indicate the 95% confidence intervals. The gray shaded area in (c) indicates the northern midlatitudes, which is the latitude band of interest in Figures (4.14-4.16).

4.4.2. Coupling of the S_{UT} to the LMS and volcanism

A scatter plot of the S_{UT}, and the ratio of S_{LMS} to PV (S/PV_{LMS}), further illustrates the coupling of the aerosol concentrations (Figure 4.14). Division by PV was employed in this case as a means of normalizing to the strong S gradient through the LMS. To highlight the connection, data from the season with large influence from the stratosphere (spring/summer), for the period with background levels (99-02) and the period intermediately affected by tropical volcanism (05-08/13), were used (dark yellow diamonds). To improve the statistics in this analysis, years with similar S/PV_{LMS} values were combined to form averages.

Data from the fall during the period of strong volcanic influence were used for comparison. Linear regression was applied to the two data sets, resulting in values of R^2 of 0.73 and 0.95, with significance levels of 85% and >99%, for the spring/summer and fall data, respectively.

The steeper slope in spring/summer is the result of greater stratosphere-troposphere transport than in the fall. The influence of the stratosphere on the S_{UT} in the season of greatest subsidence (spring/summer) appears to be 4 times stronger than in the fall.

Eventually, the LMS aerosol was transported across the tropopause to the UT, which differs vastly in composition compared to the overlying stratosphere. Until recently, neither the LMS aerosol forcing [*Andersson et al.*, 2015] nor the S_{UT} forcing [*Friberg et al.*, 2015] were included in discussions or estimates of the climatic response to volcanism.

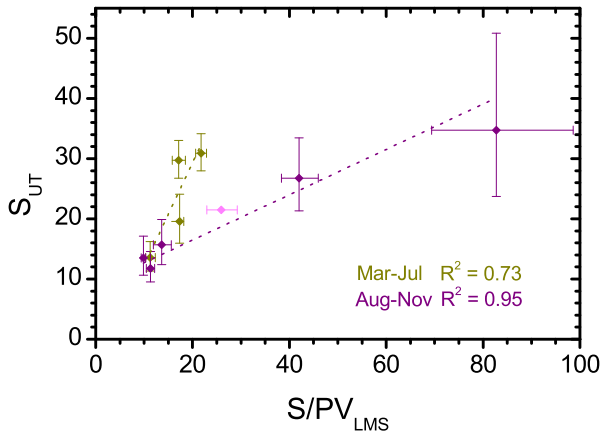

Figure 4.14.
Comparison of the geometric averages of the S_{UT} (ng m^{-3} STP) with the S/PV_{LMS} (ng m^{-3} STP PVU^{-1}), for the spring/summer data (March-July, dark yellow diamonds) and fall data (August-November, magenta diamonds), for samples taken at PVs below 5 PVU. The dashed lines represent the linear regressions for the respective season. The error bars represent the geometric standard errors. The data averaged for the spring/summer season are (in order of their S/PV_{LMS} values): 2000-2002, 2010/2013, 2005/2006, and 2007/2008, and for the fall season: 2007, 2010/2012, 2006, 2011 (Nabro), and 2009 (Sarychev). The data for 2008 (Kasatochi) (light magenta symbols) were excluded from the regression due to poor statistics.

4.5. Subsidence of volcanic SO_4 could influence cirrus

Unlike the LMS and the overlying stratosphere, the UT contains large amounts of water. Both the UT aerosol particles and water are involved in the formation of cirrus cloud ice crystals. It is therefore logical to investigate whether the volcanically influenced increase in S_{UT} could affect the radiative properties of cirrus clouds.

4.5.1. Coupling of S_{UT} to midlatitude cirrus clouds

The possible influence of the increase in S_{UT} on cirrus clouds was investigated using CR data obtained by MODIS, from northern midlatitudes (Figure 4.15). The effect was expected to be most prominent during the season of large subsidence from the stratosphere, i.e. the March-July data. However, there were too few S_{UT} data for such a comparison. Therefore, S_{LMS} data (taken at average PV values <5 PVU) were used as a proxy for S_{UT}. The CR data from the two satellites (Terra and Aqua) showed similar temporal trends (with ~20% higher CR from Aqua, as explained in Section 3.7.1), and an anti-correlation was observed between S_{UT} and CR (note the reversed scale of

S/PV_{LMS} in Figure 4.15a). Direct comparison of the CR from Terra to the S/PV_{LMS} ratio resulted in a rather good anti-correlation (R^2 = 0.63) and high significance level (99%). In the period 2001-2011, the CR decreased by 8%, while S/PV_{LMS} increased by a factor of 3-4.

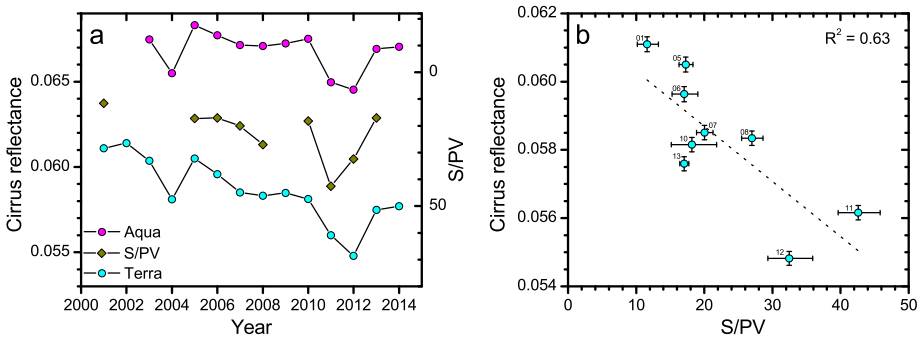

Figure 4.15.
(a) Time series of the geometric average of the S/PV (ng m^{-3} STP PVU^{-1}) (note the reversed scale), and the arithmetic average of the cirrus reflectance obtained from MODIS measurements using the satellites Aqua and Terra, for samples taken in the LMS below 5 PVU in the spring/summer (March-July). (b) A plot of CR obtained from Terra vs. values of S/PV_{LMS}, as in (a), fitted by linear regression (dotted line).

Figure 4.16a and b illustrate the geographical distribution of the CR in the northern midlatitudes, in the periods 2001-2002 and 2011-2012, respectively. The CR was obviously higher in regions with much convection, i.e. the North American continent, and the eastern parts of the oceans (where warm water is transported northwards inducing convection). Figure 4.16c shows the difference in CR between these two periods. The most pronounced decrease was seen over North America, Europe, and the north Atlantic Ocean. Excluding regions with persistent convection further increased the value of R^2 for the Terra S/PV_{LMS} comparison in Figure 4.15b (not shown here). Thus, the anti-correlation in Figure 4.15b was not caused by a change in convective activity.

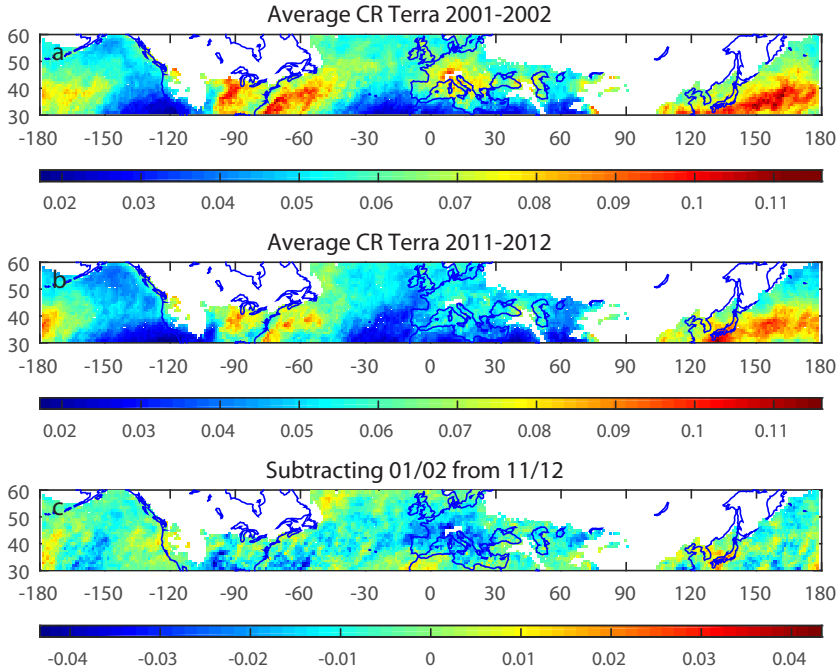

Figure 4.16.
Geographical distributions of the spring/summer (March-July) CR averaged over the period of background concentrations of S (2001-2002) (a), and the years most strongly affected by volcanism (2011-2012) (b). (c) Shows the difference in CR between the two periods in (b) and (a).

Aerosol particles can influence clouds in many ways. In the investigation presented in Paper V, several mechanisms were discussed as potential causes of the coupling of the S concentration to the cirrus cloud properties.

4.5.2. Cause of cirrus perturbations and resultant climate impact

Modelling suggests that geo-engineering the stratosphere with S would result in increased temperatures in the tropopause-region, decreasing the vertical velocities [*Kuebbeler et al.*, 2012]. Hence, ice crystal formation rates would decrease, causing optical thinning of cirrus clouds. The cloud microphysics could also be affected by increased S_{UT}. Ammonium sulfate could act as IN, i.e. if sulfuric acid becomes neutralized by ammonia it can act as IN [*Abbatt et al.*, 2006; *Hoose and Möhler*, 2012]. Thus, an increase in S_{UT} could increase the IN concentration in the UT, possibly shifting freezing from a homogeneously dominated regime to a heterogeneous one.

On the other hand, sulfuric acid could reduce the nucleation ability of IN. Hence, in a heterogeneous nucleation regime, increased S_{UT}, through downwelling from the

stratosphere, could reduce the number concentration of IN in the UT. This would cause optical thinning of cirrus clouds. A major part of the aviation soot emitted in the northern Atlantic flight corridor is spread to North America, the Atlantic Ocean, and Europe [*Zhou and Penner*, 2014], making deactivation of soot IN a viable explanation of the observed decrease in CR over these regions.

Optical thinning of cirrus clouds results in less warming. Thinner clouds absorb less longwave radiation and reflect less shortwave solar radiation; the influence being greater in the longwave interactions [*Storelvmo et al.*, 2013]. For thin clouds, CR is proportional to the COT (cloud optical thickness) [*Meyer et al.*, 2007]. In a geo-engineering modeling study, *Cirisan et al.* [2013] estimated the sensitivity of RF to changes in COT. Based on their findings, a decrease in CR of 8% would correspond to a net RF of ~-2 Wm^{-2} in the northern midlatitudes.

4.6. Volcanic aerosol and climate cooling

In recent years, much effort has been devoted to the hypothesized global warming hiatus. However, recent studies indicate a slowing down, rather than a cessation of warming. The term hiatus is therefore somewhat misleading. Also, the year in which the hiatus is supposed to have started is often given as 1998, after which the ENSO (El Niño Southern Oscillation) shifted phase, leading to cooling of the climate. Decadal variability in surface water temperatures in the Pacific Ocean has been found to strongly affect climate [*Clement and DiNezio*, 2014]. During the negative phase of the so-called 'Pacific Decadal Oscillation' (PDO), large amounts of heat are sequestered in the deep ocean. This probably led to cooling during the period 1998-2013. Furthermore, the inter-annual variability in global temperatures is large, and the observation of a hiatus is probably not statistically significant [*Rajaratnam et al.*, 2015]. In addition, *Karl et al.* [2015] found biases in the temperature records that masked some of the recent warming. Their reevaluation suggests greater 21st century warming than reported in previous studies.

Attempts to explain the hypothesized hiatus have resulted in improved insight into the factors causing decadal and inter-decadal cooling of the atmosphere. One of these is volcanism. Early estimates [*Solomon et al.*, 2011] suggested that volcanism had only a minor influence on the observed temperature trend, and that other factors were responsible for masking the inevitable temperature rise due to anthropogenic GHG emissions. In this context, the findings presented in Papers IV and V in this thesis provide new insights into one of the potential drivers of periods of climate cooling. During the period 2008-2012, most of the impact of volcanic eruptions in the northern extratropics was found to be below an altitude of 15 km, i.e. in the LMS. Excluding the LMS results in underestimation of the volcanic impact on climate of more than 30%. Furthermore, the impact of volcanism on the UT has been

disregarded. The impact of volcanic sulfate on the optical properties of cirrus clouds could cause further cooling in midlatitudes, which may regionally be of a size comparable to the direct radiative effect. The comparatively large value of RF (~-2 Wm^{-2}) suggests that volcanism can cause significant perturbations in the cirrus cloud RF. Thus, when considering the impact of volcanism on climate, it is important to include the direct radiative effect in the LMS and indirect effects in the UT. Further studies are needed to elucidate the impact of volcanism on the surface temperature of the Earth. The new perspectives presented in this thesis can lead to a broader understanding of the natural variations in temperature, and provide additional insights into the potential of geo-engineering of the stratosphere.

When external forcing (including volcanism) and internal variability associated with the ENSO are taken into account in the CMIP5 models, the predicted temperatures are much closer to the observed [*Schmidt et al.*, 2014]. Hence, including the full impact of volcanism on climate will improve current models, and likely result in more similar temperature trends as the observed.

In 2013/2014, the PDO shifted to its positive phase, releasing heat from the deep ocean [e.g. *Trenberth*, 2015]. At the same time, the volcanic aerosol load in the stratosphere was declining, and the stratospheric aerosol load is currently (2015) close to its background level. However, while the ocean circulation changes on a decadal to inter-decadal scale, volcanic eruptions perturb the stratospheric aerosol load sporadically, for periods lasting from months to a few years. It is therefore impossible to predict the future impact of volcanism on climate. Single or repeated tropopause penetration by volcanic plumes could result in small perturbations masking future global warming due to GHG, or even cooling climate.

5. Conclusions

The sulfurous component generally constitutes the major fraction of the UT and LMS aerosol. In addition, large amounts of carbonaceous aerosol are present. The concentrations of carbonaceous aerosol in the LMS were at least one order of magnitude higher than the soot concentrations in the UT/LMS reported in the literature. Furthermore, the stoichiometric relation of O/C ~0.2 suggest that the carbonaceous aerosol is of organic origin.

Regarding the sulfurous fraction, the SO_2 conversion rate in the LMS was estimated to be 45±22 days, based on samples of fresh and aged volcanic aerosol following extra-tropical eruptions. In addition to the commonly known volcanic aerosol components (sulfurous particles and ash), high concentrations of particulate C were found in both the fresh and aged volcanic aerosol. Entrainment of organic aerosol and particle-forming trace gases within volcanic jets and plumes, was proposed as likely cause.

Since roughly 2000, the aerosol concentrations in the UT/LMS have varied by a factor of over 100. This was mainly attributed to volcanic eruptions. The largest perturbations in aerosol concentrations were found to be related to extra-tropical volcanic eruptions with plumes penetrating the tropopause, as well as rapid transport in the shallow BD branches after the eruption of the tropical volcano Nabro in June 2011. Concurrent subsidence resulted in decreasing concentrations in the ensuing months.

Smaller, yet significant, perturbations associated with tropical volcanism were found in the period May 2005-July 2008. As a result of the slow transport in the deep BD branch, volcanic perturbations of the tropical stratospheric aerosol load induced perturbations in midlatitudes that lasted for years. Thus, the combination of tropical and extra-tropical volcanic eruptions was responsible for the perturbations observed in the stratospheric aerosol during most parts of the period 2005-2013.

The radiative impact of the volcanic aerosol in the LMS (altitudes <15 km) was estimated based on CALIOP observations. When including the effects of the volcanic aerosol in the LMS, the global stratospheric aerosol RF increased by >30% for the period 2008 to mid-2012. Hence, the LMS needs to be included in estimates of the effect of volcanism on climate.

The particulate S concentrations in the UT were found to be coupled to those in the LMS. Thus, subsidence of air from a volcanically perturbed stratosphere results in

perturbations in the UT, seen as increased S concentration, which could affect the properties of cirrus clouds.

The volcanic influence on the optical properties of cirrus clouds was investigated by comparing the S concentrations with satellite observations of the CR from the MODIS instrument. Interestingly, the CR was anti-correlated with the S concentration, suggesting volcanism to be affecting the optical properties of cirrus clouds, with an associated negative RF. The largest decreases in CR were observed over Europe, the northern Atlantic Ocean, and eastern parts of North America, i.e. areas with considerable air traffic. Deactivation of aircraft soot IN was proposed as an explanation. On average, the CR in northern midlatitudes decreased by 8% over the period 2001-2011, concomitant with an increase in particulate S of a factor of 3-4.

Negative RF resulted from the volcanically induced perturbations of the stratospheric aerosol load, and from changes in radiative properties of cirrus clouds. Neither the direct nor the indirect radiative effects in the UT/LMS have been included in previous estimates of the impact of volcanism on climate. Including these effects will provide more accurate estimates of the impact of volcanism on the Earth's climate, and better predictions of future surface temperatures.

6. Outlook

While the CARIBIC aerosol samples are well suited for studying the long-term and global trends of the UT/LMS aerosol concentrations, rapid changes or regional variations are more difficult to capture. A third-generation aerosol sampler and ion beam analysis system with 10 times higher time resolution is being developed by the Lund Aerosol Group. This device will significantly increase the amount of aerosol data from this little-studied part of the atmosphere. This will improve our possibility to study the UT/LMS in more detail, and allow the investigation of tropospheric sources and transport from low tropospheric altitudes. An interesting subject in this context is the transport of anthropogenic sources to the UT/LMS, and their contribution to the so-called Asian Tropopause Aerosol Layer (ATAL). Satellite data indicate that the ATAL appeared for the first time in 1998 [*Thomason and Vernier*, 2013], suggesting that the cause of the phenomenon is anthropogenic. Another interesting topic is the origin and transport of crustal material found in the UT/LMS. Future CARIBIC-based studies might also shed light on the impact of the crustal component on the climate, perhaps including possible crust-associated cloud seeding.

Further and more thorough studies are needed to elucidate the causes and implications of the findings reported in Paper V, i.e. the volcanically associated 8% decrease in the CR; specifically, regarding the mechanisms behind the decrease in CR, and its effect on climate. Combinations of aircraft-borne sampling, satellite observations and modeling are suggested to gain a better understanding of the influence of stratospheric aerosols on midlatitude cirrus clouds. Satellite observations of cirrus clouds, for example from CALIOP, are desirable to determine the horizontal and vertical distributions and the temporal trends of cirrus. These can be combined with data with improved time resolution from the next-generation CARIBIC sampling and analysis system.

Data from CALIOP, covering a period of 4½ years (2008 to mid-2012) were used to describe the radiative impact of the volcanic aerosol (Paper IV). Extending the period studied would probably provide a better understanding of the influence of the LMS on the Earth's radiative balance. Although CALIOP will soon have provided data for a decade, satellite-based aerosol data from other instruments cover other and, in some cases, longer time spans. Thus, the combination of data from several satellite-based instruments could provide valuable insight into the effect of volcanism on the LMS preceding the CALIOP data.

References

Abbatt, J. P. D., S. Benz, D. J. Cziczo, Z. Kanji, U. Lohmann, and O. Möhler (2006), Solid ammonium sulfate aerosols as ice nuclei: A pathway for cirrus cloud formation, *Science, 313*(5794), doi: 10.1126/science.1129726.

Andersson, S. M., B. G. Martinsson, J. Friberg, C. A. M. Brenninkmeijer, A. Rauthe-Schöch, M. Hermann, P. F. J. van Velthoven, and A. Zahn (2013), Composition and evolution of volcanic aerosol from eruptions of Kasatochi, Sarychev and Eyjafjallajökull in 2008–2010 based on CARIBIC observations, *Atmos. Chem. Phys., 13*, doi: 10.5194/acp-13-1781-2013.

Andersson, S. M., B. G. Martinsson, J. P. Vernier, J. Friberg, C. A. M. Brenninkmeijer, M. Hermann, P. F. J. van Velthoven, and A. Zahn (2015), Significant radiative impact of volcanic aerosol in the lowermost stratosphere, *Nature Communications*, doi: 10.1038/ncomms8692.

Appenzeller, C., J. R. Holton, and K. H. Rosenlof (1996), Seasonal variation of mass transport across the tropopause, *J. Geophys. Res.*, *101*(D10), 15071-15078.

Baker, A. K., F. Slemr, and C. A. M. Brenninkmeijer (2010), Analysis of non-methane hydrocarbons in air samples collected aboard the CARIBIC passenger aircraft, *Atmos. Meas. Tech.*, *3*(1), 311-321.

Barahona, D., A. Molod, J. Bacmeister, A. Nenes, A. Gettelman, H. Morrison, V. Phillips, and A. Eichmann (2014), Development of two-moment cloud microphysics for liquid and ice within the NASA Goddard Earth Observing System Model (GEOS-5), *Geosci. Model Dev., 7*(4), doi: 10.5194/gmd-7-1733-2014.

Bazhenov, O. E., V. D. Burlakov, S. I. Dolgii, and A. V. Nevzorov (2012), Lidar Observations of Aerosol Disturbances of the Stratosphere over Tomsk (56.5 N; 85.0 E) in Volcanic Activity Period 2006–2011, *International Journal of Optics, 2012*, doi: 10.1155/2012/786295.

Bennett, J. M. (2006), *Radiation, energy budgets & planetary temperatures*, "The Atmosphere" note set 2, Semester 1, Flinders University.

Birner, T., and H. Bönisch (2011), Residual circulation trajectories and transit times into the extratropical lowermost stratosphere, *Atmos. Chem. Phys., 10*, doi: 10.5194/acp-11-817-2011.

Boucher, O., et al. (2013), *Clouds and Aerosols. In: Climate Change 2013: The Physical Science Basis. Contribution of Working Group I to the Fifth Assessment Report of the Intergovernmental Panel on Climate Change*, (eds.) T. F. Stocker, D. Qin, G.-K. Plattner, M. Tignor, S.K. Allen, J. Boschung, A. Nauels, Y. Xia, V. Bex and P.M. Midgley, Cambridge, United Kingdom and New York, NY, USA, pp. 1535, 10.1017/CBO9781107415324.

Bourassa, A. E., A. Robock, W. J. Randel, T. Deshler, L. A. Rieger, N. D. Lloyd, E. J. T. Llewellyn, and D. A. Degenstein (2012), Large volcanic aerosol load in the stratosphere linked to Asian monsoon transport, *Science, 337*(6090), doi: 10.1126/science.1219371.

Brenninkmeijer, C. A. M., et al. (2007), Civil Aircraft for the regular investigation of the atmosphere based on an instrumented container: The new CARIBIC system, *Atmos. Chem. Phys.*, *7*(18), 4953-4976.

Brewer, A. W. (1949), Evidence for a world circulation provided by the measurements of helium and water vapour distribution in the stratosphere, *Q. J. R. Meteorol. Soc.*, *75*, 351-363.

Brühl, C., J. Lelieveld, P. J. Crutzen, and H. Tost (2012), The role of carbonyl sulphide as a source of stratospheric sulphate aerosol and its impact on climate, *Atmos. Chem. Phys., 12*, doi: 10.5194/acp-12-1239-2012.

Bönisch, H., A. Engel, J. Curtius, T. Birner, and P. Hoor (2009), Quantifying transport into the lowermost stratosphere using simultaneous in-situ measurements of SF6 and CO2, *Atmos. Chem. Phys.*, *9*, 5905–5919.

Campbell, J. R., E. J. Welton, N. A. Krotkov, K. Yang, S. A. Stewart, and M. D. Fromm (2012), Likely seeding of cirrus clouds by stratospheric Kasatochi volcanic aerosol particles near a mid-latitude tropopause fold, *Atmos. Environ., 46*, doi: 10.1016/j.atmosenv.2011.09.027.

Carn, S. A., and F. J. Prata (2010), Satellite-based constraints on explosive SO2 release from Soufrière Hills Volcano, Montserrat, *Geophys. Res. Lett., 37*, doi: 10.1029/2010GL044971.

Carn, S. A., et al. (2011), In situ measurements of tropospheric volcanic plumes in Ecuador and Colombia during TC4, *J. Geophys. Res., 116*, doi: 10.1029/2010JD014718.

Cirisan, A., P. Spichtinger, B. P. Luo, D. K. Weisenstein, H. Wernli, U. Lohmann, and T. Peter (2013), Microphysical and radiative changes in cirrus clouds by geoengineering the stratosphere, *J. Geophys. Res., 118*(10), doi: 10.1002/jgrd.50388.

Clarisse, L., D. Hurtmans, C. Clerbaux, J. Hadji-Lazaro, Y. Ngadi, and P.-F. Coheur (2012), Retrieval of sulphur dioxide from the infrared atmospheric sounding interferometer (IASI), *Atmos. Meas. Tech., 5*(3), doi: 10.5194/amt-5-581-2012.

Clement, A., and P. DiNezio (2014), The Tropical Pacific Ocean—Back in the Driver's Seat?, *Science, 343*(6174), doi: 10.1126/science.1248115.

Crutzen, P. J. (1976), The possible importance of CSO for the sulfate layer of the stratosphere, *Geophys. Res. Lett.*, *3*(2), 73-76.

Crutzen, P. J. (2006), Albedo enhancement by stratospheric sulfur injections: a contribution to resolve a policy dilemma?, *Climatic change, 77*(3), doi: 10.1007/s10584-006-9101-y.

Cziczo, D. J., K. D. Froyd, C. Hoose, E. J. Jensen, M. Diao, M. A. Zondlo, J. B. Smith, C. H. Twohy, and D. M. Murphy (2013), Clarifying the dominant sources and mechanisms of cirrus cloud formation, *Science, 340*(6138), doi: 10.1126/science.1234145.

Deshler, T. (2008), A review of global stratospheric aerosol: Measurements, importance, life cycle, and local stratospheric aerosol, *Atmos. Res.*, *90*(2), 223-232.

Dobson, G. M. B. (1956), Origin and distribution of the polyatomic molecules in the atmosphere, *Proc. R. Soc.London, Ser. A*, *236*, 187-193.

Flato, G., et al. (2013), *Evaluation of Climate Models. In: Climate Change 2013: The Physical Science Basis. Contribution of Working Group I to the Fifth Assessment Report of the Intergovernmental Panel on Climate Change* (eds.) T. F. Stocker, D. Qin, G.-K. Plattner, M. Tignor, S.K. Allen, J. Boschung, A. Nauels, Y. Xia, V. Bex and P.M. Midgley, Cambridge University Press, Cambridge, United Kingdom and New York, NY, USA.

Fortuin, J. P. F., and H. Kelder (1998), An ozone climatology based on ozonesonde and satellite measurements, *J. Geophys. Res.*, *103*(D24), 31709-31734.

Friberg, J., B. G. Martinsson, S. M. Andersson, C. A. M. Brenninkmeijer, M. Hermann, P. F. J. van Velthoven, and A. Zahn (2014), Sources of increase in lowermost stratospheric sulphurous and carbonaceous aerosol background concentrations during 1999-2008 derived from CARIBIC flights, *Tellus B, 66*, doi: 10.3402/tellusb.v66.23428.

Friberg, J., B. G. Martinsson, M. K. Sporre, S. M. Andersson, C. A. M. Brenninkmeijer, M. Hermann, P. F. J. van Velthoven, and A. Zahn (2015), Influence of volcanic eruptions on midlatitude upper tropospheric aerosol and consequences for cirrus clouds, *Earth and Space Science, 2*(7), doi: 10.1002/2015ea000110.

Fromm, M., D. T. Lindsey, R. Servranckx, G. Yue, T. Trickl, R. Sica, P. Doucet, and S. Godin-Beekmann (2010), The untold story of pyrocumulonimbus, *B. Am. Meteorol. Soc., 91*(9), doi: 10.1175/2010BAMS3004.1.

Fyfe, J. C., N. P. Gillett, and F. W. Zwiers (2013), Overestimated global warming over the past 20 years, *Nature Clim. Change*, *3*(9), 767-769.

Gettelman, A., P. Hoor, L. L. Pan, W. J. Randel, M. I. Hegglin, and T. Birner (2011), The extratropical upper troposphere and lower stratosphere, *Rev. Geophys., 49*(3), doi: 10.1029/2011RG000355.

Guan, H., R. Esswein, J. Lopez, R. Bergstrom, A. Warnock, M. Follette-Cook, M. Fromm, and L. T. Iraci (2010), A multi-decadal history of biomass burning plume heights identified using aerosol index measurements, *Atmos. Chem. Phys., 10*, doi: 10.5194/acp-10-6461-2010.

GVP (2015), Global volcanism program, Online at: http://www.volcano.si.edu/index.cfm.

Haywood, J. M., A. Jones, L. Clarisse, A. Bourassa, J. Barnes, P. Telford, N. Bellouin, O. Boucher, P. Agnew, and C. Clerbaux (2010), Observations of the eruption of the Sarychev volcano and simulations using the HadGEM2 climate model, *J. Geophys. Res., 115*(D21), doi: 10.1029/2010JD014447.

Hermann, M., F. Stratmann, M. Wilck, and A. Wiedensohler (2001), Sampling characteristics of an aircraft-borne aerosol inlet system, *Journal of Atmospheric and Oceanic Technology*, *18*(1), 7-19.

Hoerling, M. P., T. K. Schaack, and A. J. Lenzen (1991), Global objective tropopause analysis, *Mon. Weather Rev.*, *119*, 1816-1831.

Hofmann, D., J. Barnes, M. O'Neill, M. Trudeau, and R. Neely (2009), Increase in background stratospheric aerosol observed with lidar at Mauna Loa Observatory and Boulder, Colorado, *Geophys. Res. Lett., 36*(15), doi: 10.1029/2009GL039008.

Hoinka, K. P. (1997), The tropopause: Discovery, definition and demarcation, *Meteorol. z*, *6*, 281– 303.

Holton, J. R., P. H. Haynes, M. E. McIntyre, A. R. Douglas, R. B. Rood, and L. Pfister (1995), Stratosphere-troposphere exchange, *Rev. Geophys.*, *33*(4), 403-439.

Hoor, P., H. Fischer, L. Lange, J. Lelieveld, and D. Brunner (2002), Seasonal variations of a mixing layer in the lowermost stratosphere as identified by the CO-O3 correlation from in situ measurements, *J. Geophys. Res*, *107*(D5), 4044.

Hoose, C., and O. Möhler (2012), Heterogeneous ice nucleation on atmospheric aerosols: a review of results from laboratory experiments, *Atmos. Chem. Phys., 12*(20), doi: 10.5194/acp-12-9817-2012.

Hu, M., J. Peng, K. Sun, D. Yue, S. Guo, A. Wiedensohler, and Z. Wu (2012), Estimation of Size-Resolved Ambient Particle Density Based on the Measurement of Aerosol Number, Mass, and Chemical Size Distributions in the Winter in Beijing, *Environmental science & technology, 46*(18), doi: 10.1021/es204073t.

IPCC AR5 (2013), *Anthropogenic and Natural Radiative Forcing. In: Climate Change 2013: The Physical Science Basis. Contribution of Working Group I to the Fifth Assessment Report of the Intergovernmental Panel on Climate Change*, (eds.) T. F. Stocker, D. Qin, G.-K. Plattner, M. Tignor, S.K. Allen, J. Boschung, A. Nauels, Y. Xia, V. Bex and P.M. Midgley, Cambridge, United Kingdom and New York, NY, USA, pp. 1535, 10.1017/CBO9781107415324.

Johansson, S. A. E., and J. L. Campbell (1988), *PIXE: A novel technique for elemental analysis*, 347 pp., John Wiley, Hoboken, N. J.

Jost, H. J., K. Drdla, A. Stohl, L. Pfister, M. Loewenstein, J. P. Lopez, P. K. Hudson, D. M. Murphy, D. J. Cziczo, and M. Fromm (2004), In-situ observations of mid-latitude forest fire plumes deep in the stratosphere, *Geophys. Res. Lett., 31*(11), doi: 10.1029/2003GL019253.

Junge, C. E., C. W. Chagnon, and J. E. Manson (1961), A world-wide stratospheric aerosol layer, *Science*, *133*(3463), 1478-1479.

Jurkat, T., C. Voigt, F. Arnold, H. Schlager, H. Aufmhoff, J. Schmale, J. Schneider, M. Lichtenstern, and A. Dörnbrack (2010), Airborne stratospheric ITCIMS measurements of SO_2, HCl, and HNO_3 in the aged plume of volcano Kasatochi, *J. Geophys. Res.*, *115*(D2).

Jäger, H., and T. Deshler (2002), Lidar backscatter to extinction, mass and area conversions for stratospheric aerosols based on midlatitude balloonborne size distribution measurements, *Geophys. Res. Lett., 29*(19), doi: 10.1029/2002GL015609.

Jäger, H., and T. Deshler (2003), Correction to "Lidar backscatter to extinction, mass and area conversions for stratospheric aerosols based on midlatitude balloonborne size distribution measurements", *Geophys. Res. Lett., 30*(7), doi: 10.1029/2003GL017189.

Kannosto, J., A. Virtanen, M. Lemmetty, J. M. Mäkelä, J. Keskinen, H. Junninen, T. Hussein, P. Aalto, and M. Kulmala (2008), Mode resolved density of atmospheric aerosol particles, *Atmos. Chem. Phys.*, *8*(17), 5327-5337.

Karagulian, F., L. Clarisse, C. Clerbaux, A. J. Prata, D. Hurtmans, and P. F. Coheur (2010), Detection of volcanic SO_2, ash, and H_2SO_4 using the Infrared Atmospheric Sounding Interferometer (IASI), *J. Geophys. Res., 115*(D2), doi: 10.1029/2009JD012786.

Karl, T. R., A. Arguez, B. Huang, J. H. Lawrimore, J. R. McMahon, M. J. Menne, T. C. Peterson, R. S. Vose, and H.-M. Zhang (2015), Possible artifacts of data biases in the recent global surface warming hiatus, *Science, 348*(6242), doi: 10.1126/science.aaa5632.

King, M. D., W. P. Menzel, Y. J. Kaufman, D. Tanré, B.-C. Gao, S. Platnick, S. A. Ackerman, L. A. Remer, R. Pincus, and P. A. Hubanks (2003), Cloud and aerosol properties, precipitable water, and profiles of temperature and water vapor from MODIS, *IEEE Transactions on Geoscience and Remote Sensing*, *41*(2), 442-458.

Kremser, S., N. B. Jones, M. Palm, B. Lejeune, Y. Wang, D. Smale, and N. M. Deutscher (2015), Positive trends in Southern Hemisphere carbonyl sulfide (OCS), *Geophys. Res. Lett.*, doi: 10.1002/2015GL065879.

Krotkov, N. A., M. R. Schoeberl, G. A. Morris, S. A. Carn, and K. Yang (2010), Dispersion and lifetime of the SO_2 cloud from the August 2008 Kasatochi eruption, *J. Geophys. Res., 115*(D2), doi: 10.1029/2010JD013984.

Kuebbeler, M., U. Lohmann, and J. Feichter (2012), Effects of stratospheric sulfate aerosol geo-engineering on cirrus clouds, *Geophys. Res. Lett., 39*(23), doi: 10.1029/2012GL053797.

Lopez, T., S. A. Carn, C. A. Werner, D. Fee, P. Kelly, M. Doukas, M. Pfeffer, P. Webley, C. Cahill, and D. Schneider (2013), Evaluation of Redoubt Volcano's sulfur dioxide emissions by the Ozone Monitoring Instrument, *J. Volcanol. and Geoth. Res., 259*, doi: 10.1016/j.jvolgeores.2012.03.002.

Martinsson, B. G., H. N. Nguyen, C. A. M. Brenninkmeijer, A. Zahn, J. Heintzenberg, M. Hermann, and P. F. J. van Velthoven (2005), Characteristics and origin of lowermost stratospheric aerosol at northern midlatitudes under volcanically quiescent conditions based on CARIBIC observations, *J. Geophys. Res., 110*, doi: 10.1029/2004JD005644.

Martinsson, B. G., C. A. M. Brenninkmeijer, S. A. Carn, M. Hermann, K. P. Heue, P. F. J. van Velthoven, and A. Zahn (2009), Influence of the 2008 Kasatochi volcanic eruption on sulfurous and carbonaceous aerosol constituents in the lower stratosphere, *Geophys. Res. Lett., 36*, doi: 10.1029/2009GL038735.

Martinsson, B. G., J. Friberg, S. M. Andersson, A. Weigelt, M. Hermann, D. Assmann, J. Voigtländer, C. A. M. Brenninkmeijer, P. J. F. van Velthoven, and A. Zahn (2014), Comparison between CARIBIC aerosol samples analysed by accelerator-based methods and optical particle counter measurements, *Atmos. Meas. Tech., 7*, doi: 10.5194/amt-7-2581-2014.

McCormick, M. P., L. W. Thomason, and C. R. Trepte (1995), Atmospheric effects of the Mt Pinatubo eruption, *Nature*, *373*(6513), 399-404.

Meyer, K., P. Yang, and B.-C. Gao (2007), Ice Cloud Optical Depth From MODIS Cirrus Reflectance, *4*(3), 471-474.

Murphy, D. M., D. S. Thomson, and M. J. Mahoney (1998), In situ measurements of organics, meteoritic material, mercury, and other elements in aerosols at 5 to 19 kilometers, *Science*, *282*(5394), 1664-1669.

Murphy, D. M., D. J. Cziczo, P. K. Hudson, and D. S. Thomson (2007), Carbonaceous material in aerosol particles in the lower stratosphere and tropopause region, *J. Geophys. Res., 112*(D4), doi: 10.1029/2006JD007297.

Murphy, D. M., K. D. Froyd, J. P. Schwarz, and J. C. Wilson (2014), Observations of the chemical composition of stratospheric aerosol particles, *Quarterly Journal of the Royal Meteorological Society*, doi: DOI:10.1002/qj.2213.

Murphy, D. M., D. J. Cziczo, K. D. Froyd, P. K. Hudson, B. M. Matthew, A. M. Middlebrook, R. E. Peltier, A. Sullivan, D. S. Thomson, and R. J. Weber (2006), Single-particle mass spectrometry of tropospheric aerosol particles, *J. Geophys. Res., 111*(D23), doi: 10.1029/2006JD007340.

Myhre, G., et al. (2013), *Anthropogenic and Natural Radiative Forcing. In: Climate Change 2013: The Physical Science Basis. Contribution of Working Group I to the Fifth Assessment Report of the Intergovernmental Panel on Climate Change*, (eds.) T. F. Stocker, D. Qin, G.-K. Plattner, M. Tignor, S.K. Allen, J. Boschung, A. Nauels, Y. Xia, V. Bex and P.M. Midgley, Cambridge, United Kingdom and New York, NY, USA.

Nagai, T., B. Liley, T. Sakai, T. Shibata, and O. Uchino (2010), Post-Pinatubo evolution and subsequent trend of the stratospheric aerosol layer observed by mid-latitude lidars in both hemispheres, *Sola, 6*, doi: 10.2151/sola.2010-018.

Nguyen, H. N., and B. G. Martinsson (2007), Analysis of C, N and O in aerosol collected on an organic backing using internal blank measurements and variable beam size, *Nucl. Instrum. Methods Phys. Res., Sect. B, 264*, doi: 10.1016/j.nimb.2007.08.001.

Nguyen, H. N., A. Gudmundsson, and B. G. Martinsson (2006), Design and Calibration of a Multi-Channel Aerosol Sampler for Tropopause Region Studies from the CARIBIC Platform, *Aerosol Sci. Technol., 40*, doi: 10.1080/02786820600767807.

Nguyen, H. N., et al. (2008), Chemical composition and morphology of individual aerosol particles from a CARIBIC flight at 10 km altitude between 50 N and 30 S, *J. Geophys. Res., 113*, doi: 10.1029/2008JD009956.

Oram, D. E., F. S. Mani, J. C. Laube, M. J. Newland, C. E. Reeves, W. T. Sturges, S. A. Penkett, C. A. M. Brenninkmeijer, T. Röckmann, and P. J. Fraser (2012), Long-term tropospheric trend of octafluorocyclobutane (c-C4F8 or PFC-318), *Atmos. Chem. Phys., 12*, doi: 10.5194/acp-12-261-2012.

Papaspiropoulos, G., B. Mentes, P. Kristiansson, and B. G. Martinsson (1999), A high sensitivity elemental analysis methodology for upper tropospheric aerosol, *Nucl. Instrum. Methods Phys. Res., Sect. B*, *150*, 356-362.

Platnick, S., M. D. King, S. A. Ackerman, W. P. Menzel, B. A. Baum, J. C. Riédi, and R. A. Frey (2003), The MODIS cloud products: Algorithms and examples from Terra, *IEEE Transactions on Geoscience and Remote Sensing*, *41*(2), 459-473.

Prata, A. J., and C. Bernardo (2007), Retrieval of volcanic SO_2 column abundance from atmospheric infrared sounder data, *J. Geophys. Res., 112*, doi: 10.1029/2006JD007955.

Prata, F., S. A. Carn, M. Fromm, and N. A. Krotkov (2008), A-train satellite observations of the 2008 Chaitén eruption clouds, *Am. Geophys. Union Fall Meeting 2008, abstract #V43D-2183*.

Rajaratnam, B., J. Romano, M. Tsiang, and N. S. Diffenbaugh (2015), Debunking the climate hiatus, *Climatic change, 133*(2), doi: 10.1007/s10584-015-1495-y.

Ramanathan, V., and Y. Feng (2008), On avoiding dangerous anthropogenic interference with the climate system: Formidable challenges ahead, *Proceedings of the National Academy of Sciences, 105*(38), doi: 10.1073/pnas.0803838105.

Rauthe-Schöch, A., et al. (2012), CARIBIC aircraft measurements of Eyjafjallajökull volcanic clouds in April/May 2010, *Atmos. Chem. Phys., 12*, doi: 10.5194/acp-12-879-2012.

Ridley, D. A., S. Solomon, J. E. Barnes, V. D. Burlakov, T. Deshler, S. I. Dolgii, A. B. Herber, T. Nagai, R. R. Neely, and A. V. Nevzorov (2014), Total volcanic stratospheric aerosol optical depths and implications for global climate change, *Geophys. Res. Lett.*, doi: 10.1002/2014GL061541.

Robock, A. (2000), Volcanic eruptions and climate, *Rev. Geophys.*, *38*(2), 191-219.

Roelofs, G.-J., and J. Lelieveld (1997), Model study of the influence of cross-tropopause O_3 transports on tropospheric O_3 levels, *Tellus B*, *49*(1), 38-55.

Rosen, J. M. (1971), The boiling point of stratospheric aerosols, *Journal of applied meteorology*, *10*, 1044-1046.

Rosenfeld, D., and W. L. Woodley (2000), Deep convective clouds with sustained supercooled liquid water down to -37.5C, *Nature*, *405*(6785), 440-442.

Rudnick, R. L., and D. M. Fountain (1995), Nature and composition of the continental crust: a lower crustal perspective, *Rev. Geophys.*, *33*(3), 267-309.

Saarikoski, S., T. Mäkelä, R. Hillamo, P. P. Aalto, V.-M. Kerminen, and M. Kulmala (2005), Physico-chemical characterization and mass closure of size-segregated atmospheric aerosols in Hyytiälä, Finland, *Boreal Environ. Res.*, *10*, 385-400.

Santer, B. D., C. Bonfils, J. F. Painter, M. D. Zelinka, C. Mears, S. Solomon, G. A. Schmidt, J. C. Fyfe, J. N. S. Cole, and L. Nazarenko (2014), Volcanic contribution to decadal changes in tropospheric temperature, *Nature Geoscience*, *7*(3), 185-189.

Schmale, J., et al. (2010), Aerosol layers from the 2008 eruptions of Mount Okmok and Mount Kasatochi: In situ upper troposphere and lower stratosphere measurements of sulfate and organics over Europe, *J. Geophys. Res., 115*, doi: 10.1029/2009JD013628.

Schmidt, G. A., D. T. Shindell, and K. Tsigaridis (2014), Reconciling warming trends, *Nature Geoscience, 7*(3), doi: 10.1038/ngeo2105.

Schuck, T. J., C. A. M. Brenninkmeijer, F. Slemr, I. Xueref-Remy, and A. Zahn (2009), Greenhouse gas analysis of air samples collected onboard the CARIBIC passenger aircraft, *Atmos. Meas. Tech.*, *2*(2), 449-464.

Schumann, U., P. Jeßberger, and C. Voigt (2013), Contrail ice particles in aircraft wakes and their climatic importance, *Geophys. Res. Lett., 40*, doi: 10.1002/grl.50539, 2013.

Schwarz, J. P., J. R. Spackman, R. S. Gao, L. A. Watts, P. Stier, M. Schulz, S. M. Davis, S. C. Wofsy, and D. W. Fahey (2010), Global-scale black carbon profiles observed in the remote atmosphere and compared to models, *Geophys. Res. Lett., 37*, doi: 10.1029/2010GL044372.

Seifert, P., A. Ansmann, S. Groß, V. Freudenthaler, B. Heinold, A. Hiebsch, I. Mattis, J. Schmidt, F. Schnell, and M. Tesche (2011), Ice formation in ash-influenced clouds after the eruption of the Eyjafjallajökull volcano in April 2010, *J. Geophys. Res., 116*(D20), doi: 10.1029/2011JD015702.

Seinfeld, J. H., and S. N. Pandis (2012), *Atmospheric chemistry and physics: from air pollution to climate change*, 2 ed., John Wiley & Sons, Hoboken, New Jersey, ISBN: 1118591364.

Shibata, T., M. Hayashi, A. Naganuma, N. Hara, K. Hara, F. Hasebe, K. Shimizu, N. Komala, Y. Inai, and H. Vömel (2012), Cirrus cloud appearance in a volcanic aerosol layer around the tropical cold point tropopause over Biak, Indonesia, in January 2011, *J. Geophys. Res., 117*(D11), doi: 10.1029/2011JD017029.

Solomon, S., J. S. Daniel, R. R. Neely, J. P. Vernier, E. G. Dutton, and L. W. Thomason (2011), The persistently variable "background" stratospheric aerosol layer and global climate change, *Science, 333*, doi: 10.1126/science.1206027.

SPARC (2015), stratospheric processes and their role in climate, Online at: http://www.atmosp.physics.utoronto.ca/SPARC/News25/temperatures.html.

Spracklen, D. V., S. R. Arnold, J. Sciare, K. S. Carslaw, and C. Pio (2008), Globally significant oceanic source of organic carbon aerosol, *Geophys. Res. Lett.*, *35*(12), L12811.

Sprenger, M., and H. Wernli (2003), A northern hemispheric climatology of cross-tropopause exchange for the ERA15 time period (1979–1993), *J. Geophys. Res., 108*, doi: 10.1029/2002JD002636.

Storelvmo, T., J. E. Kristjansson, H. Muri, M. Pfeffer, D. Barahona, and A. Nenes (2013), Cirrus cloud seeding has potential to cool climate, *Geophys. Res. Lett., 40*(1), doi: doi:10.1029/2012GL054201.

Stramska, M. (2009), Particulate organic carbon in the global ocean derived from SeaWiFS ocean color, *Deep Sea Research Part I*, *56*(9), 1459-1470.

Surono, et al. (2012), The 2010 explosive eruption of Java's Merapi volcano—a '100-year'event, *J. Volcanol. and Geoth. Res.*, doi: 10.1016/j.jvolgeores.2012.06.018.

Thomas, H. E., I. M. Watson, S. A. Carn, A. J. Prata, and V. J. Realmuto (2011), A comparison of AIRS, MODIS and OMI sulphur dioxide retrievals in volcanic clouds, *Geomatics, Natural Hazards and Risk, 2*(3), doi: 10.1080/19475705.2011.564212.

Thomason, L., and J.-P. Vernier (2013), Improved SAGE II cloud/aerosol categorization and observations of the Asian tropopause aerosol layer: 1989–2005, *Atm. Chem. Phys.*, *13*(9), 4605-4616.

Trenberth, K. E. (2015), Has there been a hiatus?, *Science, 349*(6249), doi: 10.1126/science.aad0678.

Vanhellemont, F., D. Fussen, N. Mateshvili, C. Tétard, C. Bingen, E. Dekemper, N. Loodts, E. Kyrölä, V. Sofieva, and J. Tamminen (2010), Optical extinction by upper tropospheric/stratospheric aerosols and clouds: GOMOS observations for the period 2002–2008, *Atmos. Chem. Phys., 10*(16), doi: 10.5194/acp-10-7997-2010.

Vaughan, N. E., and T. M. Lenton (2011), A review of climate geoengineering proposals, *Climatic change, 109*(3), doi: 10.1007/s10584-011-0027-7.

Vernier, J. P., et al. (2009), Tropical stratospheric aerosol layer from CALIPSO lidar observations, *J. Geophys. Res., 114*, doi: 10.1029/2009JD011946.

Vernier, J. P., et al. (2011), Major influence of tropical volcanic eruptions on the stratospheric aerosol layer during the last decade, *Geophys. Res. Lett., 38*(12), doi: 10.1029/2011GL047563.

Zahn, A., and C. A. M. Brenninkmeijer (2003), New directions: a chemical tropopause defined, *Atmos. Environ.*, *37*(3), 439-440.

Zahn, A., J. Weppner, H. Widmann, K. Schlote-Holubek, B. Burger, T. Kühner, and H. Franke (2012), A fast and precise chemiluminescence ozone detector for eddy flux and airborne application, *Atmos. Meas. Tech., 5*, doi: 10.5194/amt-5-363-2012.

Zahn, A., C. A. M. Brenninkmeijer, W. A. H. Asman, P. J. Crutzen, G. Heinrich, H. Fischer, J. W. M. Cuijpers, and P. F. J. van Velthoven (2002), Budgets of O_3 and CO in the

upper troposphere: CARIBIC passenger aircraft results 1997–2001, *J. Geophys. Res., 107*(D17), doi: 10.1029/2001JD001529.

Zhou, C., and J. E. Penner (2014), Aircraft soot indirect effect on large-scale cirrus clouds: Is the indirect forcing by aircraft soot positive or negative?, *J. Geophys. Res.*, *119*(19), 11,303-311,320.

Paper I

Atmos. Chem. Phys., 13, 1781–1796, 2013
www.atmos-chem-phys.net/13/1781/2013/
doi:10.5194/acp-13-1781-2013

Atmospheric Chemistry and Physics Open Access

Composition and evolution of volcanic aerosol from eruptions of Kasatochi, Sarychev and Eyjafjallajökull in 2008–2010 based on CARIBIC observations

S. M. Andersson[1], B. G. Martinsson[1], J. Friberg[1], C. A. M. Brenninkmeijer[2], A. Rauthe-Schöch[2], M. Hermann[3], P. F. J. van Velthoven[4], and A. Zahn[5]

[1]Division of Nuclear Physics, Lund University, Lund, Sweden
[2]Max Planck Institute for Chemistry, Atmospheric Chemistry, Mainz, Germany
[3]Leibniz Institute for Tropospheric Research, Leipzig, Germany
[4]Royal Netherlands Meteorological Institute, de Bilt, The Netherlands
[5]Institute for Meteorology and Climate Research, Karlsruhe Institute of Technology (KIT), Germany

Correspondence to: S. M. Andersson (sandra.andersson@nuclear.lu.se)

Received: 12 April 2012 – Published in Atmos. Chem. Phys. Discuss.: 22 August 2012
Revised: 7 January 2013 – Accepted: 5 February 2013 – Published: 18 February 2013

Abstract. Large volcanic eruptions impact significantly on climate and lead to ozone depletion due to injection of particles and gases into the stratosphere where their residence times are long. In this the composition of volcanic aerosol is an important but inadequately studied factor. Samples of volcanically influenced aerosol were collected following the Kasatochi (Alaska), Sarychev (Russia) and also during the Eyjafjallajökull (Iceland) eruptions in the period 2008–2010. Sampling was conducted by the CARIBIC platform during regular flights at an altitude of 10–12 km as well as during dedicated flights through the volcanic clouds from the eruption of Eyjafjallajökull in spring 2010. Elemental concentrations of the collected aerosol were obtained by accelerator-based analysis. Aerosol from the Eyjafjallajökull volcanic clouds was identified by high concentrations of sulphur and elements pointing to crustal origin, and confirmed by trajectory analysis. Signatures of volcanic influence were also used to detect volcanic aerosol in stratospheric samples collected following the Sarychev and Kasatochi eruptions. In total it was possible to identify 17 relevant samples collected between 1 and more than 100 days following the eruptions studied. The volcanically influenced aerosol mainly consisted of ash, sulphate and included a carbonaceous component. Samples collected in the volcanic cloud from Eyjafjallajökull were dominated by the ash and sulphate component (∼45 % each) while samples collected in the tropopause region and LMS mainly consisted of sulphate (50–77 %) and carbon (21–43 %). These fractions were increasing/decreasing with the age of the aerosol. Because of the long observation period, it was possible to analyze the evolution of the relationship between the ash and sulphate components of the volcanic aerosol. From this analysis the residence time (1/e) of sulphur dioxide in the studied volcanic cloud was estimated to be 45 ± 22 days.

1 Introduction

Despite its modest size, the eruption of Eyjafjallajökull volcano in the spring of 2010 caused considerable disruption of European air traffic due to the ash and sulphate aerosol it produced. In particular ash particles are hazardous, since they can damage jet engines and disrupt avionics and navigation systems (Casadevall, 1994), whereas sulphate aerosol have been reported to cause crazing of aircraft windows (Carn et al., 2009). Above all the complex effects of volcanoes on atmospheric chemistry and physics are also of concern for climate (Ammann et al., 2003). Not only the amount of ejected material, the location of the volcano and the force of the eruption, but also the properties of volcanic aerosol play a considerable role in these contexts. Unfortunately, our present understanding of the composition of volcanically influenced

atmospheric aerosol is limited since quantitative measurements in the free troposphere and in the stratosphere are scarce. To improve this situation, we report here on the investigation of the elemental composition of volcanic aerosol sampled directly in the volcanic cloud from the Eyjafjallajökull eruption in 2010, and moreover sampled in the upper troposphere/lowermost stratosphere (UT/LMS) following eruptions of the volcanoes Kasatochi (Alaska, 2008) and Sarychev (Russia, 2009).

The scattering and absorbing properties of volcanic aerosol affect the Earth's radiation budget and thus result in temperature gradients that perturb circulation patterns and impact climate (IPCC, 2007). After the eruption of Mount Pinatubo in 1991, with a large Volcanic Explosivity Index (VEI) (Newhall and Self, 1982) of 6, the global, tropospheric temperature was estimated to have been 0.5 °C lower than the climatological average temperature. Another large eruption in Tambora (1815, VEI 7) caused an estimated drop in global mean temperature of 0.4 to 0.7 °C (McCormick et al., 1995). Stratospheric aerosols also act as surfaces for heterogeneous reactions that affect the distribution of ozone and other trace gases (IPCC, 2007). Not only massive eruptions such as those mentioned above are of importance to the stratospheric aerosol load. A study by Vernier et al. (2011) based on satellite observations shows that eruptions of lower explosivity are also an important source of stratospheric aerosol. Their effect is visible in the increase of the stratospheric aerosol layer that has occurred since 2002 after a period with little volcanic influence. This increase in the stratospheric aerosol load has also been observed in other data sets, however, anthropogenic influence cannot be ruled out (Hofmann et al., 2009; Solomon et al., 2011).

In the absence of volcanic eruptions, stratospheric aerosol is mainly found at altitudes of 20–30 km (Junge et al., 1961). This aerosol layer, referred to as the Junge layer, mainly consists of sulphate aerosol that is chiefly formed by sulphur dioxide (SO_2) produced from photo-dissociation of carbonyl sulphide (OCS) transported from the troposphere (Crutzen, 1976). However studies indicate that OCS is not enough to explain the observed aerosol load (Chin and Davis, 1995), and direct transport of SO_2 or sulphate aerosol have been suggested as important contributions to stratospheric aerosol (Pitari et al., 2002; Myhre et al., 2004). Volcanic injections however makes it difficult to determine the background state of the stratospheric aerosol layer (Solomon et al., 2011), and thereby the importance of different sources for its production. A carbonaceous component of the UT/LMS aerosol was identified by Murphy et al. (1998), which was subsequently found to be a large fraction of the aerosol (Nguyen et al., 2008; Murphy et al., 2007). Martinsson et al. (2009) found that volcanic aerosol contains a large carbonaceous component. Additional sources contributing to the aerosol load in the UT/LMS, include air traffic (Ferry et al., 1999; Kjellström et al., 1999), meteorites (Cziczo et al., 2001) and boundary layer aerosol and precursor gases transported across the tropopause (Papaspiropoulos et al., 2002; Köppe et al., 2009). Especially aerosol from forest fires can be brought to high altitudes by extreme convection, however, the frequency and global contribution of such events is poorly understood (Fromm et al., 2004, 2008). Guan et al. (2010) estimated that on average about six such events per year lead to injection of particles to altitudes above 8 km. With a frequency of one or a few events per year, volcanic eruptions contribute to stratospheric aerosol mass of similar magnitude as OCS does (Vernier et al., 2011), and in a few events per century volcanism is by far the strongest source of stratospheric aerosol (Ammann et al., 2003).

Volcanic eruptions inject large quantities of ash and gases into the atmosphere. Sulphur dioxide is the third most abundant gas in volcanic emissions, after water vapor and carbon dioxide (von Glasow et al., 2009). It is oxidized in the atmosphere thus leading to sulphate aerosol. Enhanced concentrations of stratospheric aerosol following the eruptions of El Chichón (1982) and Pinatubo (1991) had a residence time (1/e) of 10.3 and 12.0 months respectively (Jäger, 2005; Deshler, 2008). Especially the number concentration of particles larger than 1 µm in diameter was observed to increase substantially following the Pinatubo eruption (Deshler, 2008). The directly emitted ash particles exhibit a size of 2 mm or less (by definition) (Heiken and Wohletz, 1985), and show a large span in size with particle diameters down to less than 1 µm (Rose and Durant, 2009; Mather et al., 2003). Large particles sediment quickly while very fine ash particles ($<$15 µm) have been found to have a residence time of days to weeks in the UT/LMS (Rose and Durant, 2009; Niemeier et al., 2009). During the first 24 h after an eruption a rapid decrease of the fine ash ($<$25 µm) content of the volcanic cloud have been observed, likely caused by aggregation into larger particles with higher settling velocities (Rose et al., 2001). After this initial phase, ash concentrations decrease more slowly together with concentrations of SO_2. Ash and SO_2 clouds can either be travelling collocated or separated in the atmosphere. Vertical separation occurs due to the eruption style or by different sedimentation velocity of ash and SO_2, and horizontal separation due to wind shear (Thomas and Prata, 2011). Although research has shown that fine ash particles are spread and deposited over large areas (Rose and Durant, 2009), we know little about the atmospheric fate (change in composition, lifetime) of volcanic particles in the micrometer size range.

Most research into atmospheric influence of volcanic eruptions is based on remote sensing from the surface or from satellite to follow the dispersal of volcanic SO_2 clouds or to investigate the influence of eruptions on the stratospheric aerosol load. The actual composition of volcanic aerosol has been investigated by aircraft-based measurements by Martinsson et al. (2009) and Schmale et al. (2010) following the Kasatochi eruption in 2008 and recently by Schumann et al. (2011) in the volcanic cloud from Eyjafjallajökull. However these studies only consider aerosol composition from

single eruptive events and do not address evolution of the composition of volcanic aerosol in the atmosphere. In the study by Martinsson et al. (2009) a subset of the data presented in this study was used to investigate the development of the sulphurous and carbonaceous components of the volcanically influenced aerosol.

Here we present and discuss the multi elemental composition of aerosol from three eruptions with VEI 4. The volcanic aerosol was collected between one and over 100 days after the eruptions, which provides a unique opportunity to investigate the evolution of the aerosol. Aerosol sampling and measurements of trace gases were performed by the CARIBIC (Civil Aircraft for Regular Investigation of the atmosphere Based on an Instrument Container) platform operating on a passenger aircraft (Brenninkmeijer et al., 2007; www.caribic-atmospheric.com).

2 Experimental methods

Samples of volcanic aerosol particles were obtained from the CARIBIC platform during regular long-distance passenger flights in the UT/LMS following large eruptions of the Kasatochi (2008) and Sarychev (2009) volcanoes, as well as during special flights at 4–12 km altitudes on 16 May and 19 May 2010, which were conducted to investigate the composition of the volcanic clouds produced by the Eyjafjallajökull eruption (Rauthe-Schöch et al., 2012). The CARIBIC measurement container is mounted in the forward cargo bay of a Lufthansa Airbus 340–600 during four sequential flights (Brenninkmeijer et al., 2007) on a monthly basis. From Frankfurt (Germany) destinations in North and South America, South Africa and South and East Asia are reached, thus covering a large geographical area mainly in the Northern Hemisphere. Instruments in the container automatically measure concentrations of many trace gases, aerosol number concentrations and the aerosol size distribution. In addition sampling of air and aerosol particles for laboratory analysis takes place. This study concentrates on volcanically influenced aerosol samples collected between 2008 and 2010, but also uses measurements of the background aerosol collected from 1999 to 2002 (Martinsson et al., 2005) and somewhat volcanically influenced samples from 2005 to 2008.

Aerosol particles of 0.08–2 µm aerodynamic diameter were collected in a multi-channel aerosol sampler on 0.2 µm thick polyimide foils (Nguyen et al., 2006) by impaction. The upper size limit is determined by a cyclone separator placed between the aerosol inlet and the sampler, and the lower limit by the cutoff diameter of the aerosol sampler. The sampler has 16 sampling channels with 14 for sequential collection and 2 for integral samples used to monitor contamination by comparing the integral samples to the sum of the sequential samples. The sampling time for each sequential sample is typically 100 min, corresponding to a flight distance of approximately 1500 km at cruising speed, and a sampling volume of approximately 0.25 m^3 STP (Standard Temperature (273 K) and Pressure (1013 hPa)). Sampling is suspended when the outside pressure is above 350 hPa. However, during the special flights through the Eyjafjallajökull volcanic cloud, collection of aerosol at lower altitudes was allowed and the sampling time was reduced to 50 min.

Aerosol samples were analyzed by accelerator-based techniques at the Lund ion beam analysis facility using two methods to obtain elemental concentrations: PIXE (Particle-Induced X-ray Emission) and PESA (Particle Elastic Scattering Analysis). In both methods the samples were mounted in a high vacuum chamber and irradiated with a beam of 2.55 MeV protons. Concentrations of elements with atomic numbers of 16 (*S*) or more were obtained by PIXE (Johansson and Campbell, 1988), and concentrations of hydrogen, carbon, nitrogen and oxygen by PESA (Nguyen and Martinsson, 2007). PESA was implemented for analysis of samples collected after 2005. Detection limits reached from several down to 0.1 ng m^{-3} STP, depending on element. The accuracy for elemental determination by both methods is estimated to be 10 % (Nguyen and Martinsson, 2007). The PIXE technique can also detect silicon (Si) when the concentrations are high, such as in aerosol samples which are dominated by aerosol particles from volcanic eruptions. In samples with low concentrations of Si problems arise due to interference with sulphur, which is often dominant. In samples with a S/Si ratio below a critical value, these effects have been corrected for, but for larger S/Si ratios corrections were not possible and the measured Si concentrations were excluded from the results. Elements that usually are below the detection limit (Sr, Zr) were detectable in samples collected in the Eyjafjallajökull volcanic clouds, using longer than usual analysis times.

We further use data from ozone measurements performed by two instruments on the CARIBIC platform. A UV-photometer is used for accurate determination of the ozone concentration by absorption of UV light and also serves as a standard for a fast chemiluminescence detector which enables ozone detection with high temporal resolution. The accuracy is estimated to be 0.3–1 % at typical mixing ratios at a measurement frequency of 10 Hz (Zahn et al., 2012).

Also measurements of SO_2 concentrations and particle size distributions during the flights in the volcanic cloud from Eyjafjallajökull were used in this study. Concentrations of SO_2 are obtained from the CARIBIC DOAS (Differential Optical Absorption Spectroscopy) instrument (Dix et al., 2009), detecting NO_2, HCHO, HONO, BrO, OClO, O_3, SO_2 and O_4 simultaneously by measuring scattered or reflected sunlight, collected with three telescopes pointing to $-82°$, $-10°$ and $+10°$ relative to the horizon, with a temporal resolution of 8 s. During the volcanic flights the instrument was only functioning properly on May 16, measuring in the $-82°$ and $-10°$ directions (Heue et al., 2011). Particle size distributions are measured with an integrated OPC (Optical Particle Counter), which measures particles with a diameter in the

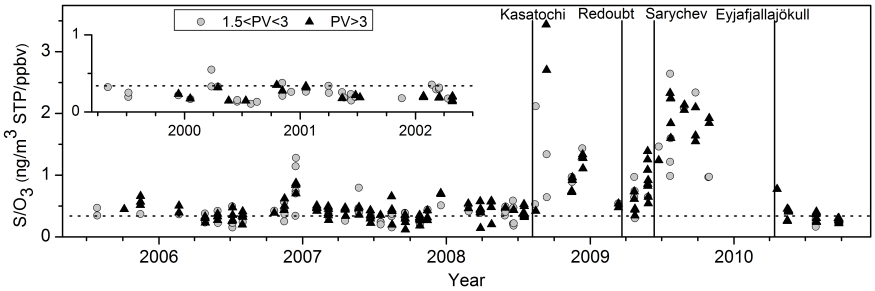

Fig. 1. Ratio of particulate sulphur to ozone concentration in aerosol samples collected in the tropopause region (grey circles) and the lowermost stratosphere (black triangles). The dotted line indicates the geometrical mean of samples collected before the eruption of Kasatochi in August 2008. The occasions of major eruptions are marked by vertical lines.

range of approximately 0.1–1µm. OPC measurements from the volcanic flight on 19 May were used in this study (Heue et al., 2011; Rauthe-Schöch et al., 2012). A time resolution of 3 min was used to calculate the OPC size distributions during this flight.

Potential vorticity (PV) at the location of the aircraft was used to determine whether collected particles were of tropospheric or stratospheric origin, the tropopause region was defined as the region between 1.5–3 PVU (Potential Vorticity Unit; $1\,\mathrm{PVU} = 10^{-6}\,\mathrm{K\,m^2\,kg^{-1}\,s^{-1}}$). PV was derived from archived ECMWF (European Centre for Medium-range Weather Forecast) analyses with a resolution of 1×1 degree in the horizontal direction and 91 vertical hybrid sigma-pressure model levels. To obtain PV at the aircraft position the PV values was interpolated linearly in latitude, longitude, log pressure and time for each sample.

The recent history of probed air was investigated by means of 5-days backward air mass trajectories, calculated every third minute along the flight route using the trajectory model TRAJKS (Scheele et al., 1996) and the horizontal and vertical wind fields provided by ECMWF.

Complementary to trajectory analysis, lidar measurements from the CALIPSO (Cloud-Aerosol Lidar and Infrared Pathfinder Satellite Observations) satellite were used. The lidar is equipped with a Nd:YAG laser producing highly polarized co-aligned beams with wavelengths of 532 and 1064 nm. Clouds and different types of aerosol particles can be identified since the shape and size of particles and droplets cause different scattering properties at these wavelengths (Winker et al., 2009).

3 Results

3.1 Identification of volcanic aerosol

A first indication of volcanic influence on CARIBIC UT/LMS aerosol samples is high concentrations of sulphur. These concentrations correspond to sulphate aerosol produced from SO_2 emitted during eruptions. Such influence is mainly seen in stratospheric samples, where the residence time of aerosol particles is long compared to the troposphere. In Fig. 1 the ratio of S/O_3 is used as an indicator of volcanic influence on stratospheric aerosol. Concentrations of S and O_3 show a correlation in absence of volcanic influence, since both sulphate and ozone are produced in the stratosphere with the aid of shortwave radiation. Consequently, high concentrations of sulphur are usually observed in association with downward transport in the stratosphere, together with elevated O_3 levels (Martinsson et al., 2009). Explosive volcanic eruptions disturb this ratio by injecting large amounts of additional sulphur. In Fig. 1, volcanic influence is indicated by elevated S/O_3 ratios following major eruptions (VEI 4) of the Kasatochi (52.18° N, 175.51° W, August, 2008), Redoubt (60.49° N, 152.74° W, March/April, 2009) and Sarychev (48.09° N, 153.20° E, June, 2009) volcanoes. The sulphurous and carbonaceous components of the aerosol related to the Kasatochi eruption were discussed in detail in the study by Martinsson et al. (2009). Fig. 1 shows that elevated S/O_3 ratios prevailed for at least four months after the Kasatochi eruption and were just reaching background levels when elevated concentrations of sulphur again were observed after the Redoubt and Sarychev eruptions in 2008. The small effects of the Eyjafjallajökull (63.63° N, 19.62° W) eruption in April/May 2010 can be explained by the fact that the emissions were poor in SO_2 and that only a small fraction of the plume reached the stratosphere (BGVN, 2010; Thomas and Prata, 2011). However,

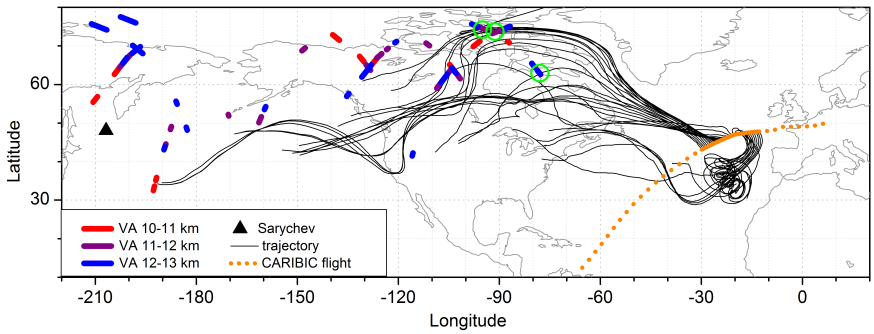

Fig. 2. Air-mass back-trajectories (thin black lines) calculated for one sample collected during the first CARIBIC flight from Frankfurt to Caracas at 23 June 2009 (orange dotted line) following the eruption of Sarychev, combined with volcanic aerosol (VA) layers at 10–13 km altitude (colored lines) obtained from CALIPSO lidar measurements at 21 June 2009. Green circles indicate where trajectories and aerosol layers intersect horizontally and vertically.

very high concentrations of crustal elements were found in three aerosol samples collected during the special flights on 16 May and 19 May 2010, strongly indicating volcanic influence. These samples were collected in the troposphere and are thus not included in Fig. 1, which only shows samples collected in the stratosphere or the tropopause region.

Further connection to the eruptions was established by using 5-days, and in one case 8-days, backward trajectory analysis for samples following the Kasatochi (Martinsson et al., 2009), Sarychev and Eyjafjallajökull eruptions. The first samples following the eruption of Redoubt were collected more than a month after the first explosion; hence trajectory analysis could not be used to verify volcanic origin. In addition, these samples show less elevation in their S/O_3 ratio than the samples following Sarychev and Kasatochi. The eruptions of Sarychev and Kasatochi emitted approximately 1.2 Tg (Haywood et al., 2010) and 2 Tg (Yang et al., 2010) of SO_2, respectively, into the atmosphere which can be compared to only 0.08 Tg by the eruption of Redoubt (Lopez et al., 2009). It is thus unlikely that the sulphate aerosol produced by the Redoubt eruption had large enough influence for a clear identification in sampled aerosol. It is possible that the elevated concentrations in the samples instead are due to downward transport of an upper branch of the aerosol produced in the preceding eruption of Kasatochi. The volcanically influenced aerosol also contains a crustal component, which will be further discussed in Sect. 3.2. Stratospheric concentrations of crustal elements such as potassium (K) and iron (Fe) show a seasonal dependence with high concentrations in spring (March to June) that seem to be connected with transport across the tropopause from the troposphere (Martinsson et al., 2005). The samples collected following the Redoubt eruption were collected at this time of the year; therefore it cannot be excluded that the crustal component of the aerosol has been transported from the boundary layer rather than been injected by the eruption. Due to the uncertainty of the source of the aerosol following the Redoubt eruption, these samples are excluded from further consideration.

Trajectory analysis performed for each of the three samples with large crustal components from the Eyjafjallajökull volcanic clouds showed that the sampled air had passed over the volcano. The transport time from the volcano to the aircraft position, and thus the age of the aerosol, was estimated to have been about 40 and 45 h for the samples collected May 16 and about 25 h for the sample collected May 19. The time for sampling within the volcanic cloud, and thereby the most likely transport path, was determined from peaks in the SO_2 and particle mass concentrations obtained from the CARIBIC DOAS and OPC instruments (Heue et al., 2011; Rauthe-Schöch et al., 2012).

Trajectory analysis conducted for samples following the Sarychev eruption was combined with lidar measurements from CALIPSO (Fig. 2). The large amount of sulphate produced during this eruption made it possible to follow the volcanic aerosol in the lidar measurements up to more than a month after the eruption. Aerosol layers detected by CALIPSO at an altitude between 10 and 13 km were identified, and this information was put together with the path of calculated air mass trajectories. By this method aerosol produced in the eruption earlier than the 5 days backward time span of the trajectories could be linked to the eruption, by investigating if the trajectories intersected these aerosol layers. Three samples collected during the first flight after the Sarychev eruption, taking place 12 days after the start of the eruption, had trajectories that clearly traversed aerosol layers.

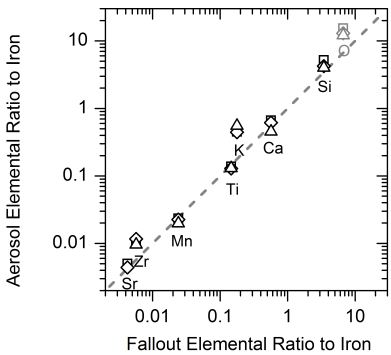

Fig. 3. Elemental ratio to iron in three aerosol samples (shown by different symbols) collected by the CARIBIC platform vs. fall out sample (SRG 5a, Sigmundsson et al., 2010). The dashed line indicates equal ratio. The oxygen content in the fallout sample is not measured and therefore indicated by grey symbols (see text for futher details).

Also samples collected during the next flight, 6 weeks after the eruption, could be connected to the aerosol produced in the eruption by this method, because the volcanic cloud could still be identified in the CALIPSO measurements.

3.2 Ash composition

The high concentrations of crustal elements in three of the samples collected during the Eyjafjallajökull eruption are important indications of volcanic origin. To further investigate this component of the aerosol it was compared to the composition of a fall-out sample of volcanic ash from the eruption site (Sigmundsson et al., 2010). The composition of erupted material can change over time and also with distance from the source due to fractionation and sedimentation (Carey and Sigurdsson, 1982). Thus it is not obvious that the fall out sample should be representative of the ash composition in the aerosol sample. Interestingly the composition for the three CARIBIC samples shows good agreement with the fallout sample for crustal elements (Fig. 3). Only the concentrations of potassium (K) and Zirconium (Zr) show some larger deviations. One explanation to the higher aerosol potassium (K) content in the CARIBIC samples could be fractioning in concentration between different sizes of ash particles in the samples analyzed, due to a larger surface area to mass ratio of small particles. Small ash particles remain in the plume longer than larger particles, and cool faster, which favors condensation of volatiles onto the smaller particles (Witham et al., 2005). Among the elements presented in Fig. 3, K happens to be the most volatile species found enriched in volcanic gases, due to degassing from the magma (Hinkley et al., 1994; Rubin, 1997). Also Zr was found in enhanced concentrations in deposits from a volcanic plume compared to the magma (Moune et al., 2005), indicating that also this element could have been abundant in the gas phase and condensed onto the ash particles.

The oxygen content (corrected for the amount of oxygen assumed bound to sulphurous aerosol in the form of sulphate) is also high compared to that of the fallout sample. The amount of oxygen in the fallout sample was not measured (indicated by grey symbols in Fig. 3), but are expressed as generalized oxygen proportions to the corresponding elements. It should however represent the approximate oxygen content, indicating that there is more oxygen in the aerosol samples. A likely explanation for the extra oxygen is that part of it is bound to the carbonaceous fraction of the aerosol (see Sect. 3.3).

The ash component of the Eyjafjallajökull aerosol is also similar to Earth's crustal composition (Rudnic and Fountain, 1995). Although analysis of rare elements such as the chalcophile metals (Bi, Cd, Cu, In, Pb and Tl), found in volcanic plumes from degassing of silicate melts (Hinkley et al., 1994), would be necessary to distinguish volcanic ash from this type of source, the high concentrations of crustal elements together with elevated sulphur concentrations in the aerosol samples are strong evidence of volcanic origin. On a final note, all of the elements, except manganese (Mn), in these three samples have the highest concentrations noted in the entire CARIBIC data set taken over a 10 years period. Therefore the composition of crustal elements in the Eyjafjallajökull aerosol samples (Fig. 3) is used here to define the ash component of volcanic aerosol.

The ash component of the sampled aerosol caused by the Kasatochi and Sarychev eruptions was identified by comparing it to the ash composition of the Eyjafjallajökull samples, as no fallout samples were available from these eruptions. Since this composition cannot be clearly distinguished from Earth's crustal composition, it was used as an indicator of volcanic ash in those samples with elevated S/O_3 levels, and for early collected samples, where trajectory analysis indicate volcanic origin. In addition the identified samples from the Kasatochi and Sarychev eruptions were collected in the summer to winter period when little influence of crustal particles in the LMS is seen (Martinsson et al., 2005). Only the three first samples following the Sarychev eruption were collected in spring when concentrations are usually elevated. For these samples however there is strong evidence of volcanic influence from the trajectory analysis and aerosol composition. Also meteoritic material can contribute to elements indicative of crustal material. Samples which are mainly influenced by meteorites can be identified by their Fe/Ni ratio (Kopp, 1997), which was used to exclude them from this study.

In Fig. 4 we include all samples having a crustal component classified to be of volcanic origin. These samples have a geometric residual sum of squares (RSS) in their elemental to iron ratios of less than two compared to the geometric mean

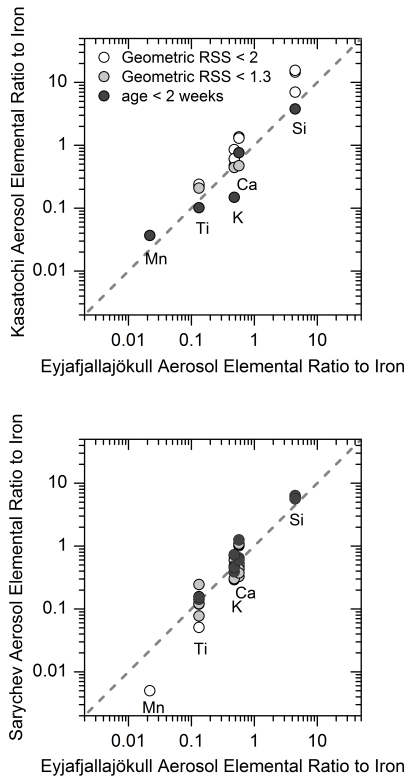

Fig. 4. Elemental ratio to iron in aerosol samples collected following eruptions of Sarychev and Kasatochi vs. geometric mean of volcanic aerosol collected in the volcanic cloud from Eyjafjallajökull. The dashed line indicates equal ratio. Samples with a Residual Sum of Squares (RSS) of less than two are included in the figures. Samples collected less than two weeks after the start of the eruptions are marked by dark circles.

of the Eyjafjallajökull aerosol samples (shown in Fig. 3). A minimum limit of at least three detected elements was applied to be able to examine the composition. Also the detection limit of undetected elements in relation to the iron content was taken into account. Samples were excluded if more than one of the elements K, Ca, Ti or Mn were missing even though they were expected to have had a concentration above the detection limit in relation to the content of Fe in the samples. One missing element was accepted to account for the risk of contamination due to mixing in the atmosphere and since it is likely that the composition of ash from different eruptions is not exactly the same. The ash composition depends on the magma type as well as on the absorption of volatiles onto the ash particles which is controlled by a number of factors such as eruption type, concentration of gases and particles and particle size (Witham et al., 2005). As can be seen from Fig. 4, Si is only represented in a few samples which is due to problems with interference with S as described in Sect. 2. Also Mn is represented only in a few samples since its concentrations in ash is low hence falling below the detection limit in samples of low ash content.

The composition of samples collected 8 days after the Kasatochi eruption and 12 days after the Sarychev eruption (indicated by dark circles in Fig. 4) show good agreement with the composition of the Eyjafjallajökull sample, except for lower concentrations of K in the sample from the Kasatochi eruption. Also samples collected one month or more after the eruptions are similar in their composition but ratios show more scatter. The larger deviations in composition in these samples indicate that the aerosols are more mixed and influenced by other sources. In addition changed emissions during the eruptions can cause variations in the composition of ash. The identified samples, classified as volcanic aerosol both by elevated S/O_3 ratios and composition of the crustal (ash) component, range in age between 8 to 128 days and 12 to 77 days from the start of the explosive phase of the Kasatochi and Sarychev eruptions, respectively. The length of these eruptions adds an uncertainty to these age estimates (1 and 5 days of explosive eruptions in the case of Kasatochi and Sarychev, respectively, BGVN, 2009; Waythomas et al., 2010).

3.3 Carbonaceous aerosol in volcanic clouds

The aerosol in volcanic clouds studied here contains a large fraction of carbonaceous aerosol. This has earlier been observed following the eruption of Kasatochi (Martinsson et al., 2009; Schmale et al., 2010) and in fresh volcanic clouds (Carn et al., 2011). A carbonaceous aerosol component has been observed in volcanic clouds from several volcanoes despite the fact that only for few volcanos lava can interact with carbonates in the crust prior to eruption. The volcanoes considered here do not belong to this category. This is corroborated by the measurements because the stoichiometric relations between carbon, oxygen, sulphur and ash elements in the sampled aerosol do not permit such an oxygen-rich form of carbon. Therefore explanations other than direct volcanic emissions need to be considered. One common source of carbonaceous material is combustion. Pyro-convection during forest fires can inject particles into the UT/LMS. However such events are not frequent and none one of the events identified in Guan et al. (2010) coincides with the eruptions studied here. Also no clearly elevated concentrations of K in excess of the ash concentration are seen in the samples, which would be expected from fires (Andreae et al., 1998). One

alternative explanation is the carbon content of the air that is entrained into the volcanic jet and lifted with the volcanic effluents. Mixing with air creates the buoyancy needed for the formation of a volcanic plume that can reach the stratosphere (Suzuki and Koyaguchi, 2010).

To obtain an estimate on the organic aerosol concentration in the region of the volcanoes studied, we consider the conditions in the boundary layer, where large numbers of observations are available. Boundary layer air contains high concentrations of carbonaceous aerosol from anthropogenic and from natural sources. Jimenez et al. (2009) report average urban organic aerosol concentrations up to 30 000 ng m^{-3} (Beijing, China) and, even at remote sites like Hyytiala, Finland the organic concentration exceeds one thousand ng m^{-3}. In a study focusing on the USA, urban regions average concentrations of several thousand ng m^{-3} were found and in rural areas the organic concentration was of the order 1000 ng m^{-3} (Hand et al., 2012). Interestingly, the Alaskan rural average organic aerosol concentration peaks in August, the month of the Kasatochi eruption, at approximately 3000 ng m^{-3}. Organic aerosol sources extend also to the oceans. Regional and seasonal variation in oceanic biological activity can be derived from SeaWiFS sensor on the OrbView2 satellite. The activity shows strong geographical and seasonal variations (Stramska, 2009). Measurements in Maze Head (Ireland) show organic aerosol concentration of several hundred ng m^{-3} connected with biologic activity in the ocean during spring to autumn (O'Dowd et al., 2004; Yoon et al., 2007). All three volcanoes studied here erupted in the biologically active part of the year. Modelling of the global distribution of yearly average organic aerosol with the ocean source included indicate high, to a large degree ocean-derived, organic aerosol concentration over the ocean surrounding island volcanoes Sarychev, Kasatochi and Eyjafjallajökull. For Sarychev a concentration of approximately 1000 ng m^{-3} was obtained, the same or somewhat lower for Kasatochi and a few hundred ng m^{-3} for Eyjafjallajökull (Spracklen et al., 2008). Additional organic material can be derived from gaseous precursors. Influence of volcanic halogen emissions on organic chemistry is important in the often OH poor volcanic clouds (von Glasow et al., 2009). In the volcanic cloud of Eyjafjalljökull chlorine radicals rapidly depleted organic trace gases to levels well below background concentrations (Baker et al., 2011). Such processes can further add particulate carbon to the volcanic cloud. The LMS particulate carbon concentration measured by CARIBIC outside directly injected volcanic clouds is approximately 100 ng m^{-3} at STP. In volcanic clouds the concentration typically is a few hundred ng m^{-3} STP, reaching more than one thousand ng m^{-3} STP in three observations of the volcanic cloud from Sarychev. The regional average particulate carbon concentrations in the boundary layer around the volcanoes studied here are thus comparable to the observations at high altitude (free troposphere, UT and LMS) in this study. Although sources in direct connection to the volcano, such as burning vegetation and sedimentary layers, also could contribute to carbonaceous aerosol, we hypothesize that organic material in entrained air constitutes a significant fraction of the particulate carbon observed in volcanic clouds.

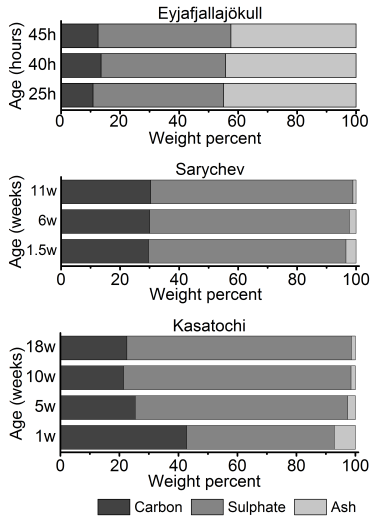

Fig. 5. Major components of aerosol samples collected following eruptions in Eyjafjallajökull, Sarychev and Kasatochi. Aerosol collected 1.5, 6 and 11 weeks after the eruption in Sarychev are shown as averages of 3, 6 and 2 samples respectivley. The composition of aerosol collected 18 weeks after the Kasatochi eruption are an average of 3 samples. The remaining aerosol compositions are each represented by only one sample. The carbonaceous fraction is averaged over all samples of the aerosol from Sarychev, see text for further details.

3.4 Major components

The main components of the samples classified as volcanic aerosol are carbon, sulphate and ash (Fig. 5). Samples influenced by Kasatochi and Sarychev are grouped with respect to age, where the compositions of aerosol collected at approximately the same time from the eruptions (i.e. from the same CARIBIC flight sequence) are presented as mean values. The carbonaceous component is presented as the mass of the measured carbon concentrations, since the stoichiometry of the carbon aerosol is unknown. The mass of sulphate (SO_4) was calculated by adding the amount of oxygen corresponding to the measured mass of sulphur, assuming that all sulphur is in the form of SO_4. In a similar manner the mass of the ash components in the Eyjafjallajökull samples were obtained by adding the mass of oxygen according to the fallout

sample presented in the table by Sigmundsson et al. (2010). Elements found in ash that could not be detected, primarily sodium (Na), magnesium (Mg), aluminum (Al) and phosphorus (P), were calculated according to the composition of the fallout sample using the relation to the iron content. The entire ash components of samples influenced by the Sarychev and Kasatochi eruptions were estimated based on their Fe content since many of the elements were below their detection limits. In these samples the mass of Fe, S and C was corrected for stratospheric background concentrations calculated as averages of samples with concentrations below the 95 percentile collected during the period from 1999 to the eruption of Kasatochi in August 2008. For S and C this correction was done with respect to the O_3 mixing ratios measured during the sampling time since they show a correlation with O_3. For Fe, the background correction was done with respect to season, divided into December–February, June–August and September–November (no samples were obtained in the period March–May). Since the samples from the Eyjafjallajökull eruption originate in lower altitudes than the CARIBIC platform usually measures, no such correction was made for them. Therefore C and S components should be considered to represent maximum estimates. However the concentrations were very high so the background influence most likely was small.

Figure 5 reveals that the samples collected following Eyjafjallajökull's eruption show little variation in their compositions, they mainly consist of ash and sulphate in about equal amounts. In contrast samples influenced by the eruptions of Kasatochi and Sarychev to a large extent consist of sulphate and carbon, while the ash component is well below 10 %. Even though the carbon and sulphate components comprise a smaller part of the mass in the Eyjafjallajökull samples compared to them influenced by the other two volcanoes, the respective concentrations are of similar magnitude as in the Kasatochi and Sarychev samples, while the ash component is approximately a factor of 10 higher in the Eyjafjallajökull samples.

The aerosol from Sarychev shows a strong dependence of the carbon-to-sulphur ratio on latitude, with increasing C/S ratio with increasing latitude, while the iron-to-sulphur ratio shows no such dependence (not shown). Possibly changing properties of the eruptions that persisted for several days and/or differences in carbonaceous aerosol precursor gases combined with transport patterns from the source could explain this latitudinal dependence. The time evolution of C can thus not be given. Instead the average C/S over the volcanically influenced samples taken from June to October 2009 was used to obtain the C component for Sarychev in Fig. 5. A decreasing fraction of ash with time is observed from Sarychev. The aerosol from the Kasatochi eruption has a simpler C-to-S relation. The sulphurous fraction shows an increase with time, whereas the ash and carbonaceous fractions decline.

3.5 Effects of sedimentation and coagulation on the composition evolution

Figure 5 shows that there is a change in the relations of the components of the Kasatochi and Sarychev volcanic aerosol with its age. The relative increase of SO_4 is likely caused by the transformation of SO_2 into SO_4 particles. Also higher rates of removal of ash (and C) might contribute to the observed pattern. Since all samples older than two weeks were taken in the stratosphere or the tropopause region, where little wet scavenging occurs, the solubility of the particles had no or only a small influence on the rate of deposition. The impact of different sedimentation rates of ash and SO_4 particles was investigated by estimating their settling velocity. In the computations the particle diameters that carry most of the mass according to the particle mass distributions were applied. For the sulphate particles, spherical droplets of sulphuric acid solution with a diameter of 0.6 µm (Martinsson et al., 2005) (corresponding to 0.76 µm aerodynamic diameter) and a density of 1600 kg m^{-3} (Yue et al., 1994) were used in the calculations. The diameter of the sulphate aerosol estimated by Martinsson et al. (2005) was obtained from the effective radius of stratospheric aerosol from lidar observations (Bauman et al., 2003) during a period with low volcanic activity. Thus the radius is underestimated for volcanic aerosol which usually exhibit larger diameters (Bauman et al., 2003; Deshler et al., 2003). Ash particles usually have substantially larger diameters (Schumann et al., 2011). The 2 µm aerodynamic diameter upper size limit of the aerosol sampler was thus used to estimate the upper limit in settling velocity of the ash. The thickness of the volcanic aerosol layers from the Sarychev and Kasatochi eruptions, through which the volcanic aerosol has to settle, was estimated by locating the altitude of volcanic aerosol during the first week after the eruptions using CALIPSO lidar measurements. After some time the identified volcanic aerosol layers are assumed to have been horizontally mixed and contributed to a more or less homogeneous aerosol layer. Therefore a cumulative altitude distribution of the volcanically influenced air from 10 km altitude and upwards was calculated, by summing all events when volcanic aerosol was observed at a certain altitude, see Fig. 6. According to the above method about 85 % of the identified aerosol following the Sarychev eruption was injected to a height between 10 and 15 km. Therefore a 5 km thick layer was assumed to have been produced. The aerosol layer formed by the Kasatochi eruption was less homogenous with 75 % of the aerosol located between 10–13 km and the remaining aerosol extending up to ∼20 km. During the 2 months we followed these volcanic clouds, the 2 µm ash particles fall a distance of about 10 % of the thickness of the volcanic aerosol layer produced by Sarychev and about 17 % of the lowest 3 km of the volcanic aerosol produced by Kasatochi. Since the aerosol samples were collected in the lower part of these layers, at 10–11.3 km, there should thus still be large amounts of 2 µm ash particles, originating in the

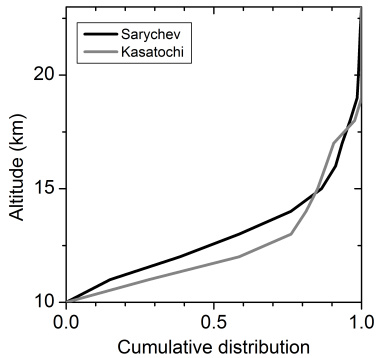

Fig. 6. Cumulative altitude distributions of volcanic injections above 10 km the first week after the Sarychev and Kasatochi eruptions. The distributions was deduced from the number of observations of volcanic aerosol layers in CALIPSO lidar measurements as a function of altitude, see the text for further details.

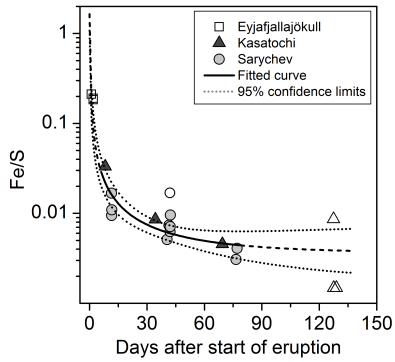

Fig. 7. Mass ratio of iron to sulphur in aerosol samples influenced by three volcanoes (marked by different symbols) vs. time since the start of the eruptions. The line shows a fit to the Fe/S ratio for the samples influenced by the Sarychev and Kasatochi eruptions. Samples shown with open symbols have been excluded from the fit.

upper part of the volcanic aerosol layers. Bearing in mind that the sulphate sedimentation was underestimated and that of ash was overestimated, this simple estimation suggests that the difference in deposition velocity between ash and sulphate particles only has minor importance for the relation between the measured ash and sulphate concentrations on the timescale considered here.

In addition, coagulation of particles needs to be considered as it can enhance the sedimentation velocity and can grow particles to diameters outside the collection range of the sampler. However the paticle concentrations in samples collected more than one week after the Kasatochi and Sarychev eruptions are low, $\sim$22 ng m^{-3} ash and $\sim$156 ng m^{-3} SO_4 in the first sample collected following the Kasatochi eruption. Calculations based on thermal coagulation (Hinds, 1999), points to that the effects of particle coagulation is very small in the concentrations encountered in these volcanic clouds. In order to simplify the estimates of coagulation, the case of monodispersed ash and sulphate particles of the same properties as described for the sedimentation calculations were used. The resulting change in the number concentration both from coagulation of ash and of sulphate particles is less than 1 % during the 2 months considered. Coagulation thus is estimated to be of minor importance because the aerosol concentrations in the observed clouds are too low for that process to be efficient.

3.6 Sulphur dioxide conversion rate in volcanic clouds

To further evaluate the evolution of the volcanic aerosol the sulphate and ash components were studied more in detail. In Fig. 7 the ratio of Fe/S shows the relation between the ash and sulphate components as a function of time after the eruptions. As the difference in sedimentation velocity of ash and sulphate particles in the 0.08–2 µm size range were estimated to be of small importance, the decreaseing trend of Fe/S is likely explained by the conversion rate of SO_2 into sulphate aerosol. The residence time of SO_2 can thus be estimated from the decrease in the Fe/S ratios. From the reaction of SO_2 with OH, which mainly controls the conversion into sulphate aerosol (Weisenstein et al., 1997), an exponential decay rate of the number concentrations of SO_2 can be derived (Seinfeld and Pandis, 2006);

$$C^n_{SO_2}(t) = C^n_{SO_2}(0) \cdot e^{-kt}, \quad (1)$$

where k is the loss rate constant. Since the depletion rate $C^n_{SO_2}(t)/dt$ of SO_2 molecules equals the production rate of SO_4, the mass concentration ratio of Fe and S can be expressed as;

$$\frac{C^n_{Fe}}{C^n_{SO_4}(t)} \propto \frac{C^m_{Fe}}{C^m_S(t)} = \frac{A}{1-e^{-kt}}, \quad (2)$$

where C^n and C^m denotes number respective mass concentrations. The constant A is the mass concentration ratio of Fe from ash and total S from SO_2 that is eventually converted to sulphate. Since the composition of volcanic aerosol depends on the eruption characteristics (magma composition, explosivity, temperature, gas release etc., Mather et al., 2003) aerosol from different eruptive events cannot be expected to have similar Fe/S ratios. Still most samples collected following the Sarychev and Kasatochi eruptions show large similarities in their Fe/S ratio with respect to age. Thus Eq. (2) was fitted to the Fe/S ratio in Sarychev and Kasatochi

samples, assuming similar emission ratio of Fe/S in the eruptions. The logarithm of the Fe/S ratios was used in the fitting to avoid over representing the large ratios appearing the first two weeks after the eruptions. Changed emissions during the eruptions as well as atmospheric conditions that affect mixing and transport also influence the composition of the aerosol. As stated earlier, the ash component was rather simple to recognize within two weeks after the eruption, and thereafter it was more influenced by other sources. Such influences could explain some of the deviations from the decreasing trend in Fig. 7. Also deviations from the average background concentrations used in the corrections have to be considered. Samples taken more than 100 days after the eruptions show large deviations from the general tendency, probably as the result of dilution of the volcanic cloud and mixing, and are excluded from the fit. One younger Sarychev sample shows large deviation compared to other samples collected at approximately the same time, and has therefore also been excluded.

Samples from the Eyjafjallajökull volcanic cloud was not included in this fit. As was seen in Fig. 5, the relative concentration of sulphate is low in samples from the Eyjafjallajökull eruption compared to the samples following Sarychev and Kasatochi, likely due to the large emissions of fine grained ash in the Eyjafjallajökull eruption (BGVN, 2010). In addition these samples were collected close to the eruption which implicates short time for conversion of SO_2 into sulphate aerosol. However the residence time of SO_2 in the troposphere where these samples were collected are considerably shorter than in the stratosphere, only hours to few days (McGonigle et al., 2004; Carn et al., 2011), leading to rapid conversion into sulphate aerosol. These samples should therefore not follow the same decay as those collected at higher altitudes. Also no background correction was made for the Eyjafjallajökull samples as mentioned earlier. An additional important aspect is initial processes in the volcanic cloud that lead to growth by aggregation and rapid sedimentation of fine ash particles (Rose et al., 2001). Such processes could be of importance during sampling in the Eyjafjallajökull volcanic clouds because they were only 1–2 days old.

The residence time of SO_2 (1/k) in the tropopause region and LMS after the eruptions of Kasatochi and Sarychev was from the fitted curve estimated to be 45 ± 22 days (mean $\pm$ standard error). The value of A, representing the ratio of total Fe and S was estimated to 0.0036 corresponding to a final ash/SO_4 mass ratio of approximately 0.016 for particles in the 0.08–2 µm size range considered here.

4 Discussion

Previous estimates of residence time of SO_2 for the volcanic cloud of Kasatochi span from 9 days (Krotkov et al., 2010), to 18 days (Karagulian et al., 2010) and up to 62 days (Jurkat et al., 2010). The residence time of SO_2 following the Sarychev eruption has been estimated to 11 days (Haywood et al., 2010). Thus there is a large spread in estimated residence times. Estimations of the conversion rate of SO_2 following the Pinatubo eruption are less dispersed; 35 days (Bluth and Doiron, 1992), 33 days (Read et al., 1993) and 25 ± 5 as well as 23 ± 5 days (Guo et al., 2004). Except in the work by Guo et al. (2004), uncertainty of the estimated residence time has not been given. Thus it is difficult to compare the validity of our estimate to others. While earlier estimates obtained for the Pinatubo eruption (satellite based) and by aircraft observations for Kasatochi (Jurkat et al., 2010) lie within our uncertainty limits, the results based on satellite observations of the Kasatochi and Sarychev volcanic clouds are considerably lower. The spread in estimated residence time, both between similar and dissimilar methods, underscore that it is valuable to perform calculations of SO_2 residence time in different volcanic clouds and by different methods, and not only rely on the more consistent results from the Pinatubo eruption.

For the Kasatochi and Sarychev eruptions, it seems like the aircraft observations of volcanic clouds (Jurkat et al., 2010; this study) result in longer residence times than the satellite based measurements (see above). Haywood et al. (2010) argue that the detection limit of the IASI satellite measurements could lead to somewhat underestimated residence time (up to 50 %). Measurements following the Kasatochi eruption based on particle detection by OSIRIS on board the satellite Odin corresponded to a SO_2 residence time of approximately 30 days (Bourassa et al., 2010). This points to that the difference between the Kasatochi measurements is connected to whether the measurements are based on detection of SO_2 or particles rather than satellite or in situ. Heard et al. (2012) modelled SO_2 and aerosol optical depth (AOD). Their results were compared with satellite observations from IASI and OSIRIS for the eruption of Sarychev. In their model SO_2 remained longer and the particle concentration rose faster than in the observations. The detection limit of the satellite SO_2 retrieval was suggested as a possible cause for the faster decrease of SO_2 in observed data, while for the AOD the inadequately modelling of nucleation were proposed as the main reason for the earlier peak of the AOD in the model as particle reached the optically active accumulation mode to fast.

Aircraft measurements suffer from the difficulties to follow a volcanic cloud as it ages, and the sampling of volcanically influenced air at one position cannot be guaranteed to be representative for the whole volcanic cloud. The methodology used in this study demands that the ratio of ash and SO_2 injected into the UT/LMS by the volcanoes were constant and that influence from coagulation has declined before the first measurement used in the estimate of the residence time. These assumptions are likely simplifications, where the former causes scatter in the data whereas coagulation would tend to cause a shorter estimate of residence time than the actual one. One important difference between

the aircraft and satellite observations is that while the in-situ measurements are constrained to a well-defined altitude, the remote sensing SO_2 instruments observes the whole atmospheric column. The altitude of the Kasatochi plume is estimated to 12.5 ± 4 km by Karagulian et al. (2010) and 10–12 km by Krotkov et al. (2010). Mixing with tropospheric air, where residence times are shorter, cannot be excluded and would have affected the satellite based estimates. Krotkov et al. (2010) suggest the rather low altitude of the Kasatochi plume and the dynamic UT/LMS in the extra tropics as an explanation for why they derive a shorter SO_2 residence time (9 days) compared to the one observed after the Pinatubo eruption, that injected material well into the stratosphere.

Finally differences in the actual residence times following the eruptions of Sarychev and Kasatochi compared to that following Pinatubo may well be caused by differences in the abundance of OH. The latitudinal dependence could thereby be of significance as Pinatubo is located in the tropics (15.13° N, 120.35° E) where OH concentrations are higher than at the mid-latitudes (Gross and Khalil, 2000), where the Kasatochi and Sarychev volcanoes are located, leading to longer residence times. Since the eruptions occurred in June (Pinatubo and Sarychev) and August (Kasatochi), there should be negligible differences in the OH concentration due to seasonal variation in the UV flux. An important factor is likely to be the altitude for which these estimates were made, since OH concentrations increase strongly above ∼20 km (Gross and Khalil, 2000). The results obtined in this study and by Jurkat et al. (2010) are based on aircraft measurements at altitudes of 7–12 km, which is just below the center of the volcanic cloud as observed by sattelites. The volcanic cloud that was observed by satellite following the Pinatubo eruption was injected well into the stratosphere to altitudes of ∼25 km (Guo et al., 2004). Thus the longer residence times meassured by aircraft might be typical for the altitude and latitude considered.

5 Conclusions

Volcanic aerosol have been collected in the tropopause region and lowermost stratosphere following major eruptions of the Kasatochi and Sarychev volcanoes, and in the troposphere in the volcanic cloud from the Eyjafjallajökull eruption in 2010. The main components of the volcanic aerosol were found to be sulphate, ash and carbonaceous material, where the source of the latter is proposed to be low-altitude tropospheric air that is entrained into the volcanic jet and plume. In samples collected in the volcanic cloud from Eyjafjallajökull ash and sulphate contributed approximately equal amounts to the total aerosol mass (∼45 %). In samples collected following Sarychev and Kasatochi ash was a minor part of the aerosol (1–7 %) while sulphate (50–77 %) and carbon (21–43 %) were dominating. These fractions changed with the age of the aerosol. In this study we could follow the evolution of volcanic aerosol during more than twice the residence time of SO_2 in a volcanic cloud. The first samples collected 1 and 1.5 weeks after the eruption of Kasatochi and Sarychev consisted of 14 % and 5 % ash relative to the mass of sulphate, respectively. After 10 and 11 weeks the ash component was still identifiable, but had decreased to about 2 % relative to the sulphate mass for both eruptions. The ash/sulphate ratio of aerosol collected following the Kasatochi and Sarychev eruptions showed a decreasing trend. From this decay the residence time of SO_2 in the tropopause region and lowermost stratosphere was estimated to be 45 ± 22 days. Previous estimates of SO_2 residence time following the Kasatochi and Sarychev eruptions by different methods based on SO_2 or sulphate detection as well as in situ or remote sensing from satellites, are of the same magnitude although distributed over a rather wide range from 9 to 62 days. In contrast more consistent residence times was observed from satellite measurements following the large eruption of Pinatubo in 1991. This emphasizes that it is more difficult to measure the conversion rates of SO_2 after intermediate eruptions. The difficulties could be connected with variability in composition, detection problem and/or the altitude distribution of SO_2 after the eruptions.

Acknowledgements. We thank all members of the CARIBIC team, especially C. Koeppel, D. S. Scharffe and S. Weber. The collaboration with Lufthansa and Lufthansa Technik is gratefully acknowledged. Aerosol measurements from CALIPSO were produced by NASA Langley Research Center. Financial support from the Swedish Research Council and the Swedish Research Council for Environments, Agricultural Sciences and Spatial Planning under grants 621-2007-4639 and 214-2009-613 is gratefully acknowledged.

Edited by: W. Birmili

References

Ammann, C. M., Meehl, G. A., Washington, W. M., and Zender, C. S.: A monthly and latitudinally varying volcanic forcing dataset in simulations of 20th century climate, Geophys. Res. Lett., 30, 1657–1661, doi:10.1029/2003GL016875, 2003.

Andreae, M. O., Wienhold, F. G., Zenker, T., Andreae, T. W., Annegarn, H., Beer, J., Cachier, H., le Canut, P., Elbert, W., Maenhaut, W., and Salma, I.: Airborne studies of aerosol emissions from savanna fires in southern Africa: 2. Aerosol chemical composition, J. Geophys Res., 103, 32119–32128, doi:10.1029/98JD02280, 1998.

Baker, A. K., Rauthe-Schöch, A., Schuck, T. J., Brenninkmeijer, C. A. M., van Velthoven, P. F. J., Wisher, A., and Oram, D. E.: Investigation of chlorine radical chemistry in the Eyjafjallajökull volcanic plume using observed depletions in non-methane hydrocarbons, Geophys. Res. Lett., 38, L13801, doi:10.1029/2011GL047571, 2011.

Bauman, J. J., Russell, P. B., Geller, M. A., and Patrick, H.: A stratospheric aerosol climatology from SAGE II and CLAES measurements: 2. Results and comparisons, 1984–1999, J. Geophys. Res., 108, 4383, doi:10.1029/2002jd002993, 2003.

BGVN, B. o. t. G. V. N.: Widespread plumes from large 11–16 June 2009 eruption34:06, 2009.

BGVN, B. o. t. G. V. N.: Large explosions from the summit crater; ash plumes close airspace in Europe, 35:04, 2010.

Bluth, G. J. S. and Doiron, S. D.: Global tracking of the SO2 clouds from the june, 1991 mount pinatubo eruptions, Geophys. Res. Lett., 19, 51–154, 1992.

Bourassa, A. E., Degenstein, D. A., Elash, B. J., and Llewellyn, E. J.: Evolution of the stratospheric aerosol enhancement following the eruptions of Okmok and Kasatochi: Odin-OSIRIS measurements, J. Geophys. Res., 115, D00L03, doi:10.1029/2009jd013274, 2010.

Brenninkmeijer, C. A. M., Crutzen, P., Boumard, F., Dauer, T., Dix, B., Ebinghaus, R., Filippi, D., Fischer, H., Franke, H., Friess, U., Heintzenberg, J., Helleis, F., Hermann, M., Kock, H. H., Koeppel, C., Lelieveld, J., Leuenberger, M., Martinsson, B. G., Miemczyk, S., Moret, H. P., Nguyen, H. N., Nyfeler, P., Oram, D., O'Sullivan, D., Penkett, S., Platt, U., Pupek, M., Ramonet, M., Randa, B., Reichelt, M., Rhee, T. S., Rohwer, J., Rosenfeld, K., Scharffe, D., Schlager, H., Schumann, U., Slemr, F., Sprung, D., Stock, P., Thaler, R., Valentino, F., van Velthoven, P., Waibel, A., Wandel, A., Waschitschek, K., Wiedensohler, A., Xueref-Remy, I., Zahn, A., Zech, U., and Ziereis, H.: Civil Aircraft for the regular investigation of the atmosphere based on an instrumented container: The new CARIBIC system, Atmos. Chem. Phys, 7, 4953–4976, doi:10.5194/acp-7-4953-2007, 2007.

Carey, S. N. and Sigurdsson, H.: Influence of particle aggregation on deposition of distal tephra from the may 18, 1980, eruption of Mount St. Helens volcano, J. Geophys. Res., 87, 7061–7072, 1982.

Carn, S. A., Krueger, A. J., Krotkov, N. A., Yang, K., and Evans, K.: Tracking volcanic sulfur dioxide clouds for aviation hazard mitigation, Nat. Hazards, 51, 325–343, doi:10.1007/s11069-008-9228-4, 2009.

Carn, S. A., Froyd, K. D., Anderson, B. E., Wennberg, P., Crounse, J., Spencer, K., Dibb, J. E., Krotkov, N. A., Browell, E. V., Hair, J. W., Diskin, G., Sachse, G., and Vay, S. A.: In situ measurements of tropospheric volcanic plumes in Ecuador and Colombia during TC4, J. Geophys. Res., 116, D00J24, doi:10.1029/2010jd014718, 2011.

Casadevall, T. J.: The 1989–1990 eruption of Redoubt Volcano, Alaska: impacts on aircraft operations, J. Volcanol. Geoth. Res., 62, 301–316, doi:10.1016/0377-0273(94)90038-8, 1994.

Chin, M. and Davis, D. D.: A reanalysis of carbonyl sulfide as a source of stratospheric background sulfur aerosol, J Geophys. Res., 100, 8993–9005, 1995.

Crutzen, P. J.: The possible importance of CSO for the sulfate layer of the stratosphere, Geophys. Res. Lett., 3, 73–76, doi:10.1029/GL003i002p00073, 1976.

Cziczo, D. J., Thomson, D. S., and Murphy, D. M.: Ablation, Flux, and Atmospheric Implications of Meteors Inferred from Stratospheric Aerosol, Science, 291, 1772–1775, 2001.

Deshler, T.: A review of global stratospheric aerosol: Measurements, importance, life cycle, and local stratospheric aerosol, Atmos. Res., 90, 223–232, doi:10.1016/j.atmosres.2008.03.016, 2008.

Deshler, T., Hervig, M., Hofmann, D., Rosen, J., and Liley, J.: Thirty years of in situ stratospheric aerosol size distribution measurements from Laramie, Wyoming (41° N), using balloon-borne instruments, J. Geophys. Res., 108, 4167, doi:10.1029/2002JD002514, 2003.

Dix, B., Brenninkmeijer, C. A. M., Frieß, U., Wagner, T., and Platt, U.: Airborne multi-axis DOAS measurements of atmospheric trace gases on CARIBIC long-distance flights, Atmos. Meas. Tech., 2, 639–652, doi:10.5194/amt-2-639-2009, 2009.

Ferry, G. V., Pueschel, R. F., Strawa, A. W., Kondo, Y., Howard, S. D., Verma, S., Mahoney, M. J., Bui, T. P., Hannan, J. R., and Fuelberg, H. E.: Effects of aircraft on aerosol abundance in the upper troposphere, Geophys. Res. Lett., 26, 2399–2402, doi:10.1029/1999GL900445, 1999.

Fromm, M., Bevilacqua, R., Stocks, B., and Servranckx, R.: New Directions: Eruptive Transport to the Stratosphere: Add Fire-Convection to Volcanoes, Atmos. Environ., 38, 163–165, doi:10.1016/j.atmosenv.2003.10.001, 2004.

Fromm, M., Shettle, E. P., Fricke, K. H., Ritter, C., Trickl, T., Giehl, H., Gerding, M., Barnes, J. E., Neill, M. O., Massie, S. T., Blum, U., McDermid, I. S., Leblanc, T., and Deshler, T.: Stratospheric impact of the Chisholm pyrocumulonimbus eruption: 2. Vertical profile perspective, J. Geophys. Res., 113, D08203, doi:10.1029/2007jd009147, 2008.

Gross, G. W. and Khalil, M. A. K.: OH concentrations from a general circulation model coupled with a tropospheric chemistry model, Chemosphere – Global Change Science, 2, 191–206, doi:10.1016/s1465-9972(99)00054-9, 2000.

Guan, H., Esswein, R., Lopez, J., Bergstrom, R., Warnock, A., Follette-Cook, M., Fromm, M., and Iraci, L. T.: A multi-decadal history of biomass burning plume heights identified using aerosol index measurements, Atm. Chem. Phys., 10, 6461–6469, doi:10.5194/acp-10-6461-2010, 2010.

Guo, S., Bluth, G., J. S., Rose, W. I., Watson, I. M., and Prata, A. J.: Re-evaluation of SO2 release of the 15 June 1991 Pinatubo eruption using ultraviolet and infrared satellite sensors, Geochem. Geophy. Geosy., 5, Q04001, doi:10.1029/2003GC000654, 2004.

Hand, J. L., Schichtel, B. A., Pitchford, M., Malm, W. C., and Frank, N. H.: Seasonal composition of remote and urban fine particulate matter in the United States, J. Geophys. Res., 117, D05209, doi:10.1029/2011JD017122, 2012.

Haywood, J. M., Clerbaux, C., Coheur, P., Degenstein, D., Braesicke, P., Jones, A., Clarisse, L., Bourassa, A., Barnes, J., Telford, P., Bellouin, N., Boucher, O., and Agnew, P.: Observations of the eruption of the Sarychev volcano and simulations using the HadGEM2 climate model, J. Geophys. Res., 115, D21212, doi:10.1029/2010JD014447, 2010.

Heard, I. P. C., Manning, A. J., Haywood, J. M., Witham, C., Redington, A., Jones, A., Clarisse, L., and Bourassa, A.: A comparison of atmospheric dispersion model predictions with observations of SO_2 and sulphate aerosol from volcanic eruptions, J. Geophys. Res., 117, D00U22, doi:10.1029/2011JD016791, 2012.

Heiken, G. and Wohletz, K.: Volcanic ash, University of California Press, Berkeley, 1985.

Heue, K. P., Brenninkmeijer, C. A. M., Baker, A. K., Rauthe-Schoch, A., Walter, D., Wagner, T., Hormann, C., Sihler, H., Dix, B., Friess, U., Platt, U., Martinsson, B. G., van Velthoven, P.

F. J., Zahn, A., and Ebinghaus, R.: SO2 and BrO observation in the plume of the Eyjafjallajokull volcano 2010: CARIBIC and GOME-2 retrievals, Atmos. Chem. Phys, 11, 2973-2989, doi:10.5194/acp-11-2973-2011, 2011.

Hinds, W. C.: Aerosol technology: properties, behavior, and measurement of airborne particles, Book, John Wiley & Sons, New York, USA, 1999.

Hinkley, T. K., Le Cloarec, M. F., and Lambert, G.: Fractionation of families of major, minor, and trace metals across the melt-vapor interface in volcanic exhalations, Geochim. Cosmochim. Ac., 58, 3255–3263, doi:10.1016/0016-7037(94)90053-1, 1994.

Hofmann, D., Barnes, J., O'Neill, M., Trudeau, M., and Neely, R.: Increase in background stratospheric aerosol observed with lidar at Mauna Loa Observatory and Boulder, Colorado, Geophys. Res. Lett., 36, L15808, doi:10.1029/2009GL039008, 2009.

IPCC: Climate Change 2007: The Physical Science Basis. Contribution of Working Group I to the Fourth Assessment Report of the Intergovernmental Panel on Climate Change, edited by: Solomon, S., Qin, D., Manning, M., Chen, Z., Marquis, M., Averyt, K. B., Tignor, M., and Miller, H. L., Cambridge University Press, Cambridge, United Kingdom and New York, NY, USA, 2007.

Jimenez, J. L., Canagaratna, M. R., Donahue, N. M., Prevot, A. S., Zhang, Q., Kroll, J. H., DeCarlo, P. F., Allan, J. D., Coe, H., Ng, N. L., Aiken, A. C., Docherty, K. S., Ulbrich, I. M., Grieshop, A. P., Robinson, A. L., Duplissy, J., Smith, J. D., Wilson, K. R., Lanz, V. A., Hueglin, C., Sun, Y. L., Tian, J., Laaksonen, A., Raatikainen, T., Rautiainen, J., Vaattovaara, P., Ehn, M., Kulmala, M., Tomlinson, J. M., Collins, D. R., Cubison, M. J., Dunlea, E. J., Huffman, J. A., Onasch, T. B., Alfarra, M. R., Williams, P. I., Bower, K., Kondo, Y., Schneider, J., Drewnick, F., Borrmann, S., Weimer, S., Demerjian, K., Salcedo, D., Cottrell, L., Griffin, R., Takami, A., Miyoshi, T., Hatakeyama, S., Shimono, A., Sun, J. Y., Zhang, Y. M., Dzepina, K., Kimmel, J. R., Sueper, D., Jayne, J. T., Herndon, S. C., Trimborn, A. M., Williams, L. R., Wood, E. C., Middlebrook, A. M., Kolb, C. E., Baltensperger, U., and Worsnop, D. R.: Evolution of organic aerosols in the atmosphere, Science, 326, 1525–1529, doi:10.1126/science.1180353, 2009.

Johansson, S. A. E. and Campbell, J. L.: PIXE: A novel technique for elemental analysis, John Wiley & Sons, New York, 1988.

Junge, C. E., Chagnon, C. W., and Manson, J. E.: A Worldwide Stratospheric Aerosol Layer, Science, 133, 1478–1479, doi:10.1126/science.133.3463.1478-a, 1961.

Jurkat, T., Voigt, C., Arnold, F., Schlager, H., Aufmhoff, H., Schmale, J., Schneider, J., Lichtenstern, M., and Dornbrack, A.: Airborne stratospheric ITCIMS measurements of SO_2, HCl, and HNO_3 in the aged plume of volcano Kasatochi, J. Geophys. Res., 115, D00L17, doi:10.1029/2010JD013890, 2010.

Jäger, H.: Long-term record of lidar observations of the stratospheric aerosol layer at Garmisch-Partenkirchen, J. Geophys. Res., 110, D08106, doi:10.1029/2004jd005506, 2005.

Karagulian, F., Clarisse, L., Clerbaux, C., Prata, A. J., Hurtmans, D., and Coheur, P. F.: Detection of volcanic SO2, ash, and H2SO4 using the Infrared Atmospheric Sounding Interferometer (IASI), J. Geophys. Res., 115, D00L02, doi:10.1029/2009JD012786, 2010.

Kjellström, E., Feichter, J., Sausenc, R., and Hein, R.: The contribution of aircraft emissions to the atmospheric sulfur budget, Atmos. Environ., 33, 3455–3465, 1999.

Kopp, E.: On the abundance of metal ions in the lower ionosphere, J. Geophys. Res., 102, 9667–9674, doi:10.1029/97ja00384, 1997.

Krotkov, N. A., Schoeberl, M. R., Morris, G. A., Carn, S., and Yang, K.: Dispersion and lifetime of the SO_2 cloud from the August 2008 Kasatochi eruption, J. Geophys. Res., 115, D00L20, doi:10.1029/2010JD013984, 2010.

Köppe, M., Hermann, M., Brenninkmeijer, C. A. M., Heintzenberg, J., Schlager, H., Schuck, T., Slemr, F., Sprung, D., Velthoven, P. F. J. v., Wiedensohler, A., Zahn, A., and Ziereis, H.: Origin of aerosol particles in the mid-latitude and subtropical upper troposphere and lowermost stratosphere from cluster analysis of CARIBIC data, Atmos. Chem. Phys., 9, 8413–8430, doi:10.5194/acp-9-8413-2009, 2009.

Lopez, T. M., Carn, S. A., Webley, P., and Pfeffer, M. A.: Evaluation of satellite derived sulfur dioxide measurements for volcano monitoring during the 2009 Redoubt eruption American Geophysical Union, Fall Meeting 2009, abstract #V51F-03, 2009.

Martinsson, B. G., Nguyen, H. N., Brenninkmeijer, C. A. M., Zahn, A., Heintzenberg, J., Hermann, M., and Velthoven, P. F. J. v.: Characteristics and origin of lowermost stratospheric aerosol at northern midlatitudes under volcanically quiescent conditions based on CARIBIC observations, J. Geophys. Res., 110, D12201, doi:10.1029/2004JD005644, 2005.

Martinsson, B. G., Brenninkmeijer, C. A. M., Carn, S. A., Hermann, M., Heue, K. P., Velthoven, P. F. J. v., and Zahn, A.: Influence of the 2008 Kasatochi volcanic eruption on sulfurous and carbonaceous aerosol constituents in the lower stratosphere, Geophys. Res. Lett., 36, L12813, doi:10.1029/2009gl038735, 2009.

Mather, T. A., Pyle, D. M., and Oppenheimer, C.: Tropospheric Volcanic Aerosol, Geophys. Monogr., 139, 189–212, doi:10.1029/139GM12, 2003.

McCormick, M. P., Thomason, L. W., and Trepte, C. R.: Atmospheric effects of the Mt Pinatubo eruption, Nature, 373, 399–404, doi:10.1038/373399a0, 1995.

McGonigle, A. J. S., Delmelle, P., Oppenheimer, C., Tsanev, V. I., Delfosse, T., Williams-Jones, G., Horton, K., and Mather, T. A.: SO_2 depletion in tropospheric volcanic plumes, Geophys. Res. Lett., 31, L13201, doi:10.1029/2004gl019990, 2004.

Moune, S., Gauthier, P.-J., Gislason, S. R., and Sigmarsson, O.: Trace element degassing and enrichment in the eruptive plume of the 2000 eruption of Hekla volcano, Iceland, Geochim. Cosmochim. Ac., 70, 461–479, doi:10.1016/j.gca.2005.09.011, 2005.

Murphy, D. M., Thomson, D. S., and Mahoney, M. J.: In situ measurements of organics, meteoritic matierial, mercury, and other elements in aerosols at 5 to 19 kilometers, Science, 282, 1664–1669, 1998.

Murphy, D. M., Cziczo, D. J., Hudson, P. K., and Thomson, D. S.: Carbonaceous material in aerosol particles in the lower stratosphere and tropopause region, J. Geophys. Res., 112, D04203, doi:10.1029/2006JD007297, 2007.

Myhre, G., Berglen, T. F., Myhre, C. E. L., and Isaksen, I. S. A.: The radiative effect of the anthropogenic influence on the stratospheric sulfate aerosol layer, Tellus B, 56, 294–299, doi:10.1111/j.1600-0889.2004.00106.x, 2004.

Newhall, C. G. and Self, S.: The Volcanic Explosivity Index (VEI): An Estimate of Explosive Magnitude for Historical Volcanism, J. Geophys. Res., 87, 1231–1238, doi:10.1029/JC087iC02p01231,

1982.
Nguyen, H. N. and Martinsson, B. G.: Analysis of C, N and O in aerosol collected on an organic backing using internal blank measurements and variable beam size, Nucl. Instrum. Methods, 264, 96–102, 10.1016/j.nimb.2007.08.001, 2007.
Nguyen, N. H., Gudmundsson, A., and Martinsson, B.: Design and calibration of a multi-channel aerosol sampler for tropopause region studies from the CARIBIC platform, Aerosol Sci. Tech., 40, 649–655, doi:10.1080/02786820600767807, 2006.
Nguyen, H. N., Martinsson, B. G., Wagner, J. B., Carlemalm, E., Ebert, M., Weinbruch, S., Brenninkmeijer, C. A. M., Heintzenberg, J., Hermann, M., Schuck, T., Velthoven, P. F. J. v., and Zahn, A.: Chemical composition and morphology of individual aerosol particles from a CARIBIC flight at 10 km altitude between 50° N and 30° S, J. Geophys. Res., 113, D23209, doi:10.1029/2008JD009956, 2008.
Niemeier, U., Timmreck, C., Graf, H.-F., Kinne, S., Rast, S., and Self, S.: Initial fate of fine ash and sulfur from large volcanic eruptions, Atmos. Chem. Phys., 9, 9043–9057, doi:10.5194/acp-9-9043-2009, 2009.
O'Dowd, C. D., Facchini, M. C., Cavalli, F., Ceburnis, D., Mircea, M., Decesari, S., Fuzzi, S., Yoon, Y. J., and Putaud, J.-P.: Biogenically driven organic contribution to marine aerosol, Nature, 431, 676–680, doi:10.1038/nature02959, 2004.
Papaspiropoulos, G., Martinsson, B. G., Zahn, A., Brenninkmeijer, C. A. M., Hermann, M., Heintzenberg, J., Fischer, H., and Velthoven, P. F. J. v.: Aerosol elemental concentrations in the tropopause region from intercontinental flights with the Civil Aircraft for Regular Investigation of the Atmosphere Based on an Instrument Container (CARIBIC) platform, J. Geophys. Res., 107, 4671, doi:10.1029/2002jd002344, 2002.
Pitari, G., Mancini, E., Rizi, V., and Shindell, D. T.: Impact of Future Climate and Emission Changes on Stratospheric Aerosols and Ozone, J. Atmos. Sci., 59, 414–440, doi:10.1175/1520-0469(2002)059<0414:iofcae>2.0.co; 2, 2002.
Rauthe-Schöch, A., Weigelt, A., Hermann, M., Martinsson, B. G., Baker, A. K., Heue, K.-P., Brenninkmeijer, C. A. M., Zahn, A., Scharffe, D., Eckhardt, S., Stohl, A., and Velthoven, P. F. J. v.: CARIBIC aircraft measurements of Eyjafjallajökull volcanic plumes in April/May 2010, Atmos. Chem. Phys., 12, 879–902, doi:10.5194/acp-12-879-2012, 2012.
Read, W. G., Froidevaux, L., and Waters, J. W.: Microwave Limb Sounder measurement of stratospheric SO2 from the Mt. Pinatubo volcano, Geophys. Res. Lett., 20, 1299–1302, 1993.
Rose, W. I. and Durant, A. J.: Fine ash content of explosive eruptions, J. Volcanol. Geoth. Res., 186, 32-39, doi:10.1016/j.jvolgeores.2009.01.010, 2009.
Rose, W. I., Bluth, G. J. S., Schneider, D. J., Ernst, G. G. J., Riley, C. M., Henderson, L. J., and McGimsey, R. G.: Observations of Volcanic Clouds in Their First Few Days of Atmospheric Residence: The 1992 Eruptions of Crater Peak, Mount Spurr Volcano, Alaska, J. Geol., 109, 677–694, 10.1086/323189, 2001.
Rubin, K.: Degassing of metals and metalloids from erupting seamount and mid-ocean ridge volcanoes: Observations and predictions, Geochim. Cosmochim. Ac., 61, 3525–3542, doi:10.1016/s0016-7037(97)00179-8, 1997.
Rudnic, L. R. and Fountain, M. D.: Nature and composition of the continental crust: a lower crustal perspective, Rev. Geophys., 33, 267–309, doi:10.1029/95RG01302, 1995.
Scheele, M. P., Siegmund, P. C., and Velthoven, P. F. J. V.: Sensitivity of trajectories to data resolution and its dependence on the starting point: In or outside a tropopause fold, Meteorol. Appl., 3, 267–273, doi:10.1002/met.5060030308, 1996.
Schmale, J., Schneider, J., Voigt, T. J., Kalesse, H., Rautenhaus, M., Lichtenstern, M., Schlager, H., Ancellet, G., Arnold, F., Gerding, M., Mattis, I., Wendisch, M., and Borrmann, S.: Aerosol layers from the 2008 eruptions of Mount Okmok and Mount Kasatochi: In situ upper troposphere and lower stratosphere measurements of sulfate and organics over Europe, J. Geophys. Res., 115, D00L07, doi:10.1029/2009JD013628, 2010.
Schumann, U., Weinzierl, B., Reitebuch, O., Schlager, H., Minikin, A., Forster, C., Baumann, R., Sailer, T., Graf, K., Mannstein, H., Voigt, C., Rahm, S., Simmet, R., Scheibe, M., Lichtenstern, M., Stock, P., Ruba, H., Schauble, D., Tafferner, A., Rautenhaus, M., Gerz, T., Ziereis, H., Krautstrunk, M., Mallaun, C., Gayet, J. F., Lieke, K., Kandler, K., Ebert, M., Weinbruch, S., Stohl, A., Gasteiger, J., Gross, S., Freudenthaler, V., Wiegner, M., Ansmann, A., Tesche, M., Olafsson, H., and Sturm, K.: Airborne observations of the Eyjafjalla volcano ash cloud over Europe during air space closure in April and May 2010, Atmos. Chem. Phys, 11, 2245–2279, doi:10.5194/acp-11-2245-2011, 2011.
Seinfeld, J. H. and Pandis, S. N.: Atmospheric chemistry and physics: from air pollution to climate change, 2nd edn., Book, John Wiley&Sons, Inc., Hoboken, N.J, 2006.
Sigmundsson, F., Hreinsdóttir, S., Hooper, A., Árnadóttir, T., Pedersen, R., Roberts, M. J., Óskarsson, N., Auriac, A., and Decriem, J.: Intrusion triggering of the 2010 Eyjafjallajökull explosive eruption, Nature 468, 426–430, doi:10.1038/nature09558, 2010.
Solomon, S., Daniel, J. S., Neely III, R. R., Vernier, J. P., Dutton, E. G., and Thomason, L. W.: The persistently variable "background" stratospheric aerosol layer and global climate change, Science, 333, 866–870, doi:10.1126/science.1206027, 2011.
Spracklen, D. V., Arnold, S. R., Sciare, J., Carslaw, K. S., and Pio, C.: Globally significant oceanic source of organic carbon aerosol, Geophys. Res.Lett., 35, L12811, doi:10.1029/2008GL033359, 2008.
Stramska, M.: Particulate organic carbon in the global ocean derived from SeaWiFS ocean color, Deep-Sea Research Part I, 56, 1459–1470, doi:10.1016/j.dsr.2009.04.009, 2009.
Suzuki, Y. J. and Koyaguchi, T.: Numerical determination of the efficiency of entrainment in volcanic eruption columns, Geophys. Res. Lett., 37, L05302, doi:10.1029/2009GL042159, 2010.
Thomas, H. E. and Prata, A. J.: Sulphur dioxide as a volcanic ash proxy during the April–May 2010 eruption of Eyjafjallajökull Volcano, Iceland, Atmos. Chem. Phys, 11, 6871–6880, doi:10.5194/acp-11-6871-2011, 2011.
Vernier, J.-P., Thomason, L. W., Pommereau, J.-P., Bourassa, A., Pelon, J., Garnier, A., Hauchecorne, A., Blanot, L., Trepte, C., Degenstein, D., and Vargas, F.: Major influence of tropical volcanic eruptions on the stratospheric aerosol layer during the last decade, Geophys. Res. Lett., 38, L12807, doi:10.1029/2011GL047563, 2011.
von Glasow, R., Bobrowski, N., and Kern, C.: The effects of volcanic eruptions on atmospheric chemistry, Chem. Geol., 263, 131–142, doi:10.1016/j.chemgeo.2008.08.020, 2009.
Waythomas, C. F., Scott, W. E., Prejean, S. G., Schneider, D. J., Izbekov, P., and Nye, C. J.: The 7–8 August 2008 eruption of

Kasatochi Volcano, central Aleutian Islands, Alaska, J. Geophys. Res., 115, B00B06, doi:10.1029/2010jb007437, 2010.

Weisenstein, D. K., Yue, G. K., Ko, M. K. W., Sze, N.-D., Rodriguez, J. M., and Scott, C. J.: A two-dimensional model of sulfur species and aerosols, J. Geophys. Res., 102, 13019–13035, doi:10.1029/97JD00901 1997.

Winker, D. M., Vaughan, M. A., Omar, A., Hu, Y. X., Powell, K. A., Liu, Z. Y., Hunt, W. H., and Young, S. A.: Overview of the CALIPSO Mission and CALIOP Data Processing Algorithms, J. Atmos. Ocean. Tech., 26, 2310–2323, doi:10.1175/2009jtecha1281.1, 2009.

Witham, C. S., Oppenheimer, C., and Horwell, C. J.: Volcanic ash-leachates: a review and recommendations for sampling methods, J. Volcanol. Geoth. Res., 141, 299–326, doi:10.1016/j.jvolgeores.2004.11.010, 2005.

Yang, K., Liu, X. O., Bhartia, P. K., Krotkov, N. A., Carn, S. A., Hughes, E. J., Krueger, A. J., Spurr, R. J. D., and Trahan, S. G.: Direct retrieval of sulfur dioxide amount and altitude from spaceborne hyperspectral UV measurements: Theory and application, J. Geophys. Res., 115, D00L09, doi:10.1029/2010jd013982, 2010.

Yoon, Y. J., Jennings, S. G., Dowd, C. D. O., Ceburnis, D., Cavalli, F., Jourdan, O., Putaud, J. P., Facchini, M. C., Decesari, S., Fuzzi, S., and Sellegri, K.: Seasonal characteristics of the physicochemical properties of North Atlantic marine atmospheric aerosols, J. Geophys. Res., 112, D04206, doi:10.1029/2005JD007044, 2007.

Yue, G. K., Poole, L. R., Wang, P. H., and Chiou, E. W.: Stratospheric aerosol acidity, density, and refractive index deduced from SAGE II and NMC temperature data J. Geophys. Res., 99, 3727–3738, doi:10.1029/93jd02989, 1994.

Zahn, A., Weppner, J., Widmann, H., Schlote-Holubek, K., Burger, B., Kuhner, T., and Franke, H.: A fast and precise chemiluminescence ozone detector for eddy flux and airborne application, Atmos. Meas. Tech., 5, 363–375, doi:10.5194/amt-5-363-2012, 2012.

Paper II

Tellus SERIES B CHEMICAL AND PHYSICAL METEOROLOGY
PUBLISHED BY THE INTERNATIONAL METEOROLOGICAL INSTITUTE IN STOCKHOLM

Sources of increase in lowermost stratospheric sulphurous and carbonaceous aerosol background concentrations during 1999–2008 derived from CARIBIC flights

By JOHAN FRIBERG[1]*, BENGT G. MARTINSSON[1], SANDRA M. ANDERSSON[1], CARL A. M. BRENNINKMEIJER[2], MARKUS HERMANN[3], PETER F. J. VAN VELTHOVEN[4] and ANDREAS ZAHN[5], [1]*Department of Physics, Lund University, Lund, Sweden;* [2]*Max Planck Institute for Chemistry, Mainz, Germany;* [3]*Leibniz Institute for Tropospheric Research, Leipzig, Germany;* [4]*Royal Netherlands Meteorological Institute, de Bilt, The Netherlands;* [5]*Institute for Meteorology and Climate Research, Karlsruhe Institute of Technology (KIT), Karlsruhe, Germany*

(Manuscript received 25 November 2013; in final form 19 February 2014)

ABSTRACT

This study focuses on sulphurous and carbonaceous aerosol, the major constituents of particulate matter in the lowermost stratosphere (LMS), based on in situ measurements from 1999 to 2008. Aerosol particles in the size range of 0.08–2 μm were collected monthly during intercontinental flights with the CARIBIC passenger aircraft, presenting the first long-term study on carbonaceous aerosol in the LMS. Elemental concentrations were derived via subsequent laboratory-based ion beam analysis. The stoichiometry indicates that the sulphurous fraction is sulphate, while an O/C ratio of 0.2 indicates that the carbonaceous aerosol is organic. The concentration of the carbonaceous component corresponded on average to approximately 25% of that of the sulphurous, and could not be explained by forest fires or biomass burning, since the average mass ratio of Fe to K was 16 times higher than typical ratios in effluents from biomass burning. The data reveal increasing concentrations of particulate sulphur and carbon with a doubling of particulate sulphur from 1999 to 2008 in the northern hemisphere LMS. Periods of elevated concentrations of particulate sulphur in the LMS are linked to downward transport of aerosol from higher altitudes, using ozone as a tracer for stratospheric air. Tropical volcanic eruptions penetrating the tropical tropopause are identified as the likely cause of the particulate sulphur and carbon increase in the LMS, where entrainment of lower tropospheric air into volcanic jets and plumes could be the cause of the carbon increase.

Keywords: lowermost stratosphere, elemental composition, volcanic aerosol, sulphurous aerosol, carbonaceous aerosol

1. Introduction

Aerosol particles play an important role in the radiation balance of the earth, with cooling and warming effects depending on particle composition. The combined aerosol effects are complex and estimated to provide a net negative radiative forcing (IPCC, 2007), which implies cooling of the earth surface. Because of the complexity and the scarcity of measurement data, the associated uncertainties are still large. Hence, it is important to learn more about particle chemical and elemental composition, not only for assessing the direct radiative effects, but also with regard to aerosol microphysical properties and, ultimately, cloud formation.

The major part of the particulate mass in the stratosphere is carried by submicrometer diameter particles (Deshler, 2008). Sedimentation velocities for such particles at these altitudes are low compared to the residence times of the air masses (Martinsson et al., 2005). Also for the upper troposphere (UT) and lowermost stratosphere (LMS), transport of air masses is of particular relevance for particles and precursor gases. We first briefly summarise some of the main

*Corresponding author.
email: johan.friberg@nuclear.lu.se

Citation: Tellus B 2014, **66**, 23428, http://dx.doi.org/10.3402/tellusb.v66.23428

aspects of the dynamics affecting this region of the atmosphere. The lower bound of the LMS is the tropopause and the upper one the 380 K isentropic surface (Hoskins, 1991; Holton et al., 1995). Large-scale transport in the stratosphere occurs via the Brewer–Dobson (BD) circulation (Brewer, 1949; Dobson, 1956), in which tropical tropospheric air is first transported upwards to the tropical stratosphere and subsequently polewards, to descend finally through the LMS into the extratropical troposphere. Air reaching the tropical stratosphere can undergo fast transport (month) to mid-latitudes in a transitional branch or be moved diabatically upwards in deeper branches of the BD circulation (years) (Gettelman et al., 2011). The downward mass flux across the 380 K isentrope varies with season. In the northern hemisphere, a maximum is found in January and a minimum in July (Appenzeller et al., 1996). The subsidence through the LMS takes months, resulting in a seasonal maximum of stratospheric influence at the tropopause in May (Tang et al., 2011). In addition, direct two-way mass exchange between the UT and LMS, through the extratropical tropopause, occurs along isentropic surfaces (Dessler et al., 1995; Sprenger and Wernli, 2003). The LMS can thus be regarded as a mixture of air from the troposphere and the stratosphere. Mixing of air in the LMS creates concentration gradients of trace gases (Lelieveld et al., 1997; Zahn and Brenninkmeijer, 2003) and particulate matter (Martinsson et al., 2005).

Studies on stratospheric aerosol composition started with Junge et al. (1961). They found a water-soluble sulphurous component, subsequently identified as sulphuric acid and water (Rosen, 1971), formed via gas to particle conversion of mainly OCS and SO_2 (Crutzen, 1976; Weisenstein et al., 1997). OCS photo-oxidises at high altitudes, within the deep BD branch, while SO_2 oxidises at all altitudes in the stratosphere. A recent study by Brühl et al. (2012) argues that OCS is the major source of non-volcanic particulate sulphur in the stratosphere, while Chin and Davis (1995) advocated that the emission rate of OCS alone is insufficient to explain the large amounts of particulate sulphur in the stratosphere. It remains unclear to what degree SO_2 from fossil fuel combustion penetrates the tropical troposphere because of difficulties to distinguish its contribution to the stratospheric aerosol from that of OCS and volcanism (Solomon et al., 2011).

Large volcanic eruptions represent the strongest source of variability in stratospheric aerosol as they can inject substantial amounts of particulate matter and SO_2 into the stratosphere (Robock, 2000). The eruption of Mount Pinatubo in 1991 was observed in the tropics (Dutton and Bodhaine, 2001) and delayed by more than half a year in the stratospheric column at mid-latitudes (Trickl et al., 2013). It perturbed the stratosphere for several years, with an estimated global surface cooling in the order of 0.5°C (McCormick et al., 1995) the year after eruption. A large decline in the aerosol load of the stratosphere was then observed in the following years (Deshler et al., 2006), until reaching a period of near-background conditions in the late 1990s.

LIDAR measurements (Hofmann et al., 2009) indicated increasing amounts of particulate matter in the stratosphere at mid-latitudes in the northern hemisphere after the year 2000. Vernier et al. (2011b) used satellite observations to address this increase and found that the trend increased after year 2005 in connection with volcanic eruptions, reaching the tropical stratosphere. The volcanic aerosol was eventually transported to mid-latitudes (Vernier et al., 2009), increasing the aerosol abundance in both the northern (Hofmann et al., 2009; Bazhenov et al., 2012) and southern hemisphere (Nagai et al., 2010). Solomon et al. (2011) estimated the effect of the stratospheric volcanic aerosol for the time period 2000–2010, to have had a mean radiative forcing of -0.1 W m^{-2}. In addition to the direct injection via explosive volcanic eruptions, Bourassa et al. (2012) found evidence that the eruption of the tropical volcano Nabro in 2011 reached the UT and was lifted to the lower stratosphere, by the South Asian monsoon, where the effluents were transported to the extratropical stratosphere within 4 weeks of the eruption. Neely et al. (2013) later found that the contribution to the stratospheric aerosol load in this period from anthropogenic emissions and that of transport within the South Asian monsoon to be small, further validating volcanic eruptions in the tropics as the main cause of perturbation.

In addition to sulphate, a carbonaceous component in stratospheric particles was observed more recently (Murphy et al., 1998) and was found to be a large fraction of the UT/LMS aerosol (Nguyen and Martinsson, 2007; Schmale et al., 2010). Using electron microscopy, PIXE (particle-induced X-ray emission) and PESA (particle elastic scattering analysis), Nguyen et al. (2008) found a mixture of sulphurous and carbonaceous components in UT and LMS particles, with LMS particles containing a framework of carbonaceous material. Martinsson et al. (2009) and Schmale et al. (2010) found a large carbonaceous component in the aerosol from the Kasatochi eruption. In a recent study, based on model results and satellite measurements of extinction ratios from SAGE, Brühl et al. (2012) suggest that organic particulate matter contributes a significant fraction to the light extinction in the LMS, as particulate sulphur concentrations from the model are insufficient to fully explain the observed light extinction in the stratosphere.

In situ measurements for elemental characterisation of particulate matter in the tropopause region are scarce. CARIBIC (Civil Aircraft for the Regular Investigation of the atmosphere Based on an Instrument Container,

www.caribic-atmospheric.com) is the first project providing in situ elemental characterisation of particulate matter in the UT and LMS on a regular basis.

In this study, the LMS background or close-to-background aerosol is investigated using the CARIBIC platform. For this purpose, datasets from the period 1999–2002 and 2005–2008 are used, spanning almost a decade (data after 2008 are omitted from this study as the LMS became perturbed by a direct injection of volcanic aerosol in Aug 2008). These data for sulphurous and carbonaceous fractions of LMS particles provide, as far as we know, the longest time series on particulate sulphur and the first long-term quantitative measurements of the particulate carbon content in the tropopause region. Aerosol concentrations are presented relative to the position of the tropopause, as temporal trends, seasonal differences and inter-annual variations. In addition, the chemical composition of the carbonaceous component is presented as stoichiometric ratios of oxygen to carbon, and aerosol sources are discussed and identified.

2. Methods

The first generation CARIBIC measurements (CARIBIC phase #1) (Brenninkmeijer et al., 1999) using intercontinental flights were performed in 1997–2002 on board a Boeing 767–300 ER from LTU International Airways providing the first long-term in situ observations of the chemical composition of aerosol particles, combined with particle number and trace gas concentrations. The present CARIBIC system (CARIBIC phase #2) is the second generation consisting of a 1.6-ton container with an extended scientific payload, sampling at cruise altitudes of 9–12 km (Brenninkmeijer et al., 2007). This new CARIBIC container is installed in a Lufthansa Airbus 340–600 on a monthly basis for four consecutive flights, since May 2005 (no aerosol samples were collected in the period May 2002–April 2005). This aircraft is equipped with a sophisticated inlet system for gases and particles. In situ measurements of aerosol particles and of trace gases (e.g. O_3, CO, NO/NO_y, VOCs, gaseous and condensed water) are carried out. Collected air samples are analysed for greenhouse gases, hydro- and halo carbons (Brenninkmeijer et al., 2007; Schuck et al., 2009; Baker et al., 2010; Oram et al., 2012). Monthly measurement flights depart from Frankfurt for destinations in South East Asia, East Asia, Southern Africa and North and South America, thus covering a large geographical area, mainly in the northern hemisphere.

2.1. Aerosol sampling

The aerosol data presented in this work from CARIBIC phase #1 and #2 have been obtained using two different inlet systems. Based on experimental studies and modelling, the CARIBIC phase #1 inlet efficiency for particle sizes of 0.1–1 μm was estimated to be 90% (Hermann et al., 2001). The present CARIBIC inlet system is described by Brenninkmeijer et al. (2007). Its sampling efficiency is estimated to be 60% at 5 μm particle diameter (Rauthe-Schöch et al., 2012), and based on modelling and experience with other aerosol inlets, its efficiency is estimated be at least 90% for particles of 0.01–1 μm diameter.

Collection of aerosol particles was undertaken by automated impactors (Nguyen et al., 2006), implemented in the CARIBIC instrument containers, collecting particles of 0.08–2 μm aerodynamic diameters. The CARIBIC phase #1 (phase #2) impactors have 14 (16) channels for sequential and integral samples. Each sequential sample is collected during typically 150 (100) minutes corresponding to flight distances of approximately 2200 (1500) km at cruise speed. The integral samples [1 (2) out of 14 (16) samples] are collected for the purpose of checking for sample contamination. The air sampling volume for a sequential sample is approximately 0.09 (0.25) m^3 STP [standard temperature (273.15 K) and pressure (1013.25 hPa)]. Sampling is suspended during take-off and landing, whenever pressure exceeds 350 hPa, to prevent mixed samples of lower tropospheric (or even boundary layer) and UT/LMS aerosol particles. Particles accelerated in 0.5 mm diameter impactor orifices are deposited in four spots (phase #2), forming a square pattern with centre distances between spots of 1.3 mm, whereas the CARIBIC phase #1 sampler collected aerosol from a single orifice (Martinsson et al., 2001). The sampling substrate consists of a 0.2 μm thin AP1™ polyimide film, a material well suited for ion beam analysis (IBA) (Papaspiropoulos et al., 1999; Nguyen and Martinsson, 2007).

2.2. Analyses of aerosol particles

Analyses were undertaken with a 2.55 MeV proton beam at the Lund IBA accelerator. The IBA measurement techniques used are PIXE and PESA. PIXE (Johansson and Campbell, 1988) was used for elements with an atomic number larger than 13 and PESA for measurements of lighter elements (hydrogen, carbon, nitrogen and oxygen). Analyses were run in two steps, using the technique described by Nguyen and Martinsson (2007). Typical elemental minimum detection limits (MDL) in units of ng m^{-3} STP are 1 (hydrogen), 15 (carbon), 7 (oxygen), 2 (sulphur) and 0.1 (iron). The accuracy of PIXE and PESA is estimated to be 10% (Nguyen and Martinsson, 2007). Concentrations below MDL were set to MDL/2. The detection frequencies, that is, the fraction of the samples with elemental concentrations above the MDL are: 100% (hydrogen),

83% (carbon), 100% (oxygen), 100% (sulphur) and 50% (iron).

Films with low deposited aerosol mass occasionally lead to significantly higher MDLs compared to the majority of the samples in the PESA analysis as a result of problems in identifying the aerosol deposit spot, which prevents analysis. This MDL problem is primarily associated with short sampling times. MDLs, in ng m^{-3}, were derived from sampled mass density, in μg cm^{-2}, on the exposed films and are thus highly dependent on sampling time. Samples with sampling times shorter than 60 minutes (caused for instance by aircraft landings) were therefore excluded to prevent these effects of high MDLs on the data set.

The analytical system used for detection of carbon was developed after 2002. Hence, no analysis of carbon was possible for samples collected with the first generation collection system. The carbon data in the present study is thus obtained from measurements with the second-generation collection system running since 2005.

2.3. Ozone measurements

We use the concurrent CARIBIC in situ ozone measurements to assist the interpretation of the variations in particulate carbon and sulphur concentrations in the UT/LMS. Two ozone analysers are currently installed in the CARIBIC container; an accurate, dual-beam UV-photometer serving as a calibrated standard instrument and a fast solid state chemiluminescence detector. The accuracy was estimated to be 2% for 10 Hz measurements (Brenninkmeijer et al., 2007; Zahn et al., 2012), while the uncertainty for the first generation CARIBIC system was 4% or 4 ppbv, whichever was larger (Zahn et al., 2002).

2.4. The tropopause definition

The dynamical tropopause, based on potential vorticity (PV) with a typical threshold value of 1.5–3.5 PVU (Potential Vorticity Units; 1 PVU = 10^{-6} K m^2 kg^{-1} s^{-1}) (Hoerling et al., 1991; Hoinka, 1997), is used for identifying samples collected in the LMS. PV values were derived from archived ECMWF (European Centre for Medium-range Weather Forecast) analyses with a resolution of 1×1 degree in the horizontal at 91 vertical hybrid sigma-pressure model levels and calculated by the Royal Netherlands Meteorological Institute, de Bilt, the Netherlands (KNMI). PV values were interpolated linearly in latitude, longitude, log pressure and time to the location of the aircraft and for each sample averaged over the duration of sampling. Samples at an average PV of over 2 PVU are accordingly regarded as stratospheric.

2.5. Exclusion of periods affected by direct injection into the LMS by extratropical, strong volcanic eruptions

Previous studies have shown a large impact on the LMS aerosol mass concentrations from volcanoes injecting directly into the LMS (Martinsson et al., 2009; Schmale et al., 2010; Andersson et al., 2013). The largest such eruptions in the period studied here (1999–2008) were Okmok (July 12, 2008) and Kasatochi (August 7–8, 2008), of which the latter strongly affected the LMS aerosol load (Martinsson et al., 2009). The first samples containing volcanic aerosol from Okmok and Kasatochi were collected by CARIBIC on August 15, 2008. Samples containing aerosol from these eruptions are excluded in our study. This refers to all LMS samples collected after August 15, 2008. After excluding samples affected by fresh volcanic clouds, this study on the background aerosol is based on 181 LMS samples, whereof 38 were from the period 1999–2002.

3. Results

3.1. Particulate sulphur and carbon concentrations in the LMS

Figure 1 shows the temporal evolution of particulate sulphur and carbon concentrations in the LMS for the period considered. The strong effect on the aerosol concentrations via a direct injection of volcanic aerosol into the extratropical LMS by the Kasatochi eruptions in August 2008, as reported by Martinsson et al. (2009) is evident, while the rest of the period represents an episode of low volcanic activity at mid-latitudes. Comparing the early sulphur data (1999–2002) with later data (2005–2008), a clear increase in concentration and variation is observed. Moreover, the concentrations increase substantially in the period 2005–2008, for both sulphur and carbon, with on average higher concentrations in 2008 than in any previous year investigated.

3.2. Vertical gradients and seasonal variations in the LMS

Ozone is formed deep in the stratosphere and is transported down to the LMS within the large-scale DB circulation. In the LMS, ozone has a chemical lifetime of >1 yr (Solomon et al., 1997; Smith et al., 2001); that is, it is basically an inert transport tracer and is solely diluted with inflowing ozone-poor tropospheric air, locally or via the lower BD branch. Thus, in the LMS ozone constitutes a reliable tracer for the degree of mixing with tropospheric air and an accurate measure for the distance above the tropopause (Sprung and Zahn, 2010). In Fig. 2, we use LMS

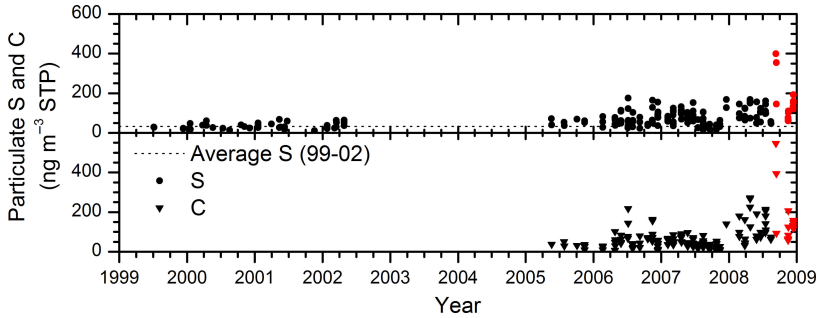

Fig. 1. Temporal variations of concentrations of particulate sulphur and carbon (ng m^{-3} STP) in the northern hemisphere LMS. Red dots illustrate observations after the eruption of Kasatochi. The dashed line shows the geometric average particulate sulphur concentrations during 1999–2002.

ozone concentrations, thus expressing distance to the tropopause, for the four different seasons. Increase in aerosol concentrations is investigated via a scatter plot of particulate sulphur vs. ozone to illustrate the vertical gradient of sulphur from the tropopause into the LMS. A linear fit is applied to the 1999–2002 data for comparison to the 2005–2008 data. This fit is based on data for all four seasons to obtain a significant number of results. Figure 2 shows the difference between the two periods much more clearly. For all seasons, over 90% of the observed concentrations in the period 05–08 is found to be higher than during 99–02, whereas measurements at lowest ozone concentrations, that is, close to the tropopause, show similar concentrations in the two periods. The difference between the periods is less pronounced during fall. In the period 05–08, the observed gradient is strongest during winter and decreases in strength

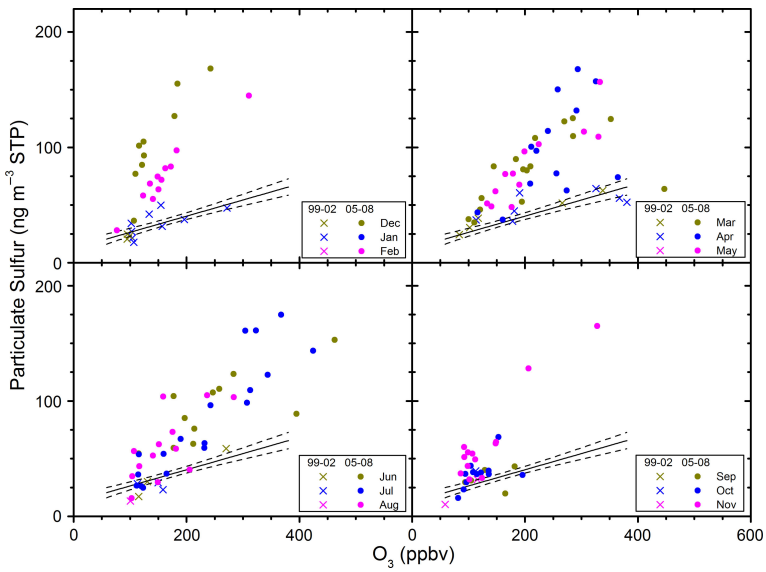

Fig. 2. Concentration of particulate sulphur vs. ozone for stratospheric samples (potential vorticity > 2 PVU) collected in the northern hemisphere. Upper left: winter (December, January, February). Upper right: spring (March, April, May). Lower left: summer (June, July, August). Lower right: fall (September, October, November). A regression model (full line), with 95% confidence interval (dashed lines) based on the 1999–2002 data is used to facilitate the comparison to the 2005–2008 data.

during spring and summer, to reach significantly lower levels in fall.

3.3. Inter-annual variations

To further explore seasonality of particulate sulphur in the LMS, the distance from the tropopause needs to be considered. We consider this using PV, a meteorological parameter with a strong gradient from the tropopause into the LMS. Hence, the sulphur to PV ratio is used in Fig. 3b and is subsequently compared to the corresponding ozone and particulate carbon ratios. The O_3/PV ratio in the LMS is primarily determined by the seasonally varying subsidence of stratospheric air in the BD circulation and thus maximises in mid-latitudes in late spring (Tang et al., 2011), at the seasonal maximum influence from the stratosphere. We observe no difference in the average O_3/PV for the periods 99–02 and 05–08, indicating that no major changes occurred in the transport from the stratosphere during this time. A sine curve fitting is applied with the relative amplitude of 0.31, as shown in Fig. 3a, which holds throughout the period 1999–2008, corroborating the absence of major changes in transport.

The contribution by downward transport of sulphurous aerosol formed in the stratosphere is evaluated in Fig. 3b, using S/PV. To account for the increase in sulphur concentrations from 99–02 to 05–08, two sine functions are used with the same relative amplitude and phase as for the O_3/PV model. In the period 05–08, the S/PV shows considerable agreement with the seasonal variation of O_3/PV with two large deviations (end of 2006 and 2007), and a tendency of higher values during 2008 compared to the two preceding years. Whereas the contribution from the deep branch is expected to follow the phase of the model, transport of SO_2 and particles in the shallow BD branch can cause deviation from this seasonal pattern. The data show that this may have been the case. Interestingly, for carbon the picture seems more complicated, as the C/PV ratio (Fig. 3c) lacks any clear resemblance to that of O_3/PV (Fig. 3a). Some larger deviations are found at the end of 2006 and 2007 and during 2008. These deviations will be further investigated in the Discussion section.

3.4. Composition of carbonaceous aerosol

Besides the very presence of carbonaceous aerosol in conjunction with sulphur and its variability, any information on its actual chemical moiety is valuable. Optical measurements of black carbon in the LMS (Schwarz et al., 2010) showed concentrations in the range of 0.1–4 ng m^{-3} STP. We are however dealing with concentrations that are up to two orders of magnitudes higher (Fig. 1), indicating that soot is only a minor constituent of the carbonaceous fraction in the LMS. The major part of the carbonaceous fraction is therefore likely to be organic.

By means of stoichiometric calculations we can use the PIXE and PESA elemental analyses to infer main properties of the chemical compounds in the samples. Previous CARIBIC measurements have shown that LMS particles have two major components, namely a sulphurous and a carbonaceous one (Nguyen and Martinsson, 2007). In addition several minor constituents can be found, with mineral particles from the earth's crust being the most frequently observed. Figure 4 illustrates the stoichiometric ratios of

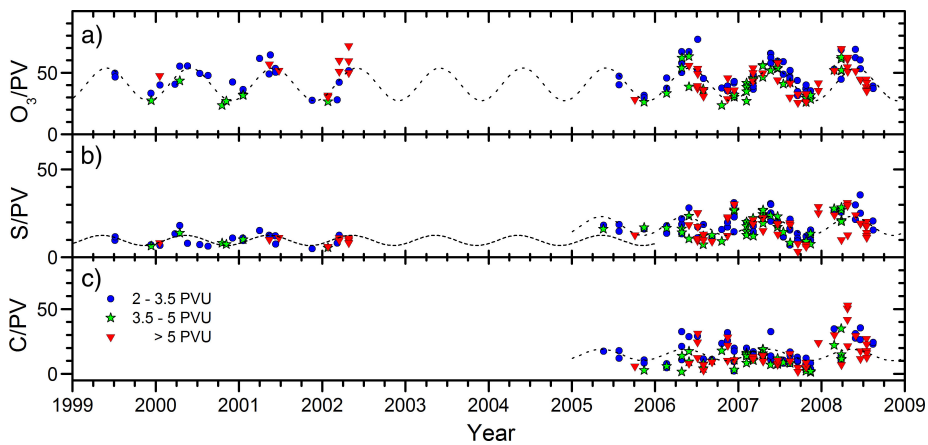

Fig. 3. Temporal trends of ratios to potential vorticity (PV) for a) ozone (ppbv PVU^{-1}), b) particulate sulphur (ng m^{-3} STP PVU^{-1}) and c) particulate carbon (ng m^{-3} STP PVU^{-1}). Sine functions, based on ozone to PV ratios in a) are used in b) and c) to guide the eye.

oxygen to sulphur against carbon to sulphur, for all LMS samples with concentrations above the MDLs of these elements (C, O and S). Oxygen is present in the sulphurous fraction and also in the crustal fraction. A crustal component was identified in 19 samples based on elemental concentration ratios between potassium, calcium, titanium and iron. The crustal contribution to the oxygen content was subtracted from the total stoichiometric amounts of oxygen shown in Fig. 4. The correction was based on the average mineral composition of the earth crust estimated by Rudnick and Fountain (1995). The contribution from the sulphurous fraction can be identified at an oxygen to sulphur ratio of 4 (O/S = 4), based on the assumption that all sulphur is present in the form of sulphate. Figure 4 indeed supports this, as most of the O/S ratios scatter at values exceeding 4. A positive trend from the line of O/S = 4 with increasing C/S ratio is present, which reflects the fraction of oxygen in the carbonaceous component. A relationship for the O/S ratios in relation to C/S ratios can be derived using a linear regression. Thus, the oxygen content in the carbonaceous fraction is obtained at an average O/C ratio of 0.2. Combined with the low concentrations of black carbon (Schwarz et al., 2010), this corroborates that the main part of carbonaceous LMS aerosol is organic.

4. Discussion

An upward trend of 5–6% per year in the background aerosol at 20–25 km altitude for the period 2000–2009 was observed using LIDAR measurements. Increasing coal combustion associated with sulphur emissions, primarily in China, was hypothesised as an explanation (Hofmann et al., 2009). However, Vernier et al. (2011b) used satellite observations to study the trend of increasing amounts of particulate matter in the stratosphere and found that several moderate volcanic eruptions with explosions reaching the tropical stratosphere had affected the aerosol load. In addition to volcanism, Vernier et al. (2011a) identified the South Asian summer monsoon as a likely transport path for aerosol and precursor gases to the tropical tropopause layer (TTL). The aerosol load in the TTL in that study was found to be fairly constant in the period 2006–2008, with a minor increase in 2008, discussed to be an effect of volcanic aerosol.

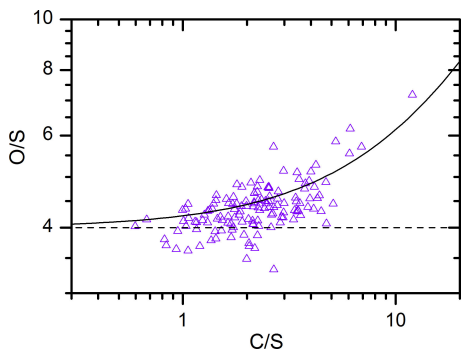

Fig. 4. Oxygen to sulphur vs. carbon to sulphur molar ratios. The dashed line represents O/S = 4, and the full line shows the best fit, i.e. O/S = 4 + 0.2 C/S.

The particulate sulphur concentration increases from the tropopause into the LMS and is significantly higher at the 380 K isentrope than at the tropopause or the UT (Martinsson et al., 2005). The same pattern but magnified appears in the period 2005–2008 (Fig. 2). The increase in aerosol concentration in the LMS in the period 2000–2009 thus indicates transport from the stratosphere, rather than from local mixing of air from the UT.

The difference in sulphur concentrations between the periods 99–02 and 05–08 is smallest in fall (Fig. 2), when ozone and particulate sulphur concentrations minimises, indicating the lowest contribution from the deep BD branch. Air mass budget analyses based on aircraft data demonstrated a strongly varying seasonal partitioning of stratospheric and tropospheric air in the LMS with a minimum influence from the deep BD branch in fall (Hoor et al., 2005). In summer and fall, the LMS is flushed with ozone-poor air from the TTL (Bönisch et al., 2009), additionally reducing the impact from the deep BD branch. This further emphasises our finding that the particulate sulphur is of stratospheric origin and varies in phase with the downward flux within the BD circulation. Bönisch et al. (2009) found the LMS above the extratropical transition layer (ExTL) to be more connected to the stratosphere than to the extratropical UT. Hence, the composition of the LMS air is essentially dependent on transport that occurs above the 380 K isentrope, that is, mixing of the deep and shallow BD branches. The shallow BD branch transports air from the tropical stratosphere to northern mid-latitudes within about 1–2 months (Bourassa et al., 2012; Flury et al., 2013), whereas transport in the deep branch takes a year or more (Holton et al., 1995).

Air transported polewards from the tropical stratosphere, experiences different exposure to photo-chemistry depending on altitude and speed along the transport paths. Whereas sulphuric acid is produced from SO_2 at all altitudes, ozone production and particulate sulphur production from OCS occur predominantly within the deep BD branch. Trace gas concentration distributions bare evidence of meridional mixing of air at high and low altitudes in the stratosphere (Gettelman et al., 1997). The ozone concentration at the 380 K isentrope varies by a factor of 2 (Fortuin and Kelder, 1998; Martinsson et al., 2005), with its maximum in March and minimum in September. That varia-

tion compares well to the corresponding O_3/PV variation in Fig. 3a, with a phase shift of 2 months (relative to the 380 K isentrope) and a peak-to-peak ratio of 1.9, indicating a strong coupling between the LMS and the stratosphere. Hence, the low ozone and sulphur concentrations in fall are results of less ozone and particulate sulphur in the air that is down-welling to the LMS as an effect of less transport via the deep BD branch, and an increasing importance of the shallow branch, during summer (Lin and Fu, 2013).

Regarding the sulphurous aerosol component we note that the approach used in Fig. 3b, based on the O_3/PV variability, does capture the overall pattern of the S/PV values. Nonetheless, several deviations from the general pattern indicate that not only OCS contributed to the observed sulphur concentrations. Regarding the C/PV values in Fig. 3c, larger deviations are seen and only a weak seasonal cycle exists. This suggests that oxidation of precursor gases in the deep BD branch in relative terms is less important for formation of particulate carbon, compared to particulate sulphur. It also indicates that other processes cause the variability in the carbon concentration. The O_3 concentration at the 380 K isentrope shows its seasonal minimum in September and maximum in March (Fortuin and Kelder, 1998; Martinsson et al., 2005). This seasonal variation is expected also in the concentration of sulphate aerosol formed from OCS, as it follows the deep BD branch, while transport of sulphate aerosol to the 380 K isentrope via the shallow BD branch can cause high S/O_3 ratios also during fall. Low ozone concentration in the LMS in winter concurrent with elevated particulate sulphur concentration is thus an indication of formation of particulate matter in SO_2-rich air that was transported in the stratosphere to mid-latitudes by the shallow BD branch. Hence to study the importance of particulate matter formation and transport in the shallow branch we use the seasonal variations of S/O_3 (Fig. 5). For the period 05–08 we have enough data to produce monthly averages. The S/O_3 is once again shown to be significantly higher in the period 05–08 than in the 99–02 ratios with a strong seasonal cycle. In the period 99–02, the S/O_3 remained fairly constant with a small increase at the turn of the year. For 05–08, the S/O_3 shows a clear saw-tooth pattern with a rapid rise from September to December. This increase in the S/O_3 indicates production and transport of sulphurous aerosol within the shallow BD branch. Revisiting the strong particulate-sulphur-to-ozone gradient in Fig. 2 during winter, we conclude that this is the consequence of down-welling of air that was transported in the shallow branch, from the overlying stratosphere, while the gradient in spring and in summer corresponds to mixing also via the deep branch.

Using Fig. 6, we can inspect deviations of particulate sulphur and carbon from seasonality in down-welling of O_3 from the stratosphere over a longer time span. During

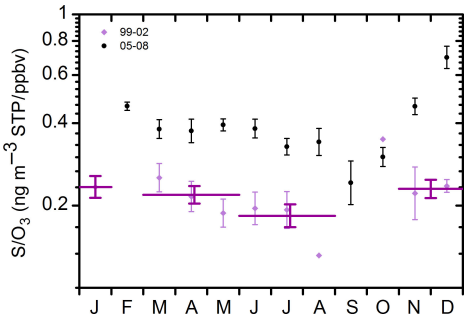

Fig. 5. Ratios of particulate sulphur to ozone mixing ratio (Unit: ng m^{-3} STP $ppbv^{-1}$) for the periods 1999–2002 and 2005–2008, expressed as monthly geometric averages (black and light purple). Purple lines denote averages in the period 1999–2002 for the months; January, March–May, June–August and November–December. Error bars represents standard errors.

05–08, there are periods (Fig. 6a) when S/O_3 values are similar to those of the period 99–02, in particular during July–October 2007. There are also large positive deviations from the geometric average of May 2005–August 2008 in the end of 2006 and in December 2007, while 2008 shows higher S/O_3 ratios compared to 2006 and 2007. A similar pattern is evident for the C/O_3 ratios in Fig. 6b. Deviations from the geometric average of the C/O_3 are essentially found in the end of 2006 and in December 2007, and during most of 2008. In fall 05–08 (Fig. 2), two of the observations have ozone and sulphur concentrations well above the average of the season. These were sampled on November 14–15, close to the end of the defined season and look more connected to the observations in the winter season.

While sulphuric acid is generally considered the main component in stratospheric and LMS aerosol much less is known of the other large component; the carbonaceous aerosol. The following two sections will address the cause of high concentrations of particulate carbon, and of the temporal trends of particulate sulphur and carbon in the LMS aerosol.

4.1. *Forest fires and biomass burning*

Combustion of biomass emits large amounts of soot and organic trace gases that lead to secondary aerosol formation (Andreae and Merlet, 2001). Episodes of increased scattering ratios coupled to pyroconvection from forest fires have been observed at altitudes above the tropopause, remaining for a month or more. A number of authors (Jost et al., 2004; Fromm et al., 2005, 2010; Damoah et al., 2006) discuss the possibility and magnitude of forest fire injection of

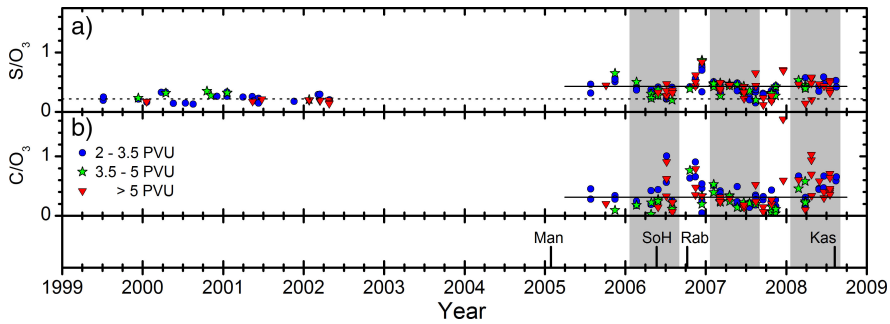

Fig. 6. Ratios of particulate sulphur and carbon concentration to ozone mixing ratio (Unit: ng m^{-3} STP $ppbv^{-1}$), for a) particulate sulphur and b) particulate carbon for stratospheric samples. Full and dashed horizontal lines represent geometric averages for the periods 2005–2008 and 1999–2002, respectively. The February–August period is indicated by a grey background. The four discussed volcanic eruptions (Manam, Soufriere Hills, Rabaul and Kasatochi) are indicated by vertical lines.

smoke particles into the LMS via pyroconvective transport. Based on optical measurements Fromm et al. (2008) estimate that a massive fire storm in Canada in the end of May 2001 injected a mass of smoke, corresponding to more than 5% of the background aerosol in the northern hemisphere lower stratosphere, that persisted until the end of summer. Such events are sporadic with uncertain occurrence frequency. Guan et al. (2010) estimate that approximately 140 plumes reached altitudes above 5 km, in the northern hemisphere, in the period 1979–2009, that is, on average less than 5 per year. Potassium (K) is one of the elements, besides carbon that is generally found in aerosol from biomass burning (Andreae and Merlet, 2001). Importantly, there is no correlation between C and K in the stratospheric CARIBIC samples ($R^2 = 0.004$), indicating that biomass burning had a negligible contribution to the LMS aerosol during the period considered here. The other large potential source of K in the LMS is crustal material. Besides K crustal particles also contain silicon, iron, titanium and calcium. Out of these elements, iron (Fe) is the element with the highest detection frequency in our samples. In Fig. 7, a scatter plot of Fe vs. K in stratospheric samples is used to study the possible impact of biomass burning and crust particles on the LMS aerosol. Aerosol from biomass burning would result in ratios <0.1 ng Fe/ng K (Andreae et al., 1998), while crustal material would be found at ratios >1 (Rudnick and Fountain, 1995). Only a few observations lie close to the 0.1 line (dashed), indicating that biomass burning has a minor impact on the LMS aerosol. A linear regression model shows a strong correlation between Fe and K, with an average ratio of 1.58 ng Fe/ng K. These observations give evidence that biomass burning is insufficient to explain the high carbon concentrations observed.

4.2. *Impact of mid-latitude volcanism*

Volcanic plumes bring high concentrations of particulate matter, SO_2 and other gases to the stratosphere. Gas to particle conversion of SO_2 in the stratosphere is fast compared to the residence times of the air mass and the entrained submicron particles. Volcanic injections of aerosol to the LMS from mid-latitude eruptions are expected to perturb the LMS for a few months or less depending on the altitude of the volcanic injection. Kasatochi's eruption in August 2008 increased the sulphurous aerosol concentrations by a factor of two in the following months. The SO_2 emissions from Okmok were estimated to be 5% (0.1 Tg) of that of Kasatochi's (2 Tg) (Yang et al., 2010; Thomas et al., 2011). In addition some minor eruptions on mid-latitudes

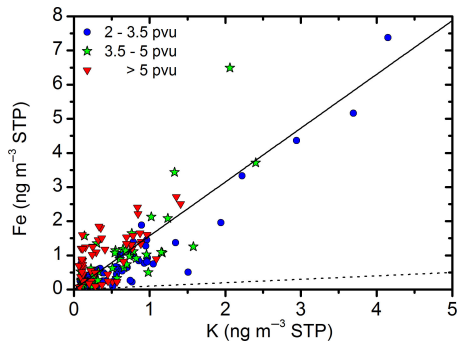

Fig. 7. Mass concentrations of Fe vs. K (ng m^{-3} STP) for stratospheric samples. Regression model shown by full line illustrating a ratio of 1.58 ng Fe/ng K. Dotted line shows Fe/K mass ratio of 0.1, a typical ratio for effluents from biomass burning.

were reported to have reached the tropopause region (Massie, 2014) in the period January 2005–August 2008. Satellite images (from OMI, GOME-2 and AIRS) tell that the SO_2 emissions from any of these eruptions were at least a factor of five lower than that from the eruption of Okmok, implying a maximum perturbation of the LMS aerosol of less than 2% in the months following one of these eruptions. Hence, it is most unlikely that the increases in aerosol concentrations from the periods 99–02 to 05–08 (Fig. 3) are caused by mid-latitude eruptions.

4.3. *Impact of tropical volcanism*

Mixing in the extratropical stratosphere occurs as air from high altitudes descends and mixes with air at lower altitudes. As a result, aerosol and trace gases injected into the tropical stratosphere can reach mid-latitudes in a time scale of months by stratospheric low altitude meridional mixing, via the shallow branch of the BD circulation, and in 1–2 yr via the deep BD branch. The time of the year of a tropical volcano's eruption is expected to affect the period of time for the effects to be observable in the LMS. Main effects from volcanic aerosol transported via the high-altitude branch may appear 2 yr after the eruption. Three tropical volcanoes had eruptions that reached the stratosphere in the time period 2003–2008, namely Manam, Soufriere Hills and Rabaul (Table 1). Based on the transport characteristics of the stratosphere the Manam eruption in January 2005 could affect the mid-latitude stratosphere primarily in 2005–2006, whereas the effects of the two eruptions in 2006 (Table 1) might be observable during late 2006, with the major effects in the downward transport in 2008. These patterns are essentially observed in measurements from the NASA satellite CALIPSO (Vernier et al., 2009, 2011b).

Volcanic aerosol is commonly considered to be composed of sulphate from the conversion of SO_2, combined with a minor fraction of ash constituents (e.g. potassium, calcium, titanium and iron) even though large amounts of carbonaceous aerosol have been observed in volcanic clouds on several occasions. Martinsson et al. (2009) found particulate carbon-to-sulphur-ratios (C/S, in terms of mass) of 2.6 in fresh plumes in the LMS, decreasing to 1 when most of the SO_2, from the eruption of Kasatochi had been converted, corresponding to an organic content of 25–50% (assuming all particulate carbon to have been organic). Measurements with mass spectrometric methods indicated organic fractions of 20–40% (Carn et al., 2011) and 20% (Schmale et al., 2010) in fresh and aged volcanic clouds, respectively. Hence, these studies indicate that particulate carbon is a major constituent of the aerosol in volcanic clouds, with a substantial effect on the stratosphere given the observations of a volcanically perturbed stratosphere in 2006–2008, as reported by Vernier et al. (2011b).

Despite a number of observations of elevated concentrations of particulate carbon in the LMS connected to volcanic clouds, little is known about the origin of this particulate carbon. In a recent study on volcanic aerosol, Andersson et al. (2013) argue, based on the global distribution of organic aerosol in the lower troposphere, that volcanic jets and plumes could bring large amounts of particulate carbon and organic trace gases to the tropopause region via entrainment of air from low altitudes. Entrainment of low altitude air to the tropical stratosphere, via jets from the three tropical volcanoes could be the cause of the observations of high particulate carbon concentrations in the present study, whereas particulate sulphur is expected from transformation of SO_2 emitted from the volcanoes. The term 'volcanic aerosol' will therefore be used for attributing, not only sulphurous, but also carbonaceous aerosol in the following sections.

It is not possible to attribute every deviation in Fig. 6 to a specific event of volcanic activity, but the main patterns will be discussed. The elevated ratios of S/O_3 and C/O_3 during the end of 2006 and December 2007, suggest down-

Table 1. Explosive volcanic eruptions most relevant for this study in the period 2005–August 2008

Eruption date[a]	Volcano	SO_2 (Tg)	VEI[a]	Longitude[a]	Latitude[a]	Altitude (km)
2005-01-27	Manam	0.09[b]	4	145	−4.1	18[b]
2006-05-20	Soufriere Hills	0.2[c]	3	−62	16.7	20[c]
2006-10-07	Rabaul	0.2[d]	4	152	−4.3	18[d]
2008-07-12	Okmok	0.1[e]	4	−168	55.3	15[f]
2008-08-07	Kasatochi	2[g]	4	−176	52.2	14[e]

[a]Volcanic Explosivity Index, from Global Volcanism Program (2011).
[b]Prata and Bernardo (2007).
[c]Carn and Prata (2010).
[d]Carn et al. (2009).
[e]Thomas et al. (2011).
[f]Massie et al. (2014).
[g]Yang et al. (2010).

ward transport of volcanic aerosol from the low altitude branch of the BD circulation, carrying aerosol from the Soufriere Hills eruption. Towards the end of 2006, in the build-up to the maximum downward transport to the LMS in December, Rabaul could also have contributed via the shallow branch of the BD. When downward transport increased during the end of 2007, the volcanic aerosol was located at higher altitudes (Vernier et al., 2009) compared to the end of 2006, and it therefore took longer for the volcanic aerosol to be transported to the LMS, resulting in deviations occurring later in the annual cycle than in 2006. The February–August periods for 2008 S/O_3 ratios are clearly elevated, and even more so for C/O_3 ratios compared to 2006 and 2007, in connection with the down-welling of aerosol from the 2006 eruptions of Soufriere Hills and Rabaul.

4.4. *Inter-annual trends*

The trend of increasing concentrations of particulate matter above the LMS, as reported by Hofmann et al. (2009) and Vernier et al. (2011b), should be expected to be visible in the particulate sulphur and/or carbon concentrations also in the LMS. The strong influence on the LMS aerosol from the Kasatochi eruption effectively eliminated the possibility to study background stratospheric aerosol after August 2008 (Martinsson et al., 2009), shown in Fig. 1. Our data have 3 yr of good coverage for the months February to the beginning of August for both sulphur and carbon, in the period 05–08, and for sulphur 2 yr in the period 99–02. This part of the year, which is also the part of the year when the LMS is strongly influenced by air from higher stratospheric altitudes, is used to study the evolution with time of particulate sulphur and carbon concentrations in the LMS. The time dependence of the 'background aerosol' concentration is investigated using Fig. 8a and b, where the averaged concentration ratios of particulate sulphur and carbon to ozone are plotted, for the February–August periods. The years 1999, 2002 and 2005 are excluded as they lack observations for several months, while the data in the February to August periods of the years 2000 and 2001 are combined in one average, because of the small number of data for these years. The observed ratios of S/O_3 and C/O_3 for the February–August periods are increasing from 2006 to 2008. This coincides with the influence from volcanic eruptions on the LMS as discussed above, and also found by Vernier et al. (2011b) in studies of the stratosphere.

The optical measurements on aerosol in the stratosphere used by Hofmann et al. (2009) and Vernier et al. (2011b) do not reveal the chemical composition of particulate matter, but rather capture the average optical effects of the particulate matter in the studied region. The trend revealed from the optical measurements might therefore be more connected to the sum of the concentrations of the major constituents

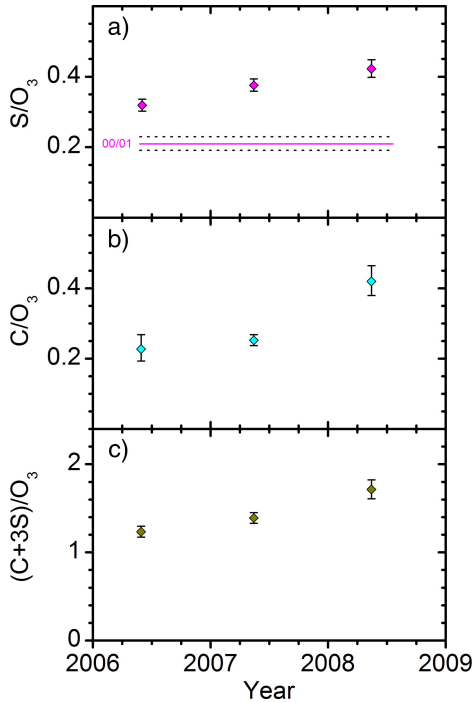

Fig. 8. Geometric average of ratios (a) particulate sulphur (b) carbon and (c) carbon + 3 sulphur concentration to ozone mixing ratio (ng m^{-3} STP $ppbv^{-1}$) for the February–August periods of 2000/2001, 2006, 2007 and 2008.

rather than with individual constituents. Hence, the trend for the sum of the two major components of the LMS aerosol, the carbonaceous and sulphurous fractions, is investigated in Fig. 8c. The sulphurous fraction is assumed to be composed of sulphate, with a mass three times that of sulphur, while the mass of the carbonaceous fraction is represented by the mass of carbon. The ratio of the sum of carbonaceous and sulphurous mass concentrations to ozone $[(C + 3S)/O_3]$ is shown in Fig. 8c for the February–August periods. A significant increase from 2006 to 2008 can be identified. This increase was 30%, with a stronger relative increase for carbon (70%; Fig. 8b) than for sulphur (23%; Fig. 8a).

Overall, a doubling is shown in the S/O_3 from the 2000/2001 to the year 2008 (Fig. 8a). Hofmann et al. (2009) found an increase at 20–25 km altitude of 6.3% $year^{-1}$ in the mid-latitudes (Boulder, 40°N) over the years 2000–2009, corresponding to a total increase of 73%. The differences to our data can be caused by difference in altitude, time period studied or measurement method. The particulate mass

concentrations presented here are particle volume oriented, whereas optical methods are basically particle surface oriented with a complicated response to particle size, shape and chemical composition. Another reason is that the data presented here pertain to the time of the year when the influence from the deep BD branch is strong.

The steady increase in S/O_3 in the LMS (Fig. 8a) combined with the sudden rise in C/O_3 from 2007 to 2008 (Fig. 8b) indicates different compositions for stratospheric aerosol in 2007 than in 2008. A comparison of particulate carbon-to-sulphur-ratios (C/S) for these years, shows a significant difference in the geometric average of 0.66–0.99, with geometric standard deviations of 1.06 and 1.08, respectively (i.e. a 1-sigma-range of 0.62–0.70 and 0.92–1.08). Could this increase in the C/S be an effect of different aerosol compositions from the different volcanic clouds?

The time span for the tropical volcanoes impact on the stratosphere is expected to depend on their penetration depth into the stratosphere. Volcanic clouds reaching high altitudes are expected to affect aerosol via the deep BD branch, while aerosol injected to lower altitudes would follow the shallow branch. Based on CALIPSO observations Vernier et al. (2009) illustrated that aerosol from the Soufriere Hills eruption reached higher altitude (>20 km) compared to that from the Rabaul eruption (≤ 18 km), by the end of 2006. Hence, a larger fraction of the Soufriere Hills aerosol is expected to be transported via the deep branch, whilst the Rabaul aerosol would to a larger extent have been transported to mid-latitudes via the shallow BD branch. As the shallow branch transports air from the tropics to mid-latitudes within months, the deep branch affects the mid-latitude stratosphere after a year or more. The composition of the mid-latitude stratospheric aerosol, down-welling to the LMS in 2007, would thus be more connected to aerosol from the eruption of Rabaul, whereas the main effects of the Soufriere Hills aerosol would be visible during 2008. Studies based on satellite measurements (Stramska, 2009) and models (Spracklen et al., 2008) indicate higher regional organic aerosol concentrations in lower tropospheric air at the time of the Soufriere Hills eruption than for that of Rabaul. The eruption of Rabaul thus had a lower potential to entrain particulate carbon in the volcanic jet and plume. As these two eruptions emitted similar amounts of SO_2 (Table 1) a higher C/S concentration ratio could be expected for the Soufriere Hills eruption in agreement with our observations.

5. Conclusions

The present work is based on measurements of LMS aerosol particle composition sampled by CARIBIC (Civil Aircraft for the Regular Investigation of the atmosphere Based on an Instrument Container, www.caribic-atmospheric.com) in the periods 1999–2002 and 2005–2008. IBA was used to derive detailed elemental concentrations, finding a sulphurous and a carbonaceous component to be dominant. The concentration of the carbonaceous component corresponded on average to approximately 25% of that of the sulphurous, in terms of mass, and could not be explained by forest fires or other types of biomass burning. Stoichiometric O/C ratios of 0.2 and the fact that the measured particulate carbon concentrations greatly exceed literature data on black carbon concentrations indicate that the carbonaceous aerosol is organic in nature.

Particulate sulphur showed a distinct concentration gradient from the tropopause into the mid-latitude LMS. The gradient was strongest during winter and weakest during fall, indicating transport from the stratosphere as the cause of high concentration of particulate sulphur in the LMS. The gradient was also significantly stronger in the period 2005–2008 than in the earlier (1999–2002) period. Variations in the particulate sulphur and carbon concentrations were compared to that of O_3 to track the effect of transport from high altitudes of the stratosphere via the deep Brewer-Dobson branch. That comparison indicated an increased importance for transport of sulphurous aerosol via the shallow BD branch in the period 2005–2008 compared to that of the earlier period, suggesting oxidation of SO_2 as a likely cause for the strengthening of the concentration gradient.

The elevation and the variations in aerosol concentrations in the period 2005–2008 are associated with varying concentrations of particulate matter above the LMS, depending on mainly three volcanic eruptions in the tropics, with plumes reaching the tropical stratosphere. Subsequent transport by the BD circulation then carried the volcanic aerosol to the LMS, resulting in the elevated concentrations of particulate matter observed by CARIBIC in the following years. Entrainment of air from low altitudes, with high concentrations of particulate carbon and organic trace gases, in volcanic jets and plumes is proposed as the cause of high concentrations of particulate carbon in the stratosphere, while sulphur is expected from the volcanic effluents. The eruption in 2006 by Soufriere Hills reached deeper into the stratosphere than Rabaul later the same year, causing a longer duration of the influence from Soufriere Hills. The higher C/S ratios during 2008 could thus be connected with higher concentrations of carbonaceous aerosol at low altitude around the Soufriere Hills volcano.

Comparison of aerosol concentrations in the LMS during the February–August periods of 2006, 2007 and 2008 reveals an increase of 30% from 2006 to 2008. The rate of increase over that period was stronger for carbon (70%) than for the other major constituent sulphur (23%), hence indicating that volcanism had a stronger relative impact on the concentration of carbonaceous than on sulphu-

rous aerosol in the stratosphere, although the increase in the absolute amount of sulphurous aerosol in the form of sulphate was larger than that of the carbonaceous aerosol.

Mass concentrations of sulphurous and carbonaceous aerosol, the two main components in the northern hemisphere mid-latitude LMS aerosol, increased in the period studied here. The former approximately doubled from the period 2000–2001 to the year 2008. This could to a large degree be attributed to intermediate volcanic eruptions in the tropics. Previous studies found an increasing stratospheric aerosol burden above 15 km altitude in the period 2000–2009, which potentially cooled the climate. This study extends these findings to the LMS.

6. Acknowledgements

We especially acknowledge C. Koeppel, D. S. Scharffe, S. Weber and all other members of the CARIBIC project. Lufthansa and Lufthansa Technik are gratefully acknowledged for enabling this scientific experiment. Financial support from the Swedish Research Council and the Swedish Research Council for Environments, Agricultural Sciences and Spatial Planning under grants 621-2007-4639 and 214-2009-613 is gratefully acknowledged.

References

Andersson, S. M., Martinsson, B. G., Friberg, J., Brenninkmeijer, C. A. M., Rauthe-Schöch, A. and co-authors. 2013. Composition and evolution of volcanic aerosol from eruptions of Kasatochi, Sarychev and Eyjafjallajökull in 2008–2010 based on CARIBIC observations. *Atmos. Chem. Phys.* **13**, 1781–1796. DOI: 10.5194/acp-13-1781–2013.

Andreae, M. O., Andreae, T. W., Annegarn, H., Beer, J., Cachier, H. and co-authors. 1998. Airborne studies of emissions from savanna fires in southern Africa. 2. Aerosol chemical composition. *J. Geophys. Res.* **103**, 32119–32128.

Andreae, M. O. and Merlet, P. 2001. Emission of trace gases and aerosols from biomass burning. *Global Biogeocheml. Cycles*. **15**, 955–966.

Appenzeller, C., Holton, J. R. and Rosenlof, K. H. 1996. Seasonal variation of mass transport across the tropopause. *J. Geophys. Res.* **101**, 15071–15078.

Baker, A. K., Slemr, F. and Brenninkmeijer, C. A. M. 2010. Analysis of non-methane hydrocarbons in air samples collected aboard the CARIBIC passenger aircraft. *Atmos. Meas. Tech.* **3**, 311–321.

Bazhenov, O. E., Burlakov, V. D., Dolgii, S. I. and Nevzorov, A. V. 2012. Lidar observations of aerosol disturbances of the stratosphere over Tomsk (56.5 N; 85.0 E) in volcanic activity period 2006–2011. *Int. J. Opt.* **2012**. DOI: 10.1155/2012/786295.

Bourassa, A. E., Robock, A., Randel, W. J., Deshler, T., Rieger, L. A. and co-authors. 2012. Large volcanic aerosol load in the stratosphere linked to Asian monsoon transport. *Science*. **337**, 78–81. DOI: 10.1126/science.1219371.

Brenninkmeijer, C. A. M., Crutzen, P. J., Fischer, H., Güsten, H., Hans, W. and co-authors. 1999. CARIBIC—Civil aircraft for global measurement of trace gases and aerosols in the tropopause region. *J. Atmos. Oceanic Technol.* **16**, 1373–1383.

Brenninkmeijer, C. A. M., Crutzen, P., Boumard, F., Dauer, T., Dix, B. and co-authors. 2007. Civil Aircraft for the regular investigation of the atmosphere based on an instrumented container: the new CARIBIC system. *Atmos. Chem. Phys.* **7**, 4953–4976.

Brewer, A. W. 1949. Evidence for a world circulation provided by the measurements of helium and water vapour distribution in the stratosphere. *Q. J. Roy. Meteorol. Soc.* **75**, 351–363.

Brühl, C., Lelieveld, J., Crutzen, P. J. and Tost, H. 2012. The role of carbonyl sulphide as a source of stratospheric sulphate aerosol and its impact on climate. *Atmos. Chem. Phys.* **12**, 1239–1253. DOI: 10.5194/acp-12-1239-2012.

Bönisch, H., Engel, A., Curtius, J., Birner, T. and Hoor, P. 2009. Quantifying transport into the lowermost stratosphere using simultaneous in-situ measurements of SF6 and CO2. *Atmos. Chem. Phys.* **9**, 5905–5919.

Carn, S. A., Froyd, K. D., Anderson, B. E., Wennberg, P., Crounse, J. and co-authors. 2011. In situ measurements of tropospheric volcanic plumes in Ecuador and Colombia during TC4. *J. Geophys. Res.* **116**, D00J24. DOI: 10.1029/2010JD014718.

Carn, S. A., Krueger, A. J., Krotkov, N. A., Yang, K. and Evans, K. 2009. Tracking volcanic sulfur dioxide clouds for aviation hazard mitigation. *Nat. Hazards.* **51**, 325–343. DOI: 10.1007/s11069-008-92284.

Carn, S. A. and Prata, F. J. 2010. Satellite-based constraints on explosive SO_2 release from Soufrière Hills Volcano, Montserrat. *Geophys. Res. Lett.* **37**, L00E22. DOI: 10.1029/2010GL044971.

Chin, M. and Davis, D. D. 1995. A reanalysis of carbonyl sulfide as a source of stratospheric background sulfur aerosol. *J. Geophys. Res.* **100**, 8993–9005.

Crutzen, P. J. 1976. The possible importance of CSO for the sulfate layer of the stratosphere. *Geophys. Res. Lett.* **3**, 73–76.

Damoah, R., Spichtinger, N., Servranckx, R., Fromm, M., Eloranta, E. W. and co-authors. 2006. A case study of pyro-convection using transport model and remote sensing data. *Atmos. Chem. Phys.* **6**, 173–185.

Deshler, T. 2008. A review of global stratospheric aerosol: measurements, importance, life cycle, and local stratospheric aerosol. *Atmos. Res.* **90**, 223–232.

Deshler, T., Anderson-Sprecher, R., Jäger, H., Barnes, J., Hofmann, D. J. and co-authors. 2006. Trends in the nonvolcanic component of stratospheric aerosol over the period 1971–2004. *J. Geophys. Res.* **111**, D01201. DOI: 10.1029/2005jd006089.

Dessler, A. E., Hintsa, E. J., Weinstock, E. M., Anderson, J. G. and Chan, K. R. 1995. Mechanisms controlling water vapor in the lower stratosphere: "a tale of two stratospheres." *J. Geophys. Res.* **100**, 23167–23172.

Dobson, G. M. B. 1956. Origin and distribution of the polyatomic molecules in the atmosphere. *Proc. R. Soc. London, Ser. A.* **236**, 187–193.

Dutton, E. G. and Bodhaine, B. A. 2001. Solar irradiance anomalies caused by clear-sky transmission variations above Mauna Loa: 1958–99. *J. Clim.* **14**, 3255–3262.

Flury, T., Wu, D. L. and Read, W. G. 2013. Variability in the speed of the Brewer–Dobson circulation as observed by Aura/MLS. *Atmos. Chem. Phys.* **13**, 4563–4575. DOI: 10.5194/acp-13-4563-2013.

Fortuin, J. P. F. and Kelder, H. 1998. An ozone climatology based on ozonesonde and satellite measurements. *J. Geophys. Res.* **103**, 31709–31734.

Fromm, M., Bevilacqua, R., Servranckx, R., Rosen, J., Thayer, J. P. and co-authors. 2005. Pyro-cumulonimbus injection of smoke to the stratosphere: observations and impact of a super blowup in northwestern Canada on 3–4 August 1998. *J. Geophys. Res.* **110**, D08205. DOI: 10.1029/2004JD005350.

Fromm, M., Lindsey, D. T., Servranckx, R., Yue, G., Trickl, T. and co-authors. 2010. The untold story of pyrocumulonimbus. *Bull. Am. Meteorol. Soc.* **91**, 1193–1209. DOI: 10.1175/2010BAMS3004.1.

Fromm, M., Torres, O., Diner, D., Lindsey, D., Vant Hull, B. and co-authors. 2008. Stratospheric impact of the Chisholm pyrocumulonimbus eruption: 1. Earth-viewing satellite perspective. *J. Geophys. Res.* **113**, D08202. DOI: 10.1029/2007JD009153.

Gettelman, A., Holton, J. R. and Rosenlof, K. H. 1997. Mass fluxes of O_3, CH_4, N_2O and CF_2Cl_2 in the lower stratosphere calculated from observational data. *J. Geophys. Res.* **102**, 19149–19159.

Gettelman, A., Hoor, P., Pan, L. L., Randel, W. J., Hegglin, M. I. and co-authors. 2011. The extratropical upper troposphere and lower stratosphere. *Rev. Geophys.* **49**, RG3003. DOI: 10.1029/2011RG000355.

Guan, H., Esswein, R., Lopez, J., Bergstrom, R., Warnock, A. and co-authors. 2010. A multi-decadal history of biomass burning plume heights identified using aerosol index measurements. *Atmos. Chem. Phys.* **10**, 6461–6469. DOI: 10.5194/acp-10-6461-2010.

GVP 2011. Global Volcanism Program. Online at: http://www.volcano.si.edu/index.cfm

Hermann, M., Stratmann, F., Wilck, M. and Wiedensohler, A. 2001. Sampling characteristics of an aircraft-borne aerosol inlet system. *J. Atmos. Ocean. Technol.* **18**, 7–19.

Hoerling, M. P., Schaack, T. K. and Lenzen, A. J. 1991. Global objective tropopause analysis. *Mon. Weather Rev.* **119**, 1816–1831.

Hofmann, D., Barnes, J., O'Neill, M., Trudeau, M. and Neely, R. 2009. Increase in background stratospheric aerosol observed with lidar at Mauna Loa Observatory and Boulder, Colorado. *Geophys. Res. Lett.* **36**, L15808. DOI: 10.1029/2009GL039008.

Hoinka, K. P. 1997. The tropopause: discovery, definition and demarcation. *Meteorol. Z.* **6**, 281–303.

Holton, J. R., Haynes, P. H., McIntyre, M. E., Douglas, A. R., Rood, R. B. and co-authors. 1995. Stratosphere–troposphere exchange. *Rev. Geophys.* **33**, 403–439.

Hoor, P., Fischer, H. and Lelieveld, J. 2005. Tropical and extratropical tropospheric air in the lowermost stratosphere over Europe: a CO-based budget. *Geophys. Res. Lett.* **32**. DOI: 10.1029/2004GL022018.

Hoskins, B. J. 1991. Towards a PV-θ view of the general circulation. *Tellus, Ser AB.* **43**, 27–35.

Intergovernmental Panel on Climate Change. 2007. *Contribution of Working Group I to the Fourth Assessment Report of the Intergovernmental Panel on Climate Change, 2007*. (eds. S. Solomon, et al.). Cambridge University Press, Cambridge, United Kingdom and New York, NY, USA.

Johansson, S. A. E. and Campbell, J. L. 1988. *PIXE: A Novel Technique for Elemental Analysis*. John Wiley, Hoboken, NJ.

Jost, H. J., Drdla, K., Stohl, A., Pfister, L., Loewenstein, M. and co-authors. 2004. In-situ observations of mid-latitude forest fire plumes deep in the stratosphere. *Geophys. Res. Lett.* **31**, L11101. DOI: 10.1029/2003GL019253.

Junge, C. E., Chagnon, C. W. and Manson, J. E. 1961. A world-wide stratospheric aerosol layer. *Science*. **133**, 1478–1479.

Lelieveld, J., Bregman, B., Arnold, F., Bürger, V., Crutzen, P. J. and co-authors. 1997. Chemical perturbation of the lowermost stratosphere through exchange with the troposphere. *Geophys. Res. Lett.* **24**, 603–606.

Lin, P. and Fu, Q. 2013. Changes in various branches of the Brewer–Dobson circulation from an ensemble of chemistry climate models. *J. Geophys. Res.* **118**, 73–84. DOI: 10.1029/2012JD018813.

Martinsson, B. G., Brenninkmeijer, C. A. M., Carn, S. A., Hermann, M., Heue, K. P. and co-authors. 2009. Influence of the 2008 Kasatochi volcanic eruption on sulfurous and carbonaceous aerosol constituents in the lower stratosphere. *Geophys. Res. Lett.* **36**, L12813. DOI: 10.1029/2009GL038735.

Martinsson, B. G., Nguyen, H. N., Brenninkmeijer, C. A. M., Zahn, A., Heintzenberg, J. and co-authors. 2005. Characteristics and origin of lowermost stratospheric aerosol at northern midlatitudes under volcanically quiescent conditions based on CARIBIC observations. *J. Geophys. Res.* **110**, D12201. DOI: 10.1029/2004JD005644.

Martinsson, B. G., Papaspiropoulos, G., Heintzenberg, J. and Hermann, M. 2001. Fine mode particulate sulphur in the tropopause region measured from intercontinental flights (CARIBIC). *Geophys. Res. Lett.* **28**, 1175–1178.

Massie, S. T. 2014. *AURA Cloud/Aerosol/SO2Working Group*. Online at: http://avdc.gsfc.nasa.gov/PDF/volcano.pdf

McCormick, M. P., Thomason, L. W. and Trepte, C. R. 1995. Atmospheric effects of the Mt Pinatubo eruption. *Nature*. **373**, 399–404.

Murphy, D. M., Thomson, D. S. and Mahoney, M. J. 1998. In situ measurements of organics, meteoritic material, mercury, and other elements in aerosols at 5 to 19 kilometers. *Science*. **282**, 1664–1669. DOI: 10.1126/science.282.5394.1664.

Nagai, T., Liley, B., Sakai, T., Shibata, T. and Uchino, O. 2010. Post-Pinatubo evolution and subsequent trend of the stratospheric aerosol layer observed by mid-latitude lidars in both hemispheres. *Sola*. **6**, 69–72. DOI: 10.2151/sola.2010-018.

Neely III, R. R., Toon, O. B., Solomon, S., Vernier, J. P., Alvarez, C. and co-authors. 2013. Recent anthropogenic increases in SO_2 from Asia have minimal impact on stratospheric aerosol. *Geophys. Res. Lett.* **40**, 999–1004. DOI: 10.1002/grl.50263.

Nguyen, H. N., Gudmundsson, A. and Martinsson, B. G. 2006. Design and calibration of a multi-channel aerosol sampler for tropopause region studies from the CARIBIC platform. *Aerosol Sci. Technol.* **40**, 649–655. DOI: 10.1080/02786820600767807.

Nguyen, H. N. and Martinsson, B. G. 2007. Analysis of C, N and O in aerosol collected on an organic backing using internal

blankmeasurements and variable beam size. *Nucl. Instrum. Methods Phys. Res. Sect. B.* **264**, 96–102. DOI: 10.1016/j.nimb.2007.08.001.

Nguyen, H. N., Martinsson, B. G., Wagner, J. B., Carlemalm, E., Ebert, M. and co-authors. 2008. Chemical composition and morphology of individual aerosol particles from a CARIBIC flight at 10 km altitude between 50 N and 30 S. *J. Geophys. Res.* **113**, D23209. DOI: 10.1029/2008JD009956.

Oram, D. E., Mani, F. S., Laube, J. C., Newland, M. J., Reeves, C. E. and co-authors. 2012. Long-term tropospheric trend of octafluorocyclobutane (c-C4F8 or PFC-318). *Atmos. Chem. Phys.* **12**, 261–269. DOI: 10.5194/acp-12-261-2012.

Papaspiropoulos, G., Mentes, B., Kristiansson, P. and Martinsson, B. G. 1999. A high sensitivity elemental analysis methodology for upper tropospheric aerosol. *Nucl. Instrum. Methods Phys. Res. Sect. B.* **150**, 356–362.

Prata, A. J. and Bernardo, C. 2007. Retrieval of volcanic SO_2 column abundance from atmospheric infrared sounder data. *J. Geophys. Res.* **112**, D20204. DOI: 10.1029/2006JD007955.

Rauthe-Schöch, A., Weigelt, A., Hermann, M., Martinsson, B. G., Baker, A. K. and co-authors. 2012. CARIBIC aircraft measurements of Eyjafjallajökull volcanic clouds in April/May 2010. *Atmos. Chem. Phys.* **12**, 879–902. DOI: 10.5194/acp-12-879-2012.

Robock, A. 2000. Volcanic eruptions and climate. *Rev. Geophys.* **38**, 191–219.

Rosen, J. M. 1971. The boiling point of stratospheric aerosols. *J. Appl. Meteorol.* **10**, 1044–1046.

Rudnick, R. L. and Fountain, D. M. 1995. Nature and composition of the continental crust: a lower crustal perspective. *Rev. Geophys.* **33**, 267–309.

Schmale, J., Schneider, J., Jurkat, T., Voigt, C., Kalesse, H. and co-authors. 2010. Aerosol layers from the 2008 eruptions of Mount Okmok and Mount Kasatochi: in situ upper troposphere and lower stratosphere measurements of sulfate and organics over Europe. *J. Geophys. Res.* **115**, D00L07. DOI: 10.1029/2009JD013628.

Schuck, T. J., Brenninkmeijer, C. A. M., Slemr, F., Xueref-Remy, I. and Zahn, A. 2009. Greenhouse gas analysis of air samples collected onboard the CARIBIC passenger aircraft. *Atmos. Meas. Tech.* **2**, 449–464.

Schwarz, J. P., Spackman, J. R., Gao, R. S., Watts, L. A., Stier, P. and co-authors. 2010. Global-scale black carbon profiles observed in the remote atmosphere and compared to models. *Geophys. Res. Lett.* **37**, L18812. DOI: 10.1029/2010GL044372.

Smith, J. B., Hintsa, E. J., Allen, N. T., Stimpfle, R. M. and Anderson, J. G. 2001. Mechanisms for midlatitude ozone loss: heterogeneous chemistry in the lowermost stratosphere? *J. Geophys. Res.* **106**, 1297–1309.

Solomon, S., Borrmann, S., Garcia, R. R., Portmann, R., Thomason, L. and co-authors. 1997. Heterogeneous chlorine chemistry in the tropopause region. *J. Geophys. Res.* **102**, 21411–21429.

Solomon, S., Daniel, J. S., Neely, R. R., Vernier, J. P., Dutton, E. G. and co-authors. 2011. The persistently variable ''background'' stratospheric aerosol layer and global climate change. *Science.* **333**, 866–870. DOI: 10.1126/science.1206027.

Spracklen, D. V., Arnold, S. R., Sciare, J., Carslaw, K. S. and Pio, C. 2008. Globally significant oceanic source of organic carbon aerosol. *Geophys. Res. Lett.* **35**, L12811.

Sprenger, M. and Wernli, H. 2003. A northern hemispheric climatology of cross-tropopause exchange for the ERA15 time period (1979–1993). *J. Geophys. Res.* **108**(D12), 8521. DOI: 10.1029/2002JD002636.

Sprung, D. and Zahn, A. 2010. Acetone in the upper troposphere/lowermost stratosphere measured by the CARIBIC passenger aircraft: distribution, seasonal cycle, and variability. *J. Geophys. Res.* **115**, D16301. DOI: 10.1029/2009JD012099.

Stramska, M. 2009. Particulate organic carbon in the global ocean derived from SeaWiFS ocean color. *Deep Sea Res. Part I.* **56**, 1459–1470.

Tang, Q., Prather, M. J. and Hsu, J. 2011. Stratosphere–troposphere exchange ozone flux related to deep convection. *Geophys. Res. Lett.* **38**, L03806. DOI: 10.1029/2010GL046039.

Thomas, H. E., Watson, I. M., Carn, S. A., Prata, A. J. and Realmuto, V. J. 2011. A comparison of AIRS, MODIS and OMI sulphur dioxide retrievals in volcanic clouds. *Geomatics Nat. Hazards Risk.* **2**(3), 217–232. DOI: 10.1080/19475705.2011.564212.

Trickl, T., Giehl, H., Jäger, H. and Vogelmann, H. 2013. 35 yr of stratospheric aerosol measurements at Garmisch-Partenkirchen: from Fuego to Eyjafjallajökull, and beyond. *Atmos. Chem. Phys.* **13**, 5205–5225. DOI: 10.5194/acp-13-5205-2013.

Vernier, J. P., Pommereau, J. P., Garnier, A., Pelon, J., Larsen, N. and co-authors. 2009. Tropical stratospheric aerosol layer from CALIPSO lidar observations. *J. Geophys. Res.* **114**, D00H10. DOI: 10.1029/2009JD011946.

Vernier, J. P., Thomason, L. W. and Kar, J. 2011a. CALIPSO detection of an Asian tropopause aerosol layer. *Geophys. Res. Lett.* **38**, L07804. DOI: 10.1029/2010GL046614.

Vernier, J. P., Thomason, L. W., Pommereau, J. P., Bourassa, A., Pelon, J. and co-authors. 2011b. Major influence of tropical volcanic eruptions on the stratospheric aerosol layer during the last decade. *Geophys. Res. Lett.* **38**, L12807. DOI: 10.1029/2011GL047563.

Weisenstein, D. K., Yue, G. K., Ko, M. K. W., Sze, N. D., Rodriguez, J. M. and co-authors. 1997. A two-dimensional model of sulfur species and aerosols. *J. Geophys. Res.* **102**, 13019–13035.

Yang, K., Liu, X., Bhartia, P. K., Krotkov, N. A., Carn, S. A. and co-authors. 2010. Direct retrieval of sulfur dioxide amount and altitude from spaceborne hyperspectral UV measurements: theory and application. *J. Geophys. Res.* **115**, D00L09.

Zahn, A. and Brenninkmeijer, C. A. M. 2003. New directions: a chemical tropopause defined. *Atmos. Environ.* **37**, 439–440.

Zahn, A., Brenninkmeijer, C. A. M., Asman, W. A. H., Crutzen, P. J., Heinrich, G. and co-authors. 2002. Budgets of O_3 and CO in the upper troposphere: CARIBIC passenger aircraft results 1997–2001. *J. Geophys. Res.* **107**(D17), 4337. DOI: 10.1029/2001JD001529.

Zahn, A., Weppner, J., Widmann, H., Schlote-Holubek, K., Burger, B. and co-authors. 2012. A fast and precise chemiluminescence ozone detector for eddy flux and airborne application. *Atmos. Meas. Tech.* **5**. DOI: 10.5194/amt-5-363-2012.

Paper III

Atmos. Meas. Tech., 7, 2581–2596, 2014
www.atmos-meas-tech.net/7/2581/2014/
doi:10.5194/amt-7-2581-2014

Atmospheric Measurement Techniques
Open Access

Comparison between CARIBIC Aerosol Samples Analysed by Accelerator-Based Methods and Optical Particle Counter Measurements

B. G. Martinsson[1], J. Friberg[1], S. M. Andersson[1], A. Weigelt[2,*], M. Hermann[2], D. Assmann[2], J. Voigtländer[2], C. A. M. Brenninkmeijer[3], P. J. F. van Velthoven[4], and A. Zahn[5]

[1]Division of Nuclear Physics, Lund University, Lund, Sweden
[2]Leibniz Institute for Tropospheric Research, Leipzig, Germany
[3]Division of Atmospheric Chemistry, Max Planck Institute for Chemistry, Mainz, Germany
[4]Royal Netherlands Meteorological Institute (KNMI), De Bilt, The Netherlands
[5]Institute of Meteorology and Climate Research, Forschungszentrum Karlsruhe, Karlsruhe, Germany
[*]now at: Institute for Coastal Research, Helmholtz-Zentrum Geesthacht, Geesthacht, Germany

Correspondence to: B. G. Martinsson (bengt.martinsson@nuclear.lu.se)

Received: 5 February 2014 – Published in Atmos. Meas. Tech. Discuss.: 1 April 2014
Revised: 4 July 2014 – Accepted: 10 July 2014 – Published: 19 August 2014

Abstract. Inter-comparison of results from two kinds of aerosol systems in the CARIBIC (Civil Aircraft for the Regular Investigation of the atmosphere Based on a Instrument Container) passenger aircraft based observatory, operating during intercontinental flights at 9–12 km altitude, is presented. Aerosol from the lowermost stratosphere (LMS), the extra-tropical upper troposphere (UT) and the tropical mid troposphere (MT) were investigated. Aerosol particle volume concentration measured with an optical particle counter (OPC) is compared with analytical results of the sum of masses of all major and several minor constituents from aerosol samples collected with an impactor. Analyses were undertaken with the following accelerator-based methods: particle-induced X-ray emission (PIXE) and particle elastic scattering analysis (PESA). Data from 48 flights during 1 year are used, leading to a total of 106 individual comparisons. The ratios of the particle volume from the OPC and the total mass from the analyses were in 84 % within a relatively narrow interval. Data points outside this interval are connected with inlet-related effects in clouds, large variability in aerosol composition, particle size distribution effects and some cases of non-ideal sampling. Overall, the comparison of these two CARIBIC measurements based on vastly different methods show good agreement, implying that the chemical and size information can be combined in studies of the MT/UT/LMS aerosol.

1 Introduction

The particles of the atmospheric aerosol have a broad spectrum of sources, where the anthropogenic contribution often can be difficult to quantify due to influences from natural sources at background conditions (Andreae and Rosenfeld, 2008). Despite being trace constituents of the atmosphere, particles are of considerable concern, such as adverse health effects and premature deaths (Pope III and Dockery, 2006) and climate change (IPCC, 2013), where in the latter case the direct and indirect effects of atmospheric particles can act as to mask the climate impact of greenhouse gases (Schwartz et al., 2010).

In this study the aerosol at 9–12 km altitude is investigated, thus dealing with the upper troposphere (UT) and the lowermost stratosphere (LMS) in the extratropics and the middle troposphere (MT) in the tropics. The vast majority of all studies of atmospheric aerosol concerns surface conditions. Aircraft measurements and remote sensing from the surface (Mattis et al., 2010) or from satellites, such as the NASA satellite CALIPSO (Vernier et al., 2011), are used to study the aerosol at higher altitudes. Besides information on scattered intensity for a given wavelength, multi-wavelength measurements combined with assumptions on particle composition and shape has been used to estimate particle size distribution in the 0.1 to above 1 µm diameter range (Bauman et

al., 2003). Smaller particles cannot be detected by remote sensing, and therefore also most of the aerosol dynamics cannot be studied. In addition, aerosol chemical information is normally not available by remote sensing except in very special circumstances (Rinsland et al., 1994). Remote sensing thus needs to be complemented by in situ observations of particle size distributions and composition in order to study sources and processes forming the aerosol. Research aircraft and balloons have been used for in situ studies of particle formation (de Reus et al., 1998), particle size distributions (Deshler et al., 2003) and particle chemical composition (Huebert et al., 2004). Based on the use of in-service passenger aircraft, long-term aerosol observations have been undertaken from the CARIBIC (Civil Aircraft for the Regular Investigation of the atmosphere Based on a Instrument Container) platform for the years 1997–2002 and 2005 to present (Brenninkmeijer et al., 1999, 2007) concerning particle chemical composition (Martinsson et al., 2001) and particle number concentrations (Hermann et al., 2003).

Aerosol particles in the 9–12 km altitude region contain a significant fraction of sulfurous aerosol (Dibb et al., 2000; Xu et al., 2001; Martinsson et al., 2001, 2005; Kojima et al., 2004). The carbonaceous fraction is another major component of the aerosol in this region (Murphy et al., 1998, 2006; Nguyen et al., 2008, Friberg et al., 2014). Black carbon constitutes a small fraction of the total carbon (Schwarz et al., 2010; Friberg et al., 2014). Occasionally chemical elements connected with crustal matter and fires are observed (Papaspiropoulos et al., 2002), which on rare occasions can have a strong influence on aerosol particle concentration (Eguchi et al., 2009; Dirksen et al., 2009; Fromm et al., 2010). Particles from explosive volcanism have strong effects on the studied region at times, affecting the climate (Ammann et al., 2003; Solomon et al., 2011), stratospheric ozone (McCormick et al., 1995) and aviation (Gislason et al., 2011). The aerosol particles in volcanic clouds contain besides the ash component (Schumann et al., 2011; Andersson et al., 2013) large sulphurous and carbonaceous components (Martinsson et al., 2009; Schmale et al., 2010; Carn et al., 2011).

The size distribution of the aerosol in the lowermost stratosphere is also strongly influenced by volcanism (Bauman et al., 2003). Hervig and Deshler (2002) compared balloon-borne optical particle counter (OPC) measurements with satellite-based measurements of extinction for several wavelengths from SAGE II and HALOE and found good agreement during periods of strong volcanic influence, whereas the OPC registered considerably higher particle surface area than the satellites during periods with little volcanic influence.

The study presented here deals with two very different CARIBIC aerosol measurements. Particle volume is obtained by integrating the size distributions obtained from an OPC. Subsequently these results are compared with the aerosol mass from samples that were analysed with PIXE (particle-induced X-ray emission) and PESA (particle elastic scattering analysis) for concentrations of all major and several minor chemical elements. Together these different measurements can deepen our understanding of the atmospheric aerosol by this combination of chemical and physical information. However, to reach that goal an assessment of the degree of agreement between the two measurements is needed. Therefore this paper is devoted to the comparison of the total particle volume concentration obtained from the CARIBIC OPC and the total mass concentration obtained from the analyses of the CARIBIC aerosol samples.

2 Methods

The measurements presented here were undertaken from the CARIBIC observatory (Brenninkmeijer et al., 2007; www.caribic-atmospheric.com/) where a large number of trace gases are measured and aerosol particles are characterized with respect to size distribution and composition during monthly sets of usually four intercontinental flights at 9–12 km altitude. The CARIBIC system comprises an instrumented container that is connected to a multiple probe inlet system for trace gases and aerosol that is permanently mounted on the belly of a Lufthansa Airbus A340-600. Concentrations of CO, O_3, NO/NO_y, VOCs, gaseous and condensed water are determined, and air samples collected are analysed for greenhouse gases, hydro and halo carbons (Brenninkmeijer et al., 2007; Schuck et al., 2009; Baker et al., 2010; Oram et al., 2012). Aerosol particle number concentration measurements down to a diameter of 4 nm are undertaken with three condensation particle counters (CPC, TSI model 7610; Hermann et al., 2003), and for the particle size distribution in the diameter range $\sim$130–$\sim$1000 nm a 16-channel OPC (RION, KS-93) is used (Rauthe-Schöch et al., 2012). Furthermore, aerosol samples are collected for subsequent analysis with respect to all major and several minor constituents (Martinsson et al., 2001; Nguyen et al., 2006; Nguyen and Martinsson, 2007). Details of the inlet system are described by Brenninkmeijer et al. (2007). The efficiency of the aerosol inlet is estimated to be 60 % for 5 µm diameter particles (Rauthe-Schöch et al., 2012). Based on modelling and previous experience the efficiency of the inlet is estimated to exceed 90 % for particles in the size range 0.01–1 µm diameter.

This comparison of the CARIBIC OPC and the analytical results obtained from the aerosol sampler span 1 year from April 2011 to March 2012. The measurements were undertaken during flights from Frankfurt in Germany to northern South America (24 flights), western North America (14), the Indian subcontinent (8) and eastern Asia (2), thus spanning a large region from 120° W to 120° E and 10 to 75° N. The average flight altitude was 10 900 m with a span of 9500 to 11 900 m. For those samples collected in clouds the average air temperature was below 230 K, implying that the

clouds were dominated of ice particles (Koop et al., 2000; Rosenfeld and Woodley, 2000). The meteorological modelling along the CARIBIC flight paths indicates that each sample affected by clouds encountered hydrometeors that in most cases consisted to 100 % of ice, the lowest fraction of ice being 99 % (http://www.knmi.nl/samenw/campaign_support/CARIBIC/). This is consistent with measured temperatures.

The aerosol sampling requires the longest sampling time of the two methods, thereby determining the amount of data available. For the investigated period of 1 year, 153 aerosol samples are available. This number available for comparison is lower by constraints that, of course, OPC data should be available and that uncertainties in total mass due to detection limit should be within ±5 % (described below). In addition, clouds were found to seriously affect the comparison. Therefore also measurements of gaseous and total water concentrations should be available for identification of samples collected in cloudy conditions. These requirements together reduce the number of samples available for the comparison to 106. The OPC – aerosol sampler intercomparison primarily deals with the integrated particle volume concentration obtained from the OPC (C_V) and the total aerosol mass concentration obtained as the sum of all major and several minor constituents of the aerosol samples (C_m).

2.1 Aerosol sampling and analysis

CARIBIC aerosol samples are collected by impaction on a 0.2 µm polyimide film, Proline-10, from Moxtek Inc., Orem, Utah, USA. The sampling unit contains three kinds of nozzles. Here nozzles connected the 14 channels that were sequentially activated for sampling and subsequent PIXE/PESA (Particle-Induced X-ray Emission/Particle Elastic Scattering Analysis) analysis were used. The typical sampling time for each sequential sample is 100 min. The collection efficiency of the sampler is 97 % ± 4 % for particles with aerodynamic diameter larger than 0.2 µm, and the 50 % cut-off diameter is 0.08 µm (Nguyen et al., 2006).

A cyclone separator placed up-stream of the sampler limits the upper particle size to 2 µm aerodynamic diameter. The penetration of the cyclone by particles smaller than 1 µm diameter has been measured to be 100 % ± 3 % (Nguyen et al., 2006). This cyclone is used exclusively for the aerosol sampler, implying that the OPC, to be described below, does not have the same definition of the upper size limit.

The collected samples were analysed for elemental composition by ion beam analysis (IBA). For sulphur (S) and elements with larger atomic number PIXE is used (Johansson and Campbell, 1988). The lower limit of the PIXE analysis of this study with respect to atomic number is connected with spectral interference, see Andersson et al. (2013) for further details. Hydrogen (H), carbon (C), nitrogen (N) and oxygen (O) are analysed by PESA. The analytical setup has been optimised with respect to sampling substrate and analytical parameters for PIXE (Papaspiropoulos et al., 1999) and PESA (Nguyen and Martinsson, 2007). During the time period of this study the detection efficiencies (i.e. the fraction of the samples where the element was detected) for H, C, N, O and S were 100, 96, 82, 95 and 100 %. Minor constituents were detected less frequently, like for instance potassium (K) 41 %, iron (Fe) 44 % and nickel (Ni) 30 %. The accuracy of the analyses is estimated to 10 % (Papaspiropoulos et al., 2002; Nguyen and Martinsson, 2007).

The total aerosol mass concentration (in ng m^{-3} STP; standard temperature and pressure) was obtained as the sum of all elemental mass concentrations. An element that was not detected in a sample was represented by the half of its minimum detection limit (MDL) which was added to the sum of the elements. When more than 5 % of that sum was from undetected elements (represented by half the MDL) the measurement was discarded, implying that the total mass concentration given has a ±5 % uncertainty due to elemental concentrations below the MDL. This requirement implied that only samples with detection of all the five major elements, H, C, N, O and S, were selected for this analysis. Uncertainties slightly larger than 5 % could appear for samples with a significant crustal component because some of the crustal elements, most notable silicon, are not analysed with adequate detection limits. This could lead to an underestimation of the crustal component by approximately 41 % according to average crust composition (Weaver and Tarney, 1984). For the two samples with the largest mass fractions of crust, containing 22 and 13 %, respectively, the total mass concentration could thus be underestimated by 9 and 5 %, respectively.

Combining the uncertainties of the sampling efficiency (4 and 3 %), elemental analysis (10 %) and effects from the minimum detection limit (5 %) the combined uncertainty of the mass concentration obtained from sampling and analysis becomes 12 %.

The aerosol sampler has demonstrated excellent properties in calibration procedures (Nguyen et al., 2006). Calibration results were obtained using liquid aerosol consisting of dioctyl serbacate (DOS) with traces of uranine. The performance of impactors is, however, sensitive to particle material as well as the amount of mass deposited. Solid particles can bounce off the sampling substrate, and in that way be lost. Bounce-off can be counteracted by the use of a coating of the impaction surface. Pak et al. (1992) showed that a coating of Apiezon-L grease needs to be more than 9 µm thick to obtain close to 100 % impactor collection efficiency for solid particles, whereas silicon oil shows more promising properties with rather high efficiency at 0.3 µm thickness. However, applying such a thickness would result in a factor of 2.5 thicker sampling substrate causing typically a factor 1.6 worse PIXE detection limits (if contamination in the coating process can be avoided). The effect on carbon detection can be expected to be much stronger, because the coating thickness variance will be added to that of the polyimide film which is low (Nguyen and Martinsson, 2007). Given the usually low

UT/LMS aerosol concentrations and the short sampling time, minimum detections limits are very important. Therefore no coating of the impaction surface was used. This should not be seen as a general recommendation, but rather as an adaption to a special measurement situation with respect to required detection limits and properties of MT/UT/LMS particles. Overloaded impactor substrates could suffer blow-off, where a sizable fraction of a solid or semi-solid deposit is blown away from the impaction zone. Impactors overloaded with liquid particles may wet the surface of the sampling substrate, causing a drift of deposited material away from the impaction region. Mass deposited away from this region might be outside the area where the analytical beam impinges on the sample. That mass will not interact with the beam thus causing too low measured concentrations.

In order to study the influence from the distorting effects on the aerosol samples of this study, all the 106 samples were photographed using a Canon EOS 550D with an EFS 15–85 mm lens. A photodiode placed behind the sample was used for illumination. The images were systematically evaluated based on the appearance of the deposit. Evidence of bounce-off could be found for one group of samples. Liquid samples wetting the surface outside the impaction region could also be observed, whereas no signs of large features at the outer part of the sample indicative of blow-off were obtained from any of the samples. Each of the four orifices of the impactor nozzle should produce a deposit, thus causing a square pattern of four deposits with a distance of 0.9 mm to the centre of the sampling substrate. The samples were classified in four basic groups. The first group, type 1, contains samples with no deviation from the ideal appearance, see Fig. 1a. Some samples contain low amounts of deposited mass, making identification of secondary deposition pattern more difficult. Type 1 samples are subdivided in normal (type 1.1) and low-loaded (1.2) samples. Frequently thin filaments of deposit stretching outside the regular impaction area were found (type 2, Fig. 1b). The type 2 samples are subdivided according to (2.1) wetting only inside the analytical beam area, (2.2) minor wetting outside the beam area and (2.3) considerable wetting outside the beam area. When the impactor jet meets the sampling surface the air flows out over the surface in all directions. Because of the fact that the present impactor contains four jets this outflow causes an interaction between the jets, causing secondary deposition of bounce-off-particles in between the ordinary deposition area. This is manifested by a deposition spot in the centre (Fig. 1c). In some cases a cross can be discerned, marking the outflow path of air from the central area. These type 3 samples were subdivided into three categories: (3.1) central spot discerned, (3.2) cross discerned and (3.3) cross clearly visible, in expected order of increasing severity of the bounce-off problem observed. Several images reveal tiny spots outside the central deposition area. This could be caused by imperfection of the polyimide film or it could be single particles that have bounced. A few samples have a large number of tiny spots outside the regular deposition area. When the number of spots over the 16 mm diameter polyimide film exceeded 15, the samples were classified as type 4. Otherwise they were classified according to the appearance of central deposit. An example of these type 4 samples is shown in Fig. 1d.

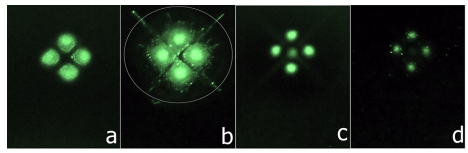

Figure 1. Photographic images of aerosol deposits from the CARIBIC aerosol sampler, where particles are collected from four impactor orifices. **(a)** Type 1: four spots of deposit (detected mass 100 ng). **(b)** Type 2: thin filaments of liquid aerosol out from the main deposit (670 ng). **(c)** Type 3: four spots and a secondary deposition pattern (92 ng). **(d)** Type 4: several small spots outside the deposition area (32 ng). The ellipse in **(b)** illustrates the beam size which is 5.5 mm vertically and 5.5/cos(23°) horizontally.

The different deposition types were summarized by a qualitative indicator (QI) expressing qualitatively the problem with losses for each sample based on the deposition pattern. QI = 0 are the samples where no significant losses are expected. The deposit types with QI = 0 are 1.1, 1.2, 2.1 and 2.2. Samples indicating discernible losses (QI = 1) comprise only type 3.1 samples. Sample deposits indicating more serious losses (QI = 2) include deposit types 2.3, 3.2, 3.3 and 4. Classification in these main and sub categories will be used in the evaluation of the comparison between the sampler and OPC.

To further substantiate the findings from images of the samples, use will be made of results from the elemental analysis itself. All samples are analysed in two steps, the first with a large ion beam area (5.5 mm diameter with beam current 150 nA and duration of 200 s per sample) used only for quantitative PIXE analysis. The second method, used for relative PIXE and PESA analyses, is based on a small beam (1 mm diameter). This small-beam analysis is based on three irradiations (beam current 15 nA with duration 3×200 s per sample), one over the aerosol deposit and two blank irradiations outside the main deposit area of the impactor at 4 mm distance from the deposit centre at opposite sides (Nguyen and Martinsson, 2007). These two internal blank measurements can be utilized to obtain an estimate of aerosol deposit outside the 5.5 mm diameter beam of the quantitative PIXE analysis. They should represent an area from the outer bound of the large beam to an outer bound where half of this doughnut area is inside a 4 mm radius. A circle with 4 mm radius has approximately twice the area of the beam in the slightly tilted sample plane (23°). Adding the same surface area outside the 4 mm radius, the blank spots can be

seen as to represent an area twice the size of the large beam, between diameters 5.5 and 9.5 mm. The estimated mass deposited is the areal density of an element (in ng cm^{-2}) multiplied with the surface area. To estimate non-ideal deposition outside the primary impactor deposition area the ratio between the mass deposited between 5.5 and 9.5 mm diameter (m_{udet}) and the mass detected in the quantitative analysis within 5.5 mm diameter (m_{det}) is formed. This ratio can only be formed for elements detected with PIXE because of the strong signal of H, C, N and O from the polyimide sampling substrate. The major aerosol constituent sulphur is detected with PIXE, and will therefore serve as the element used for estimation of deposition outside the main deposition area of the impactor. From Fig. 1c it is clear that secondary deposition is inhomogeneous in the vicinity of the impactor jets. It is not clear to what degree the secondary deposition pattern reaches outside the irradiated area of the sample. Therefore the m_{udet} / m_{det} ratios should be treated with some caution, especially for sample types 3.2 and 3.3. Additionally, this ratio only describes the aerosol components internally mixed with the sulphate aerosol. Components of other size modes, like crustal particles, may behave differently, as will be shown in Sect. 3.1. Samples with QI = 0, i.e. samples showing no visible imperfections in the deposition pattern, have m_{udet} / m_{det} ratios narrowly distributed around 0.03 indicating that 3 % of the aerosol deposit was outside the 5.5 mm ion beam used in the quantitative PIXE analysis. All samples were therefore corrected by that percentage to account for regular deposition outside the analysed area.

The analyses of the aerosol samples are undertaken in high vacuum of approximately 10^{-5} hPa. The samples remain at this pressure for 6 h, the duration of both analytical steps for a batch of 21 samples. This will cause losses of chemical compounds with a vapour pressure larger than the order of 10^{-7} Pa at room temperature (Martinsson, 1987; Deiters and Randzio, 2007). The main aerosol components observed in the analysed UT/LMS samples over the years are sulphurous and carbonaceous components, but sometimes also a significant crustal component can be observed. The sulphate compounds common in the atmosphere are not lost during analysis when particles, like in this study, are deposited onto a thin substrate, unless an external heating source is used (Martinsson and Hansson, 1988; Mentes et al., 2000). Among other common inorganic salts of the atmospheric aerosol, sodium chloride is stable during analysis, whereas ammonium nitrate will evaporate, if present. The occasional crustal component is expected to remain in the sample during analysis. The atmospheric carbonaceous aerosol component contains a broad range of vapour pressures. Therefore a definition of what is analysed is of need (Martinsson, 1987). In this case the IBA analytical definition most likely deviates from that during the OPC measurements, implying that the amount of carbonaceous aerosol determined by IBA could be smaller than the amount present during the OPC measurements.

2.2 Optical particle counter

For CARIBIC, a KS-93 OPC (RION CO., Ltd., Japan) was modified and applied for the first time onboard aircraft. The KS-93 has a diode laser with 830 nm wavelength, a lower detection limit of about 120 nm particle diameter, a robust synthetic quartz optical cell and is relatively small in size ($135 \times 280 \times 150$ mm), which makes it all well suited for airborne atmospheric research. The modified OPC is mounted together with the flow control system and the data acquisition in a 19″ rack unit. For data analysis the signals of the three OPC internal amplifiers are recorded with a real-time data acquisition system (PXI, National Instruments, USA) with 3 µs resolution. As the signal of one particle has an average duration of about 60 to 90 µs, each pulse is resolved with 20 to 30 data points. This data acquisition allows a free choice of the sampling time and number of channels. For the present analysis particle pulse heights were sorted into 16 channels and averaged over 300 s. For CARIBIC, the KS-93 signal output is improved by applying particle free sheath air (0.135 L min^{-1}) around the aerosol sampling air (0.015 L min^{-1}). In this configuration the CARIBIC OPC yields reliable data for particles larger than about 130 nm (optical diameter). The largest particle diameter which can be size-resolved is between 1.0 and 1.3 µm and depends on the particle refractive index and the respective calibration curve. However, as can be seen in Fig. 8, most of the volume distributions in the UT/LMS have their maximum in the particle size range between 300 and 600 nm. Hence the analysis in this study does not strongly depend on the OPC upper particle diameter limit. For the present analysis a theoretical response function based on spherical particles and the Mie theory was used (van de Hulst, 1981; Bohren and Huffman, 1983). This curve was related to the signal output by calibrating the OPC with latex and ammonium sulfate particles in the laboratory. Note that the OPC also counts particles larger than the upper size limit, but cannot determine their exact size. These particles are assigned to the largest particle size channel, which is therefore biased and not used in the analysis here. Uncertainties of the OPC data evaluation originate mainly from the "unknown", hence to be estimated particle refractive index, and the accuracy of the sampling air flow. They amount to ~ 10 % in particle size and ~ 19 % for the particle number concentration. Due to the cubed dependence of the particle volume on diameter the combined uncertainty of C_{V} becomes 50 %. For CARIBIC, the refractive index was calculated using literature values of the UT particle chemical composition (44 % H_2SO_4, 44 %, $(NH_4)_2SO_4$, 10 % organic carbon and 2 % soot) and a mixing rule to $1.479–0.0143i$. This refractive index was applied for the whole OPC size range. Additional information of the OPC unit is given in Rauthe-Schöch et al. (2012).

2.3 Additional methods

Besides the data from the OPC and the aerosol sampler, measurements of water are used to identify measurements that were influenced by clouds. The CARIBIC inlet system houses a forward-facing inlet tube for total water (H_2O_{tot}; being the sum of cloud water/ice and gaseous water) and one sideways-facing inlet tube for gaseous water (H_2O_{gas}) only. These two inlet lines are connected with two water vapour sensors, a chilled mirror frost point hygrometer (FPH) measuring total water (time resolution 10–180 s) and a two-channel photoacoustic laser spectrometer (PAS) detecting H_2O_{tot} and H_2O_{gas} (time resolution: $\sim$ 5 s). The PAS data are calibrated post-flight using the FPH data showing a total uncertainty of approximately 0.5 K (verified by regular laboratory-based cross-checks to high precision FHP instrument MWB LX-373). The calibrated PAS data have a precision of 2 % or 0.5 ppmv (whichever is higher).

We use the dynamical tropopause to differentiate between tropospheric and stratospheric air. This tropopause is based on the strong gradient in potential vorticity (PV) in the tropopause region (Hoerling et al., 1991; Hoinka, 1997). The PV along the flight track was obtained from archived European Centre for Medium-Range Weather Forecasts (ECMWF) analyses with a resolution of 1×1 degree in the horizontal and at 91 vertical hybrid sigma-pressure model levels. The PV was interpolated linearly in longitude, latitude, log pressure and time to the position of the aircraft. Based on PV, air masses were classified as tropospheric for average PV < 1.5 PVU (potential vorticity units; 1 PVU = 10^{-6} K m^2 kg^{-1} s^{-1}), and as belonging to the tropopause region for 1.5 < PV < 3 PVU. The samples taken in the LMS are subdivided in three groups of varying depth into the LMS, 3–5 PVU, 5–7 PVU and measurements taken in air masses with PV > 7 PVU.

3 Results and discussion

The primary measure used in the comparison between the OPC and the aerosol samples is the ratio of the OPC particle volume concentration (C_V) to the total mass concentration (C_m) obtained as the sum of the elemental concentrations from PIXE and PESA analysis of the aerosol samples. Figure 2 shows the 1 year data used to evaluate the relative performance of the two methods that are based on completely different physical principles. From the distribution it is clear that a large fraction of the measurements (85 %) have C_V / C_m ratios from 0.55 to 1.55 cm^3 g^{-1}. Out of the 106 samples 14 were found to have C_V / C_m ratios larger than the 1.55 cm^3 g^{-1} upper limit of this range and three were below the lower limit. The causes contributing to these 17 outliers will be investigated next.

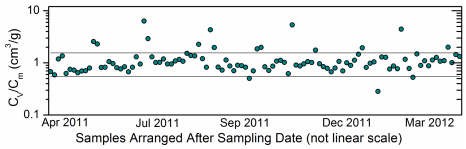

Figure 2. One year time series from CARIBIC measurements of the ratio of aerosol elemental concentrations from samples analysed with PIXE and PESA (C_m) and particle volume concentrations obtained from the OPC (C_V).

3.1 Examination of outlying data points

To shed light on the causes of outlying C_V / C_m ratios, the measurement situation, elemental composition features, size distribution and aerosol sample deposit patterns will be scrutinized. First the special case of sampling in clouds will be studied. Based on the CARIBIC measurements of gaseous and total water mixing ratios, intercepted clouds are detected (Brenninkmeijer et al., 2007). Figure 3a shows the C_V / C_m ratio related to the cloud ice concentration. Approximately half of the samples were obtained without any contact with clouds. The degree of cloud contact of the other samples varies strongly (note the logarithmic scale). When the cloud ice concentration is high, several measurements show high C_V / C_m ratio. The aerosol inlet is designed to collect particles of a few micrometre in diameter or smaller. When the inlet approaches particles at a cruise speed of 230 m s^{-1}, large particles that hit the leading edge of the shroud or, less likely the inlet cone itself, can disintegrate adding artifactual particles to the sampling airstream (Korolev et al., 2011). Because the leading edges and rim of the CARIBIC inlet have a surface-coating of nickel, we evaluated the connection between nickel elemental concentration and cloud ice concentrations. Figure 3b demonstrates a strong correlation for cloud ice concentration above 5 ppmv with aerosol sample nickel mass fractions larger than 0.05 %, indeed showing that, besides break-up of ice particles, the inlet contributes nickel when measuring inside clouds. This group of 10 samples will be further investigated, starting with photographic images of the aerosol samples to inspect the deposition patterns of the samples.

Out of this group of 10 instances four occurred in the tropics, five in the extra-tropical UT and one in the tropopause region. Figure 4a contains indeed a very incoherent message on the connection between deposition pattern and cloud influence or C_V / C_m ratio. Four of the samples show clear signs of losses based on a non-ideal deposition pattern (QI = 2; one type 3.2 and three type 4), four show traces of secondary deposition and the remaining two samples are classified as QI = 0 samples. The two samples most affected by clouds, sample No. 1 and 2, have deposition pattern type 4. They also have the two highest C_V / C_m ratios. The type 4 samples

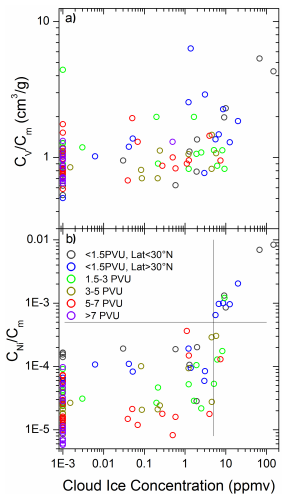

Figure 3. (a) Dependence of the ratio of particle volume to mass concentrations from OPC and IBA measurements (C_V / C_m), respectively, on average cloud ice concentration during each sampling period. **(b)** The latter related to the mass fraction of nickel in the samples. Note, in order to display zero cloud ice concentration in the logarithmic scale, 10^{-3} ppmv was added to each data point.

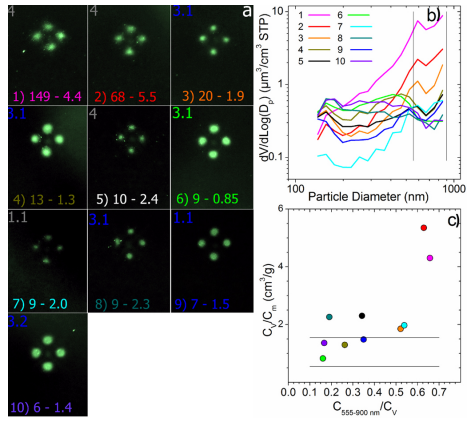

Figure 4. (a) Aerosol deposition pattern for samples affected by ice clouds. Numbers on bottom of pictures are measurement number, cloud ice concentration (ppmv) and OPC volume to IBA mass concentration ratio (C_V / C_m; cm^3 g^{-1}). The numbers in the top left corners show the aerosol deposit classification and their colour indicates air mass type according to the legend of Fig. 3. **(b)** Particle volume size distribution for measurements affected by clouds. Numbers in legends are measurement numbers in **(a)**. **(c)** C_V / C_m related to particle volume fraction in the four OPC channels of the largest sizes (555–900 nm). The colour of distributions in **(b)** and markers in **(c)** corresponds to bottom text colours in **(a)**.

are, as will be shown later, rather unusual, suggesting that the artefact particles generated at the inlet have a high probability for bounce-off and become spread over the surface. The volume size distributions of Fig. 4b are typical of artefactual particles due to particle break-up in clouds and do not appear in the absence of clouds. High values of the C_V / C_m ratio (Fig. 4c) are connected with high concentrations of large particles. It is also clear that there is a strong correlation between nickel in the aerosol samples and cloud ice concentration (Fig. 3b) likely originating in collisions between ice particles and materials of the walls of the inlet (Murphy et al., 2004). However, the amount of nickel collected in the sampler is much less than the signal registered in the OPC channels for large particles. Bounce-off could cause reduced collection efficiency of these newly formed, solid particles in the aerosol sampler. Another difficulty arises from the fact that the OPC measurements are based on the assumption of a sulphate-dominated aerosol, thus causing large sizing uncertainties for nickel particles due to the use of inadequate refractive index in the data evaluation. Additionally, nickel has a large density (8.9 g cm^{-3}) implying that the cyclone in front of the sampler catches particles approximately a factor of 3 smaller in terms of geometrical diameter compared to 2 µm aerodynamic diameter cut-off. Hence it is likely that a large fraction of the particles registered by the OPC is outside the range of the sampler, thus further adding to the uncertainties. It is clear that the large diameter channels of the CARIBIC OPC are severely affected by clouds, as are the CARIBIC nickel concentration measurements from the aerosol samples.

Measurements where the crustal component is significant were identified from the iron concentration and its relative concentration to potassium, calcium and titanium. Six samples have a relative iron concentration (C_{Fe} / C_m) larger than 0.3 %, corresponding to a crustal fraction (C_{crust} / C_m) of approximately 6 % according to average crust composition (Weaver and Tarney, 1984). The deposition patterns of crust-containing samples (Fig. 5a and, for sample No. 1, Fig. 4a) all show signs of losses. Five of the samples have QI = 2 and the remaining sample QI = 1. The C_V / C_m ratio is connected with the deposition pattern to a higher degree than the cloud-influenced samples. The size distributions of measurements with a strong crustal component are shown in Fig. 5b. The size distribution of the cloud-affected measurement (No. 1) differs markedly from the other crust-influenced measurements with high concentrations of the largest particles artificially produced in the inlet. Yet, all but sample No. 12 show high concentration in the OPC channel for the largest particles. Crustal particles usually are larger than

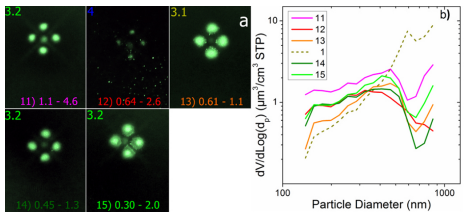

Figure 5. (a) Particle deposition patterns on the aerosol samples with a strong crustal component. Sample No., C_{Fe} / C_m mass ratio (%) and C_V / C_m ($cm^3\,g^{-1}$) are shown in the bottom of the images. Numbers in top left corners show deposition pattern and the colour indicates air mass type according to the legend of Fig. 3. **(b)** Volume size distributions from the OPC for samples with an Fe fraction larger than 0.3 % of the particle mass. Sample 1 (dashed) is also affected by clouds.

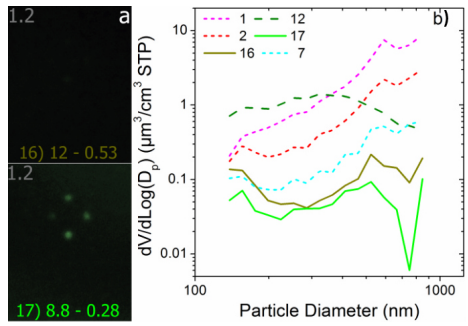

Figure 6. (a) Particle deposition patterns on the aerosol samples with a strong carbonaceous component. Sample No., C / S mass ratio and C_V / C_m ($cm^3\,g^{-1}$) are shown in the bottom of the images. Numbers in top left corners show deposition pattern and the colour indicates air mass type according to the legend of Fig. 3. **(b)** Volume size distributions from the OPC for samples with C / S mass ratio larger than 5. Samples also affected by clouds (short dashed in **b**) [No. 1 (C / S = 32), 2 (12) and 7 (6.2)], as well as those affected by crust (dashed) [No. 12 (9.5)], are shown only in **(b)**. Images of deposition patterns for these samples are displayed in Figs. 4 and 5, respectively.

sulphurous/carbonaceous particles indicating that the crustal particles mainly appear in the OPC channels for the largest particle sizes. Crustal particles differ significantly from the sulphate OPC calibration substance in refractive index as well as in particle shape, implying that the uncertainty of the OPC sizing of the crustal particles is large. The density of crustal particles is comparatively high, usually around $2.7\,g\,cm^{-3}$. This increases the probability that particles in the upper channels of the OPC are outside the upper aerodynamic limit of the aerosol sampler. The balance of these circumstances indicates that a mismatch in particle size range of the OPC and the aerosol sampler contributes to the high C_V / C_m ratios as well as non-ideal collection of crustal particles demonstrated by the deposition patterns.

The ratio of carbon (C) to sulphur (S) mass concentration varies by a factor of more than 100 between the samples in this study. Such variability in composition will of course affect the refractive index of the particles. Here samples with mass concentration ratio C / S > 5 will be examined. The mass of sulphate aerosol composed H_2SO_4 – $(NH_4)_2SO_4$ can be estimated to be 4 times the mass of S, implying that the carbonaceous component in these samples most likely is larger than the sulphurous fraction. Six of the 106 samples in this study had C / S mass concentration ratios larger than 5. Three of these samples were affected by clouds and one contained crust, which strongly affect the results of the comparison between the OPC and the sampler. The remaining two samples (Fig. 6a) show rather faint deposition patterns, the deposit of sample No. 16 being barely visible. Both of them are classified as type 1.2. These two measurements differ markedly from the cloud-affected and crust-containing samples with respect to size distribution (Fig. 6b) by showing a mode of small particles (most clear for sample 16). This indicates that a fraction of the particles escapes detection in the OPC while collected by the sampler having a much lower cut-off. This could be the cause of low C_V / C_m ratios. Also deviations of the actual optical properties from the refractive index assumed in the size attribution could be significant for these carbon-rich particles, e.g. underestimation of the soot fraction would lead to underestimation of C_V.

After the examination of the influence from clouds, crust and C / S composition 11 of the 17 outliers with respect to C_V / C_m ratio have been identified. The remaining six outliers are shown in Fig. 7. It is clear that the sampling failed to produce quantitative collection for samples 18–20 (Fig. 7a). The remaining measurements (No. 21, 22 and 23) show good sampling characteristics. The size distribution of sample 23, (Fig. 7b) indicates that a significant fraction of the particle volume can be found on particles smaller than the lowest size channel of the OPC, thus causing a low C_V / C_m ratio. The other two measurements (21 and 22) were taken in the LMS and display unusually large particles. This point will be discussed further in the next section.

3.2 Problems connected with the size distributions

To further evaluate the relation between the measurements with the OPC and the aerosol sampler, the size distributions will be examined. Difference in size range between the OPC (measuring 130–900 nm optical diameter) and the sampler (80–2000 nm aerodynamical diameter) could cause mismatch between the measurements, as discussed above. Assuming that the OPC measurements approximately resemble

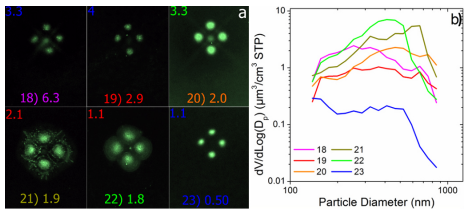

Figure 7. Samples outside the C_V / C_m range of 0.55–1.55 cm^3 g^{-1} marked in Fig. 2 that cannot be connected with cloud, crust or large carbonaceous fraction. **(a)** Particle deposition patterns on the aerosol samples with measurement No. and C_V / C_m (cm^3 g^{-1}) at bottom of the images. Numbers in top left corners show deposition pattern and the colour indicates air mass type according to the legend of Fig. 3. **(b)** Volume size distributions from the OPC.

the geometrical diameter the measurements would have the same upper size limit for particles of density of 5 g cm^{-3}. A lower density, usually true for atmospheric aerosol particles, would move the upper OPC limit downwards in aerodynamical size. In Fig. 8 particle volume size distributions are shown for all measurements not shown in Sect. 3.1 arranged according to the measurement region, i.e. UT, MT and LMS. It is clear that almost all measurements indicate that the particle volume outside the upper size limit of the OPC is small, implying that problems with mismatching upper size limits usually are small outside clouds (Fig. 4a) and in measurements with a strong crustal component (Fig. 5b).

The lower limits in particle size of the OPC and the impactor coincide at a particle density of approximately 0.4 g cm^{-3}. This low value implies that size distributions with large volume in the channel for the smallest particles might be underrepresented in terms of total particle volume from the OPC. Some size distributions show high concentrations in the two smallest particle channels without having a dominant mode of larger particles. These distributions could be expected to be most affected in the C_V / C_m ratio by particle volume outside the lower OPC measurement limit. In the tropics three measurements were taken in the fresh volcanic cloud from the eruption of Nyamurgira (DR Congo) in November 2011 with particle volume (and mass) concentrations similar to those deep into the LMS, see measurements 26, 27 and 28 in Fig. 8a (red vertical scale). These measurements together with 29 and 32 have C_V / C_m ratios of 0.69, 0.79, 0.80, 0.90 and 1.3 cm^3 g^{-1}. The low C_V / C_m ratios together with the size distributions of the measurements in the fresh volcanic cloud thus indicate some particle volume outside the OPC measurement range. All the measurements from the extratropical UT (Fig. 8b) have size distributions that indicate particle volume outside the lower size limit. However, the size distributions alone cannot explain variability in the C_V / C_m ratio of 0.77–1.4 cm^3 g^{-1}, for example

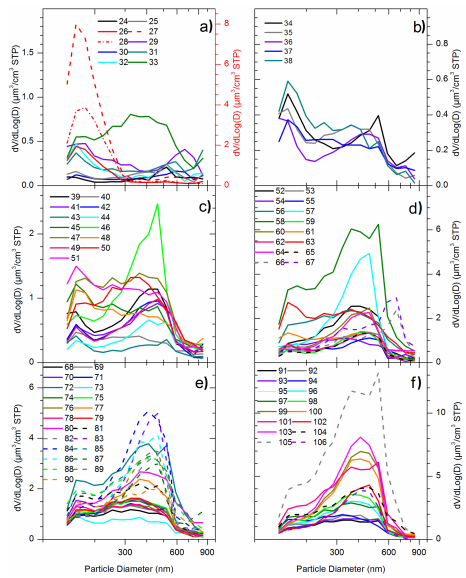

Figure 8. Particle volume distributions from the OPC for measurements without influence from clouds, high crustal or carbonaceous fractions. The legends show measurement number. **(a)** Tropics middle troposphere. Measurements 26–28 are shown on the axis to the right. **(b)** Extratropical UT (PV < 1.5 PVU). **(c)** Tropopause region (1.5 < PV < 3 PVU). **(d)** LMS 3 < PV < 5 PVU. **(e)** LMS 5 < PV < 7 PVU. **(f)** LMS PV > 7 PVU.

distributions 34 and 38 (the smallest and largest C_V / C_m ratio in this group) are similar both in terms of the distribution of small particles and relative particle volume for large particles. Measurements from the tropopause region (Fig. 8c) in some cases, in particular measurements 40, 43, 45 and 51, show significant concentration in the two lowest OPC channels without a dominant mode of larger particles. The respective C_V / C_m ratios are 0.83, 0.89, 1.0 and 1.2 cm^3 g^{-1}. All the measurement numbers are arranged in order of increasing C_V / C_m ratio in each of Fig. 8a–f. Presence of particles outside the lower size limit thus cannot explain the variability in the C_V / C_m ratio for measurements in the tropopause region. Finally, in Fig. 8d–f it can be seen that problems with particle volume outside the lower particle size limit are minor for the LMS aerosol. In conclusion it is clear that most size distributions from the MT tropics and the UT extratropics, and some of those from the tropopause region, indicate particle volume outside the lower size limit of the OPC, although it is not a major factor behind the variability of the C_V / C_m ratio. Measurements taken in the LMS do not indicate this problem.

In addition to investigating the conditions at the lower and upper size limit of the OPC, patterns associated with the volume mean diameter (VMD) will be examined. Figure 9 shows the C_V / C_m ratio related to the VMD. There is no clear correlation between these parameters for the tropospheric and tropopause region measurements. For measurements taken in the LMS weak correlation is found in the PV range 3–5 PVU, whereas the 5–7 PVU and PV > 7 PVU ranges show a clear correlation, i.e. when VMD increases from 270 to 360 nm (where most of these measurements are found) the C_V / C_m ratio in the LMS increases from 0.7 to 1.2 $cm^3\,g^{-1}$. Two of the measurements (red stars) in Fig. 9 are the two outliers (measurements 21 and 22 in Fig. 7) where no reason for the deviation could be found. Figure 9 indicates that the VMD is important for the observed deviation. As already pointed out, LMS size distributions show no sign of problems with the lower or upper size limits of the OPC measurements. However, the OPC response to particle size needs to be considered. Besides dependence on composition (refractive index) and particle shape, the calibration curve for a given composition is complicated. The range 0.7–1.2 $cm^3\,g^{-1}$ in C_V / C_m ratio corresponds to approximately ±25 % around the central value. If for the present, we disregard problems with the aerosol sampling and analysis this would indicate 25 % particle volume measurement uncertainty, corresponding to a range of a modest 8 % in terms of particle diameter for particles deep into the LMS.

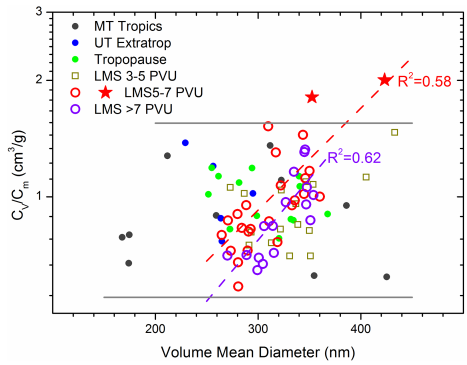

Figure 9. Dependence on volume mean diameter of the ratio of particle volume concentration (C_V, from the OPC) to mass concentration (C_m, from the aerosol samples). Purple and red lines are exponential fits to PV > 7 PVU and 5 < PV < 7 PVU data, respectively. Red stars are measurements classified as outliers where no explanation could be found in Sect. 3.1.

3.3 Problems in aerosol sampling and analysis

It is clear that problems in the aerosol sampling were responsible for some of the outliers with respect to the C_V / C_m ratio. The aerosol sampler collection efficiency shows excellent characteristics for liquid particles (Nguyen et al., 2006) and the errors from the PIXE and PESA analyses are small. However, solid particles could affect the sampling efficiency. Therefore all sample images not already dealt with in the previous sections (i.e. Figs. 4–7) will be investigated with respect to deposition pattern to find out to what degree the sampling suffered from losses.

Figure 10 shows the aerosol deposits of the samples taken in the tropical middle troposphere, the extratropical upper troposphere and the tropopause region. Ten tropical samples do not belong to the categories of outliers that were presented in Sect. 3.1. The aerosol sampling in the tropics usually worked well with seven QI = 0 (i.e. deposit types 1.1, 1.2, 2.1 and 2.2) samples and three samples with QI = 1 (deposit type 3.1), whereas none of the samples showed indications of severe losses (QI = 2; deposit types 2.3, 3.2, 3.3 and 4). Only five samples in Fig. 10 were taken in the extratropical UT. Three showed no signs of losses, one indicated minor losses and one major losses. Out of the 13 samples taken in the tropopause region, six showed no signs of losses, six minor losses and one sample indicated major losses. Overall, of the 28 samples from these three sampling regions 57, 36 and 7 % had QIs 0, 1 and 2, respectively.

The stratospheric samples are displayed in Fig. 11. Deposits with filaments wetting the surface of the polyimide film become more common in the stratosphere. Out of the 16 samples from the lowest stratospheric level, 3 < PV < 5 PVU (Fig. 11), 12 show no signs of losses (QI = 0), three show minor losses and one indicates significant losses (QI = 2). Deeper into the stratosphere, the PV range 5–7 PVU, 23 samples are available. Seventeen are of QI = 0, three of QI = 1 and three of QI = 2. Further up in the stratosphere, PV > 7 PVU, 15 out of 16 have QI = 0 and the only sample with QI = 2 shows wetting of the sampling substrate that is deemed to cause significant losses (type 2.3). Together the samples from the three stratospheric sampling levels have QI values of 0, 1 and 2 in 80, 11 and 9 % of the cases. Thus the fraction of the samples with major sampling problems is similar in the troposphere/tropopause and stratosphere, whereas a larger fraction of the stratospheric samples showed no signs of reduced collection efficiency.

Table 1 provides further overview of the classification with respect to aerosol deposit of the samples. Out of the total of 106 samples, 67 have deposit types that do not indicate losses in the sampling (QI = 0), 21 indicates minor losses (QI = 1) and 18 more severe losses (QI = 2). Eighty-three samples do not belong to the outlier categories clouds, crust, large carbonaceous fraction or the outlier samples presented in Fig. 7. Out of these 83 samples 72 % show no signs of losses (QI = 0) and 8 % have deposition patterns indicating major losses (QI = 2). It is clear that C_V / C_m shows a dependence on QI which is stronger when all samples are considered in comparison with when the four outlier

Table 1. Classification based on photographic images of all samples.

Category	Explanation	No. Samples Excl. outliers (All)[a]	C_V / C_m^b Excl. outliers (All)[a]	QI[c]
Type 1 – the expected pattern				
1.1	medium–high-loaded samples	26 (30)	0.86 (0.91)	0
1.2	low-loaded samples	1 (3)	[0.63] (0.45)	0
Type 2 – wetting of sampling substrate by liquid				
2.1	wetting only within beam area	28 (29)	0.89 (0.92)	0
2.2	minor wetting outside beam area	5 (5)	0.89 (0.89)	0
2.3	considerable wetting outside beam area	1 (1)	[1.3 (1.3)]	2
Type 3 – secondary deposition pattern				
3.1	central spot visible	16 (21)	1.0 (1.1)	1
3.2	cross visible	3 (7)	1.1 (1.5)	2
3.3	cross clearly visible	1 (3)	[1.1] (2.4)	2
Type 4 – large number of particles outside main deposit				
4		2 (7)	1.4 (2.6)	2
Qualitative Indicator (QI[c])				
0	types 1.1, 1.2, 2.1, 2.2	60 (67)	0.87 (0.88)	0
1	type 3.1	16 (21)	1.0 (1.1)	1
2	types 2.3, 3.2, 3.3, 4	7 (18)	1.2 (2.0)	2
All QI	all types	83(106)	0.93 (1.1)	All

[a] Referring to all samples except samples in the categories cloud, crust, C / S composition and "outliers" presented in Sect. 3.1 and to all samples in the study, respectively. [b] Geometrical average ($cm^3\,g^{-1}$) for each category. [ ] marks C_V / C_m of categories containing only one sample. [c] Qualitative indicator on the degree that the relation between measured to actual concentrations for the aerosol samples could be affected.

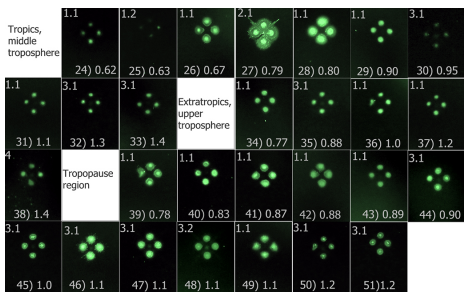

Figure 10. Photographic images of particle deposition patterns for middle troposphere tropics, extratropical upper troposphere and tropopause region samples not presented in Figs. 4–7. The upper left corner of each image shows the classification code of the deposit according to Table 1, and in the lower part sample number and C_V / C_m ($cm^3\,g^{-1}$) are shown. The bright lines in the image of sample 43 are caused by reflection in wrinkles present in this polyimide film.

categories are excluded see Table 1. The average C_V / C_m of the latter samples belonging with QI = 0 is $0.87\,cm^3\,g^{-1}$. The average of all the 83 samples is $0.93\,cm^3\,g^{-1}$, implying that the 23 samples with QI = 1 and QI = 2 increase the average C_V / C_m by 6 %.

It is clear that the deposition pattern based on qualitative classification of the samples in part can explain variability in the C_V / C_m ratio. Thereto we will briefly compare these results with measurements outside the regular 5.5 mm diameter proton beam used for quantitative analysis as explained in Sect. 2.1. Figure 12a shows the ratio of estimated, undetected sulfur mass outside the beam area of 5.5 mm diameter and the mass detected within the beam area, m_{udet} / m_{det}, in relation to particulate S concentration. Small, filled symbols indicate that particulate S was not detected in the two blank spots. These samples are represented by half the detection limit. It can be seen that particulate S could not be detected in the blank spots for samples with QI = 0 when the concentration was less than $100\,ng\,m^{-3}$ STP. This is also true for most of the QI = 1 samples (type 3.1), whereas most of the QI = 2 samples show detection with high m_{udet} / m_{det} ratio in that concentration range. For samples with particulate S concentration higher than $100\,ng\,m^{-3}$ STP the m_{udet} / m_{det} is low with a few exceptions. When relating m_{udet} / m_{det} to the C_V / C_m ratio for the samples where particulate S was detected in the blank spots a high degree of consistency can be found (Fig. 12b). m_{udet} / m_{det} is in all but one case low when the C_V / C_m ratio is low, and the deposit types are to a high degree of QI = 0 and 1. In the other end both the parameters usually are high and almost all samples have QI = 2. The agreement between the different measures further supports the consistency of the two different CARIBIC aerosol

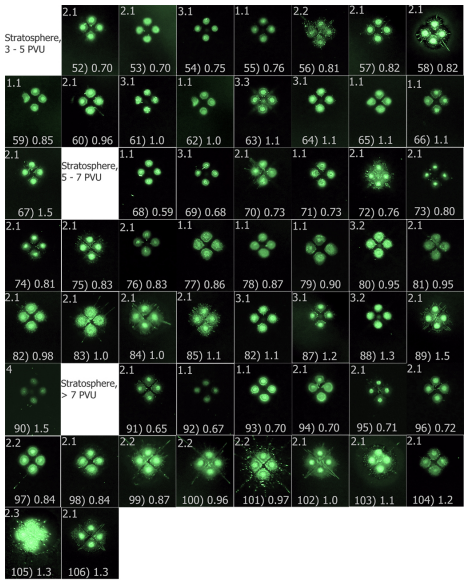

Figure 11. Photographic images of particle deposition patterns for stratospheric samples not presented in Figs. 4–7. Upper left corner of each image shows the classification code of the deposit according to Table 1, and in the lower part are sample number and C_V / C_m ($cm^3\,g^{-1}$).

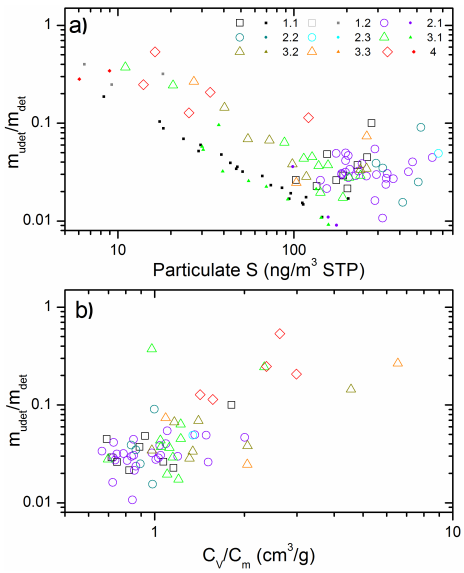

Figure 12. Ratio of estimated particulate sulphur mass outside the analytical beam (m_{udet}) to detected mass (m_{det}) related to **(a)** atmospheric particulate sulphur concentration and **(b)** the ratio total particle volume from the OPC (C_V) and total mass from the analyses of the aerosol samples (C_m). Particulate sulphur was detected in the analytical area of all samples. Open samples show analyses where sulphur was detected also outside the analytical area, whereas the small, closed symbols show samples where sulphur was not detected.

measurement methods. The m_{udet} / m_{det} ratio also provides an internal measure on the quality of a sample with respect to non-ideal effects in sampling with impactors.

3.4 Apparent particle density

To avoid bias from the outlier categories they are not retained in the data set used to further investigate the relation between the particle volume from the OPC and the mass from the sampling and analysis. The 83 measurements that did not belong to the outlier categories were all in the C_V / C_m range of 0.55–1.55 $cm^3\,g^{-1}$. Figure 13 shows C_V related to C_m. It is obvious that these measurements correlate well over approximately a factor of 50 in C_m and C_V ranges. The relative spread in the data (logarithmic scale) is essentially independent of the concentration, implying causes other than statistical for the variability within the 0.55–1.55 $cm^3\,g$ C_V / C_m range. By computing the geometric average (for consistency not the arithmetic average) of the ratio between C_m and C_V an estimate of the density of the aerosol particles is obtained. This apparent particle density becomes 1.08 $g\,cm^{-3}$. It is clear that non-ideal sampling affected some of the measurements. Removing these measurements result in the density 1.15 $g\,cm^{-3}$. The main components of the UT/LMS aerosol are sulphurous and carbonaceous aerosol. Occasionally the aerosol also contains a significant crustal fraction. The density of pure sulphuric acid is 1.84 $g\,cm^{-3}$, which could be somewhat lowered by mixing with water. Other possible forms of sulphate are ammonium bisulphate and ammonium sulphate with densities of 1.78 and 1.77 $g\,cm^{-3}$, respectively. The C / S elemental concentration ratio varies between 0.3 and 30 in the samples of this study. The carbonaceous fraction is to a large degree organic (Friberg et al., 2014). Probably the organic component acts as to lower the density of the particles, but likely not down to 1.15 $g\,cm^{-3}$. Previous measurements at remote location (Saarikoski et al., 2005; Kannosto et al., 2008) and an urban location (Hu et al., 2012) estimate the density of sub-micrometer atmospheric particles to approximately 1.5 $g\,cm^{-3}$. The apparent density of 1.15 $g\,cm^{-3}$ from this study is 30 % lower, thus calling for a discussion of the patterns behind this apparent density.

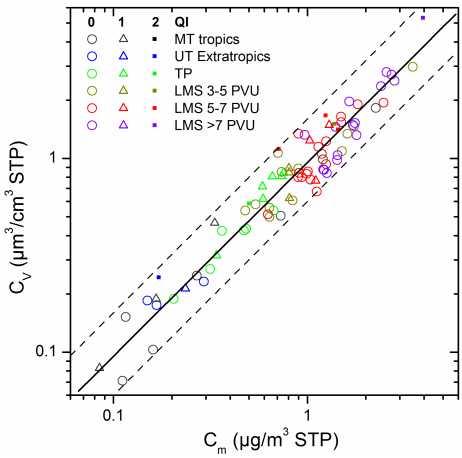

Figure 13. Particle volume concentration obtained from the OPC as a function of mass concentration from the aerosol samples taken at three PV levels in the stratosphere, the tropopause, the extratropical UT and the middle troposphere of the tropics. The colour of the symbols shows sampling location and the shape shows the quality indicator (QI) of the samples.

The measurements with the OPC and the elemental analyses of the samples are undertaken at approximately the same temperature. However, the analyses are undertaken in high vacuum, which can induce losses of organic material from the samples (Sect. 2.1). The composition and therefore the volatility of the organic fraction of the aerosol are not known. Therefore the losses during analysis cannot be estimated directly. The average carbon-to-sulphate mass ratio in samples of this study is 0.37, the ratio being higher in the troposphere (0.75) than in the stratosphere (0.26). To increase the apparent density to a value of $1.5\,\mathrm{g\,cm^{-3}}$ by increasing the carbon concentration in an attempt to reach more plausible value, the carbon concentrations need to be multiplied by approximately 2. This would increase the carbon-to-sulphate mass ratio average over all samples to 0.8, and for stratospheric samples carbon to sulphate mass ratio would become larger than 0.5, which is not in line with studies based on another analytical method (Murphy et al., 2006, 2007). In addition, studies of volcanic aerosol based on CARIBIC aerosol samples (Martinsson et al., 2009) agree well with studies based on other methods (Schmale et al., 2010; Carn et al., 2011) in the relation between the carbonaceous and sulphurous fractions of the aerosol. The increase of the carbonaceous fraction to reach $1.5\,\mathrm{g\,cm^{-3}}$ density would bring our volcanic measurements into disagreement with the mentioned other studies.

Losses of organic material would thus only explain part of the difference to previous observations at other locations. The uncertainties of the mass from the aerosol samples disregarding evaporative losses, is estimated to 12 %. The combined uncertainty in the number concentration and particle size combine to 50 % uncertainty in the particle volume determinations from the OPC. Taking the combined uncertainties of the two measurements into account, the observed apparent density is not deviating from previous observations.

4 Conclusions

Two aerosol measurement methods aboard the CARIBIC platform for studies of the upper troposphere (UT) and the lowermost stratosphere (LMS) were compared. The particle volume concentration (C_V) obtained from the CARIBIC optical particle counter (OPC) and total mass concentrations (C_m) obtained from aerosol samples analysed for all major and several minor constituents by ion beam analysis were compared by forming the ratio of the two measurements (C_V / C_m). 89 of the 106 measurements investigated have a C_V / C_m ratio confined to a rather narrow interval of 0.55–$1.55\,\mathrm{cm^3\,g^{-1}}$. Problems in the aerosol sampling were identified by photographic images of the deposition pattern, where secondary deposits indicate non-ideal sampling characteristics. Out of the 17 measurements outside the usual C_V / C_m range of 0.55–$1.55\,\mathrm{cm^3\,g^{-1}}$, six were connected with ice particles forming artificial particles in the inlet severely affecting total particle volume collected by the OPC and, in most cases, the aerosol deposition pattern of the samples. Three of the outliers were caused by non-ideal sampling of crustal particles and to some degree by problems with refractive index of the OPC and mismatch of the size ranges of the two measurements. Two of the measurements that were dominated by carbonaceous aerosol were below the usual C_V / C_m range because part of the size distribution was below the lower size limit of the OPC, and, probably due to a mismatch of the refractive index of the actual particles and that used in the OPC calibration. Of the remaining six measurements three showed poor sampling efficiency and the fourth mismatch in size range. The remaining two samples could be associated with the complicated relation between particle size and OPC signal, which was manifested by a correlation between particle volume mean diameter and the C_V / C_m ratio.

84 % of the measurements have C_V / C_m ratios within the range of 0.55–$1.55\,\mathrm{cm^3\,g^{-1}}$. The volume and mass concentrations span approximately a factor of 50 without significant change in relative residuals, thus indicating causes other than statistical for the variability. From this correlation the apparent average density of the particles was estimated to $1.15\,\mathrm{g\,cm^{-3}}$ after removal of 6 % bias from non-ideal sampling effects of the impactor. This apparent particle density is lower than previous estimates by 30 %. The combined

uncertainties of the two methods, however, accommodate this difference.

Visual inspection and classification of the samples aerosol deposits was found to be an efficient means to identify samples where non-ideal sampling appeared, which was corroborated by the C_V / C_m ratio. The analytical methodology utilizing blank spots of the sample provided further insights to the problem of non-ideal impactor sampling. This method can be applied routinely with minimal effort, thus providing the means to significantly reduce problems, however moderate in this study, from impactor sampling imperfections.

In conclusion, two methods based on widely different principles were inter-compared over a range of a factor of 50 in atmospheric aerosol concentration. The composition expressed as the ratio between the two main aerosol components in the aerosol particles, carbon and sulphur, varied over a range of a factor 100 thus further illustrating the variable condition in the UT/LMS. Except for a few outliers that could be connected with ice clouds, crust, size range mismatch or non-ideal sampling, a strong correlation between the two methods indicates that in most cases the CARIBIC aerosol sampling/analysis and OPC produce consistent and reliable results. This implies that the CARIBIC measurements with the OPC and the aerosol sampler can be combined to further understand the physical and chemical nature of the upper tropospheric and lowermost stratospheric aerosol.

Acknowledgements. We especially acknowledge C. Koeppel, D. S. Scharffe, S. Weber and all other members of the CARIBIC project. Lufthansa and Lufthansa Technik are gratefully acknowledged for enabling this scientific experiment. Financial support from the Swedish Research Council for Environments, Agricultural Sciences and Spatial Planning under grant 214-2009-613 is gratefully acknowledged.

Edited by: W. Maenhaut

References

Ammann, C. M., Meehl, G. A., Washington, W. M., and Zender, C. S.: A monthly and latitudinally varying volcanic forcing dataset in simulations of 20th century climate, Geophys. Res. Lett., 30, 1657, doi:10.1029/2003GL016875, 2003.

Andersson, S. M., Martinsson, B. G., Friberg, J., Brenninkmeijer, C. A. M., Rauthe-Schöch, A., Hermann, M., van Velthoven, P. F. J., and Zahn, A.: Composition and evolution of volcanic aerosol from eruptions of Kasatochi, Sarychev and Eyjafjallajökull in 2008–2010 based on CARIBIC observations, Atmos. Chem. Phys., 13, 1781–1796, doi:10.5194/acp-13-1781-2013, 2013.

Andreae, M. O. and Rosenfeld, D.: Aerosol-cloud-precipitation interactions, Part 1. The nature and sources of cloud-active aerosols, Earth-Sci. Rev., 89, 13–41, 2008.

Baker, A. K., Slemr, F., and Brenninkmeijer, C. A. M.: Analysis of non-methane hydrocarbons in air samples collected aboard the CARIBIC passenger aircraft, Atmos. Meas. Tech., 3, 311–321, doi:10.5194/amt-3-311-2010, 2010.

Bauman, J. J., Russell, P. B., Geller, M. A., and Patrick, H.: A stratospheric aerosol climatology from SAGE II and CLAES measurements: 2. Results and comparisons, 1984–1999, J. Geophys. Res., 108, 4383, doi:10.1029/2002JD002993, 2003

Bohren, C. F. and Huffman, D. R.: Absorption and Scattering of Light by Small Particles, 1st Edn., p. 530, New York: John Wiley & Sons, 1983.

Brenninkmeijer, C. A. M., Crutzen, P. J., Fischer, H., Güsten, H., Hans, W., Heinrich, G., Heintzenberg, J., Hermann, M., Immelmann, T., Kersting, D., Maiss, M., Nolle, M., Pitscheider, A., Pohlkamp, H., Scharffe, D., Specht, K., and Wiedensohler, A.: CARIBIC civil aircraft for global measurement of trace gases and aerosols in the tropopause region, J. Atmos. Ocean. Tech., 16, 1373–1383, 1999.

Brenninkmeijer, C. A. M., Crutzen, P., Boumard, F., Dauer, T., Dix, B., Ebinghaus, R., Filippi, D., Fischer, H., Franke, H., Frieß, U., Heintzenberg, J., Helleis, F., Hermann, M., Kock, H. H., Koeppel, C., Lelieveld, J., Leuenberger, M., Martinsson, B. G., Miemczyk, S., Moret, H. P., Nguyen, H. N., Nyfeler, P., Oram, D., O'Sullivan, D., Penkett, S., Platt, U., Pupek, M., Ramonet, M., Randa, B., Reichelt, M., Rhee, T. S., Rohwer, J., Rosenfeld, K., Scharffe, D., Schlager, H., Schumann, U., Slemr, F., Sprung, D., Stock, P., Thaler, R., Valentino, F., van Velthoven, P., Waibel, A., Wandel, A., Waschitschek, K., Wiedensohler, A., Xueref-Remy, I., Zahn, A., Zech, U., and Ziereis, H.: Civil Aircraft for the regular investigation of the atmosphere based on an instrumented container: The new CARIBIC system, Atmos. Chem. Phys., 7, 4953–4976, doi:10.5194/acp-7-4953-2007, 2007.

Carn, S. A., Froyd, K. D., Anderson, B. E., Wennberg, P., Crounse, J., Spencer, K., Dibb, J. E., Krotkov, N. A., Browell, E. V., Hair, J. W., Diskin, G., Sachse, G., and Vay, S. A.: In situ measurements of tropospheric volcanic plumes in Equador and Colombia during TC^4, J. Geophys. Res., 116, D00J24, doi:10.1029/2010JD014718, 2011.

Deiters, U. K. and Randzio, S. L.: A combined determination of phase diagrams of assymetric binary mixtures by equations of state and transitiometry, Fluid Phase Equilibr., 260, 87–97, 2007

de Reus, M., Ström, J., Kulmala, M., Pirjola, L., Lelieveld, J., Schiller, C., and Zöger, M.: Airborne aerosol measurements in the tropopause region and the dependence of new particle formation on preexisting particle number concentration, J. Geophys. Res., 103, 31255–31263, 1998.

Deshler, T., Hervig, M. E., Hofmann, D. J., Rosen, J. M., and Liley, J. B.: Thirty years of in situ stratospheric aerosol size distribution measurements from Laramie, Wyoming (41° N), using balloon-borne instruments, J. Geophys. Res., 108, 4167, doi:10.1029/2002JD002514, 2003.

Dibb, J. E., Talbot, R. W., and Scheuer, E. M.: Composition and distribution of aerosols over the North Atlantic during the subsonic assessment ozone and nitrogen oxide experiment (SONEX), J. Geophys. Res., 105, 3709–3717, doi:10.1029/1999JD900424, 2000.

Dirksen, R. J., Boersma, K. F., de Laat, J., Stammes, P., van det Werf, G. R., Martin, M. V., and Kelder, H. M.: An aerosol boomerang: Rapid around-the-world transport of smoke from the December 2006 Australian forest fires observed from space, J. Geophys. Res., 114, D21201, doi:10.1029/2009JD012360, 2009.

Eguchi, K., Uno, I., Yumimoto, K., Takemura, T., Shimizu, A., Sugimoto, N., and Liu, Z.: Trans-pacific dust transport: integrated analysis of NASA/CALIPSO and a global aerosol transport model, Atmos. Chem. Phys., 9, 3137–3145, doi:10.5194/acp-9-3137-2009, 2009.

Friberg, J., Martinsson, B. G., Andersson, S. M., Brenninkmeijer, C. A. M., Hermann, M., van Velthoven, P. J. F., and Zahn, A.: Sources of increase in LMS sulfurous and carbonaceous aerosol background concentrations during 1999–2008 from CARIBIC flights, Tellus B, 66, 23428, doi:10.3402/tellusb.v66.23428, 2014.

Fromm, M., Lindsey, D. T., Servranckx, R., Yue, G., Trickl, T., Sica, R., Douchet, P., and Godin-Beekmann, S.: The untold story of pyrocumulonimbus, B. Am. Meteorol. Soc., 91, 1193–1209, doi:10.1175/2010BAMS3004.1, 2010.

Gislason, S. R., Hassenkam, T., Nedel, S., Bovet, N., Eiriksdottir, E. S., Alfredsson, H. A., Hem, C. P., Balogh, Z. I., Dideriksen, K., Oskarsson, N., Sigfusson, B., Larsen, G., and Stripp, L. S.: Characterization of Eyjafjallajökull volcanic ash particles and protocol for rapid risk assessment, P. Natl. Acad. Sci. USA, 108, 7307–7312, 2011.

Hermann, M., Heintzenberg, J., Wiedensohler, A., Zahn, A., Heinrich, G., and Brenninkmeijer, C. A. M.: Meridional distributions of aerosol particle number concentrations in the upper troposphere and lower stratosphere obtained by Civil Aircraft for Regular Investigation of the Atmosphere Based on an Instrument Container (CARIBIC) flights, J. Geophys. Res., 108, 4114, doi:10.1029/2001JD001077, 2003.

Hervig, M. and Deshler, T.: Evaluation of aerosol measurements from SAGE II, HALOE, and balloon-borne optical particle counters, J. Geophys. Res., 107, 4031, doi:10.1029/2001JD000703, 2002.

Hoerling, M. P., Schaak, T. K., and Lenzen, A. J.: Global objective tropopause analysis, Mon. Weahter Rev., 119, 1816–1831, 1991.

Hoinka, K. P.: The tropopause discovery, definition and demarcation, Meteorol. Z., 6, 281–303, 1997.

Hu, M., Peng, J., Sun, K., Yue, D., Guo, S., Wiedensohler, A., and Wu, Z.: Estimation of size-resolved ambient particle density based on the measurement of aerosol number, mass and chemical size distributions in the winter in Beijing, Environ. Sci. Technol., 46, 9941–9947, doi:10.1021/es204073t, 2012.

Huebert, B., Bertram, T., Kline, J., Howell, S., Eatough D., and Blomquist, B.: Measurements of organic and elemental carbon in Asian outflow during ACE-Asia from the NSF/NCAR C-130, J. Geophys. Res., 109, D19S11, doi:10.1029/2004JD004700, 2004.

IPCC: Climate Change 2013: The Physical Science Basis. Contribution of working group I to the fifth assessment report of the Intergovernmental Panel on Climate Change, edited by: Stocker, T. F., Qin, D., Plattner, G.-K., Tignor, M. M. B., Allen, S. K., Boschung, J., Nauels, A., Xia, Y., Bex, V., and Midgley, P. M., Cambridge University Press, United Kingdom and New York, NY, USA, 1535 pp., 2013.

Johansson, S. A. E. and Campbell, J. L.: PIXE: A novel technique for elemental analysis, 347 pp., John Wiley, Hoboken, N. J., 1988.

Kannosto, J., Virtanen, A., Lemmetty, M., Mäkelä, J. M., Keskinen, J., Junninen, H., Hussein, T., Aalto, P., and Kulmala, M.: Mode resolved density of atmospheric aerosol particles, Atmos. Chem. Phys., 8, 5327–5337, doi:10.5194/acp-8-5327-2008, 2008.

Kojima, T., Buseck, P. R., Wilson, J. C., Reeves, J. M., and Mahoney, M. J.: Aerosol particles from tropical convective systems: Cloud tops and cirrus anvils, J. Geophys. Res., 109, D12201, doi:10.1029/2003JD004504, 2004.

Koop, T., Luo, B., Tsias, A., and Peter, T.: Water activity as the determinant for homogeneous ice nucleation in aqueous solutions, Nature, 406, 611–614, 2000

Korolev, A. V., Emery, E. F., Strapp, J. W., Cober, S. G., Isaac, G. A., Wasey, M., and Marcotte, D.: Small ice particles in tropospheric clouds: Fact or artifact?, B. Am. Meteorol. Soc., 92, 967–973, doi:10.1175/2010BAMS2935.1, 2011.

Martinsson, B. G.: An external beam PIXE/PESA setup for characterization of fine aerosols, Nucl. Instr. Meth. B, 22, 356–363, 1987.

Martinsson, B. G. and Hansson, H.-C.: Ion beam thermography – analysis of chemical compounds using ion beam techniques, Nucl. Instr. and Meth. B, 34, 203–208, 1988.

Martinsson, B. G., Papaspiropoulos, G., Heintzenberg, J., and Hermann, M.: Fine mode particulate sulphur in the tropopause region from intercontinental commercial flights, Geophys. Res. Lett., 28, 1175–1178, 2001.

Martinsson, B. G., Nguyen, H. N., Brenninkmeijer, C. A. M., Zahn, A., Heintzenberg, J., Hermann, M., and van Velthoven, P. F. J.: Characteristics and origin of lowermost stratospheric aerosol at northern midlatitudes under volcanically quiescent conditions based on CARIBIC observations, J. Geophys. Res., 110, D12201, doi:10.1029/2004JD005644, 2005.

Martinsson, B. G., Brenninkmeijer, C. A. M., Carn, S. A., Hermann, M., Heue, K.-P., van Velthoven, P. F. J., and Zahn, A.: Influence of the 2008 Kasatochi volcanic eruption on sulfurous and carbonaceous aerosol constituents in the lower stratosphere, Geophys. Res. Lett., 36, L12813, doi:10.1029/2009GL038735, 2009.

Mattis, I., Siefert, P., Müller, D., Tesche, M., Hiebesch, A., Kanitz, T., Schmidt, J., Finger, F., Wandinger, U., and Ansmann, A.: Volcanic aerosol layers observed with multiwavelength Raman lidar over central Europe in 2008–2009, J. Geophys Res., 115, D00L04, doi:10.1029/2009JD013472, 2010.

McCormick, M. P., Thomason, L. W., and Trepte, C. R.: Atmospheric effects of the Mt Pinatubo eruption, Nature, 373, 399–404, 1995.

Mentes, B., Papaspiropoulos, G., and Martinsson, B. G.: Ion-beam thermography analysis of the H_2SO_4 – $(NH_4)_2SO_4$ system in aerosol samples, Nucl. Instr. Meth. B, 168, 533–542, 2000.

Murphy, D. M., Thomson, D. S., and Mahoney, M. J.: In situ measurements of organics, meteoritic material, mercury, and other elements in aerosols at 5 to 19 kilometers, Science, 282, 5394, doi:10.1126/science.282.5394.1664, 1998.

Murphy, D. M., Cziczo, D. J., Hudson, P. K., Thomson, D. S., Wilson, J. C., Kojima, T., and Buseck, P. R.: Particle generation and resuspension in aircraft inlets when flying in clouds, Aerosol Sci. Technol., 38, 401–409, 2004.

Murphy, D. M., Cziczo, D. J., Froyd, K. D., Hudson, P. K., Matthew, B. M., Middlebrook, A. M., Peltier, R. E., Sullivan, A., Thomson, D. S., and Weber, R. J.: Single-particle mass spectrometry of tropospheric aerosol particles, J. Geophys. Res., 111, D23S32, doi:10.1029/2006JD007340, 2006.

Murphy, D. M., Cziczo, D. J., Hudson, P. K., and Thomson, D. S.: Carbonaceous material in aerosol particles in the lower strato-

sphere and tropopause region, J. Geophys. Res., 112, D04203, doi:10.1029/2006JD007297, 2007.

Nguyen H. N. and Martinsson B. G.: Analysis of C, N and O in aerosol collected on an organic backing using internal blank measurements and variable beam size, Nucl. Instr. Meth. B, 264, 96–102, 2007.

Nguyen, H. N., Gudmundsson, A., and Martinsson, B. G.: Design and calibration of a multi-channel aerosol sampler for studies of the tropopause region from the CARIBIC platform, Aerosol Sci. Technol., 40, 649–655, 2006.

Nguyen, H. N., Martinsson, B. G., Wagner, J. B., Carlemalm, E., Ebert, M., Weinbruch, S., Brenninkmeijer, C. A. M., Heintzenberg, J., Hermann, M., Schuck, T., van Velthoven, P. F. J., and Zahn, A.: Chemical composition and morphology of individual aerosol particles from a CARIBIC fight at 10 km altitude between 50° N and 30° S, J. Geophys. Res., 113, D23209, doi:10.1029/2008JD009956, 2008.

Oram, D. E., Mani, F. S., Laube, J. C., Newland, M. J., Reeves, C. E., Sturges, W. T., Penkett, S. A., Brenninkmeijer, C. A. M., Röckmann, T., and Fraser, P. J.: Long-term tropospheric trend of octafluorocyclobutane (c-C_4F_8 or PFC-318), Atmos. Chem. Phys., 12, 261–269, doi:10.5194/acp-12-261-2012, 2012.

Pak, S. S., Liu, B. Y. H., and Rubow, K. L.: Effects of coating thickness on particle bounce in inertial impactors, Aerosol Sci. Technol., 16, 141–150, 1992

Papaspiropoulos, G., Mentes, B., Kristiansson, P., and Martinsson, B. G.: A high sensitivity elemental analysis methodology for upper tropospheric aerosol, Nucl. Instr. Meth. B, 150, 356–362, 1999.

Papaspiropoulos, G., Martinsson, B. G., Zahn, A., Brenninkmeijer, C. A. M., Hermann, M., Heintzenberg, J., Fischer, H., and van Velthoven, P. F. J.: Aerosol elemental concentrations in the tropopause region from intercontinental flights with the CARIBIC platform, J. Geophys. Res., 107, 4671, doi:10.1029/2002JD002344, 2002.

Pope III, C. A. and Dockery, D. W.: Health effects of fine particulate air pollution: Lines that connect, J. Air Waste Manage., 56, 709–742, 2006.

Rauthe-Schöch, A., Weigelt, A., Hermann, M., Martinsson, B. G., Baker, A. K., Heue, K.-P., Brenninkmeijer, C. A. M., Zahn, A., Scharffe, D., Eckhardt, S., Stohl, A., and van Velthoven, P. F. J.: CARIBIC aircraft measurements of Eyjafjallajökull volcanic clouds in April/May 2010, Atmos. Chem. Phys., 12, 879–902, doi:10.5194/acp-12-879-2012, 2012.

Rinsland, C. P., Yue, G. K., Gunson, M. R., Zander, R. and Abrams, M. C.: Mid-infrared extinction by sulphate aerosols from the Mt Pinatubo eruption, J. Quart. Radiat. Transfer, 52, 241–252, 1994.

Rosenfeld, D. and Woodley, W. L.: Deep convective clouds with sustained supercooled liquid water down to −37.5 °C, Nature, 405, 440–442, 2000.

Saarikoski, S., Mäkälä, T., Hillamo, R., Aalto, P. P., Kerminen, V.-M., and Kulmala, M.: Physico-chemical characterization and mass closure of size-segregated atmospheric aerosols in Hyytiälä, Finland, Boreal Environ. Res., 10, 385–400, 2005.

Schmale, J., Schneider, J., Jurkat, T., Voight, C., Kalesse, H., Rautenhaus, M., Lichtenstern, M., Schlager, H., Ancellet, G., Arnold, F., Gerding, M., Mattis, I., Wendisch, M., and Borrmann, S.: Aerosol layers from the 2008 eruptions of Mount Okmok and Mount Kasatochi: In situ upper troposphere and lower stratosphere measurements of sulfate and organics over Europe, J. Geophys. Res., 115, D00L07, doi:10.1029/2009JD013628, 2010.

Schuck, T. J., Brenninkmeijer, C. A. M., Slemr, F., Xueref-Remy, I., and Zahn, A.: Greenhouse gas analysis of air samples collected onboard the CARIBIC passenger aircraft, Atmos. Meas. Tech., 2, 449–464, doi:10.5194/amt-2-449-2009, 2009.

Schumann, U., Weinzierl, B., Reitebuch, O., Schlager, H., Minikin, A., Forster, C., Baumann, R., Sailer, T., Graf, K., Mannstein, H., Voigt, C., Rahm, S., Simmet, R., Scheibe, M., Lichtenstern, M., Stock, P., Rüba, H., Schäuble, D., Tafferner, A., Rautenhaus, M., Gerz, T., Ziereis, H., Krautstrunk, M., Mallaun, C., Gayet, J.-F., Lieke, K., Kandler, K., Ebert, M., Weinbruch, S., Stohl, A., Gasteiger, J., Groß, S., Freudenthaler, V., Wiegner, M., Ansmann, A., Tesche, M., Olafsson, H., and Sturm, K.: Airborne observations of the Eyjafjalla volcano ash cloud over Europe during air space closure in April and May 2010, Atmos. Chem. Phys., 11, 2245–2279, doi:10.5194/acp-11-2245-2011, 2011.

Schwartz, S. E., Charlson, R. J., Kahn, R. A., Ogren, J. A., and Rodhe, H.: Why hasn't earth warmed as much as expected?, J. Climate, 23, 2453–246, 2010.

Schwarz, J. P., Spackman, J. R., Gao, R. S., Watts, L. A., Stier, P., Schulz, M., Davis, S. M., Wofsy, S. C., and Fahey, D. W.: Global-scale black carbon profiles observed in the remote atmosphere and compared to models, Geophys. Res. Lett., 37, L18812, doi:10.1029/2010GL044372, 2010.

Solomon, S., Daniel, J. S., Neely III, R. R., Vernier, J.-P., Dutton, E. G., and Thomason, L. W.: The persistently variable "background" stratospheric aerosol layer and global climate change, Science, 333, 866–870, 2011.

Van de Hulst, H. C.: Light Scattering by Small Particles, 2nd Edn., 23 pp., 124–126, New York: Dover Publications, ISBN: 0-486-64228-3, 1981.

Vernier, J.-P., Thomason, L. W., Pommereau, J.-P., Bourassa, A., Pelon, J., Garnier, A., Hauchecorne, A., Blanot, L., Trepte, C., Degenstein, D., and Vargas, F.: Major influence of tropical volcanic eruptions on the stratospheric aerosol layer during the last decade, Geophys. Res. Lett., 38, L12807, doi:10.1029/2011GL047563, 2011.

Weaver, B. L. and Tarney, J.: Empirical approach to estimating the composition of the continental crust, Nature, 310, 575–577, 1984.

Xu, L., Okada, K., Iwasaka, Y., Hara, K., Okuhara, Y., Tsutsumi, Y., and Shi, G.: The composition of individual aerosol particle in the troposphereand stratosphere over Xianghe (39.45° N, 117.0° E), China, Atmos. Environ., 35, 3145–3153, doi:10.1016/S1352-2310(00)00532-X, 2001.

Paper IV

nature COMMUNICATIONS

ARTICLE

Received 18 Dec 2014 | Accepted 29 May 2015 | Published 9 Jul 2015

DOI: 10.1038/ncomms8692 OPEN

Significant radiative impact of volcanic aerosol in the lowermost stratosphere

Sandra M. Andersson[1], Bengt G. Martinsson[1], Jean-Paul Vernier[2,3], Johan Friberg[1], Carl A.M. Brenninkmeijer[4], Markus Hermann[5], Peter F.J. van Velthoven[6] & Andreas Zahn[7]

Despite their potential to slow global warming, until recently, the radiative forcing associated with volcanic aerosols in the lowermost stratosphere (LMS) had not been considered. Here we study volcanic aerosol changes in the stratosphere using lidar measurements from the NASA CALIPSO satellite and aircraft measurements from the IAGOS-CARIBIC observatory. Between 2008 and 2012 volcanism frequently affected the Northern Hemisphere stratosphere aerosol loadings, whereas the Southern Hemisphere generally had loadings close to background conditions. We show that half of the global stratospheric aerosol optical depth following the Kasatochi, Sarychev and Nabro eruptions is attributable to LMS aerosol. On average, 30% of the global stratospheric aerosol optical depth originated in the LMS during the period 2008–2011. On the basis of the two independent, high-resolution measurement methods, we show that the LMS makes an important contribution to the overall volcanic forcing.

[1] Department of Physics, Lund University, P.O. Box 118, Lund 22100, Sweden. [2] Science Systems and Applications, Inc., Parkway, Suite 200, Hampton, Virginia 23666, USA. [3] NASA Langley Research Center, 11 Langley Boulevard, Hampton, Virginia 23681, USA. [4] Max Planck Institute for Chemistry, Department of Atmospheric Chemistry, Hahn-Meitner Weg 1, Mainz 55128, Germany. [5] Leibniz Institute for Tropospheric Research, Department of Experimental Aerosol and Cloud Microphysics, Permoserstrasse 15, Leipzig 04318, Germany. [6] Royal Netherlands Meteorological Division of Chemistry and Climate, Climate Research, P.O. Box 201, De Bilt 3730AE, The Netherlands. [7] Institute for Meteorology and Climate Research, Atmospheric Trace Gases and Remote Sensing, Karlsruhe Institute of Technology (KIT), P.O. Box 3640, Karlsruhe 76021, Germany. Correspondence and requests for materials should be addressed to B.G.M. (email: bengt.martinsson@nuclear.lu.se).

Early 21th century global warming has been overestimated by almost all simulations of historical climate change in the latest phase of the Coupled Model Intercomparison Project (CMIP5)[1,2]. This divergence between simulated and observed warming rates could be evidence of serious model errors in the climate sensitivity to anthropogenic greenhouse gas increases[3], or to systematic model deficiencies in representing natural internal variability[4,5]. It has been shown that tropical Pacific cooling due to increased subduction and upwelling[6,7] and variations in solar[2] and volcanic aerosol forcing[5,8] contribute to the discrepancy because they are not realistically described in CMIP5 simulations of recent climate change. Volcanic eruptions induce 'persistent variability' in the stratospheric aerosol layer[8–10]. Sulfur dioxide from volcanic eruptions forms sulfate particles that reflects sunlight back to space, exerting a cooling effect[11]. The CMIP5 historical simulations did not account for observed increases in volcanic aerosol loadings after the year 2000.

Most satellite-based estimates of global stratospheric aerosol optical depth (AOD) rely on occultation and other limb viewing measurements made at altitudes above the 380 K potential temperature level (on average, above 15-km altitude)[9,10,12]. These data have been used in a wide range of different climate studies, but do not include the lowermost stratosphere (LMS)[5,8,13–15]. The LMS lies between the 380 K potential temperature level (at ~17-km altitude in the tropics and 14 km at mid-latitudes) and the underlying tropopause (coinciding with the 380 K potential temperature level in the tropics and at ~10 (11) km at mid-latitudes in winter (summer)), and constitutes over 40% of the stratospheric mass[16]. The stratosphere above 380 K potential temperature is connected to the troposphere by an upward flow across the tropical tropopause via the Brewer–Dobson circulation. At mid- and high latitudes, the LMS receives seasonally varying fractions of subsiding stratospheric air from higher altitudes, and is also affected by tropospheric air crossing the extratropical tropopause. These flow patterns cause characteristic concentration gradients of trace gases[17,18] and aerosols[19]. Volcanic aerosols reach the LMS either by direct injection in the extratropics or by transport from above via the Brewer–Dobson circulation[18].

Global estimates of the contribution from volcanism to stratospheric aerosols have historically been performed by limb viewing satellite instruments, such as SAGE II[20] (Stratospheric Aerosol and Gas Experiment), GOMOS[21] (Global Ozone Monitoring by Occultation of Stars) and presently OSIRIS[22] (Optical Spectrograph and Infrared Imaging System). Their long line of sight is obscured by the occurrence of clouds close to the tropopause and by dense volcanic clouds. These problems make it difficult to use OSIRIS for observations below 380 K potential temperature[23,24], and also limit the use of SAGE II[25].

Recently, it has been suggested that the LMS contributes significantly to stratospheric AOD[24]. For the time period from 2000 to 2013, Ridley *et al.*[26] estimated that 30–70% of the total stratospheric AOD was from volcanic aerosols in the LMS. The latter study made use of ground-based lidar retrievals, the Aerosol Robotic Network (AERONET) of sun photometers, and balloon-borne measurements. The lack of vertically resolved aerosol information in the AERONET measurements limits their ability to reliably partition the tropospheric and stratospheric contributions to the AOD.

The results presented here rely on independent observational measurements from two different sources. The first source is the nadir viewing lidar on the Cloud-Aerosol Lidar and Infrared Pathfinder Satellite Observation (CALIPSO)[27] satellite. This instrument measures from the stratosphere down to the ground with high vertical resolution, thus enabling aerosol observations in the upper troposphere (UT) and LMS. The second source of information is from analyses of aerosol samples collected by the IAGOS-CARIBIC program (In-service Aircraft for a Global Observing System—Civil Aircraft for the Regular Investigation of the atmosphere Based on an Instrument Container), a passenger aircraft-based observatory[28]. IAGOS-CARIBIC was operational for most of the period 1999–2013, permitting study of the LMS in the Northern Hemisphere (NH). The global stratosphere up to 35-km altitude was investigated with CALIPSO during the period 2008 to early 2012, which covers several of the larger volcanic eruptions. We use the 2008 Kasatochi eruption to study the detailed post-eruption vertical structure of the LMS aerosol. Our study attempts to quantify the radiative influence of the LMS aerosol relative to the radiative impact of total stratospheric AOD (measured at a wavelength of 532 nm). In contrast to previous work, we explicitly resolve the vertical 'fine structure' of the aerosol loadings after a series of volcanic eruptions. During the period 2008–2011, volcanic activity was most pronounced in the NH. The Southern Hemisphere (SH) was generally close to background conditions during this period, showing radiative properties that can be explained by stratospheric circulation and stratosphere–troposphere exchange.

Results

IAGOS-CARIBIC observations. IAGOS-CARIBIC observations are performed regularly at altitudes of 9–12 km, which is in the free troposphere in the tropics and in the UT/LMS in the extratropics. Measurements during intercontinental flights provided sampling of the LMS in the NH. The majority of these samples (90%) were collected between 30° N and 65° N. To identify volcanic influence on aerosol sampled in the LMS, we use S/O_3, the ratio of particulate elemental sulfur to *in situ* ozone. This is a powerful tracer[29] because the (non-volcanic) background S/O_3 ratio is set high in the stratosphere before transport into the LMS. The S/O_3 time series in the LMS (Fig. 1), obtained from near-monthly intercontinental IAGOS-CARIBIC flights, show clear evidence of influence from volcanic eruptions (Table 1). After a period of little volcanic influence during 1999–2002, large S/O_3 ratios (increases of up to a factor of 16 relative to background) were measured following three extratropical eruptions between 2008 and 2011. Elevated S/O_3 is also associated with a number of tropical eruptions between 2005 and 2012 (ref. 30). The effects of tropical eruptions on the mid- to high-latitude LMS region appear a few months to more than a year after the eruptions, due to the time required for transport from the tropics[18]. In 2013, the LMS aerosol concentrations again approached the background levels of 1999–2002.

Volcanic aerosol from the eruption of Kasatochi in August 2008 (see insert in Fig. 1) was first measured by the CARIBIC observatory over eastern Europe 1 week after the eruption[29]. Samples collected within 2 months after the eruption showed large variation in their S/O_3 ratios, while those collected after longer than 2 months were more homogeneous as a result of mixing in the atmosphere. Elevated S/O_3 ratios indicate that the LMS was influenced by Kasatochi at least until March 2009, seven months after the eruption. The S/O_3 ratios increased again following multiple eruptions of the Redoubt volcano in March/April 2009.

CALIPSO observations. While the majority of CARIBIC measurements are made at cruise altitude (between 9 and 12 km), CALIPSO scans the entire stratospheric aerosol column. The distribution of aerosol produced by the eruption of Kasatochi is clearly shown by the scattering ratio (the ratio of the measured scattering to the modelled molecular scattering), an optical equivalent to the mixing ratio (Fig. 2). The eruption injected ash

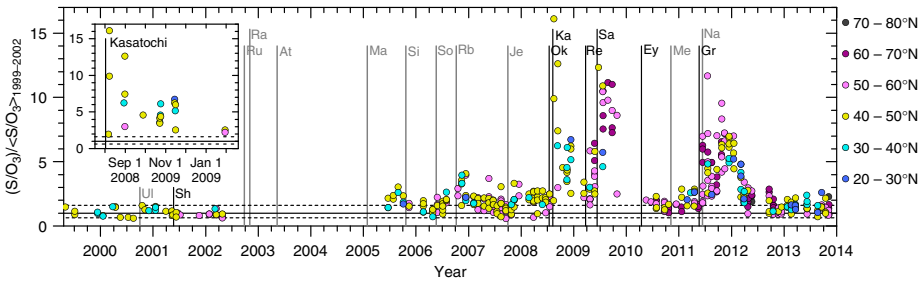

Figure 1 | Identification of volcanic aerosol in the LMS. IAGOS-CARIBIC time series of S/O_3 (ng m^{-3} STP p.p.b. v^{-1}) in the LMS, normalized by average S/O_3 during the 1999–2002 period of low volcanic influence. Major tick marks relate to Jan 1. The measurements were made at 9–12-km altitude, and the marker colour indicates the latitude band of aerosol sampling. Each measurement point corresponds to 100 (150 in 1999–2002) min of aerosol sampling. The full line indicates the geometrical average and the dashed lines the minimum and maximum S/O_3 ratio during the 1999–2002 period, normalized to its geometrical average of that period. The start dates of tropical (grey) and NH extratropical (black) eruptions that affected the stratosphere of the NH are denoted by vertical lines. The eruptions are: Ul (Ulawun), Sh (Sheveluch), Ru (Ruang), Ra (Reventador), At (Anatahan), Ma (Manam), Si (Sierra Negra), So (Soufrière Hills), Rb (Rabaul), Je (Jebel at Tair), Ok (Okmok), Ka (Kasatochi), Re (Redoubt), Sa (Sarychev), Ey (Eyjafjallajökull), Me (Merapi), Gr (Grimsvötn) and Na (Nabro), see Table 1 for details. The inset gives details for the Kasatochi eruption.

Table 1 | Volcanic eruptions in the 21th century that affect (or have the potential to affect) the aerosol loading of the stratosphere.

Volcano		Date	Lat.	Long.	VEI*	SO_2 (Tg)
Ulawun	Ul	29 Sep 2000	5° S	151° E	4	†
Sheveluch	Sh	22 May 2001	57° N	161° E	4	†
Ruang	Ru	25 Sep 2002	2° N	125° E	4	0.03 (ref. 50)
Reventador	Ra	3 Nov 2002	0° S	78° W	4	0.07 (ref. 50
Anatahan	At	10 May 2003	16° N	146° E	3	0.03 (ref. 50)
Manam	Ma	27 Jan 2005	4° S	145° E	4	0.09 (ref. 50)
Sierra Negra	Si	22 Oct 2005	1° S	91° W	3	†
Soufrière Hills	So	20 May 2006	17° N	62° W	3	0.2 (ref. 51)
Rabaul	Rb	7 Oct 2006	4° S	152° E	4	0.2 (ref. 50)
Jebel at Tair	Je	30 Sep 2007	16° N	42° E	3	0.08 (ref. 52)
Chaitén	Ch	2 May 2008	43° S	73° W	4	0.01 (ref. 53)
Okmok	Ok	12 Jul 2008	53° N	168° W	4	0.1 (ref. 52)
Kasatochi	Ka	7 Aug 2008	52° N	176° W	4	1.7 (ref. 52)
Redoubt	Re	23 Mar 2009	60° N	153° W	3	0.01 (ref. 54)
Sarychev	Sa	12 Jun 2009	48° N	153° E	4	1.2 (ref. 55)
Eyjafjallajökull	Ey	14 Apr 2010	64° N	20° W	4	†
Merapi	Me	5 Nov 2010	8° S	110° E	4	0.4 (ref. 56)
Grimsvötn	Gr	21 May 2011	64° N	17° W	4	0.4 (ref. 57)
Puyehue-Cordón Caulle	Pu	6 Jun 2011	41° S	72° W	5	0.3 (ref. 57)
Nabro	Na	12 Jun 2011	13° N	42° E	4	1.5 (ref. 57)

Lat., latitude; Long., longitude.
*VEI = Volcanic Explosivity Index (from Global Volcanism Program (http://www.volcano.si.edu/)).
†Not available.

and gases into two layers: one above 15 km that eventually spread over the entire NH, and one below 15 km in the NH LMS and extratropical UT. During the first few weeks after the eruption, the amount of aerosol increased due to the conversion of SO_2 into sulfate particles[31,32]. The volcanic particles produced in the LMS had almost vanished by November 2008 through export to the troposphere, from where they were efficiently removed. The LMS volcanic aerosol concentrations increased again after subsidence of the upper cloud (Fig. 2), thus explaining the elevated S/O_3 ratios observed by CARIBIC in December 2008 (see inset in Fig. 1).

Most of the aerosol from the Kasatochi eruption is found in the lower volcanic cloud. This is clear from examining aerosol scattering averaged over the extratropics (Fig. 3), which is optically equivalent to the aerosol concentration. The lower volcanic cloud had a relatively short but very large effect on the aerosol concentrations in the LMS, lasting ~2.5 months. The subsequent effect from the upper branch prolonged the volcanic influence on the LMS.

Discussion

In addition to the Kasatochi eruption, the Sarychev and Nabro eruptions (Table 1) clearly increased the global stratospheric AOD between 2008 and mid-2012, both above and below 15-km altitude (Fig. 4a). At least four other volcanic eruptions also had

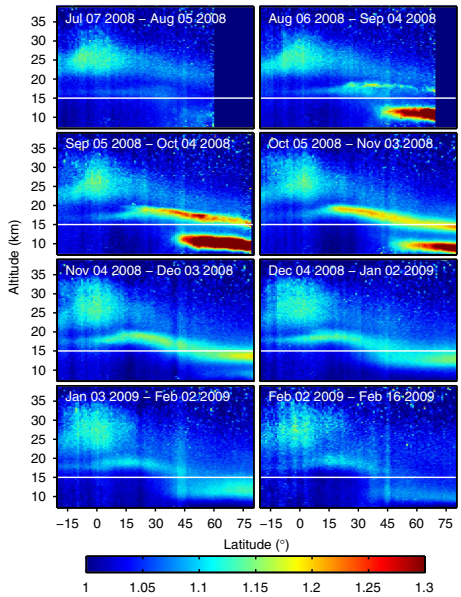

Figure 2 | Latitude and altitude distributions of Kasatochi volcanic aerosol. Distribution of the Kasatochi volcanic aerosol from CALIPSO measurements. Results are monthly and zonally averaged scattering ratios ((measured total scattering)/(modelled air molecular scattering)) from July 2008 to Feb 2009. Positive latitude values refer to the NH and negative to the SH. For Feb 2009, only 2 weeks of data were available. The feature in the tropics at 25 km, which is enhanced in the scattering ratio due to the weak scattering from air molecules at high altitudes, is already present before the eruption of Kasatochi, and is likely related to tropical upwelling and particle formation. High-latitude data are missing in the top two panels because of the limited latitudinal extent of the CALIPSO night-time data during the summer season. The white line indicates 15-km altitude.

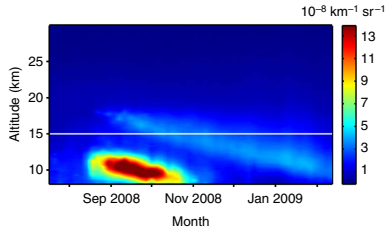

Figure 3 | Downward transport of Kasatochi volcanic aerosol. Time evolution from July 2008 to Feb 2009 of aerosol scattering as a function of altitude, spatially averaged over 40° N–80° N. Tick marks relate to the first day of a month. Results are shown as total backscatter from CALIPSO minus molecular backscatter. The white line indicates 15-km altitude.

some influence on the stratospheric aerosol loading in this period. The contribution of the LMS to total stratospheric aerosol is evident from a comparison of the global AOD calculated for the 15–35-km altitude range (the range used in almost all previous studies) and the total AOD between the tropopause to 35 km (Fig. 4a). For August to November 2008, the lower limit for calculating the integrated AOD was set to 2 km below the tropopause to include the total effect from the Kasatochi eruption, since the aerosol produced partly resided in the UT (see above).

To estimate the impact from the three largest eruptions between 2008 and mid-2012, the background AOD and radiative forcing during this time period were set to the values in the relatively quiescent periods between the Kasatochi, Sarychev and Nabro eruptions. Time integration over the elevated AOD during the three periods (Fig. 4a) then provides the total influence (grey areas in Fig. 4a) for the duration of appreciable impact of an eruption. From the integrated stratospheric AODs without and with the LMS included for the Kasatochi, Sarychev and Nabro eruptions, we found that altitudes below 15 km accounted for large fractions of the integrated AOD from these eruptions, namely 68, 54 and 41%.

Next, we estimate the fraction of the total, global stratospheric AOD attributable to aerosol in the LMS (f_{LMS}) over the entire 2008 to mid-2012 time period (Fig. 4b). The fraction is low (generally 20–30%) in periods between the three main eruptions. The f_{LMS} exceeds 50% 1 month after the Kasatochi eruption, and exceeds 40% after the Sarychev eruption. The Nabro eruption also yielded f_{LMS} values $>30\%$. Our results for the years 2008–2011 show an average f_{LMS} of 30%. This result is at the lower limit of the previous estimate of 30–70% for the years 2000–2013 by Ridley *et al*[26]. There are a number possible explanations for this finding. Ridley *et al.*[26] estimated stratospheric AOD based on data from the AERONET network of sun photometers. Because AERONET does not provide vertically resolved AOD data, this method has to rely on a model of the vertical distribution of the tropospheric AOD to estimate the stratospheric AOD. The time resolution of this approach is also limited, and the AOD impact of individual eruptions cannot be clearly resolved[26].The vertically resolved measurements from CALIPSO and IAGOS-CARIBIC permit a clearer separation between stratospheric and tropospheric AOD, and provide a new and independent assessment of the radiative impact of aerosol in the LMS.

In the following, we investigate f_{LMS} of the two hemispheres. The f_{LMS} is generally higher in the NH, and clearly shows an identifiable influence from the major eruptions (Fig. 4b). Three of the 4 years analysed display deep minima of f_{LMS} in July to August, with the exception of 2009 (which is masked by the Sarychev eruption). This annual minimum coincides with the minimum in size of the NH LMS[16] and the summer flushing of the LMS with tropical tropospheric air due to the weakened subtropical jet[17].

The SH was influenced by the eruptions of Merapi and Puyehue-Cordón Caulle. The SH f_{LMS} shows an annual variation pattern that is briefly disrupted in 2011 by the Puyehue-Cordón Caulle eruption. As in the case of the NH, the SH f_{LMS} has minima during all 5 years. These are evident in January to March, coinciding with the SH LMS minimum in size. The small influence from volcanism in the SH makes further investigation of the stratosphere–troposphere exchange feasible, because a large fraction of the stratospheric aerosol is formed in the Junge layer from carbonyl sulfide (OCS). The fraction of the LMS air that originates in that part of the stratosphere varies over the year, from $\sim$60% in the winter spring to 20% in the summer autumn[33,34]. With roughly 40% of the stratospheric air mass found in the LMS[16], we estimate that the LMS fraction of the aerosol-rich stratospheric air varies between 12 and 27% over the year. This estimate agrees well both in size and seasonal variation with our estimate of the observed f_{LMS} of the SH, indicating that

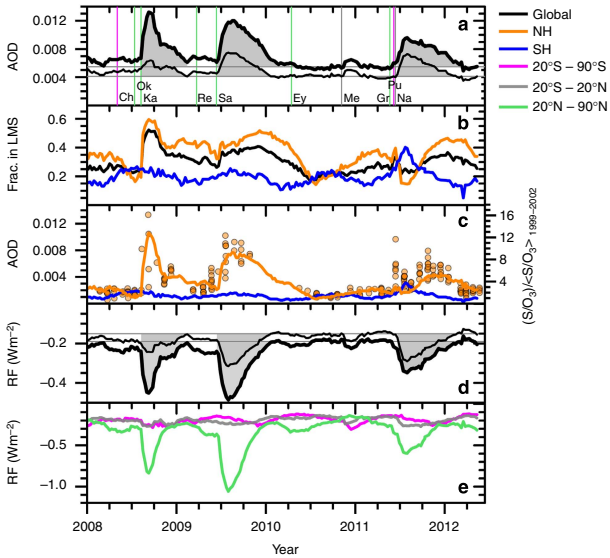

Figure 4 | Volcanic influence on global and regional aerosol radiative parameters. (**a**) Global AOD at 532-nm wavelength calculated using the integrated CALIPSO aerosol scattering from 15 to 35-km altitude (thin line) and from the tropopause to 35 km (thick line). Major tick marks relate to Jan 1. The volcanic eruption dates are denoted by vertical lines, colour coded according to latitude. The eruptions are: Ch (Chaitén), Ok (Okmok), Ka (Kasatochi), Re (Redoubt), Sa (Sarychev), Ey (Eyjafjallajökull), Me (Merapi), Gr (Grimsvötn), Pu (Puyehue-Cordón Caulle) and Na (Nabro), see Table 1 for details. The grey horizontal lines indicate the estimated background AOD of the 2008 to mid-2012 time period, and the shading denotes the total integrated volcanic AOD from the Kasatochi, Sarychev and Nabro eruptions. (**b**) The fraction of total AOD from the LMS. (**c**) AOD in the LMS from CALIPSO (lines) and S/O_3 in the NH from CARIBIC (circles). (**d**) As in **a**, but net radiative forcing (RF) calculated from AOD shown in **a**. (**e**) Stratospheric net radiative forcing in three regions equal in surface area.

during background conditions the LMS holds ~20% of the stratospheric aerosol.

All of the volcanic eruptions studied here increased the relative importance of the LMS. We speculate that most volcanic eruptions affecting the stratosphere will probably induce such an increase. This is obvious for extratropical eruptions injecting SO_2 directly to the LMS. Tropical eruptions can also be expected to increase f_{LMS}. At background conditions, a large fraction of the stratospheric aerosol is formed from OCS in the deep branch of the Brewer–Dobson circulation at altitudes of 25–30 km, because intense ultraviolet radiation is required to oxidize OCS in a first step to form sulfuric acid aerosol. Formation of sulfate aerosol from volcanic SO_2 takes place also at low stratospheric altitudes, which increases the aerosol transport in the shallow branch of the Brewer–Dobson circulation having a shorter residence time than the deep branch. A shorter residence time of the aerosol before entering the LMS increases the relative importance of the aerosol in the LMS.

Figure 4c shows the AOD of the SH and NH LMS obtained from CALIPSO LIDAR measurements, together with IAGOS-CARIBIC measurements of particulate sulfur. The IAGOS-CARIBIC measurements were taken in the NH, and were sampled in a strong concentration gradient arising from mixing of air across the extratropical tropopause. Because of this sharp gradient, the ratio to ozone (rather than the absolute concentration) is more representative of the volcanic additions to the LMS aerosol[29]. The IAGOS-CARIBIC measurements in proximity to volcanic eruptions exhibit large variability, which is subsequently reduced by atmospheric mixing. In contrast, the CALIPSO data are averaged hemispherically, thus smearing out small-scale spatial variability. This difference in spatial sampling is apparent after the Grimsvötn eruption, which causes a short but intense S/O_3 peak in the aircraft measurements, but has only a small signature in the CALIPSO observations. The effluents of that eruption were injected in the UT and the tropopause region, thus explaining the rapid decline and the comparatively weak response in the CALIPSO measurements. In addition, most of the IAGOS-CARIBIC observations were made at latitudes >55° N, outside of the latitude limit for CALIPSO night-time measurements (see Fig. 2). Aside from this difference, the CALIPSO and IAGOS-CARIBIC measurements—which were made with completely different instruments—show similar temporal variability.

In the following, we investigate the contribution of volcanic aerosol in the LMS region to recent climate change. We estimate this contribution by calculating radiative forcing using AOD estimates integrated over both 15–35 km and the tropopause − 35-km ranges (Fig. 4d). Our calculations are a function of both season and latitude (Fig. 5). As in the case of the AOD results described earlier, the radiative forcing is integrated for the Kasatochi, Sarychev and Nabro eruptions. We find that 56, 44 and 23% of the total radiative forcing from these eruptions originated from below 15 km.

The relationship between AOD and radiative forcing is affected by a variety of factors, including the latitudinal and seasonal variation in cloud cover, surface albedo and solar zenith angle. The extratropical location of the LMS introduces a dependence of

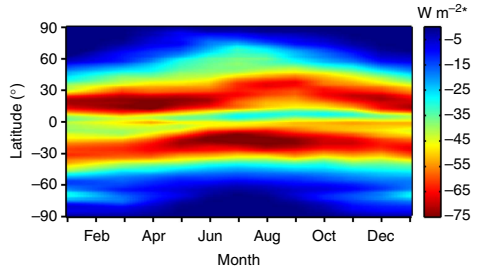

Figure 5 | Radiative forcing sensitivity to stratospheric AOD. Geographical and seasonal dependences of the average net radiative forcing for AOD = 1 at wavelength 532 nm. Tick marks relate to the first day of a month. Data are averaged over the period 2008–2011, and normalized by relative latitude area (*). The structures result from variability in daylength, upscatter fraction, surface albedo, cloudiness and transmission down to the aerosol layer.

radiative forcing on the seasonal variation in the number of sunlight hours. For Kasatochi, a clear elevation of the LMS AOD (defined here as the time period when the LMS AOD exceeded 50% of its peak value for a specific eruption) lasted from mid-August to the end of October. The influence from Sarychev extended from mid-2009 until the end of that year. This implies that both eruptions had their main impacts approximately centred on the time of the autumn equinox. The dominant part of the aerosol from the tropical Nabro eruption was advected north; Nabro's main impact on the LMS AOD occurred from the end of August to mid-February. Since this time of the year is characterized by few daylight hours, the radiative impact of the Nabro eruption in the LMS region was markedly reduced.

The eruptions studied here have clear geographical signatures (Fig. 4e). The NH extratropics were most affected by the three large eruptions described above, even in case of the near-equatorial Nabro eruption. A complete description of the volcanic aerosol loading from the total stratosphere, including the LMS region, will improve our understanding of the global- and regional-scale climatic effects of recent volcanic activity[5]. Such information will be useful for studies seeking to quantify the role of volcanism in the present 'slow-down' in global-mean surface warming[2].

The IPCC best estimate of volcanically induced radiative forcing (from ref. 35) is based only on stratospheric measurements above 380 K in potential temperature[12], resulting in an aerosol radiative forcing of -0.11 (-0.15 to -0.08) W m^{-2} during the period 2008–2011. Our results indicate that inclusion of the LMS increases the global stratospheric AOD by 45% and global radiative forcing by >30% during this 4-year period. This substantially increases the estimated radiative forcing and surface cooling. These findings provide considerable motivation for repeating CMIP5 simulations of historical climate change with improved estimates of AOD for the total stratosphere.

Methods

IAGOS-CARIBIC sampling and analysis. We used data from the IAGOS-CARIBIC observatory (www.caribic-atmospheric.com) which is based on a 1.5 ton measurement container transported onboard a long-range passenger aircraft. Measurements are typically made during four consecutive flights per month[28]. Aerosol sampling in IAGOS-CARIBIC is based on impaction of particles of 0.08–2.0-μm diameter onto 0.2-μm-thick polyimide films[36]. The time resolution is 100 min (150 min before 2005), which corresponds to a spatial resolution of ~1,500 km. Collected particles were analysed for elemental composition by two accelerator-based methods: Particle Induced X-ray Emission and Particle Elastic Scattering Analysis[37] at the Lund ion beam accelerator facility. The accuracy is estimated to be 10% (ref. 38). We also use O_3 mixing ratios obtained from IAGOS-CARIBIC, which have an accuracy of 0.3–1% (ref. 39). Particle size distributions were measured in 16 size channels in the diameter range of 0.13–0.9 μm with an optical particle counter[38]. The dynamical tropopause was used for classification of samples, where those taken in air masses with average potential vorticity (PV) >2 PVU (1 PVU = 10^{-6} K m^2 kg^{-1} s^{-1}) were classified as stratospheric. PV was obtained from ECMWF (European Centre for Medium-Range Weather Forecasts (ECMWF, http://www.ecmwf.int/)) reanalysis data at a 1 × 1 degree horizontal resolution and 91 vertical hybrid sigma-pressure levels.

CALIPSO data processing. The CALIPSO satellite performs ~15 orbits per day, with a 16 day repeat cycle, and covers the globe between 82° S and 82° N (ref. 27). We use lidar data from the CALIPSO Level 1 night-time output of the 532-nm parallel and perpendicular polarized channels. Data were processed based on the method developed by Vernier, *et al.*[40], including a shift of aerosol-free reference altitude from 30–34 km to 36–39 km. Each satellite swath was averaged horizontally to 1° latitudinal resolution and 180-m vertical resolution. Cloud pixels were identified and removed using a 5% threshold on the depolarization ratio to create a cloud mask[40]. The cloud mask was expanded upwards by 360 m to reduce the probability of missing faint upper edges of the clouds, and downwards towards the surface to remove attenuated signals from below the cloud. The final products used in this study are scattering ratios (measured total backscatter divided by calculated molecular backscatter) and aerosol scattering (measured total backscatter minus calculated molecular backscatter). The molecular scattering was modelled based on air and ozone molecule number concentrations[41,42], using ozone number density and pressure from the Global Modelling and Assimilation Office (GMAO, http://gmao.gsfc.nasa.gov/) and temperature from the ECMWF. The aerosol scattering and scattering ratios were further averaged longitudinally over swaths from several days to achieve a time resolution of 8 days or 1 month.

Aerosol optical depth. The conversion of aerosol scattering to AOD is dependent on particle size distribution. IAGOS-CARIBIC size distributions are available from mid-2010. The particle number concentrations increased appreciably after the Nabro eruption, and the size distributions shift slightly towards larger sizes compared with periods of low volcanic influence. However, the latter differences are small and all the size distributions are similar to that of the stratospheric background aerosol in 1999 (ref. 43). Therefore, the stratospheric background size distribution[43] was used for the entire period with the conversion factor 50 between aerosol scattering and particle extinction[44].

AOD is obtained by integration over the atmospheric depth. Because the tropopause altitude varies in time and space, zonal averaging was performed over (appropriately weighted) latitudinally varying altitude ranges. Wintertime data at latitudes ranging from 60° S to 90° S were removed because of frequent occurrence of polar stratospheric clouds that could not be effectively screened by the cloud mask. Polar stratospheric clouds in the NH occurred much less frequently and could be identified and removed manually. Further restrictions on data availability at high latitudes arise from the fact that CALIPSO night-time data do not extend to the poles in the summer season (the maximum latitudinal extent ranges from 55° to 80° over the year). The scattering of these regions were estimated based on extrapolation of neighbouring data. Due to the relatively small surface area contribution from high latitudes (~7% from 60° to 90°S/N) uncertainties of actual aerosol concentrations in these regions are expected to have a relatively small effect on the calculated global AOD.

Radiative forcing. A simple box model[45] was used to calculate short-wave instantaneous radiative forcing (ΔF) for AODs derived from CALIPSO data:

$$\Delta F = F_0 T^2 (1 - f_c)(1 - A_s)^2 \beta \delta, \quad (1)$$

where $F_0 = 1{,}361$ W m^{-2} is the solar constant, A_s is the surface albedo, f_c the cloud fraction, β the upscatter fraction and δ the AOD. For the calculations of two-way transmission (T^2) of incident light above an aerosol layer, the stratospheric aerosol was approximated as thin layers at 12.5 and 17.5-km altitude to represent average aerosol altitudes in the LMS and between 15 and 20 km. The net radiative forcing (including the long-wave component) is estimated to be 70% of the short-wave forcing[46]. The monthly mean surface albedo and cloud fraction were obtained from the ECMWF ERA-interim meteorological reanalysis project[47]. The two-way transmission was calculated at 532 nm as a function of solar zenith angle. Upscatter fractions for sulfuric acid particles as a function of particle size and solar zenith angle were deduced from Nemesure *et al.*[48] Extinction coefficients of solar radiation on sulfuric acid aerosol were calculated, using the size distribution of background aerosol in 1999 (ref. 43). The extinction coefficients were used to integrate over the upscatter fraction for aerosol particles with radii in the range 0.029–0.679 μm.

The resulting radiative forcing is thus sensitive to variation in latitude and season through the dependence on daylight hours, solar zenith angle and the variation in cloud cover and surface albedo (Fig. 5), whereas the effect of the zenith

angle on solar insolation and AOD cancel each other out[48]. The sensitivity of the radiative forcing to the AOD is obtained from the distribution in Fig. 5, where the global average radiative forcing for AOD = 1 is $-23\ W\ m^{-2}$, consistent with data from literature[49].

References

1. Fyfe, J. C., Gillett, N. P. & Zwiers, F. W. Overestimated global warming over the past 20 years. *Nat. Clim. Change* **3,** 767–769 (2013).
2. Flato, G. *et al.* in *Climate Change 2013: The Physical Science Basis* (Cambridge Univ. Press, 2013).
3. Ramanathan, V. & Feng, Y. On avoiding dangerous anthropogenic interference with the climate system: formidable challenges ahead. *Proc. Natl Acad. Sci. USA* **105,** 14245–14250 (2008).
4. Carslaw, K. S. *et al.* Large contribution of natural aerosols to uncertainty in indirect forcing. *Nature* **503,** 67–71 (2013).
5. Santer, B. D. *et al.* Volcanic contribution to decadal changes in tropospheric temperature. *Nat. Geosci.* **7,** 185–189 (2014).
6. England, M. H. *et al.* Recent intensification of wind-driven circulation in the Pacific and the ongoing warming hiatus. *Nat. Clim. Change* **4,** 222–227 (2014).
7. Meehl, G. A. & Teng, H. CMIP5 multi-model hindcasts for the mid-1970s shift and early 2000s hiatus and predictions for 2016–2035. *Geophys. Res. Lett.* **41,** 1711–1716 (2014).
8. Solomon, S. *et al.* The persistently variable 'background' stratospheric aerosol layer and global climate change. *Science* **333,** 866–870 (2011).
9. Vernier, J.-P. *et al.* Major influence of tropical volcanic eruptions on the stratospheric aerosol layer during the last decade. *Geophys. Res. Lett.* **38,** L12807 (2011).
10. Bourassa, A. E. *et al.* Large volcanic aerosol load in the stratosphere linked to Asian monsoon transport. *Science* **337,** 78–81 (2012).
11. Robock, A. Volcanic eruptions and climate. *Rev. Geophys.* **38,** 191–219 (2000).
12. Sato, M., Hansen, J. E., McCormick, M. P. & Pollack, J. B. Stratospheric aerosol optical depths, 1850–1990. *J. Geophys Res.* **98,** 22987–22994 (1993).
13. Kravitz, B., Robock, A. & Bourassa, A. Negligible climatic effects from the 2008 Okmok and Kasatochi volcanic eruptions. *J. Geophys Res.* **115,** D00L05 (2010).
14. Haywood, J. M. *et al.* Observations of the eruption of the Sarychev volcano and simulations using the HadGEM2 climate model. *J. Geophys. Res.* **115,** D21212 (2010).
15. Haywood, J. M., Jones, A. & Jones, G. S. The impact of volcanic eruptions in the period 2000–2013 on global mean temperature trends evaluated in the HadGEM2-ES climate model. *Atmos. Sci. Lett.* **15,** 92–96 (2014).
16. Appenzeller, C., Holton, J. R. & Rosenlof, K. H. Seasonal variation of mass transport across the tropopause. *J. Geophys. Res.* **101,** 15071–15078 (1996).
17. Hoor, P., Fischer, H., Lange, L., Lelieveld, J. & Brunner, D. Seasonal variations of a mixing layer in the lowermost stratosphere as identified by the CO-O3 correlation from in situ measurements. *J. Geophys. Res* **107,** 4044 (2002).
18. Bönisch, H., Engel, A., Curtius, J., Birner, T. & Hoor, P. Quantifying transport into the lowermost stratosphere using simultaneous in-situ measurements of SF 6 and CO2. *Atoms. Chem. Phys.* **9,** 5905–5919 (2009).
19. Martinsson, B. G. *et al.* Characteristics and origin of lowermost stratospheric aerosol at northern midlatitudes under volcanically quiescent conditions based on CARIBIC observations. *J. Geophys Res.* **110,** D12201 (2005).
20. Mauldin, III L. E., Zaun, N. H., McCormick, M. P., Guy, J. H. & Vaughan, W. R. Stratospheric Aerosol and Gas Experiment II instrument: a functional description. *Opt. Eng.* **24,** 307–312 (1985).
21. Kyrölä, E. *et al.* GOMOS on Envisat: an overview. *Adv. Space Res.* **33,** 1020–1028 (2004).
22. Llewellyn, E. *et al.* The OSIRIS instrument on the Odin spacecraft. *Can. J. Phys.* **82,** 411–422 (2004).
23. Bourassa, A. E., Degenstein, D. A., Elash, B. J. & Llewellyn, E. J. Evolution of the stratospheric aerosol enhancement following the eruptions of Okmok and Kasatochi: Odin-OSIRIS measurements. *J. Geophys Res.* **115,** D00L03 (2010).
24. Fromm, M. *et al.* Correcting the record of volcanic stratospheric aerosol impact: Nabro and Sarychev Peak. *J. Geophys Res.* **119,** 10,343–310,364 (2014).
25. Thomason, L. & Vernier, J.-P. Improved SAGE II cloud/aerosol categorization and observations of the Asian tropopause aerosol layer: 1989–2005. *Atoms. Chem. Phys.* **13,** 4605–4616 (2013).
26. Ridley, D. *et al.* Total volcanic stratospheric aerosol optical depths and implications for global climate change. *Geophys. Res. Lett.* **41,** 7763–7769 (2014).
27. Winker, D. M. *et al.* The CALIPSO Mission: a Global 3D View of Aerosols and Clouds. *Bull. Am. Meteorol. Soc.* **91,** 1211–1229 (2010).
28. Brenninkmeijer, C. A. M. *et al.* Civil Aircraft for the regular investigation of the atmosphere based on an instrumented container: the new CARIBIC system. *Atmos. Chem. Phys.* **7,** 4953–4976 (2007).
29. Martinsson, B. G. *et al.* Influence of the 2008 Kasatochi volcanic eruption on sulfurous and carbonaceous aerosol constituents in the lower stratosphere. *Geophys. Res. Lett.* **36,** L12813 (2009).
30. Friberg, J. *et al.* Sources of increase in lowermost stratospheric sulphurous and carbonaceous aerosol background concentrations during 1999-2008 derived from CARIBIC flights. *Tellus B* **66,** 23428 (2014).
31. Bluth, G. J. S., Doiron, S. D., Schnetzler, C. C., Krueger, A. J. & Walter, L. S. Global tracking of the SO2 clouds from the june, 1991 Mount-Pinatubo eruptions. *Geophys. Res. Lett.* **19,** 151–154 (1992).
32. Andersson, S. M. *et al.* Composition and evolution of volcanic aerosol from eruptions of Kasatochi, Sarychev and Eyjafjallajökull in 2008–2010 based on CARIBIC observations. *Atoms. Chem. Phys.* **13,** 1781–1796 (2013).
33. Hoor, P., Fischer, H. & Lelieveld, J. Tropical and extratropical tropospheric air in the lowermost stratosphere over Europe: A CO-based budget. *Geophys. Res. Lett.* **32** (2005).
34. Gettelman, A. *et al.* The extratropical upper troposphere and lower stratosphere. *Rev. Geophys.* **49,** RG3003 (2011).
35. Myhre, G. *et al.* in *Climate Change 2013: The Physical Science Basis.* (Cambridge Univ. Press, 2013).
36. Nguyen, N. H., Gudmundsson, A. & Martinsson, B. Design and calibration of a multi-channel aerosol sampler for tropopause region studies from the CARIBIC platform. *Aerosol Sci. Technol.* **40,** 649–655 (2006).
37. Nguyen, H. N. & Martinsson, B. G. Analysis of C, N and O in aerosol collected on an organic backing using internal blank measurements and variable beam size. *Nucl. Instrum. Methods Phys. Res. Sect. B* **264,** 96–102 (2007).
38. Martinsson, B. G. *et al.* Comparison between CARIBIC aerosol samples analysed by accelerator-based methods and optical particle counter measurements. *Atmos. Meas. Tech.* **7,** 2581–2596 (2014).
39. Zahn, A. *et al.* A fast and precise chemiluminescence ozone detector for eddy flux and airborne application. *Atmos. Meas. Tech.* **5,** 363–375 (2012).
40. Vernier, J. P. *et al.* Tropical stratospheric aerosol layer from CALIPSO lidar observations. *J. Geophys. Res.* **114,** D00H10 (2009).
41. Vernier, J.-P. *et al.* Overshooting of clean tropospheric air in the tropical lower stratosphere as seen by the CALIPSO lidar. *Atmos. Chem. Phys.* 9683–9696 (2011).
42. Hostetler, C. A. *et al.* CALIOP AlgorithmTheoretical Basis Document (ATBD): Calibration and level 1 data products. Document PC-SCI-201, NASA Langley Research Center, Hampton, VA, USA (2006).
43. Jäger, H. & Deshler, T. Lidar backscatter to extinction, mass and area conversions for stratospheric aerosols based on midlatitude balloonborne size distribution measurements. *Geophys. Res. Lett.* **29** 19 1929 (2002).
44. Jäger, H. & Deshler, T. Correction to 'Lidar backscatter to extinction, mass and area conversions for stratospheric aerosols based on midlatitude balloonborne size distribution measurements'. *Geophys. Res. Lett.* **30,** 1382 (2003).
45. Charlson, R. J., Langner, J., Rodhe, H., Leovy, C. & Warren, S. Perturbation of the northern hemisphere radiative balance by backscattering from anthropogenic sulfate aerosols. *Tellus A* **43,** 152–163 (1991).
46. Lacis, A., Hansen, J. & Sato, M. Climate forcing by stratospheric aerosols. *Geophys. Res. Lett.* **19,** 1607–1610 (1992).
47. Dee, D. *et al.* The ERA-Interim reanalysis: configuration and performance of the data assimilation system. *Q. J. Roy. Meteor. Soc.* **137,** 553–597 (2011).
48. Nemesure, S., Wagener, R. & Schwartz, S. E. Direct shortwave forcing of climate by the anthropogenic sulfate aerosol: sensitivity to particle size, composition, and relative humidity. *J. Geophys. Res.* **100,** 26105–26116 (1995).
49. Hansen, J. *et al.* Efficacy of climate forcings. *J. Geophys. Res.* **110,** D18104 (2005).
50. Prata, A. J. & Bernardo, C. Retrieval of volcanic SO_2 column abundance from atmospheric infrared sounder data. *J. Geophys. Res.* **112,** D20204 (2007).
51. Carn, S. A. & Prata, F. J. Satellite-based constraints on explosive SO2 release from Soufrière Hills Volcano, Montserrat. *Geophys. Res. Lett.* **37,** L00DE22 (2010).
52. Thomas, H. E. *et al.* A comparison of AIRS, MODIS and OMI sulphur dioxide retrievals in volcanic clouds. *Geomat. Nat. Haz. Risk* **2,** 217–232 (2011).
53. Prata, F. *et al.* A-train satellite observations of the 2008 Chaitén eruption clouds. Am. Geophys. Union Fall Meeting 2008, abstract #V43D-2183 (2008).
54. Lopez, T. *et al.* Evaluation of readout volcano's sulfur dioxide emissions by the ozone monitoring instrument. *J. Volcanol. Geoth. Res.* **259,** 290–307 (2013).
55. Haywood, J. M. *et al.* Observations of the eruption of the Sarychev volcano and simulations using the HadGEM2 climate model. *J. Geophys. Res.* **115** (2010) doi:10.1029/2010JD014447.
56. Surono, P. J. *et al.* The 2010 explosive eruption of Java's Merapi volcano–A "100-year" event. *J. Volcanol. Geoth. Res.* **241–242,** 121–135 (2012).
57. Clarisse, L. *et al.* Retrieval of sulphur dioxide from the infrared atmospheric sounding interferometer (IASI). *Atmos. Meas. Tech.* **5,** 581–594 (2012).

Acknowledgements

We acknowledge all members of the CARIBIC project and Lufthansa and Lufthansa Technik for enabling the CARIBIC observatory. We also thank André Ahlgren for support with programming. Aerosol measurements from CALIPSO were produced by NASA Langley Research Center. We thank the German Federal Ministry of Education and Research (BMBF) for financing the instruments operation as part of the Joint Project IAGOS-D. We also thank the German Research Foundation (DFG) for their financial support of the data analysis within the Priority Programme 1,294 (HALO). Financial support from Frankfurt Airport AG is gratefully acknowledged.

Author contributions

S.M.A. and B.G.M. performed data processing, analysis, computations and wrote the paper. They contributed to measurements of CARIBIC aerosol elemental concentrations. J.-P.V. supervised CALIPSO data processing and provided recalibration data. J.F. contributed to the analysis and to measurements of CARIBIC aerosol elemental concentrations. C.A.M.B. was responsible for the operation of the CARIBIC container with the help of A.Z. and M.H.; and M.H., P.F.J.v.V. and A.Z. provided CARIBIC aerosol size distribution, meteorology and ozone data, respectively.

Additional information

Competing financial interests: The authors declare no competing financial interests.

Reprints and permission information is available online at http://npg.nature.com/reprintsandpermissions/

How to cite this article: Andersson, S. M. *et al.* Significant radiative impact of volcanic aerosol in the lowermost stratosphere. *Nat. Commun.* 6:7692 doi: 10.1038/ncomms8692 (2015).

Paper V

AGU PUBLICATIONS

Earth and Space Science

RESEARCH ARTICLE
10.1002/2015EA000110

Key Points:
- CARIBIC particulate sulfur concentrations combined with MODIS cirrus reflectance
- Downwelling volcanic aerosol influence UT sulfurous aerosol concentrations
- Volcanic aerosol decreased midlatitude cirrus cloud reflectance

Correspondence to:
J. Friberg,
johan.friberg@nuclear.lu.se

Citation:
Friberg J., B. G. Martinsson, M. K. Sporre, S. M. Andersson, C. A. M. Brenninkmeijer, M. Hermann, P. F. J. van Velthoven, and A. Zahn (2015), Influence of volcanic eruptions on midlatitude upper tropospheric aerosol and consequences for cirrus clouds, *Earth and Space Science*, *2*, 285–300, doi: 10.1002/2015EA000110.

Received 15 APR 2015
Accepted 24 JUN 2015
Accepted article online 29 JUN 2015
Published online 24 JUL 2015

Influence of volcanic eruptions on midlatitude upper tropospheric aerosol and consequences for cirrus clouds

Johan Friberg[1], Bengt G. Martinsson[1], Moa K. Sporre[1], Sandra M. Andersson[1], Carl A. M. Brenninkmeijer[2], Markus Hermann[3], Peter F. J. van Velthoven[4], and Andreas Zahn[5]

[1]Department of Physics, Lund University, Lund, Sweden, [2]Max Planck Institute for Chemistry, Mainz, Germany, [3]Leibniz Institute for Tropospheric Research, Leipzig, Germany, [4]Royal Netherlands Meteorological Institute, de Bilt, Netherlands, [5]Institute for Meteorology and Climate Research, Karlsruhe Institute of Technology, Karlsruhe, Germany

Abstract The influence of downwelling stratospheric sulfurous aerosol on the UT (upper troposphere) aerosol concentrations and on cirrus clouds is investigated using CARIBIC (Civil Aircraft for Regular Investigation of the Atmosphere Based on an Instrument Container observations) (between 1999–2002 and 2005–2013) and the cirrus reflectance product from Moderate Resolution Imaging Spectroradiometer (MODIS). The initial period, 1999–2002, was volcanically quiescent after which the sulfurous aerosol in the LMS (lowermost stratosphere) (S_{LMS}) became enhanced by several volcanic eruptions starting 2005. From 2005 to 2008 and in 2013, volcanic aerosol from several tropical eruptions increased S_{LMS}. Due to consequent subsidence, the sulfur loading of the upper troposphere (S_{UT}) was increased by a factor of 2.5 compared to background levels. Comparison of S_{LMS} and S_{UT} during the seasons March–July and August–November shows a close coupling of the UT and LMS. Finally, the relationship between S_{LMS} and the cirrus cloud reflectance (CR) retrieved from MODIS spectrometer (on board the satellites Terra and Aqua) is studied. S_{LMS} and CR show a strong anticorrelation, with a factor of 3.5 increase in S_{LMS} and decrease of CR by $8 \pm 2\%$ over the period 2001–2011. We propose that the increase of S_{LMS} due to volcanism has caused the coinciding cirrus CR decrease, which would be associated with a negative radiative forcing in the Northern Hemisphere midlatitudes.

1. Introduction

The present study focuses on particulate matter collected in the upper troposphere (UT) and lowermost stratosphere (LMS) by the passenger aircraft based CARIBIC (Civil Aircraft for Regular Investigation of the Atmosphere Based on an Instrument Container) observatory [*Brenninkmeijer et al.*, 2007]. The transport of air enriched in ozone and particulate sulfur from the stratosphere into the troposphere can be monitored by CARIBIC throughout the seasons and years. Although the cruise altitude is nearly constant, the variable altitude of the extratropical tropopause allows the retrieval of vertical profiles across the tropopause and a sampling both in the UT and in the LMS. By this, CARIBIC can follow the fate of stratospheric aerosol.

The sulfurous fraction is the major component of stratospheric aerosol [*Deshler*, 2008; *Rosen*, 1971]. Recent studies [*Martinsson et al.*, 2009; *Murphy et al.*, 1998; *Schmale et al.*, 2010] find that the aerosol also contains significant amounts of carbonaceous species. In addition, small crustal [*Andersson et al.*, 2013] and meteoric [*Murphy et al.*, 2014] components are found in stratospheric aerosol particles.

The two largest sources of sulfuric acid particles in the stratosphere are the photolysis/oxidation of OCS and SO_2 [*Crutzen*, 1976; *Weisenstein et al.*, 1997], with a minor contribution from direct injection of sulfurous particles from the tropical troposphere. SO_2 forms sulfuric acid at all altitudes in the stratosphere via oxidation by radicals, while OCS is photooxidized chiefly at higher altitudes in the stratosphere. Injections of particulate matter via volcanism are by far the source inducing most variability in the stratospheric aerosol [*Robock*, 2000]. Remote sensing at lidar stations (in Boulder, Colorado, and in Mauna Loa, Hawaii) revealed a trend of increasing aerosol burden in the stratosphere (20–25 km altitude) in the period 2000–2009 [*Hofmann et al.*, 2009], which was later shown to be caused by volcanism in the tropics [*Vernier et al.*, 2011]. The stratosphere's increasing aerosol concentration has been found to cause a negative radiative forcing of $-0.1\,Wm^{-2}$ [*Solomon et al.*, 2011]. Later studies

[*Andersson et al.*, 2015; *Ridley et al.*, 2014] find that also volcanic aerosol in the LMS contributes significantly to the climate forcing in that period. These findings indicate that volcanism is a major cause for the deviations between the actual and predicted [*Flato et al.*, 2013] global warming since year 2000.

The Brewer-Dobson circulation transports air from the tropical tropopause via the middle and upper stratosphere (deep branch) and quasi-horizontally (shallow branch) to midlatitude and high latitude [*Holton et al.*, 1995]. The deep branch brings air with high concentrations of O_3 and sulfuric acid particles from the Junge layer to lower altitudes where it mixes with air from the lower branch. Whereas the deep branch transports air to midlatitudes within years, the shortcut via the lower branch requires only a few months.

The LMS is restricted downward by the tropopause, while its upper boarder is defined as the 380 K isentrope [*Holton et al.*, 1995]. Stratospheric air with high concentrations of O_3 and particulate sulfur that reaches the LMS undergoes mixing with air from the troposphere. On a local scale, mixing through the tropopause results in a 2–3 km thick layer with strong vertical gradients of trace gases [*Hoor et al.*, 2004; *Pan et al.*, 2004], called the extratropical tropopause transition layer. Seasonality in the strength of the transport paths results in seasonally varying proportions of stratospheric and tropospheric air in the LMS leading to, for example, varying ozone concentrations during the year, with the highest concentrations in spring and lowest during fall [*Zahn and Brenninkmeijer*, 2003]. Via observations of trace gas concentrations, *Bönisch et al.* [2009] revealed a seasonal cycle in the mean age of air in the LMS, decreasing from spring to fall.

Mixing through the tropopause eventually leads to transport of sulfur-rich stratospheric aerosol to the midlatitude UT, where particulate sulfur concentrations are substantially lower compared to the LMS [*Martinsson et al.*, 2005]. Sulfur compounds can also be transported from the surface by deep convection and warm conveyor belts and then lead to particle formation in the UT. *Guan et al.* [2010] report that large forest fires contributed to about 10 occurrences of pyroconvection, in 2006–2009, that could have transported biomass burning smoke to UT altitudes. Particles from this source type contain mostly carbonaceous matter with traces of metals such as potassium [*Reid et al.*, 2005]. However, *Murphy et al.* [2006] found that UT particles generally contain mixtures of sulfurous and carbonaceous components. Most of them contained no potassium, suggesting pyroconvection to be only a minor source of UT aerosol. Investigating particle morphologies, *Nguyen et al.* [2008] established that the sulfurous and carbonaceous components are internally mixed residing in different parts of the particles.

Aerosol particles in the UT are involved in the formation of cirrus clouds. Cirrus ice crystals either form homogeneously via freezing of supercooled solution droplets or heterogeneously when water crystallizes directly on ice nuclei (IN) [*Pruppacher and Klett*, 1997]. Mineral dust and metallic particles have been proposed to be the main suppliers of IN in the UT [*Cziczo et al.*, 2013; *DeMott et al.*, 2003]. Soot particles may also act as IN but at lower temperatures than mineral dust [*Hoose and Möhler*, 2012]. Recent measurements indicate that soot IN concentrations from aircraft have been underestimated [*Schumann et al.*, 2013], and the question whether soot particles from aviation affect cirrus properties has been the focus of several modeling studies recently. *Gettelman and Chen* [2013] found no effect on cirrus from aviation soot while *Zhou and Penner* [2014] found the soot to significantly alter the cirrus cloud properties. The different outcomes of the studies are caused by the different assumptions regarding the nucleation efficiency of soot. Besides soot, jet engines emit metallic elements [*Agrawal et al.*, 2008] that might add somewhat to the concentration of IN in the UT. Coating of IN, by compounds such as sulfuric acid, has in laboratory experiments been found to decrease aerosol particle effectiveness to act as IN [*Hoose and Möhler*, 2012].

Homogeneous nucleation was for many years considered to be the dominant formation mechanism for cirrus clouds [*Jensen et al.*, 2010], and in situ measurements of temperature, relative humidity, ice water content, particle size, and fall velocities have been found to confirm this [*Mitchell et al.*, 2011]. However, a recent study, investigating ice particle residuals [*Cziczo et al.*, 2013], indicates that heterogeneous freezing is the dominant mechanism for cirrus clouds over Central America and parts of North America. Heterogeneous ice nucleation has recently been incorporated in model studies of cirrus clouds [*Barahona et al.*, 2014; *Kuebbeler et al.*, 2014; *Storelvmo and Herger*, 2014]. One such study, *Barahona et al.* [2014], finds homogeneous freezing to be the dominant mechanism globally except over central Asia, the Arctic, and the west coast of North America. However, *Zhou and Penner* [2014] find that if aircraft soot emissions

provide additional IN, they could shift the freezing regime from homogeneous to heterogeneous freezing over North America, Europe, and the North Atlantic Ocean.

Whether or not volcanic aerosols injected into the stratosphere can affect cirrus clouds in the UT has been the topic of several research papers and the conclusions differ. One satellite study found an increase in high-level cloudiness after the El Chichon and Mount Pinatubo eruptions [*Song et al.*, 1996], while other satellite studies found no changes in cirrus properties after the Mount Pinatubo eruption [*Luo et al.*, 2002; *Wylie and Menzel*, 1999]. Moreover, modeling studies of the same event using only homogeneous nucleation theory find increased ice crystal number concentrations in cirrus clouds after the eruption [*Karcher and Lohmann*, 2002; *Lohmann et al.*, 2003]. Recently, a satellite study by *Campbell et al.* [2012] found cirrus clouds formed by seeding from a stratospheric layer of volcanic aerosol from the Kasatochi eruption in 2008.

Cirrus clouds are estimated to have an overall larger impact on the long-wave than on the short-wave radiation, resulting in a net warming of the surface [*Boucher et al.*, 2013; *Chen et al.*, 2000]. Estimations of radiative forcing from cirrus clouds hold considerable uncertainties [*Boucher et al.*, 2013] depending on a range of factors [*Baran*, 2009] including ice crystal shape, size, number concentration, cloud coverage, cloud thickness, and temperature [*Fusina et al.*, 2007].

In recent studies we investigated variations in the LMS aerosol concentrations during periods of tropical [*Friberg et al.*, 2014] and extratropical [*Andersson et al.*, 2013; *Martinsson et al.*, 2009] volcanism. We now investigate the influence on midlatitude UT aerosol concentrations of volcanic aerosol from the LMS, based on elemental analyses of aerosol samples collected by CARIBIC between 1999 and 2013. Perturbation of LMS aerosol by volcanism during these 15 years ranged from low to moderate. With the direct impact of volcanic aerosol in the UT/LMS having been addressed by *Andersson et al.* [2015], we now present a comparison between measured UT/LMS aerosol concentrations and MODIS (Moderate Resolution Imaging Spectroradiometer) retrieved cirrus reflectance (CR), in the light of the indirect climate impact of volcanism.

2. Methods

The period 1999–2013 was covered by CARIBIC in a near monthly rhythm, except for the 2.5 year period mid-2002 to 2005, which was used for a transition from CARIBIC 1 (Boeing 767 ER aircraft, leaving Düsseldorf and Munich airports) [*Brenninkmeijer et al.*, 1999] to CARIBIC 2 (Airbus A340-600 aircraft based in Frankfurt) [*Brenninkmeijer et al.*, 2007]. The CARIBIC system is currently based on a 1.5 t automated measurement container constituting a compact laboratory. The container is installed monthly for 2–6 consecutive flights in a Lufthansa passenger Airbus A340-600, which has been retrofitted for this task with a permanent inlet system having inlet probes for water vapor, cloud water, aerosol, and trace gases. So far about 100 publications deal with methods and results (www.caribic-atmospheric.com). The CARIBIC system is part of IAGOS (In situ Aircraft for a Global Observing System, www.iagos.org)

2.1. Air-Inlet for Aerosol Sampling

Different inlet systems were used for CARIBIC phases #1 and #2. The inlet used in phase #1 had an estimated sampling efficiency of 90% for 0.1–1 μm particles [*Hermann et al.*, 2001]. The presently used system (phase #2) has a sampling efficiency of 60% for 5 μm particles and a high transmission (>90%) for submicron particles [*Martinsson et al.*, 2014; *Rauthe-Schöch et al.*, 2012]. A cyclone with close to 100% transmission for submicron particles [*Nguyen et al.*, 2006] and a cutoff size of 2 μm are installed to reduce the influence from larger particles.

2.2. The Aerosol Sampler

Aerosol particles with aerodynamic diameters of 0.08–2 μm were collected using an automated aerosol sampler with close to 100% collection efficiency [*Nguyen et al.*, 2006] based on the use of impactors. Particles were deposited on 0.2 μm thin AP1™ polyimide films [*Papaspiropoulos et al.*, 1999]. Similar impactors were used during phases #1 and #2. The phase #2 (phase #1) device consists of 14 (12) channels for sequential samples. In addition, 2 channels were used to collect integral samples, to check for contaminations. Typical air volumes of 0.25 (0.09) m^3 STP (standard temperature and pressure) were sampled during 100 (150) min or 1500 (2200) km flight distance. Sampling is suspended when the pressure exceeds 350 hPa (landing and takeoff cycles) to avoid sampling of aerosol from lower altitudes.

2.3. Aerosol Composition Analysis

Chemical characterization of aerosol particles was obtained using PIXE (particle-induced X-ray emission) [*Johansson and Campbell*, 1988]. Samples were irradiated by a proton beam of 2.55 MeV at the Lund ion beam analysis facility. Elemental concentrations were derived for elements with atomic numbers larger than 15, with an estimated accuracy of 10% [*Martinsson et al.*, 2014; *Papaspiropoulos et al.*, 1999]. Here we focus on the sulfur data, which have a typical minimum detection limit (MDL; detection of an element with a confidence of 99%) of 2 ng m^{-3} STP. Sulfur concentrations below MDL were set to MDL/2. Detection frequencies for sulfur were 99% (UT) and 100% (LMS).

2.4. Sampling in the Midlatitude UT/LMS

Because the CARIBIC aircraft collects samples in a narrow altitude interval (9–12 km above sea level), either the extratropical UT/LMS or the tropical middle troposphere is investigated. However, due to the movement of the tropopause level relative to the aircraft flight track, air masses with vertical distances relative to the tropopause from 5 km below the tropopause to 5 km above the tropopause are probed [*Zahn et al.*, 2014]. At midlatitude and high latitude the tropopause is frequently crossed. In the present study, samples collected on latitudes south of 30°N were excluded to keep the influence from tropical air low.

2.4.1. The Dynamical Tropopause

We used potential vorticity (PV) to define the tropopause. PV values were derived from archived ECMWF (European Centre for Medium-range Weather Forecast) analyses with a resolution of 1° × 1° in the horizontal at 91 vertical hybrid sigma-pressure model levels. PV values were interpolated linearly in latitude, longitude, log pressure, and time to the location of the aircraft and for each sample averaged over the duration of sampling. Generally, PV values of 1.5–3.5 potential vorticity unit (PVU) [*Hoerling et al.*, 1991; *Hoinka*, 1997] are employed for defining the dynamical tropopause. Here we use 2 PVU.

2.4.2. Classification of UT and LMS Samples

Samples with an average PV $>$ 2 PVU were classified to be stratospheric, while UT samples were those below 1.5 PVU. The sampling time for the impactor is relatively long, sometimes resulting in samples representing air from both the UT and the LMS. To eliminate a bias in the UT aerosol concentration from samples partially taken in the LMS, samples collected at average PV lower than 1.5 PVU were excluded from this investigation, if the aircraft had crossed the tropopause (2 PVU) during the sampling interval.

2.5. Exclusion of Samples Affected by Fresh Volcanic Aerosol

Volcanic clouds reaching the UT/LMS can enhance the background aerosol concentrations tremendously. In the weeks following an eruption the emitted SO_2 is converted to sulfate and the resulting volcanic aerosol mixes at various degrees with the background. Moreover, fresh volcanic aerosol injected in the UT is susceptible to scavenging by precipitation formation. Therefore, samples collected within 30 days after volcanic eruptions that reached the extratropical UT/LMS (listed in Table 1) were excluded to prevent bias from patchiness in aerosol concentrations and influence from large ash particles. An extremely high particulate sulfur concentration was observed for one additional sample (August 2001). Trajectory analysis shows direct transport from the area of an eruption of Bezymianny, at the Kamchatka peninsula, Russia. Hence, this sample happened to have been collected in a fresh volcanic cloud was also excluded.

2.6. Contour Graphs

The geographical distribution of particulate sulfur concentration is illustrated by using a contour graph. It was produced by splitting each sample into 10 equidistant parts along the flight track, and the average position of the aircraft in longitude × latitude was calculated for each part, yielding 10 sample parts of typically 150 km along the flight route. These parts were assigned aerosol concentrations according to the analytical results and were sorted into and averaged on a longitude × latitude grid of 5° × 5°, and a center-weighted 2-D smoothing was performed. Grid cells with fewer than 10 samples in their eight nearest surrounding grid cells were excluded to reduce the impact from regions where few observations were made. The data were then 2-D interpolated to 1° × 1° (longitude × latitude) to form the presented graph. A similar contour graph was created illustrating the geographical variation of potential vorticity.

Table 1. Volcanic Eruptions in the Tropics and in the Northern Extratropics, Identified to Have Influenced the Particulate Sulfur Concentrations in the LMS (Also Marked in Figure 3) in the Period 1999–2013

Eruption Date[a]	Volcano	SO_2 (Tg)	VEI[a]	Longitude[a]	Latitude[a]
01-27-2005	Manam	0.09[b]	4	145	−4.1
05-20-2006	Soufriere Hills	0.2[c]	3	−62	16.7
10-07-2006	Rabaul	0.2[d]	4	152	−4.3
07-12-2008	Okmok	0.1[e]	4	−168	55.3
08-07-2008	Kasatochi	2[f]	4	−176	52.2
03-20-2009	Redoubt	0.08[g]	3	−153	60.5
06-12-2009	Sarychev	1.2[h]	4	153	48.1
05-21-2011	Grimsvötn	0.4[i]	4	−17.3	64.4
06-12-2011	Nabro	1.5[i]	4	41.7	13.4

[a]Volcanic explosivity index, from *Global Volcanism Program* [2011].
[b]*Prata and Bernardo* [2007].
[c]*Carn and Prata* [2010].
[d]*Carn et al.* [2009].
[e]*Thomas et al.* [2011].
[f]*Yang et al.* [2010].
[g]*Lopez et al.* [2009].
[h]*Haywood et al.* [2010].
[i]*Clarisse et al.* [2012].

2.7. Satellite Measurements

We use satellite data of cirrus clouds from the MODIS instruments. One MODIS instrument is placed on the satellite Terra, launched in December 1999, and the other on Aqua, launched in May 2003. Terra has a descending orbit while Aqua has an ascending orbit and their equatorial crossing times are 10:30 and 13:30 local solar time [*Platnick et al.*, 2003]. MODIS is a whiskbroom scanning radiometer with 36 wavelength channels spread between 0.620 and 14.4 μm. One of these channels, centered at 1.38 μm, was selected specifically for the study of cirrus clouds [*Gao and Kaufman*, 1995]. Incoming solar radiation at 1.38 μm is either reflected and scattered by the cirrus clouds or completely absorbed by the underlying atmosphere due to high water vapor absorption at this wavelength [*Gao et al.*, 2002; *Meyer and Platnick*, 2010]. However, 1–10% of the atmospheric water vapor is normally located above the cirrus clouds which results in attenuation of the 1.38 μm signal. To quantify this attenuation, a scaling factor is calculated from the slope of scatterplots of the reflectance in the 1.38 μm channel versus the reflectance from a cannel in the visible spectrum (0.66 μm) [*Gao et al.*, 2002]. Each MODIS granule (2030 × 1354 pixels) is divided into 16 subgranules, and a scaling factor is calculated for each of these subgranules. The scaling factors are then interpolated to avoid a chessboard effect, and the reflectance from the cirrus clouds for each pixel is calculated [*Gao et al.*, 2002; *Meyer and Platnick*, 2010]. Our analysis is based on the Level 3 monthly averaged CR with a resolution of 1° × 1°.

During dry atmospheric conditions not all solar radiation at 1.38 μm will be absorbed by the underlying atmosphere. Hence, reflection from the surface or lower lying clouds can contaminate the CR product [*Meyer and Platnick*, 2010]. The atmospheric water vapor product from MODIS has therefore been used to screen out dry atmospheric conditions. Similar results were obtained when using the total column water vapor from the ECMWF. The limit was set to 0.4 cm after recommendation from B.-C. Gao (personal communication, 2014) and investigation of the CR and atmospheric water vapor data. Since the same area is to be used for all monthly averages, pixels that have atmospheric water vapor less than 0.4 cm during the investigated years are removed from the entire data set. This was done for Terra and Aqua separately, but the areas included are very similar, see Figure 1. It is mainly continental areas over central North America and Asia, in particular ranges of high mountains, that are excluded but also some small ocean areas east of these continents. In order to compare the MODIS-retrieved CR against the CARIBIC measurements, only data from 30°N to 60°N are used to form average monthly cirrus products. Due to the latitude dependence of temperature and therefore atmospheric water vapor concentration, the fraction of pixels that are too dry increases with latitude. To avoid bias from this phenomenon, zonal averages were computed using 1° × 1° pixels. These averages were then weighted according to area in order to obtain the average CR for 30–60°N. An estimation of the uncertainty in the averages was calculated using error propagation on the standard deviation of the daily mean of each 1° × 1° pixel. Internal checkups of the MODIS instrument on Terra were carried out

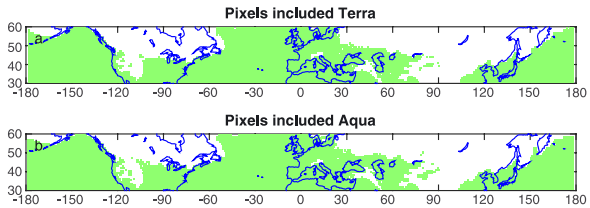

Figure 1. Illustration of the geographical areas included in the calculations of the MODIS cirrus reflectance for (a) Terra and (b) Aqua.

during spring and summer year 2000. The data from this period were not used. The averaged Aqua CR values are somewhat higher (13–19%) than the Terra values. This could be caused by the later overpass time of Aqua which enables more convective activity and thereby larger contribution from cirrus anvils to the CR.

3. Results

3.1. Geographical Distributions of Sulfur and PV

CARIBIC measurements over the years cover latitudes 30°S to 70°N and longitudes 120°W to 120°E. Figure 2a provides a geographical view of the particulate sulfur concentrations at 9-12 km altitude for all samples, tropospheric and stratospheric. The concentration clearly depends on the geographical location of sampling. A strong latitudinal gradient of the concentration of particulate sulfur is observed, with higher concentration in the North Hemisphere (NH) midlatitudes, than in the subtropics. *Martinsson et al.* [2005] found a correlation of sulfur and PV in the LMS, due to downwelling of particulate sulfur from the higher altitudes. A comparison of the geographical distribution of particulate sulfur concentrations (Figure 2a) and that of the average PV during sampling (Figure 2b) indicates the possible stratospheric origin of high sulfur concentrations. Downwelling of sulfur-rich stratospheric air can strongly enhance the particulate sulfur mass concentrations in the midlatitudes tropopause region. The samples in the subtropics are somewhat influenced by stratospheric air, while the tropical samples are purely tropospheric. The gradient to the tropics could also be caused by other differences in source patterns as well as by more efficient wet scavenging of the hygroscopic sulfur particles in the tropics by deep convective clouds. The following sections deal with the coupling of the LMS and midlatitude UT.

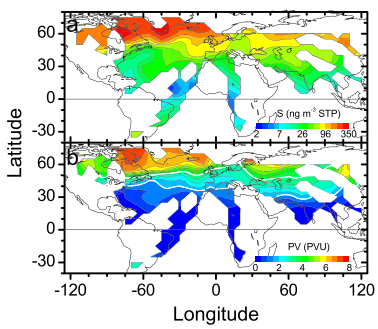

Figure 2. Contour graphs illustrating the geographical distribution of (a) particulate sulfur concentrations and (b) PV, based on all aerosol samples collected by CARIBIC in the period 1999–2013. The white lines in Figure 2b mark the PV isopleths of 1.5 and 3.5 PVU, the range in PV where the dynamical tropopause normally is set.

3.2. Volcanic Influence on Particulate Sulfur in the Midlatitude UT

Over the 15 year time span considered, particulate sulfur concentrations in the UT and LMS vary by a factor of about 100 (Figure 3). In parts of this period the LMS serves as a reservoir of volcanic aerosol that eventually is transported to the midlatitude UT. To investigate a coupling between the UT and LMS we will group data depending on the magnitude of volcanic influence on the aerosol concentrations. In the LMS, the sulfur concentrations need to be normalized by PV in order to compensate for the strong gradient of sulfur in the LMS and to highlight deviations from the nonvolcanically influenced particulate sulfur distribution. UT data are scarce as most of the midlatitude

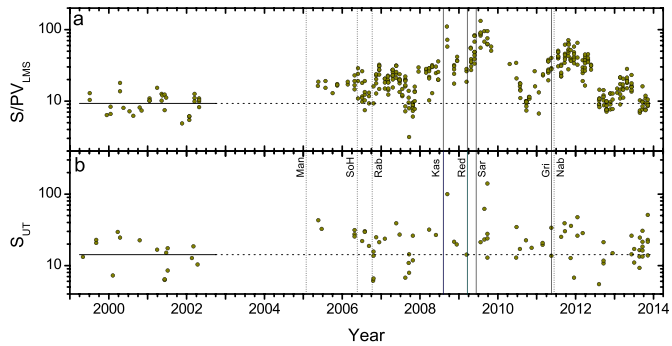

Figure 3. Temporal variations in the northern midlatitude of (a) S/PV values in the LMS (S/PV_{LMS}; ng m^{-3} STP/PVU) and (b) sulfur concentrations in the UT (S_{UT}; ng m^{-3} STP). The horizontal lines show the geometric averages for the period 1999–2002. The vertical lines mark the volcanic eruptions identified to have influenced the particulate sulfur concentrations in the LMS. The vertical dashed and full lines represent the eruptions in the tropics and northern midlatitudes, respectively. Data for the 30 days following these eruptions are excluded, also in the following figures.

samples were collected in the LMS. Thus, details in the variability in sulfur concentrations do not show as clearly in the UT as in the LMS. We will therefore use the LMS sulfur concentrations as a more distinct measure of the magnitude of the volcanic influence in the UT/LMS and divide the data into groups depending on the volcanic influence.

3.3. Grouping Data Depending on Volcanic Influence

The average S/PV ratio for the period 1999–2002 was low (Figure 3), indicating a time of low volcanic impact on the stratosphere [*Martinsson et al.*, 2005]. However, particulate sulfur was affected by volcanic aerosol to various degrees after the year 2005. The 3 year period mid-2002 to mid-2005 was not monitored by CARIBIC but is known to have had little volcanic activity [*Myhre et al.*, 2013].

In the period May 2005 to July 2008 the LMS aerosol was influenced by three volcanic eruptions in the tropics (Manam, Soufriere Hills, and Rabaul). They injected large amounts of SO_2 (Table 1) into the tropical stratosphere [*Vernier et al.*, 2011] that was subsequently, while being oxidized, transported to midlatitudes within the Brewer-Dobson (BD) circulation. Subsequent downwelling [*Friberg et al.*, 2014] explains the observed increase in the LMS sulfur concentrations from the 1999–2002 baseline. A concomitant increase in UT sulfur concentrations is evident (Figure 3).

Figure 3 shows several large peaks in S/PV, starting with the Kasatochi explosion in 2008, which eventually decline [*Martinsson et al.*, 2009] by transport across the tropopause into the UT. Extratropical volcanism then caused peaks of varying magnitudes in 2009–2010 [*Andersson et al.*, 2013] and in spring 2011, followed by an eruption of the tropical volcano Nabro. Nabro emitted about the same amount of SO_2 (1.5 Tg) as Kasatochi and Sarychev did (Table 1). After transport from the tropics to midlatitudes, downwelling through the LMS explains the observed rise in S/PV from late summer 2011. Volcanic clouds reaching the tropical stratosphere can affect the extratropical LMS for years via transport in the deep BD branch. However, the long-lasting perturbations after Nabro were limited to the first half of the year 2012, because most of the transport took place in the tropical transition layer or in the lower BD branch [*Bourassa et al.*, 2012]. Finally, remaining aerosol particles from the Nabro explosion transported in the deep BD branch slightly elevated the concentration level in spring/summer 2013.

Next, the data are divided into the following groups: (1) background conditions, (2) samples affected by direct injections into the LMS, and (3) samples influenced by volcanic aerosol downwelling from the stratosphere from above the 380 K isentrope. Thus, we derive the following:

1. The years 1999–2002 as the period that represents background levels.

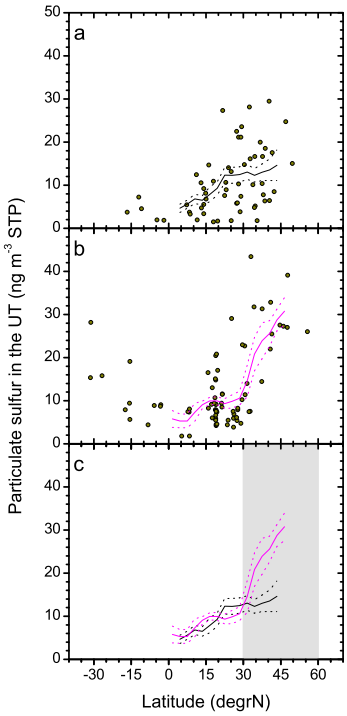

Figure 4. The latitudinal variation of particulate sulfur in the UT during (a) March–July 99–02 and (b) March–July 05–08/13 (c) a direct comparison of the averaged profiles shown as lines in Figures 4a and 4b. The dashed lines illustrate the 95% confidence interval. The grey shaded area in Figure 4c marks the northern midlatitudes, the latitude band of interest in the following figures and discussions.

2. Midlatitude eruptions penetrating the extratropical tropopause can cause a large impact on the LMS that lasts for months depending on their penetration depths. The combined injections from Kasatochi, Redoubt, and Sarychev caused such perturbations in the period August 2008 to December 2009.
3. When volcanic clouds have reached the tropical stratosphere the aerosol can induce long-term impact on the LMS aerosol concentration by transport to midlatitudes in the deep BD branch. Over the 15 years studied here, such perturbations occurred during several periods, with largely varying magnitudes. These periods are split in two categories based on the volcanic eruptions effect on the sulfur concentrations in the LMS, because averaging large concentration differences would complicate the forthcoming analyses. Category 3a represents periods strongly affected by volcanism (i.e., the period after Nabro's eruption, late summer 2011 to summer 2012), while category 3b combines an intermediately affected LMS (i.e., the periods May 2005 to July 2008 (until the Kasatochi eruption) and the year 2013).

In spite of the scarcity of UT data there are similarities in its variability in sulfur concentrations to that of the S/PV in the LMS. Peaks and periods of high S/PV in the LMS are reflected to some degree in the UT (Figure 3). For example, the peaks after the eruptions of Kasatochi and Sarychev, the decreasing concentrations from spring/summer to fall in 2006 and 2007, and the increased sulfur concentrations after the eruption of Nabro. These similarities indicate that the aerosol concentrations in the UT can be affected strongly by the LMS.

3.4. Impact on UT/LMS Aerosol From Tropical Volcanism

To explore the influence from tropical volcanism on the aerosol concentrations in the midlatitude UT we compare sulfur concentrations from the periods May 2005 to July 2008 and 2013 (Category 3b) to that of the period 1999–2002 (Category 1) (hereinafter termed periods 05-08/13 and 99–02, respectively).

The LMS contains a larger proportion of midstratospheric air in spring and summer, compared to fall when a large fraction of the LMS' air is of recent tropospheric origin [*Bönisch et al.*, 2009]. Hence, in the period 05-08/13 elevated aerosol concentrations are expected in the LMS and midlatitude UT during spring when volcanic aerosol is brought down from higher altitudes, while concentrations in fall are expected to be more connected to the aerosol concentrations in the troposphere. We explore seasonal differences by combining data from the two periods into one season of large stratospheric influence (March–July) and one season with large tropospheric influence (September–November).

3.4.1. Latitude Dependence of Particulate Sulfur UT Concentration

The latitudinal distribution of UT sulfur is displayed in Figure 4, revealing a clear tendency of increasing concentrations from the tropics to higher latitudes. For March–July, this gradient is more pronounced in the periods 05-08/13 than during 99–02 (Figures 4a and 4b). A direct comparison of the March–July moving averages (Figure 4c) shows similar concentration levels in the tropics and part of the subtropics.

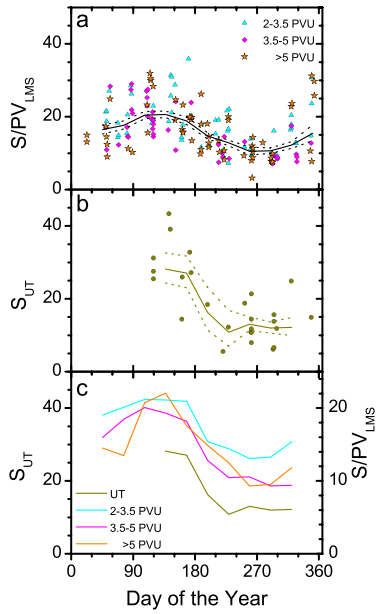

Figure 5. Illustration of the seasonal variation of (a) S/PV at different PV intervals in the LMS (S/PV_{LMS}; ng m^{-3} STP/PVU), (b) the particulate sulfur concentration in the UT (S_{UT}; ng m^{-3} STP), and (c) a direct comparison of the S/PV_{LMS} to the S_{UT}. The full and dashed lines illustrate the moving geometric averages with 95% confidence interval.

While the 05-08/13 periods show a steep increase with latitude, north of 30°N, the increase observed for the period 99–02 is not significant. This difference is largest at 45°N, which is the northernmost latitude for the average of 99–02, where the sulfur concentrations of 05-08/13 are twice that of 99–02. Hence, aerosol from tropical volcanic eruptions is detectable not only in the stratosphere but also in the midlatitude UT.

3.4.2. Seasonal Variation in the Midlatitude UT and LMS

The 05-08/13 data will now be further investigated in order to explore the origin of the particulate sulfur in the midlatitude UT and the cause of its seasonally varying concentrations. In Figure 5, the seasonally varying concentrations in the midlatitude UT are compared to the S/PV of different depths (PV levels) into the LMS.

In the LMS, high S/PV is observed in spring (Figure 5a) [*Friberg et al.*, 2014] with a reduction during summer that reaches a minimum around August–October. The maximum coincides with the downwelling of stratospheric air from the deep BD branch carrying particulate sulfur to the LMS. The minimum in August–October again illustrates the small contribution from the deep BD branch in the LMS during late summer and fall.

We observe large similarities in the variation of sulfur in the UT to that in the LMS with the maximum concentrations found in May. In Figure 5c, a comparison of the moving averages for the sulfur concentrations in the UT and that of the S/PV in the LMS shows that the seasonal variations span approximately a factor of 2. In fall, the S/PV values close to the tropopause are higher than at higher PV values. However, this is not caused by higher sulfur concentrations at the lower PV values. Instead, it is an effect of a very weak dependence on PV of the sulfur concentrations in the LMS during fall [*Friberg et al.*, 2014], resulting in high S/PV for low PV values.

4. Discussion

The strong similarities in the seasonally varying sulfur concentrations in the LMS and in the UT (Figure 5) indicate a high degree of coupling of their aerosol concentrations. Combined with previous findings of perturbations of the LMS from tropical volcanic injections transported to the LMS, these findings point to a strong influence from volcanism on the UT particulate sulfur concentration during the years 05-08/13.

To further investigate the impact of volcanism and the coupling of the UT and LMS we will extend the study with a direct comparison of the sulfur concentrations in the UT with the S/PV values in the LMS.

4.1. Transport of Volcanic Aerosol From the LMS to the UT

4.1.1. Volcanic Impact in Spring/Summer

To compare LMS and UT concentrations directly one needs to account for the variability in the transport across the extratropical tropopause. We therefore use the March–July data for a comparison in the season of large stratospheric influence. To deal with the scarcity of observations in the UT we group the years together, based on each year's average S/PV in the LMS, thus improving statistics. The years 2009 and 2011 are excluded in this comparison as midlatitude eruptions that reached the UT/LMS (Redoubt,

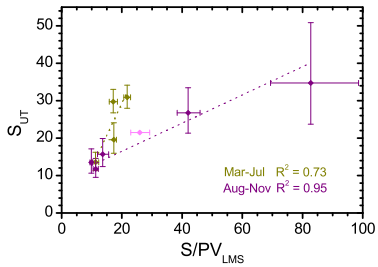

Figure 6. Comparison of the geometric averages of the particulate sulfur concentrations in the UT (S_{UT}; ng m^{-3} STP) to the S/PV in the LMS (S/PV$_{LMS}$; ng m^{-3} STP/PVU), for the seasons March–July (dark yellow diamonds) and August–November (magenta diamonds), for samples taken at PVs below 5 PVU. The dashed lines represent the linear regressions for the respective season. The error bars represents the geometric standard errors. The years that have been averaged for the season March–July, in order of their S/PV$_{LMS}$, are 2000–2002, 2010/2013, 2005/2006, and 2007/2008, while the August–November are 2007, 2010/2012, 2006, 2011 (Nabro), and 2009 (Sarychev). The 2008 (Kasatochi) data (light magenta, diamond) were excluded in the regression due to its poor statistics.

Sarychev, and Grimsvötn) occurred during the spring/summer. The year 2012 is excluded since only one UT observation is available. This results in four groups of years for comparison of the LMS and UT (2000–2002, 2010/2013, 2005/2006, and 2007/2008). The average sulfur concentrations in the UT and average S/PV in the LMS are compared in Figure 6 (dark yellow data points). Samples taken in air masses with PV values of less than 5 PVU are used here as they are expected to be more connected to the sulfur concentrations in the UT than those taken farther away from the tropopause [*Bönisch et al.*, 2009]. A positive correlation ($R^2 = 0.73$), with a significance level of 85%, emerges with a factor of 2.5 increase in the UT concentrations, ranging from 13 ng m^{-3} STP in the years 2000–2002 to 32 ng m^{-3} STP in 2007/2008. This correlation further indicates that downwelling from the stratosphere affects the aerosol concentration in the UT.

4.1.2. Volcanic Impact in Fall

For data taken in the fall, we have the possibility to extend the UT/LMS comparison to include the years that were affected by direct injections to the LMS by extratropical volcanism. To gain better statistics we extend the fall season to include August.

Aerosol samples collected in the August–November months after Kasatochi (August 2008), Sarychev (June 2009), and Nabro (June 2011) were all largely affected by volcanism. As Kasatochi exploded in August, samples from August and September 2008 are excluded.

The coupling between the LMS and UT is further explored via a comparison of the fall data (Figure 6, magenta data points) for the years when the LMS was strongly affected by volcanism (2008, 2009, and 2011) to that of the less affected years (2006, 2007, and 2012). Unfortunately, comparison to the period 99–02 is not possible, as only two observations of the sulfur concentrations in the LMS in fall are available. A linear regression of the fall data, results in a strong correlation ($R^2 = 0.95$) of high significance (>99%). The 2008 (Kasatochi) data are omitted in this calculation as only one observation from the UT is available. The strong correlation in fall, combined with the correlation found during spring/summer (see section 4.1.1), indicates that downwelling from the stratosphere strongly affects the particulate sulfur concentration in the UT. Interestingly, the slope in spring/summer is a factor 4 larger than in fall. The higher slope is attributed to increased stratosphere-to-troposphere transport [*Sprenger and Wernli*, 2003], resulting in a stronger influence from stratospheric aerosol in the UT.

4.2. Implications of Volcanic Impact on the UT

Whereas stratospheric aerosol affects Earth's radiation budget directly, tropospheric aerosol can affect the budget also indirectly, namely, by altering the occurrence and properties of clouds. In the previous sections the variability of sulfur in the northern midlatitude UT was found to be caused (i) by the seasonally varying subsidence of high-stratospheric air and (ii) by the varying contribution of volcanic aerosol mixed-in from the LMS. Next we will investigate whether volcanism influences the radiation budget via interaction with cirrus clouds.

4.2.1. Comparison to the MODIS Retrieved Cirrus Reflectance

To explore a possible impact of downwelling stratospheric aerosol on cirrus clouds, the particulate sulfur concentration measured during CARIBIC is compared to the CR retrieved by MODIS (see section 2.7). Because of the scarcity of UT data we use the S/PV in the LMS as a reasonable proxy for the UT particulate sulfur, as validated above (using samples collected below 5 PVU as in Figure 6). Only the season with

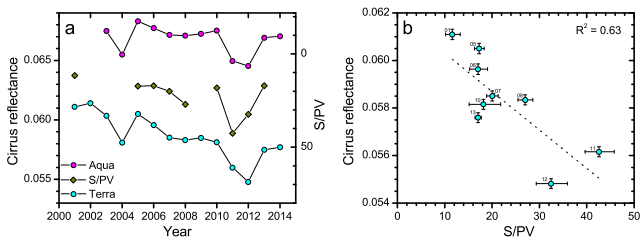

Figure 7. (a) Time series of the geometric average S/PV in the LMS (S/PV_{LMS}; ng m^{-3} STP/PVU) (note the reversed scale) and the arithmetic average of the MODIS-retrieved parameter, cirrus reflectance (CR) from Aqua and Terra, for samples taken below 5 PVU in the season March–July. (b) A comparison of S/PV and Terra's CR as in Figure 7a. A linear regression fit is shown as a dotted line.

largest stratospheric impact on the UT/LMS (March–July) is investigated here. The comparison is illustrated as time series (Figure 7a) of each year's average S/PV from CARIBIC and CR from the Terra and Aqua satellites. While no CARIBIC measurements were performed in the years 2003 and 2004, also the years 2002 and 2009 need to be excluded since too few months of CARIBIC data are available for these years.

The year-to-year changes of the CR of both satellites agree very well, in which the average Aqua values are ~20% higher, see explanation in section 2.7. The year-to-year variability and the general trend in S/PV are anticorrelated to CR; note the inverted scale of S/PV (Figure 7a). S/PV increases gradually from 2001 until 2011/2012 as a result of volcanism, whereas CR decreases. The increase in CR after the year 2012 coincides with less volcanic aerosol in the LMS. Unfortunately, maintenance of the CARIBIC aircraft in the year 2014 resulted in too few measurement months to include that year in the comparison, but the volcanic activity is known to have been low. The rate of CR decrease of Aqua is slightly weaker than that of Terra, which could be caused by stronger influence of convection. Since the CR obtained by Terra is less influenced by convective activity, it is expected to be more sensitive to changes in the UT/LMS conditions, which in this case concerns changes in the sulfur concentrations. We therefore use the CR of Terra to illustrate the close coupling of S/PV and CR as a scatterplot (Figure 7b). A linear regression reveals a good anticorrelation between CR and S/PV ($R^2 = 0.63$) with a significance level of 99%, even though the two parameters compared were obtained using fundamentally different measurement methods (the corresponding results for Aqua are $R^2 = 0.74$, significance level of 99%). The relative decrease in CR between 2001 and 2011 is $8 \pm 2\%$, while the particulate sulfur concentration in LMS increased by a factor of 3–4 during this time.

In Figure 8, the average CR during 2 years of low volcanic influence (2001–2002) is compared to the average CR during the 2 years of highest volcanic influence on the LMS/UT (2011–2012). The observed CR is generally higher over areas where convection is common since this gives rise to anvils (Figures 8a and 8b). This can be seen in the eastern parts of the oceans where warm water is transported northward resulting in convection and over the North American continent where convection also is common during this season. The CR decreases from 2001–2002 to 2011–2012 for large parts of the NH midlatitudes, see Figure 8c, and the largest decreases are found over Europe, the Atlantic Ocean, the North American continent, and the mid-Pacific Ocean. Change in the location or decrease in convective activity over the eastern parts of the oceans or the North American continent may cause a change in the CR (Figure 8c). However, limiting the computations to areas without persistent convection slightly increased the correlation between the Terra CR and S/PV. Hence, the anticorrelation seen in Figure 7b cannot be explained by a change in convective activity. In the following section possible causes for the anticorrelation will be discussed.

4.2.2. Cloud Microphysics and Climate

Recent geoengineering (GE) studies suggest that increased stratospheric sulfurous aerosol concentration can decrease cirrus cloud reflectance in a homogeneous nucleation regime. The GE aerosol increases temperatures and decreases vertical velocities in the tropopause region, which reduce the ice crystal formation rate, leading to optically thinner clouds [*Kuebbeler et al.*, 2012].

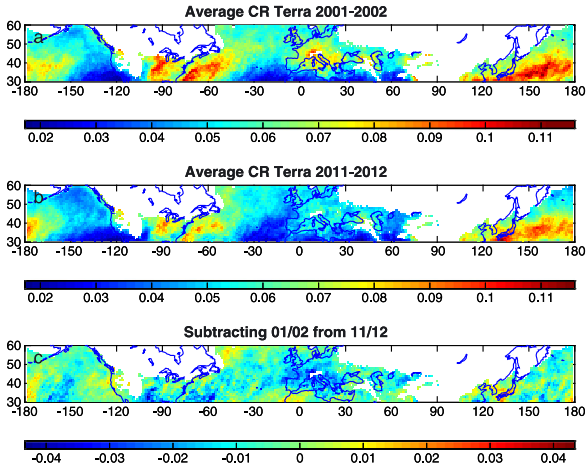

Figure 8. Geographical distributions of the March–July CR averaged over the years of (a) background concentrations of sulfur (2001–2002), (b) years of strongest influence of volcanism (2011–2012), and (c) the difference in CR between the years in Figures 8b and 8a.

Sulfurous aerosol could also shift the freezing mechanism of the cirrus clouds from homogeneous to heterogeneous. If the sulfuric acid is neutralized by ammonia, the downwelling LMS aerosol could act as IN [*Abbatt et al.*, 2006; *Hoose and Möhler*, 2012]. Increases in IN concentrations could shift the freezing mechanism from homogenous to heterogeneous, creating optically thinner cirrus clouds with fewer, larger ice crystals. Seeding of cirrus clouds have been found to make them optically thinner, except in pure heterogeneous freezing regimes [*Storelvmo and Herger*, 2014].

In a heterogeneous nucleation regime, a decrease in the amount of IN would reduce the number of ice crystals in the cirrus clouds, making them optically thinner. Sulfuric acid aerosol downwelling from the LMS may interact with some of the IN present in the UT, reducing their nucleation abilities and that way decrease the number of IN. Deactivation of soot IN from aviation could provide an explanation to the pronounced CR decrease over the Atlantic, North America, and Europe, as a large fraction of the soot emitted from the aviation corridor over the northern Atlantic ends up in this region [*Zhou and Penner*, 2014].

One of the discussed mechanisms, or a combination of them, may have caused the decrease in CR seen in Figures 7 and 8. A decrease in CR implies that the clouds are optically thinner and both reflect less shortwave radiation and absorb less longwave radiation. Because the latter effect dominates, a decrease in CR corresponds to a smaller greenhouse effect from cirrus clouds [*Storelvmo et al.*, 2013].

The strong response of 8% decrease in CR to a 3.5-fold increase of S/PV in the LMS indicates a substantial radiative forcing. Making use of the fact that CR and cloud optical thickness (COT) are linearly dependent for thin clouds [*Meyer et al.*, 2007], and the sensitivity of net radiative forcing to changes in COT according to *Cirisan et al.* [2013, their Figure 8] the maximum decrease of 8% of CR in the time period studied corresponds to approximately $-2\,\mathrm{Wm}^{-2}$ in net radiative forcing at NH midlatitudes. This regional result pertains to the season March to July.

5. Conclusions

This study focuses on particulate sulfur in the Northern Hemisphere's upper troposphere (UT) and lowermost stratosphere (LMS) in the period 1999–2013 measured by the CARIBIC observatory. Particulate sulfur

concentrations varied by a factor of about 100 in this period, mainly as a result of volcanic injections. The sulfurous aerosol concentration in the UT was strongly connected to that in the LMS, as downwelling aerosol constituted the major fraction of the UT particulate sulfur concentration in the periods of volcanic influence.

During the 15 year time span, the UT/LMS was perturbed by volcanism to various degrees. The lowest sulfur concentrations were observed in 1999–2002, a volcanically quiescent period. The largest perturbations were found not only after extratropical volcanic eruptions, specifically in 2008 (Kasatochi) and 2009 (Sarychev), but also in fall 2011 to spring 2012 after an eruption of the tropical volcano Nabro.

In the periods 2005–2008 and 2013, the variability in sulfur concentration was dominated by downwelling of volcanic aerosol from tropical volcanism that was transported through the stratosphere. In that period, the LMS sulfur concentration peaked in May as a result of downwelling of air transported in the deep Brewer-Dobson branch. The same seasonal variation was found in the UT, illustrating a strong coupling of the LMS and the UT. Downwelling of volcanic aerosol was found to more than double the spring and summer UT particulate sulfur concentrations compared to the background levels.

A comparison of sulfur concentrations to satellite observations of the MODIS retrieved cirrus reflectance (CR) from the satellites Terra and Aqua, for the season of largest stratospheric impact on the UT and LMS (March–July), resulted in strong anticorrelations ($R^2 = 0.63$ (Terra), $R^2 = 0.72$ (Aqua). The CR and thereby the cloud optical thickness (COT) decreased by 8% in the period 2001–2011. During this time the particulate sulfur concentration increased by a factor of 3.5 in the LMS. The strongest reduction in CR occurs over North America, the North Atlantic, and Europe, where soot ice nuclei (IN) from aviation [*Schumann et al.*, 2013] could shift the cirrus freezing mechanism from homogeneous to heterogeneous [*Zhou and Penner*, 2014], making deactivation of IN by volcanic sulfate aerosol a conceivable explanation for the observed reduction in CR. However, more research is needed to establish the definite mechanism.

Previous studies have shown that volcanism induced a significant radiative forcing after the turn of the millennium [*Santer et al.*, 2014; *Solomon et al.*, 2011] by the direct effect from stratospheric aerosol. New findings of the importance of LMS aerosol in this respect further increase this estimated forcing [*Andersson et al.*, 2015; *Ridley et al.*, 2014]. The tropical Pacific cooling [*England et al.*, 2014; *Meehl and Teng*, 2014], variations in solar forcing [*Flato et al.*, 2013], and volcanic aerosol forcing occurring after the year 2000 [*Santer et al.*, 2014; *Solomon et al.*, 2011] are not captured by the CMIP5 (Coupled Model Intercomparison Project Phase 5) models used by the Intergovernmental Panel on Climate Change, resulting in overestimation of the global warming over the last 15 years [*Flato et al.*, 2013; *Fyfe et al.*, 2013]. Here we introduce an indirect effect from volcanic aerosol that can contribute further explanation of the mismatch of model results and observations.

Acknowledgments

We especially acknowledge C. Koeppel, D.S. Scharffe, S. Weber, and all other members of the CARIBIC project. Lufthansa and Lufthansa Technik are gratefully acknowledged for enabling this scientific experiment. Frankfurt Airport is gratefully acknowledged for financial support. Contact the authors for CARIBIC data. The satellite data from the MODIS instruments were supplied by the United States National Aeronautics and Space Agency (http://ladsweb.nascom.nasa.gov/index.html). We are grateful to B.-C. Gao for guidance concerning MODIS cirrus reflectance data.

References

Abbatt, J. P. D., S. Benz, D. J. Cziczo, Z. Kanji, U. Lohmann, and O. Mohler (2006), Solid ammonium sulfate aerosols as ice nuclei: A pathway for cirrus cloud formation, *Science*, *313*(5794), 1770–1773.

Agrawal, H., A. A. Sawant, K. Jansen, J. W. Miller, and D. R. Cocker III (2008), Characterization of chemical and particulate emissions from aircraft engines, *Atmos. Environ.*, *42*, 4380–4392.

Andersson, S. M., B. G. Martinsson, J. Friberg, C. A. M. Brenninkmeijer, A. Rauthe-Schöch, M. Hermann, P. F. J. van Velthoven, and A. Zahn (2013), Composition and evolution of volcanic aerosol from eruptions of Kasatochi, Sarychev and Eyjafjallajökull in 2008–2010 based on CARIBIC observations, *Atmos. Chem. Phys.*, *13*, doi:10.5194/acp-13-1781-2013.

Andersson, S. M., B. G. Martinsson, J.-P. Vernier, J. Friberg, C. A. M. Brenninkmeijer, M. Hermann, P. F. J. van Velthoven, and A. Zahn (2015), Significant radiative impact of volcanic aerosol in the lowermost stratosphere, *Nat. Commun.*, *6*, doi:10.1038/ncomms8692.

Barahona, D., A. Molod, J. Bacmeister, A. Nenes, A. Gettelman, H. Morrison, V. Phillips, and A. Eichmann (2014), Development of two-moment cloud microphysics for liquid and ice within the NASA Goddard Earth Observing System Model (GEOS-5), *Geosci. Model Dev.*, *7*(4), doi:10.5194/gmd-7-1733-2014.

Baran, A. J. (2009), A review of the light scattering properties of cirrus, *J. Quant. Spectros. Radiat. Transfer*, *110*(14), doi:10.1016/j.jqsrt.2009.02.026.

Bönisch, H., A. Engel, J. Curtius, T. Birner, and P. Hoor (2009), Quantifying transport into the lowermost stratosphere using simultaneous in-situ measurements of SF6 and CO_2, *Atmos. Chem. Phys.*, *9*, 5905–5919.

Boucher, O., et al. (2013), Clouds and aerosols, in *Climate Change 2013: The Physical Science Basis. Contribution of Working Group I to the Fifth Assessment Report of the Intergovernmental Panel on Climate Change*, Cambridge Univ. Press, Cambridge, U. K., and New York.

Bourassa, A. E., A. Robock, W. J. Randel, T. Deshler, L. A. Rieger, N. D. Lloyd, E. J. T. Llewellyn, and D. A. Degenstein (2012), Large volcanic aerosol load in the stratosphere linked to Asian monsoon transport, *Science*, *337*(6090), doi:10.1126/science.1219371.

Brenninkmeijer, C. A. M., P. J. Crutzen, H. Fischer, H. Güsten, W. Hans, G. Heinrich, J. Heintzenberg, M. Hermann, T. Immelmann, and D. Kersting (1999), CARIBIC-Civil aircraft for global measurement of trace gases and aerosols in the tropopause region, *J. Atmos. Oceanic Technol.*, *16*(10), 1373–1383.

Brenninkmeijer, C. A. M., et al. (2007), Civil aircraft for the regular investigation of the atmosphere based on an instrumented container: The new CARIBIC system, *Atmos. Chem. Phys.*, *7*(18), 4953–4976.

Campbell, J. R., E. J. Welton, N. A. Krotkov, K. Yang, S. A. Stewart, and M. D. Fromm (2012), Likely seeding of cirrus clouds by stratospheric Kasatochi volcanic aerosol particles near a mid-latitude tropopause fold, *Atmos. Environ.*, *46*, doi:10.1016/j.atmosenv.2011.09.027.

Carn, S. A., and F. J. Prata (2010), Satellite-based constraints on explosive SO2 release from Soufrière Hills Volcano, Montserrat, *Geophys. Res. Lett.*, *37*, L00E22, doi:10.1029/2010GL044971.

Carn, S. A., A. J. Krueger, N. A. Krotkov, K. Yang, and K. Evans (2009), Tracking volcanic sulfur dioxide clouds for aviation hazard mitigation, *Nat. Hazards*, *51*(2), doi:10.1007/s11069-008-9228-4.

Chen, T., W. B. Rossow, and Y. Zhang (2000), Radiative effects of cloud-type variations, *J. Clim.*, *13*(1), 264–286.

Cirisan, A., P. Spichtinger, B. P. Luo, D. K. Weisenstein, H. Wernli, U. Lohmann, and T. Peter (2013), Microphysical and radiative changes in cirrus clouds by geoengineering the stratosphere, *J. Geophys. Res. Atmos.*, *118*, 4533–4548, doi:10.1002/jgrd.50388.

Clarisse, L., D. Hurtmans, C. Clerbaux, J. Hadji-Lazaro, Y. Ngadi, and P.-F. Coheur (2012), Retrieval of sulphur dioxide from the infrared atmospheric sounding interferometer (IASI), *Atmos. Meas. Tech.*, *5*(3), doi:10.5194/amt-5-581-2012.

Crutzen, P. J. (1976), The possible importance of CSO for the sulfate layer of the stratosphere, *Geophys. Res. Lett.*, *3*(2), 73–76, doi:10.1029/GL003i002p00073.

Cziczo, D. J., K. D. Froyd, C. Hoose, E. J. Jensen, M. Diao, M. A. Zondlo, J. B. Smith, C. H. Twohy, and D. M. Murphy (2013), Clarifying the dominant sources and mechanisms of cirrus cloud formation, *Science*, *340*(6138), doi:10.1126/science.1234145.

DeMott, P. J., D. J. Cziczo, A. J. Prenni, D. M. Murphy, S. M. Kreidenweis, D. S. Thomson, R. Borys, and D. C. Rogers (2003), Measurements of the concentration and composition of nuclei for cirrus formation, *Proc. Natl. Acad. Sci. U.S.A.*, *100*(25), 14,655–14,660.

Deshler, T. (2008), A review of global stratospheric aerosol: Measurements, importance, life cycle, and local stratospheric aerosol, *Atmos. Res.*, *90*(2), 223–232.

England, M. H., S. McGregor, P. Spence, G. A. Meehl, A. Timmermann, W. Cai, A. S. Gupta, M. J. McPhaden, A. Purich, and A. Santoso (2014), Recent intensification of wind-driven circulation in the Pacific and the ongoing warming hiatus, *Nat. Clim. Change*, *4*(3), 222–227.

Flato, G., J. Marotzke, B. Abiodun, P. Braconnot, S. Chou, W. Collins, P. Cox, F. Driouech, S. Emori, and V. Eyring (2013), Evaluation of climate models, in *Climate Change 2013: The Physical Science Basis. Contribution of Working Group I to the Fifth Assessment Report of the Intergovernmental Panel on Climate Change*, pp. 741–866, Cambridge Univ. Press, Cambridge.

Friberg, J., B. G. Martinsson, S. M. Andersson, C. A. M. Brenninkmeijer, M. Hermann, P. F. J. van Velthoven, and A. Zahn (2014), Sources of increase in lowermost stratospheric sulphurous and carbonaceous aerosol background concentrations during 1999–2008 derived from CARIBIC flights, *Tellus B*, *66*.

Fusina, F., P. Spichtinger, and U. Lohmann (2007), Impact of ice supersaturated regions and thin cirrus on radiation in the midlatitudes, *J. Geophys. Res.*, *112*, D24S14, doi:10.1029/2007JD008449.

Fyfe, J. C., N. P. Gillett, and F. W. Zwiers (2013), Overestimated global warming over the past 20 years, *Nat. Clim. Change*, *3*(9), 767–769.

Gao, B.-C., and Y. J. Kaufman (1995), Selection of the 1.375-um MODIS channel for remote sensing of cirrus clouds and stratospheric aerosols from space, *J. Atmos. Sci.*, *52*(23), 4231–4237.

Gao, B.-C., P. Yang, W. Han, R.-R. Li, and W. J. Wiscombe (2002), An algorithm using visible and 1.38-μm channels to retrieve cirrus cloud reflectances from aircraft and satellite data, *Geosci. Remote Sens., IEEE Trans.*, *40*(8), 1659–1668.

Gettelman, A., and C. Chen (2013), The climate impact of aviation aerosols, *Geophys. Res. Lett.*, *40*, 2785–2789, doi:10.1002/grl.50520.

Guan, H., R. Esswein, J. Lopez, R. Bergstrom, A. Warnock, M. Follette-Cook, M. Fromm, and L. T. Iraci (2010), A multi-decadal history of biomass burning plume heights identified using aerosol index measurements, *Atmos. Chem. Phys.*, *10*, doi:10.5194/acp-10-6461-2010.

GVP (2011), Global Volcanism Program. [Availble at http://www.volcano.si.edu/index.cfm, 15 March 2012.]

Haywood, J. M., A. Jones, L. Clarisse, A. Bourassa, J. Barnes, P. Telford, N. Bellouin, O. Boucher, P. Agnew, and C. Clerbaux (2010), Observations of the eruption of the Sarychev volcano and simulations using the HadGEM2 climate model, *J. Geophys. Res.*, *115*, D21212, doi:10.1029/2010JD014447.

Hermann, M., F. Stratmann, M. Wilck, and A. Wiedensohler (2001), Sampling characteristics of an aircraft-borne aerosol inlet system, *J. Atmos. Oceanic Technol.*, *18*(1), 7–19.

Hoerling, M. P., T. K. Schaack, and A. J. Lenzen (1991), Global objective tropopause analysis, *Mon. Weather Rev.*, *119*, 1816–1831.

Hofmann, D., J. Barnes, M. O'Neill, M. Trudeau, and R. Neely (2009), Increase in background stratospheric aerosol observed with lidar at Mauna Loa Observatory and Boulder, Colorado, *Geophys. Res. Lett.*, *36*, L15808, doi:10.1029/2009GL039008.

Hoinka, K. P. (1997), The tropopause: Discovery, definition and demarcation, *Meteorol. Z*, *6*, 281–303.

Holton, J. R., P. H. Haynes, M. E. McIntyre, A. R. Douglas, R. B. Rood, and L. Pfister (1995), Stratosphere-troposphere exchange, *Rev. Geophys.*, *33*(4), 403–439, doi:10.1029/95RG02097.

Hoor, P., C. Gurk, D. Brunner, M. I. Hegglin, H. Wernli, and H. Fischer (2004), Seasonality and extent of extratropical TST derived from in-situ CO measurements during SPURT, *Atmos. Chem. Phys.*, *4*(5), 1427–1442.

Hoose, C., and O. Möhler (2012), Heterogeneous ice nucleation on atmospheric aerosols: A review of results from laboratory experiments, *Atmos. Chem. Phys.*, *12*(20), doi:10.5194/acp-12-9817-2012.

Jensen, E. J., L. Pfister, T. P. Bui, P. Lawson, and D. Baumgardner (2010), Ice nucleation and cloud microphysical properties in tropical tropopause layer cirrus, *Atmos. Chem. Phys.*, *10*(3), 1369–1384.

Johansson, S. A. E., and J. L. Campbell (1988), *PIXE: A Novel Technique for Elemental Analysis*, 347 pp., John Wiley, Hoboken, N. J.

Karcher, B., and U. Lohmann (2002), A parameterization of cirrus cloud formation: Homogeneous freezing including effects of aerosol size, *J. Geophys. Res.*, *107*(D23), 4698, doi:10.1029/2001JD001429.

Kuebbeler, M., U. Lohmann, and J. Feichter (2012), Effects of stratospheric sulfate aerosol geo-engineering on cirrus clouds, *Geophys. Res. Lett.*, *39*, L23803, doi:10.1029/2012GL053797.

Kuebbeler, M., U. Lohmann, J. Hendricks, and B. Karcher (2014), Dust ice nuclei effects on cirrus clouds, *Atmos. Chem. Phys.*, *14*(6), 3027–3046.

Lohmann, U., B. Karcher, and C. Timmreck (2003), Impact of the Mount Pinatubo eruption on cirrus clouds formed by homogeneous freezing in the ECHAM4 GCM, *J. Geophys. Res.*, *108*(D18), 4568, doi:10.1029/2002JD003185.

Lopez, T. M., S. A. Carn, P. Webley, M. A. Pfeffer, M. P. Doukas, P. J. Kelly, C. A. Werner, F. Prata, D. J. Schneider, and C. F. Cahill (2009), Evaluation of satellite derived sulfur dioxide measurements for volcano monitoring during the 2009 Redoubt eruption, *AGU, Fall Meeting 2009*, abstract #V51F-03.

Luo, Z. Z., W. B. Rossow, T. Inoue, and C. J. Stubenrauch (2002), Did the eruption of the Mt. Pinatubo Volcano affect cirrus properties?, *J. Clim.*, *15*(19), 2806–2820.
Martinsson, B. G., H. N. Nguyen, C. A. M. Brenninkmeijer, A. Zahn, J. Heintzenberg, M. Hermann, and P. F. J. van Velthoven (2005), Characteristics and origin of lowermost stratospheric aerosol at northern midlatitudes under volcanically quiescent conditions based on CARIBIC observations, *J. Geophys. Res.*, *110*, D12201, doi:10.1029/2004JD005644.
Martinsson, B. G., C. A. M. Brenninkmeijer, S. A. Carn, M. Hermann, K. P. Heue, P. F. J. van Velthoven, and A. Zahn (2009), Influence of the 2008 Kasatochi volcanic eruption on sulfurous and carbonaceous aerosol constituents in the lower stratosphere, *Geophys. Res. Lett.*, *36*, L12813, doi:10.1029/2009GL038735.
Martinsson, B. G., J. Friberg, S. M. Andersson, A. Weigelt, M. Hermann, D. Assmann, J. Voigtländer, C. A. M. Brenninkmeijer, P. J. F. van Velthoven, and A. Zahn (2014), Comparison between CARIBIC aerosol samples analysed by accelerator-based methods and optical particle counter measurements, *Atmos. Meas. Tech.*, *7*, doi:10.5194/amt-7-2581-2014.
Meehl, G. A., and H. Teng (2014), CMIP5 multi-model hindcasts for the mid-1970s shift and early 2000s hiatus and predictions for 2016–2035, *Geophys. Res. Lett.*, *41*, 1711–1716, doi:10.1002/2014GL059256.
Meyer, K., and S. Platnick (2010), Utilizing the MODIS 1.38 μm channel for cirrus cloud optical thickness retrievals: Algorithm and retrieval uncertainties, *J. Geophys. Res.*, *115*, D24209, doi:10.1029/2010JD014872.
Meyer, K., P. Yang, and B.-C. Gao (2007), Ice cloud optical depth from MODIS cirrus reflectance, *IEEE Geosci. Rem. Sens. Lett.*, *4*(3), 471–474.
Mitchell, D. L., R. P. Lawson, and S. Mishra (2011), *Cirrus Clouds and Climate Engineering: New Findings on Ice Nucleation and Theoretical Basis*, INTECH Open Access Publisher.
Murphy, D. M., D. S. Thomson, and M. J. Mahoney (1998), In situ measurements of organics, meteoritic material, mercury, and other elements in aerosols at 5 to 19 kilometers, *Science*, *282*(5394), 1664–1669.
Murphy, D. M., D. J. Cziczo, K. D. Froyd, P. K. Hudson, B. M. Matthew, A. M. Middlebrook, R. E. Peltier, A. Sullivan, D. S. Thomson, and R. J. Weber (2006), Single-particle mass spectrometry of tropospheric aerosol particles, *J. Geophys. Res.*, *111*, D23S32, doi:10.1029/2006JD007340.
Murphy, D. M., K. D. Froyd, J. P. Schwarz, and J. C. Wilson (2014), Observations of the chemical composition of stratospheric aerosol particles, *Q. J. R. Meteorol. Soc.*, *140*, 1269–1278.
Myhre, G., D. Shindell, F. Bréon, W. Collins, J. Fuglestvedt, J. Huang, D. Koch, J. Lamarque, D. Lee, and B. Mendoza (2013), Anthropogenic and natural radiative forcing, in *Climate Change 2013: The Physical Science Basis. Contribution of Working Group I to the Fifth Assessment Report of the Intergovernmental Panel on Climate Change*, edited by T. F. Stocker et al., Cambridge Univ. Press, Cambridge, U. K., and New York.
Nguyen, H. N., A. Gudmundsson, and B. G. Martinsson (2006), Design and calibration of a multi-channel aerosol sampler for tropopause region studies from the CARIBIC platform, *Aerosol Sci. Technol.*, *40*, doi:10.1080/02786820600767807.
Nguyen, H. N., et al. (2008), Chemical composition and morphology of individual aerosol particles from a CARIBIC flight at 10 km altitude between 50°N and 30°S, *J. Geophys. Res.*, *113*, D23209, doi:10.1029/2008JD009956.
Pan, L. L., W. J. Randel, B. L. Gary, M. J. Mahoney, and E. J. Hintsa (2004), Definitions and sharpness of the extratropical tropopause: A trace gas perspective, *J. Geophys. Res.*, *109*, D23103, doi:10.1029/2004JD004982.
Papaspiropoulos, G., B. Mentes, P. Kristiansson, and B. G. Martinsson (1999), A high sensitivity elemental analysis methodology for upper tropospheric aerosol, *Nucl. Instrum. Methods Phys. Res., Sect. B*, *150*, 356–362.
Platnick, S., M. D. King, S. A. Ackerman, W. P. Menzel, B. A. Baum, J. C. Riedi, and R. A. Frey (2003), The MODIS cloud products: Algorithms and examples from Terra, *IEEE Trans. Geosci. Remote*, *41*(2), 459–473.
Prata, A. J., and C. Bernardo (2007), Retrieval of volcanic SO_2 column abundance from atmospheric infrared sounder data, *J. Geophys. Res.*, *112*, D20204, doi:10.1029/2006JD007955.
Pruppacher, H. R., and J. D. Klett (1997), *Microphysics of Clouds and Precipitation*, Kluwer Acad., Dordrecht, Netherlands.
Rauthe-Schöch, A., et al. (2012), CARIBIC aircraft measurements of Eyjafjallajökull volcanic clouds in April/May 2010, *Atmos. Chem. Phys.*, *12*, doi:10.5194/acp-12-879-2012.
Reid, J. S., R. Koppmann, T. F. Eck, and D. P. Eleuterio (2005), A review of biomass burning emissions Part II: Intensive physical properties of biomass burning particles, *Atmos. Chem. Phys.*, *5*(3), 799–825.
Ridley, D. A., S. Solomon, J. E. Barnes, V. D. Burlakov, T. Deshler, S. I. Dolgii, A. B. Herber, T. Nagai, R. R. Neely, and A. V. Nevzorov (2014), Total volcanic stratospheric aerosol optical depths and implications for global climate change, *Geophys. Res. Lett.*, *41*, 7763–7769, doi:10.1002/2014GL061541.
Robock, A. (2000), Volcanic eruptions and climate, *Rev. Geophys.*, *38*(2), 191–219, doi:10.1029/1998RG000054.
Rosen, J. M. (1971), The boiling point of stratospheric aerosols, *J. Appl. Meteorol.*, *10*, 1044–1046.
Santer, B. D., C. Bonfils, J. F. Painter, M. D. Zelinka, C. Mears, S. Solomon, G. A. Schmidt, J. C. Fyfe, J. N. S. Cole, and L. Nazarenko (2014), Volcanic contribution to decadal changes in tropospheric temperature, *Nat. Geosci.*, *7*(3), 185–189.
Schmale, J., et al. (2010), Aerosol layers from the 2008 eruptions of Mount Okmok and Mount Kasatochi: In situ upper troposphere and lower stratosphere measurements of sulfate and organics over Europe, *J. Geophys. Res.*, *115*, D00L07, doi:10.1029/2009JD013628.
Schumann, U., P. Jeßberger, and C. Voigt (2013), Contrail ice particles in aircraft wakes and their climatic importance, *Geophys. Res. Lett.*, *40*, 2867–2872, doi:10.1002/grl.50539.
Solomon, S., J. S. Daniel, R. R. Neely, J. P. Vernier, E. G. Dutton, and L. W. Thomason (2011), The persistently variable "background" stratospheric aerosol layer and global climate change, *Science*, *333*, doi:10.1126/science.1206027.
Song, N. H., D. O. Starr, D. J. Wuebbles, A. Williams, and S. M. Larson (1996), Volcanic aerosols and interannual variation of high clouds, *Geophys. Res. Lett.*, *23*(19), 2657–2660, doi:10.1029/96GL02372.
Sprenger, M., and H. Wernli (2003), A northern hemispheric climatology of cross-tropopause exchange for the ERA15 time period (1979–1993), *J. Geophys. Res.*, *108*(D12), 8521, doi:10.1029/2002JD002636.
Storelvmo, T., and N. Herger (2014), Cirrus cloud susceptibility to the injection of ice nuclei in the upper troposphere, *J. Geophys. Res. Atmos.*, *119*, 2375–2389.
Storelvmo, T., J. E. Kristjansson, H. Muri, M. Pfeffer, D. Barahona, and A. Nenes (2013), Cirrus cloud seeding has potential to cool climate, *Geophys. Res. Lett.*, *40*, 178–182, doi:10.1029/2012GL054201.
Thomas, H. E., I. M. Watson, S. A. Carn, A. J. Prata, and V. J. Realmuto (2011), A comparison of AIRS, MODIS and OMI sulphur dioxide retrievals in volcanic clouds, *Geomat. Nat. Hazard. Risk*, *2*(3), doi:10.1080/19475705.2011.564212.
Vernier, J. P., et al. (2011), Major influence of tropical volcanic eruptions on the stratospheric aerosol layer during the last decade, *Geophys. Res. Lett.*, *38*, L12807, doi:10.1029/2011GL047563.
Weisenstein, D. K., G. K. Yue, M. K. W. Ko, N. D. Sze, J. M. Rodriguez, and C. J. Scott (1997), A two-dimensional model of sulfur species and aerosols, *J. Geophys. Res.*, *102*(D11), 13,019–13,035, doi:10.1029/97JD00901.

Wylie, D. P., and W. P. Menzel (1999), Eight years of high cloud statistics using HIRS, *J. Clim.*, *12*(1), 170–184.
Yang, K., X. Liu, P. K. Bhartia, N. A. Krotkov, S. A. Carn, E. J. Hughes, A. J. Krueger, R. J. D. Spurr, and S. G. Trahan (2010), Direct retrieval of sulfur dioxide amount and altitude from spaceborne hyperspectral UV measurements: Theory and application, *J. Geophys. Res.*, *115*, D00L09, doi:10.1029/2010JD013982.
Zahn, A., and C. A. M. Brenninkmeijer (2003), New directions: A chemical tropopause defined, *Atmos. Environ.*, *37*(3), 439–440.
Zahn, A., E. Christner, P. F. J. Velthoven, A. Rauthe-Schöch, and C. A. M. Brenninkmeijer (2014), Processes controlling water vapor in the upper troposphere/lowermost stratosphere: An analysis of 8 years of monthly measurements by the IAGOS-CARIBIC observatory, *J. Geophys. Res. Atmos.*, *119*, 11,505–11,525, doi:10.1002/2014JD021687.
Zhou, C., and J. E. Penner (2014), Aircraft soot indirect effect on large-scale cirrus clouds: Is the indirect forcing by aircraft soot positive or negative?, *J. Geophys. Res. Atmos.*, *119*, 11,303–11,320.

Printed by Media-Tryck, Lund University 2016

Johan Friberg has a background in Engineering Nanoscience, material science and measurement technology. He was introduced to aerosol particles during his master thesis, where he worked with polymeric nanofiber production to improve air-filters. This thesis focuses on how volcanic aerosol particles influence the climate by scattering solar radiation and altering cloud properties. Volcanism was found to perturb the Earth's radiative balance, masking some of the effects of recent anthropogenic warming.

LUND UNIVERSITY
Faculty of Engineering
Department of Physics
ISRN LUTFD2/(TFKF-1047)/1 - 73 (2015)
ISBN 978-91-7623-591-1